# VYSOKÉ UČENÍ TECHNICKÉ V BRNĚ

BRNO UNIVERSITY OF TECHNOLOGY

## STŘEDOEVROPSKÝ TECHNOLOGICKÝ INSTITUT VUT

CENTRAL EUROPEAN INSTITUTE OF TECHNOLOGY BUT

## NÁVRH NOVÝCH ELEKTRODOVÝCH MATERIÁLŮ S KATALYZÁTOREM PRO ELEKTROCHEMICKÉ SNÍMÁNÍ A ENERGETICKÉ APLIKACE

DESIGNING NOVEL CATALYST LOADED ELECTRODE MATERIALS TOWARDS ELECTROCHEMICAL SENSING TO ENERGY APPLICATIONS

### DIZERTAČNÍ PRÁCE
DOCTORAL THESIS

**AUTOR PRÁCE**
AUTHOR

Akshay Kumar Kandambath Padinjareveetil, M.Sc.

**ŠKOLITEL**
SUPERVISOR

prof. RNDr. Martin Pumera, Ph.D.

BRNO 2023

**ABSTRACT**

The exponential increase in energy crises along with rising health issues is causing enormous risks to the survival of human life on Earth. Immense research is being undertaken currently to find an ideal solution to overcome these global challenges. Employing electrochemical energy technologies are thus in high demand to mitigate the growing energy requirements along with fabricating newer electrocatalysts that are cheap, efficient, and durable for utilization of such devices for large-scale commercial applications. Although several catalyst materials are being periodically studied, there is a need for more advanced studies in this direction. In the present study, newer catalyst fabrication techniques are introduced to develop application-specific catalysts for hydrogen and ammonia production. Also, with the broadening scope of the 3D-printing technology in recent times, electrocatalysts fabrication via this technology towards electrocatalytic applications such as hydrogen production, ammonia synthesis, and carbon dioxide mitigation are discussed in detail. In addition to catalysis, the current thesis also evaluates the potential possibilities of using 3D-printing technology for healthcare applications such as electrochemical sensors and emergency applications. In short, the thesis aims to provide an understanding of the recent advancements in electrocatalyst fabrications along with providing a fundamental foundation in designing, and engineering active electrode materials for energy conversion and electrochemical sensing applications.

## ABSTRAKT

Exponenciální nárůst potřeby energie spolu s rostoucími nároky na zdravotnický sektor způsobuje velká rizika pro přežití lidstva na Zemi. V současné době probíhá intenzivní výzkum s cílem nalézt ideální řešení k překonání těchto globálních výzev. Využití elektrochemických energetických technologií je velmi žádané pro zmírnění rostoucích energetických požadavků ve spojení s výrobou novějších elektrokatalyzátorů, které jsou levné, účinné a odolné pro využití takových zařízení pro komerční aplikace ve velkém měřítku. Ačkoli se opakovaně studuje několik katalytických materiálů, existuje potřeba dalšího výzkumu katalyzátorů. V této studii jsou představeny nové techniky přípravy katalyzátorů pro vývoj aplikací těchto katalyzátorů pro výrobu vodíku a amoniaku. S rozšiřujícím se rozsahem technologie 3D tisku je také podrobně diskutována výroba elektrokatalyzátorů prostřednictvím této technologie s důrazem na elektrokatalytické aplikace, jako je výroba vodíku, syntéza amoniaku a redukce oxidu uhličitého. Kromě katalýzy tato práce také hodnotí potenciální možnosti využití technologie 3D tisku pro biomedicínské aplikace, jako jsou elektrochemické sensory. V sourhnu, práce si klade za cíl výzkum pokročilých elektrokatalůyzátorů spolu s poskytnutím vhledu do navrhování a konstrukci materiálů aktivních elektrod pro přeměnu energie a aplikace elektrochemických sensorů.

**Key words**

Electrocatalysts, 3D-printing, hydrogen evolution reaction, ammonia production, sensing, doping, dip-coating, graphene, MXene, MAX, TMDs, MOF

**Klíčová slova**

Elektrokatalyzátory, 3D tisk, Uývoj vodíku, výroba amoniaku, detekce, dopování, pokovování, grafen, MXen, MAX, TMD, MOF

**Declaration**

I declare that the matter presented in this work entitled "Designing novel catalyst loaded electrode materials towards electrochemical sensing to energy applications", are the results of the work carried out by me at the CEITEC, Brno University of Technology, under the supervision of Prof. Martin Pumera. The contents are expressed in my own words and I have adequately cited and referenced the original sources. I also declare that I have adhered to all principles of academic honesty and integrity and have not misrepresented or fabricated or falsified any idea/data/fact/source in my submission.

Brno. 30-10-2023.

(author's signature)

Akshay Kumar Kandambath Padinjareveetil

**Bibliographic citation**

Kandambath Padinjareveetil, Akshay Kumar. (2023) *Designing novel catalyst loaded electrode materials towards electrochemical sensing to energy applications* [Doctoral dissertation] Brno University of Technology, Central European Institute of Technology.

## Acknowledgements

Brno. 30-10-2023

(author's signature)

Akshay Kumar Kandambath Padinjareveetil

**Table of Contents**

**Index of Abbreviations**

| | |
|---|---|
| HER | Hydrogen evolution reaction |
| NRA | Nitrate reduction to ammonia |
| $CO_2R$ | Carbon dioxide reduction |
| $ERCO_2$ | Electrochemical reduction of carbon dioxide |
| 2D | Two dimensional |
| 3D | Three dimensional |
| FDM | Fused deposition modeling |
| 3D-CE | Three dimensional carbon electrode |
| RHE | Reversible hydrogen electrode |
| SHE | Standard hydrogen electrode |
| DMF | Dimethylformamide |
| $H_2$ | Hydrogen |
| RGO | Reduced graphene oxide |
| TMDs | Transition metal dichalcogenide |
| MOFs | Metal–organic framework |
| FE | Faradaic efficiency |
| Cu | Copper |

# List of Publications

1. <u>Akshay Kumar K. Padinjareveetil</u>, Ghosh, O. Alduhaish, Martin Pumera\*, *Metal-plated 3D-printed electrode for electrochemical detection of carbohydrates*, **Electrochem. Commun**. 2020, 120, 106827, doi.org/10.1016/j.elecom.2020.106827.

2. <u>Akshay Kumar K. Padinjareveetil</u>, K. Ghosh, O. Alduhaish, Martin Pumera\*, *Dip-coating of MXene and transition metal dichalcogenides on 3D-printed nanocarbon electrodes for the hydrogen evolution reaction*, **Electrochem. Commun**. 2021, 122, 106890 doi.org/10.1016/j.elecom.2020.106890.

3. <u>Akshay Kumar K. Padinjareveetil</u>, Martin Pumera\*, *3D-Printing to Mitigate COVID-19 Pandemic*, **Adv. Funct. Mater**. 2021, 31, doi.org/10.1002/adfm.202100450.

4. <u>Akshay Kumar K. Padinjareveetil</u>, O. Alduhaish, Martin Pumera\*, *Electrocatalytic activity of layered MAX phases for the hydrogen evolution reaction,* **Electrochem. Commun**. 2021, 125, 106977, https://doi.org/10.1016/j.elecom.2021.106977.

5. <u>Akshay Kumar K. Padinjareveetil</u>, O. Alduhaish, S. F. Adil, Martin Pumera\*, *Grafting of Pd on Covalently and Noncovalently Modified N-Doped Graphene for Electrocatalysis*, **Adv. Mater. Interfaces**, 2022, 2102317, doi.org/10.1002/admi.202102317.

6. <u>Akshay Kumar K. Padinjareveetil</u>, Martin Pumera\*, *Advances in Designing 3D-Printed Systems for CO₂ Reduction,* **Adv. Mater. Interfaces**, 2023, 10, 8, 2201734, https://doi.org/10.1002/admi.202201734.

7. <u>Akshay Kumar K. Padinjareveetil</u>, Martin Pumera\*, *Engineering 3D Printed Structures Towards Electrochemically Driven Green Ammonia Synthesis: A Perspective*, **Adv. Mater. Technologies**, 2023 ,10, 8, 2201734, https://doi.org/10.1002/admt.202202080.

8. Stefan Wert, Christian Iffelsberger, <u>Akshay Kumar K. Padinjareveetil</u>, and Martin Pumera\*, *Edges of Layered FePSe₃ Exhibit Increased Electrochemical and Electrocatalytic Activity Compared to Basal Planes*, **ACS Appl. Electron. Mater.** 2023, 5, 2, 928–934, https://doi.org/10.1021/acsaelm.2c01493.

9. <u>Akshay Kumar K. Padinjareveetil</u>, Juan V. Perales-Rondon, Dagmar Zaoralová, Michal Otyepka, Osamah Alduhaish, and Martin Pumera\* *Fe-MOF Catalytic Nanoarchitectonic toward Electrochemical Ammonia Production*, **ACS Appl. Mater. Interfaces**, 2023, 15, 40, 47294–47306, https://doi.org/10.1021/acsami.3c12822.

**List of Articles not included in thesis (Submitted/Under review)**

10. Kalyan Ghosh, Siowwoon Ng, Petr Lazar, <u>Akshay Kumar K. Padinjareveetil</u>, Jan Michelicka, and Martin Pumera*, *2D Germanane-MXene Heterostructures for Cations Intercalation in Energy Applications*, Submitted, Last Update on: 20-10-2023.

11. <u>Akshay Kumar K. Padinjareveetil</u>, and Martin Pumera*, *MXenes for Energy Storage and Electrocatalytic Applications via Mechanical Downsizing*, Submitted, Last Update on: 20-10-2023.

12. <u>Akshay Kumar K. Padinjareveetil</u>, Martin Pykal, Aristides Bakandritsos, Radek Zbořil, Michal Otyepka, and Martin Pumera*, *Real Time Tracking of Nanoconfined Water-Assisted Ion Transfer in Functionalized Graphene Derivatives Supercapacitor Electrodes,* Submitted, Last Update on: 20-10-2023.

# CHAPTER 1

# 1. Introduction

Energy has always been a very important aspect for the sustenance of life on earth. Although the energy demands have been supported by non-renewable sources over generations, the excessive utilization of it has led to disastrous impacts. In the present scenario, the rapid growth in the population, increasing consumption of fossil fuels, and climate change hazards have resulted in a massive global energy crisis.[1–3] Further, rising carbon dioxide ($CO_2$) and methane ($CH_4$) levels are worsening the conditions.[4–8] Live statistics provided by NASA's global climate change, on temperature rise, inclining $CO_2$ and $CH_4$ levels, rise in sea level and ocean warming are clear signs of the forthcoming disaster.[9] For mitigating the above concerns, along with countering the huge demand for energy in the near future, stringent and quick measures are therefore the need of the hour.[10,11]

Developing green and sustainable electrochemical technology such as energy storage and conversion can be a viable solution to this crisis.[12,13] To run these electrochemical energy devices, electrocatalysis at the electrodes is essential. Also, electrocatalysis has significant merits over conventional techniques, accounting to its ideal operational conditions at ambient temperatures and pressures.[14–17] Further, in order to carry out electrocatalysis efficiently, the need for electrocatalysts are vital as these electrocatalysts minimize the overpotential of various reactions during the oxidation and reduction reactions. Finding catalysts beyond the state-of-the-art by evaluating several classes of bulk and layered materials,[18–20] downsizing and modifying them via various strategies to fabricate application specific catalysts using possible technological advancements such as 3D-printing,[21,22] doping,[23,24] anchoring,[25] functionalizing,[26,27] patterning[28] etc., are some of the approaches taken by the researchers to find a feasible solution to the rising concerns. Also, such studies are crucial for their commercialization of these technologies as well.

In short, a large amount of scientific work today is exploring the possibility of obtaining abundant, clean, renewable, efficient, and eco-friendly strategies for energy related applications. The focus of our studies also extends to developing strategies towards efficient storage/conversion of renewable sources, to make them available on demand. Hitherto, hydrogen production,[20,29] ammonia synthesis,[30] $CO_2$ reduction,[7] $CO_2$ capture continue to be high end topics, that are employed to resolve the energy crisis and environmental issues.

Subsequently, the healthcare community has evolved during the years and immense studies and research are currently operational for fighting health issues, and also finding solutions for rapid detection and diagnosis of various diseases. For instance, increased concentration of sugar in the blood can lead to a chronic long lasting disorder called diabetes mellitus.[31,32] In extreme cases they can lead to stroke and damage to various internal and external human organs such as eyes, nerves, and kidneys. Statistically, there is a rapid increase in the number of diabetic patients across the globe,[32,33] and the traditional approach of detecting sugar levels will have to be improved. Electrochemical sensing could be considered as an effective strategy to diagnose diseases and disorders.[34] Various studies are underway to fabricate devices/ electrodes that are rapid, cheap, accurate, and easy to handle. Currently, although glucose oxidase enzyme based electrochemical biosensors are used for blood glucose detection[35,36] yet, researchers are more curious in broadening the scope towards non-enzymatic glucose sensors.[37,38] The non-enzymatic glucose sensors are interesting as they eliminate the problems related to the complexity in using enzymes accounting to issues such as denaturation, poor stability, immobilization issues etc. Yet, in the present conditions, it's well evident that the field has to progress a lot in terms of sensitivity and selectivity. Electrode surfaces are a key parameter in the enhancing performance of the non-enzymatic glucose sensor.[33,37] Employing more advanced techniques such as 3D-printing as a tool for fabricating electrochemical

sensors could be interesting. The potential scope of 3D-printing technology will be discussed in subsequent sections.

## 1.1. Electrochemical energy technologies

Electrochemistry deals with the study of the relationship between electricity and chemical reactions wherein it acts as an effective tool to probe reactions associated with electron transfer. Vast studies associated with the production of electrical energy from chemical reactions and/or chemical changes associated with given electrical current are branched to several other domains. These electrochemical energy technologies are discussed in detailed in following sections. Furthermore, depending upon the intended product or application, electrocatalysts are designed to drive the electrochemical reactions.

### 1.1.1 Hydrogen production

Considering the above discussions on the importance of fuels, molecular hydrogen gas ($H_2$) can be regarded as an efficient and appropriate fuel, pertaining to its significance in mitigating the expected energy crisis in the future.[20,39] Electrocatalytic hydrogen evolution reaction (HER) can be considered as a promising and feasible approach towards $H_2$ production via 'water splitting' or 'water electrolysis', which has been of interest to the scientific community over the past several years.[18,40–42] Also, its ability to deliver carbon free clean energy products makes it highly desirable, and can be a promising alternative to fossil fuel. Electrochemical water splitting involves two main processes where water ($H_2O$) breaks down into $H_2$ and oxygen ($O_2$) upon the application of electric current. During the process (**Figure 1**), $H^+$ (two protons) ions are reduced at cathode (HER: $2H^+ + 2e^- = H_2$), and oxidation of $H_2O$ occurs at the anode (OER: $2H_2O = O_2 + 4H^+ + 4e^-$).[18] In short, electrochemical water splitting can be

considered as an ideal, efficient, clean and sustainable strategy towards $H_2$ production.[43,44] The main advantage of $H_2$ is its high calorific value and the byproduct it delivers on combustion such as pollution-free water, making it highly attractive as an energy carrier and promising for future low-carbon energy systems.[20,29,41,45] Hence, efficient, clean and renewable techniques to deliver $H_2$ is a key strategy towards effective accomplishment of the hydrogen based energy technology.
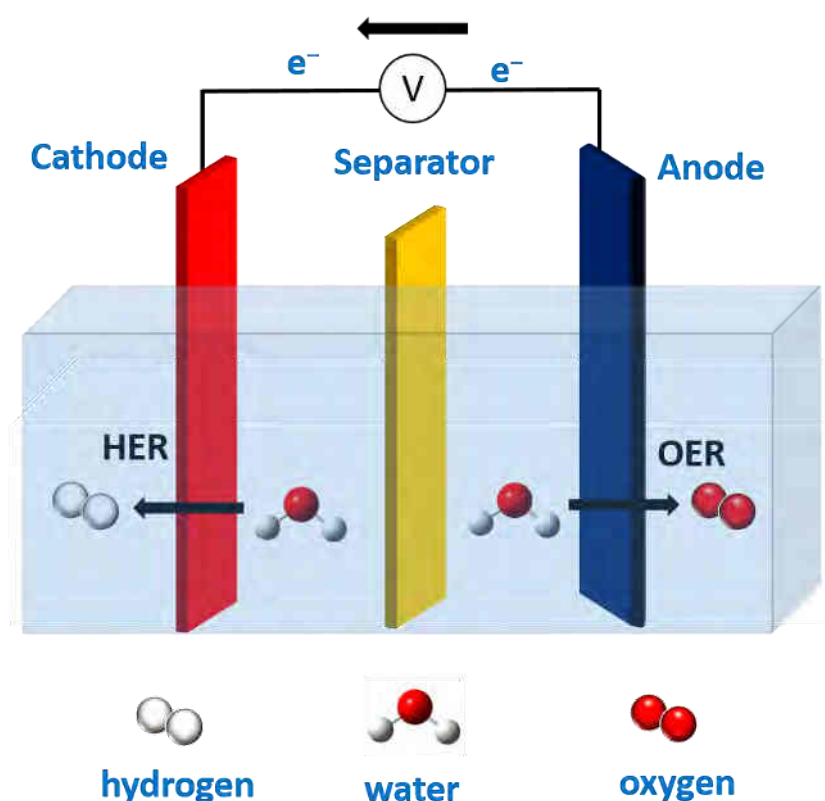


Figure 1. Schematic representation of electrochemical water splitting process.

Several studies have already been conducted in this domain, yet strategies for improving the technique, and/or catalyst material are being conducted regularly, for designing electrocatalysts exhibiting enhanced performance for large scale applications. For instance, platinum (Pt)-based catalysts are found to be ideal for this application, yet limitations such as high cost, and low abundance, calls for newer approaches.[46–48] In short, several researchers

today are focusing on the direction of designing catalysts that are cost-effective, deliver high activity, high surface area, good electrical conductivity, efficient, durable, and eventually employable for large scale commercialization.

Efficiency of the HER catalysis and mechanism is further evaluated using Tafel slopes.[49] It represents the increment in overpotential that is needed to enhance current density by one order of magnitude. The kinetics of the catalyst is evaluated by three major pathways based on their ability to convert protons in aqueous media to hydrogen molecules electrochemically. The Tafel equation is given by the formula; $\eta = b \log |j| + a$, where $\eta$ = overpotential, b = Tafel slope, and j = current density. Further, according to the Tafel analysis, the slope values are identified from the slow-rate step in the HER mechanism which is given by [25,50]

1) Volmer reaction (hydrogen adsorption)

$$H_3O^+ + e^- \rightarrow H_{ads} + H_2O; \; b \approx 120 \; mV \; dec^{-1}$$
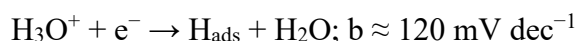
2) Heyrovsky reaction (electrochemical hydrogen desorption desorption)

$$H_3O^+ + H_{ads} + e^- \rightarrow H_2 + H_2O; \; b \approx 40 \; mV \; dec^{-1}$$
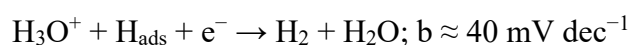
3) Tafel reaction (recombination of adsorbed hydrogen atoms; desorption)

$$H_{ads} + H_{ads} \rightarrow H_2; \; b \approx 30 \; mV \; dec^{-1}$$
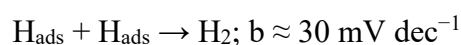
In principle, smaller Tafel slopes accounts to better HER catalysis.[49] Stability, activity, selectivity are other crucial factors that are evaluated systematically to understand the potential of electrocatalysts.[51,52] The $H_2$ generated via HER can be employed as fuel for electricity, automobiles, internal fuel cells in electric motor vehicles etc. In short, water electrolysis can be ideally used for production of cheap, carbon free and sustainable $H_2$ at a large scale. Zero carbon emission and high energy density are other added advantages of

hydrogen energy. However, this approach, although interesting, has a long way to go in resolving limitations associated with technique or finding alternatives to lower the entire cost of the set up with better efficiency. For instance, electrochemical splitting in aqueous systems is inhibited by multiple factors, and thus will require an additional potential to enhance/drive the reaction forward called overpotential.

### 1.1.2 Ammonia synthesis

Ammonia production is also considered to be a very crucial and most impactful discovery of the last century, owing to its vast applications benefit for various industrial and non-industrial purposes.[53,54] Interestingly, ammonia is considered to be an important next generation energy carrier accounting to high gravimetric energy density (3 kWh kg$^{-1}$), and high hydrogen storage capacity (17.65 wt.%) and added advantages such as convenient storage and transportation, make them highly desirable and in demand.[11] Conventional techniques such as Haber–Bosch are typically employed for large-scale ammonia production.[55] However, harsh operating conditions, energy-intensive processes with excessive emission of $CO_2$ calls for better and improved techniques. Although, electrochemical nitrogen reduction reaction,[56] is considered as a possible remedy, especially due to its mild operating conditions, high energy consumed for breaking nitrogen triple bonds, the competitive HER, low selectivity and faradaic efficiency (FE) and have made researchers to put forward better approaches.[11] Nitrate reduction to ammonia (NRA) (**Figure 2)** is one such potential field wherein appropriate utilization of technology would pave way towards a two-fold advantage for addressing both the issues of energy crisis and also strategies to mitigate excessive nitrate, especially in the water bodies. NRA involves a complex 8 electron (e$^-$) transfer process, where multiple nitrogen-containing species from +5 to −3 valence states are involved and proceed via a series

of complex routes. The general mechanism of NRA with respect to standard hydrogen electrode (SHE) is illustrated in equation 1 along with its respective reduction potential.
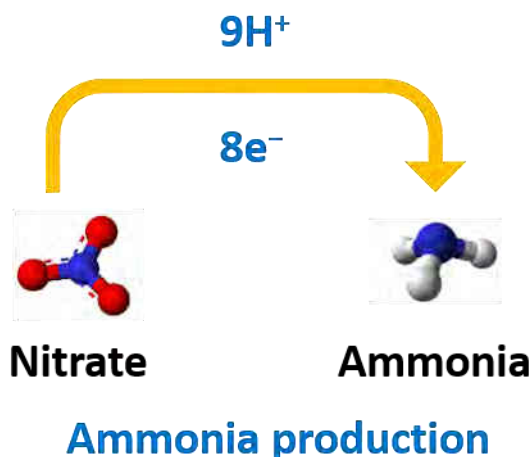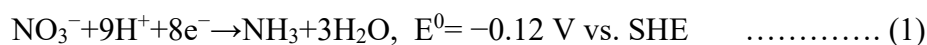
$$NO_3^- + 9H^+ + 8e^- \rightarrow NH_3 + 3H_2O, \ E^0 = -0.12 \ V \ vs. \ SHE \quad \ldots\ldots\ldots\ldots (1)$$



Figure 2. Schematic representation of electrochemical reduction of nitrate to ammonia.

In principle, designing electrocatalysts for NRA is now gaining massive attention, with several catalysts being periodically studied for delivering appreciable FE, and stability that are required for practical applications. From an experimentation point of view, the classical approach to conduct NRA experiments includes the use of electrolytic experiments at various potentials in specific experimental cells (such as H cells).[11,57] The electrocatalysts are usually assembled at the cathodic end of the experimental cell along with the reference electrode, while the counter electrode is assembled at the other end of the cell. After the electrolysis experiments, the products at the cathodic end are quantified for ammonia, nitrate and nitrite using ultraviolet–visible (UV–vis) spectroscopy.[57,58] Quantification of each product such as ammonia, nitrate, nitrite is carried out using specific reagents and the final results would deliver information on the potential of the electrocatalysts employed for NRA. ^{1}H NMR

experiments are also conducted to compare the reliability of colorimetric methods and to confirm the sources of ammonia.

### 1.1.3 Carbon dioxide mitigation strategies

$CO_2$, a major greenhouse gas, has significantly impacted the present climatic conditions and affects the innate carbon cycle of the Earth.[59,60] Combustion of fossil fuel is one of the predominant sources of the rising $CO_2$ levels in the atmosphere. Although several strategies (decarbonization, carbon sequestration, carbon recycling etc.,) and technological advancements are happening from time to time, the field is still at its infancy.[7] Electrochemical $CO_2$ reduction is an advanced approach to mitigate the $CO_2$ level wherein the $CO_2$ produced is efficiently converted to low-carbon fuels, chemicals etc., to be used as an industrial feedstock. $CO_2$ is a very stable molecule and its reduction to respective products are generally thermodynamically uphill reactions, accounting to high chemical and electrochemical stability of C=O bond. Thus, to enhance the kinetically slow reduction reaction, the need for ideal active electrocatalysts is significantly necessary.[7,61–63]
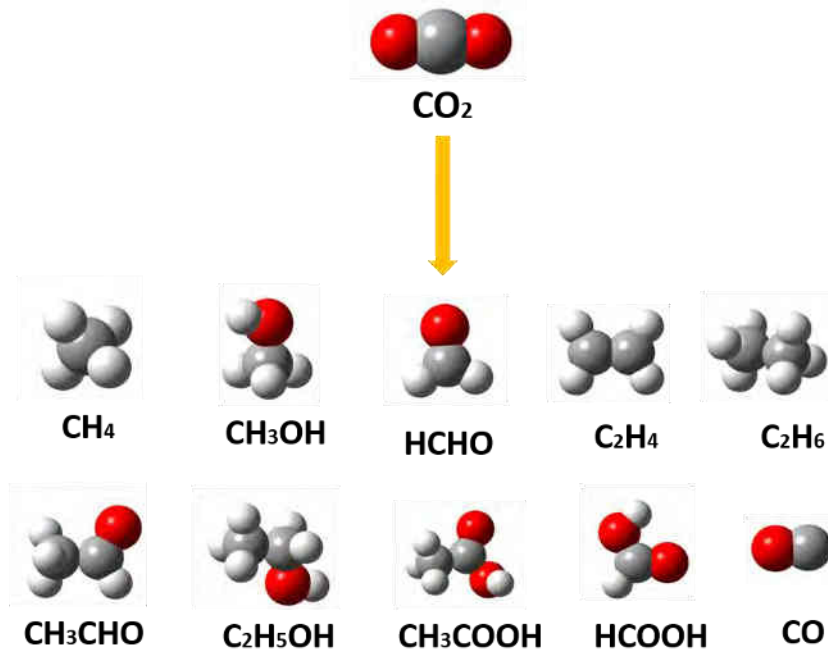
Figure 3. Schematic representation of electrochemical $CO_2$ reduction reaction and possible products as part of the reaction. Reproduced with permission from reference.[7] © 2023 The Authors. Advanced Materials Interfaces published by Wiley-VCH GmbH.

The task is to find an ideal electrocatalysts to minimize the overpotential for C=O, and drive the reaction ideally towards targeted products. Cathodic electrochemical reduction of $CO_2$ ($ERCO_2$) is given by the following general expression (2)

$$xCO_2 + nH^+ + ne^- \rightarrow product + yH_2O \ldots\ldots\ldots\ldots (2)$$
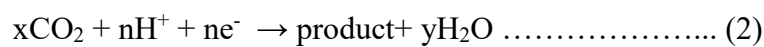
Electrochemical half reaction for $ERCO_2$ undergoes various electron pathways to deliver various products (Figure 3). The electrode potential of $ERCO_2$ (versus SHE) is shown in Table 1.[7]

| Electrochemical $CO_2$ reduction (possible half-reactions) | Electrode potentials (V vs SHE) at pH 7 |
|---|---|
| $CO_2$ (g) + e$^-$ → *COO$^-$ | −1.90 |
| $CO_2$ (g) + 2H$^+$ + 2e$^-$ → HCOOH (l) | −0.61 |
| $CO_2$ (g) + H$_2$O (l) + 2e$^-$ → HCOO$^-$ (aq) + OH$^-$ | −0.43 |
| $CO_2$ (g) + 2H$^+$ + 2e$^-$ → CO (g) + H$_2$O (l) | −0.53 |
| $CO_2$ (g) + H$_2$O (l) + 2e$^-$ → CO (g) + 2OH$^-$ | −0.52 |
| $CO_2$ (g) + 4H$^+$ + 2e$^-$ → HCHO (l) + H$_2$O (l) | −0.48 |
| $CO_2$ (g) + 3H$_2$O (l) + 4e$^-$ → HCHO (l) + 4OH$^-$ | −0.89 |
| $CO_2$ (g) + 6H$^+$ (l) + 6e$^-$ → CH$_3$OH (l) + H$_2$O (l) | −0.38 |
| $CO_2$ (g) + 5H$_2$O (l) + 6e$^-$ → CH$_3$OH (l) + 6OH$^-$ | −0.81 |
| $CO_2$ (g) + 8H$^+$ + 8e$^-$ → CH$_4$ (g) + 2H$_2$O (l) | −0.24 |
| $CO_2$ (g) + 6H$_2$O (l) + 8e$^-$ → CH$_4$ (g) + 8OH$^-$ | −0.25 |
| 2CO$_2$ (g) + 12H$^+$ + 12e$^-$ → C$_2$H$_4$ (g) + 4H$_2$O (l) | 0.06 |
| 2CO$_2$ (g) + 8H$_2$O (l) + 12e$^-$ → C$_2$H$_4$ (g) + 12OH$^-$ | −0.34 |
| 2CO$_2$ (g) + 12H$^+$ + 12e$^-$ → CH$_3$CH$_2$OH (l) + 3H$_2$O (l) | 0.08 |
| 2CO$_2$ (g) + 9H$_2$O (l) + 12e$^-$ → CH$_3$CH$_2$OH (l) + 12OH$^-$ (l) | −0.33 |

**Table 1.** Electrochemical potentials corresponding to various electrochemical $CO_2$ reduction reactions and resulting products. Adapted with permission from reference.[64] © 2017 The Authors. Published by WILEY-VCH Verlag GmbH & Co. KGaA, Weinheim.

## 1.2 3D-Printing technology

3D-Printing, also called additive manufacturing has received massive attention both from industries and academic circles owing to its rapid prototyping ability.[11,65–67] Advantages such as fabricating customised and complex printed structures with varied geometry, shape and size, low waste generation, scalability etc are the added advantages of this technique. Today, this technology has advanced to several domains mitigating and overcoming several issues faced by the conventional manufacturing technologies. The expansion of this technology to various disciplines has prompted the current study to employ 3D-printed electrocatalysts substrates as active catalysts/substrates for electrochemical[17,68,69] and sensing applications.[33]
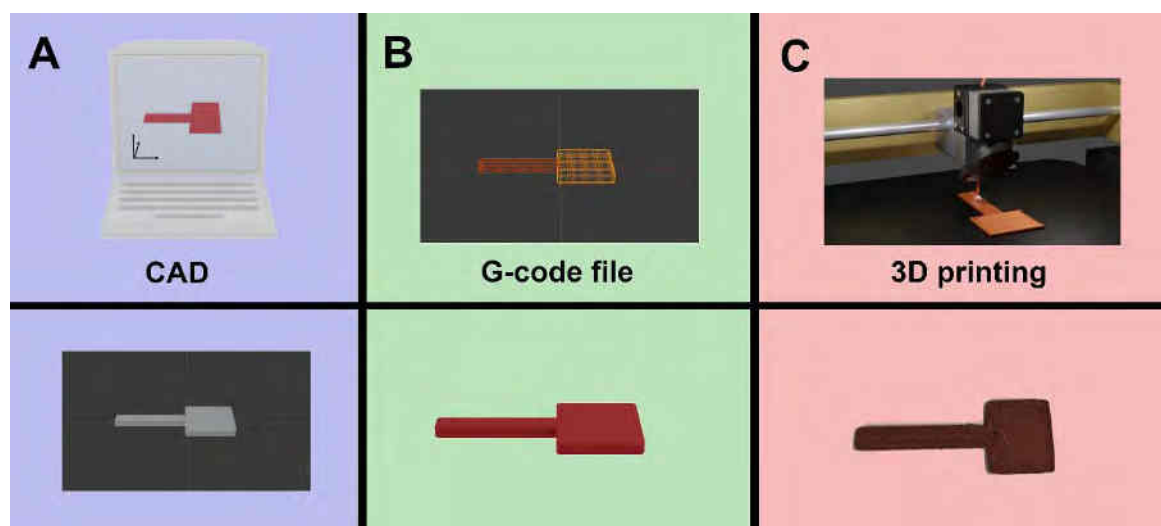


Figure 4. Schematic representation of electrode fabrication A) modeling B) G code file format configuration C) 3D-Printing of modeled structure. Reproduced with permission from reference.[11] © 2023 The Authors. Advanced Materials Technologies published by Wiley-VCH GmbH.

In short, material design based on the targeted applications is an added asset towards the fabrication of electrocatalysts and/or sensors for desired applications.[11] Modeling desired 3D

structures is the initial task conducted. This is usually executed using a using computer-aided design (CAD) 3D modeling software. Post modeling of the 3D structure (Figure 4A), it is converted to a standard format file called stereolithography file format (STL). This is followed by slicing of designed structure using another software, to procure G code file (Figure 4B). This file constitutes the key information of the modeled design and instructions for printing. Later, the G code is opened in the 3D printer and is set for final printing. During printing, active material components are oriented sequentially on top of each other, until the final modeled 3D structure is procured (Figure 4C).
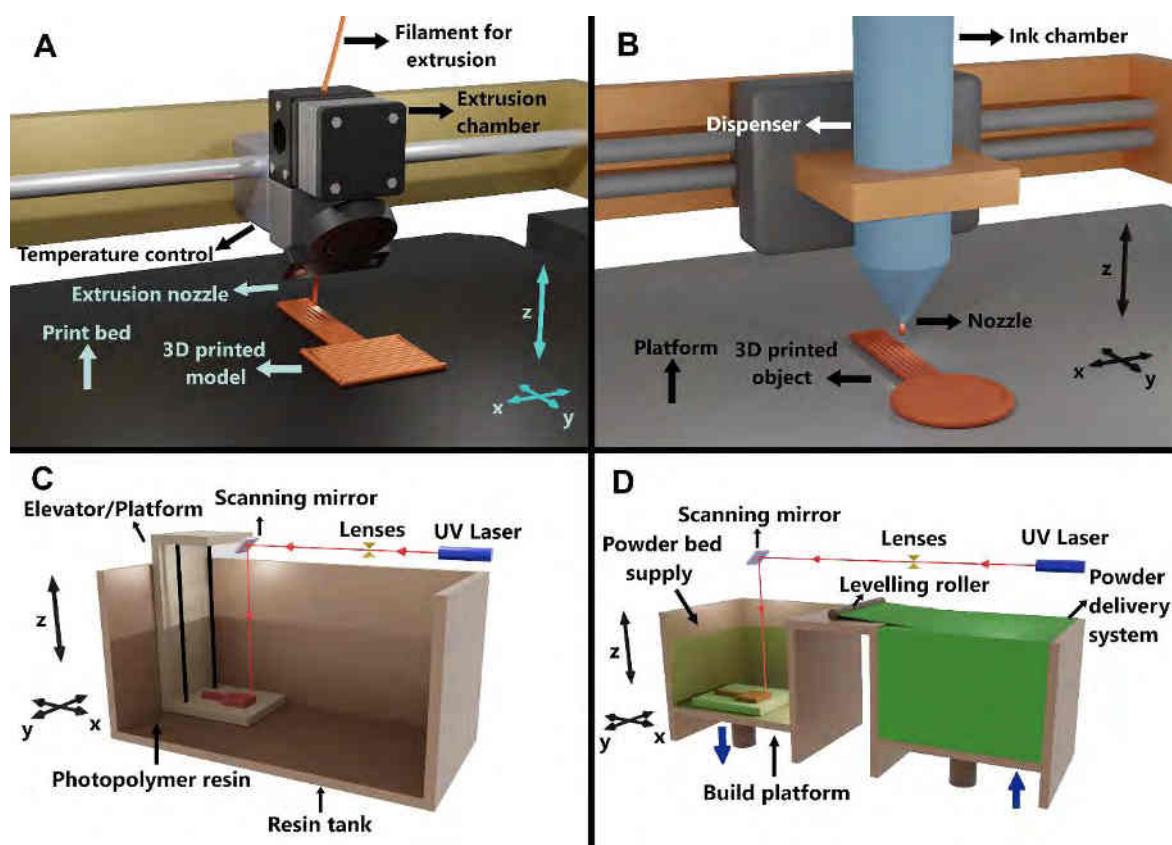


Figure 5. Schematic representations of various 3D-printing techniques: A) fused deposition modeling, B) direct ink writing, C) stereolithography, and D) selective laser sintering. Reproduced with permission from reference.[11] © 2023 The Authors. Advanced Materials Technologies published by Wiley-VCH GmbH.

The precursor materials, involve carbon/polymer, metal/polymer based filaments, composites, ceramics etc. The printing technology have advanced with time and some of the well-known techniques include extrusion based fused deposition modeling (FDM; Figure 5A) and direct ink writing (Figure 5B), stereolithography (Figure 5C) metal based selective laser sintering (Figure 5D), selective laser melting, electron beam melting, etc.

Out of the several 3D-printing techniques, extrusion based FDM or fused filament fabrication (FFF) is considered as one of the ideal approaches towards designing 3D-printed electrodes, catalyst, substrate, and sensing platforms. In this technique filaments are extruded in a layer-by-layer fashion until a final 3D-printed structure is obtained.[11,22,70,71] At laboratory scale, FDM Prusa 3D-printer is employed for fabricating 3D-printed electrodes (Figure 6A). Figure 6B depicts graphene/polylactic acid (PLA) (black magic) filaments and Figure 6C showcases the image of 3D-printed carbon electrodes (3D-CE) procured from black magic filament. Figure 6D represents the spool of metal/PLA filament which is copper (Cu)/PLA, and Figure 6E represents the image of the 3D-printed Cu electrodes.
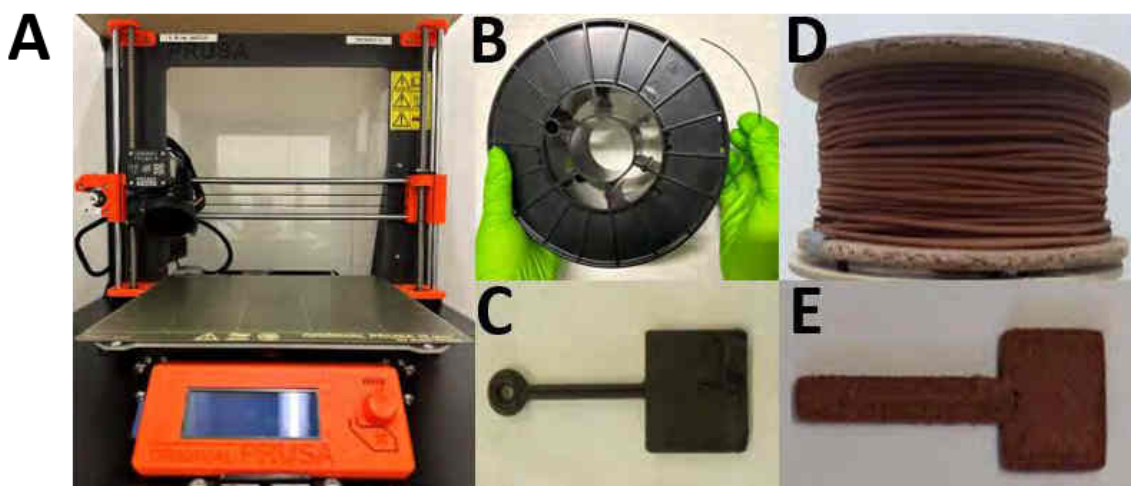


Figure 6. A) Prusa FDM 3D printer employed for printing B) Spool of commercial graphene/PLA filament C) 3D-printed carbon electrodes D) Spool of commercial copper/PLA filament E) 3D-printed copper electrodes.

PLA helps for ideal extrusion of filaments and provides structural integrity to the printed structure. However, the 3D-printed electrodes possess poor electrocatalytic properties accounting to the non-conductive PLA along with the carbon matrix. Hence, it calls for post-printing treatments such as activation techniques that can aid towards improving the surface properties by lowering the amount of PLA in the printed matrix and increasing the overall conductivity of the printed structure.[72,73] Employing solvent such as dimethylformamide (DMF) is one of the well-known techniques that are employed towards activation of carbon based electrodes. Meanwhile, sintering is the ideal technique employed towards removing of PLA from metal substrates.

### 1.2.1 3D-Printing technology towards electrocatalysis

Serval electrocatalytic application has been briefly introduced in the above sections of 1.1. It is well known that electrocatalysts play a vital role in enhancing the reaction to obtain the desired product. Several materials are being evaluated by researchers, periodically, to develop ideal, scalable, and cost-effective catalysts for various applications.[74,75] Surface modifications, material engineering, doping, integrating nanoparticles, etc., are employed to fabricate active electrode materials for desired applications, and evaluated systematically.[25]

Interestingly, with the increasing demand for designing electrocatalysts, there has been a rapid advancement in newer technologies in the past few years for devising catalysts and/or substrates such as the 3D-printing technique.[17,43,76,77] The widening potential of 3D-printing technology is one such aspect which can help towards the fabrication of 3D-printed structures towards various electrocatalytic applications owing to the advantages such as quick fabrication, easiness and flexibility in design of complex structures, waste minimization,

scope for mass customization etc. They are also interesting due to their ability to overcome the shortcomings faced using conventional methods such as high cost, intensive labor, and immense time consumption for the fabrication of active structures. Also recently, several studies have come up with employing 3D-printed electrocatalysts as active substrates towards energy conversion applications.[17,72,76,77] Specifically, this includes HER,[78,79] $CO_2$ reduction[7,80,81] and very recently towards ammonia synthesis.[11,82] Nanostructuring of both metal or carbon based electrodes surfaces can further enhance the catalytic properties of 3D-printed structures for various catalytic applications.[11] Geometry, porosity, size, post-printing treatments are also crucial parameters in devising active material substrates. Hence, enhancing the scope of this field could be vital, with technological advancements in the domain of 3D-printing improving the possibilities of this field towards fabrication of complete electrolysis cells or reactors for energy production.

## 1.2.2 3D-Printing technology towards electrochemical sensing applications

Interestingly, along with catalysis, today the advancements in 3D-printing technology can also aid towards the fabrication of non-enzymatic 3D-printed sensors for multiple applications, including the detection of sugar level in blood.[33] The diabetic condition results from a rise in the amount of sugar concentration in blood. The concentration range from 3.9–6.2 mM is considered to be normal. The level of blood sugar can be measured using several devices. However, the development of newer and efficient devices to detect the level of blood sugar can be highly advantageous. Scientists today are eyeing towards formulating sensors that are time-specific, quick, less expensive, and efficient in monitoring the sugar level. The concept of non-enzymatic sensors that can be used to design 3D-printed substrates via certain improvements, introduces a technique that is faster, reliable, and precise for sensing

applications.[33] In short, by employing ideal strategies such as surface modification of 3D-printed electrode using specific materials can aid in fabrication of an active 3D electrode substrate making this technology ideal for electrochemical sensing (such as sugars) and for several other applications as well.

# CHAPTER 2

# 2. State –of-the-Art

## 2.1. Hydrogen evolution reaction

HER is considered to be the most studied reaction in electrocatalysis, and fabricating ideal electrocatalysts to minimize the HER overpotential is in huge demand currently. In other words, lower the overpotential better the HER activity, wherein electrocatalysts play a vital role towards lowering the overpotential and increase efficiency for HER.[45,83,84] Conventionally, Pt based electrocatalysts are shown to be superior towards HER,[85,86] delivering ideal hydrogen binding energy and Gibbs free energy for atomic hydrogen adsorption, low overpotential, low Tafel slope, and high exchange current density for HER. Further, electrocatalyst materials such as Ir[87,88] and Ru-based[89,90] materials have also been reported for HER. However, high-expense and limited abundance has called for newer cost-effective, and durable catalyst materials, to produce hydrogen for large scale applications.[91,92] Interestingly, non-noble metals (transition metals) were later found to take up the momentum as active HER catalysts, as they are low cost, abundant, varied combinations, comparable electronic structure, and showcased promising and stable HER activity under large current densities.[92–94] This sets of catalysts includes self-supported,[95,96] doped,[97,98] single atom catalysts[99,100] etc. 2D materials catalysts are also actively employed for HER applications.[29,101,102] Despite all these advancements in this field, massive research is still being undertaken relentlessly toward the fabrication of clean, and efficient electrocatalysts via various technologies that can aid towards minimizing the overpotential, and enhancing hydrogen production.

Thus, in this work, studies are carried out on 2D material engineered electrocatalysts such as graphene,[25] MXenes,[49] transition metal dichalcogenides (TMDs), and a multiple set of MAX phases based materials.[18]
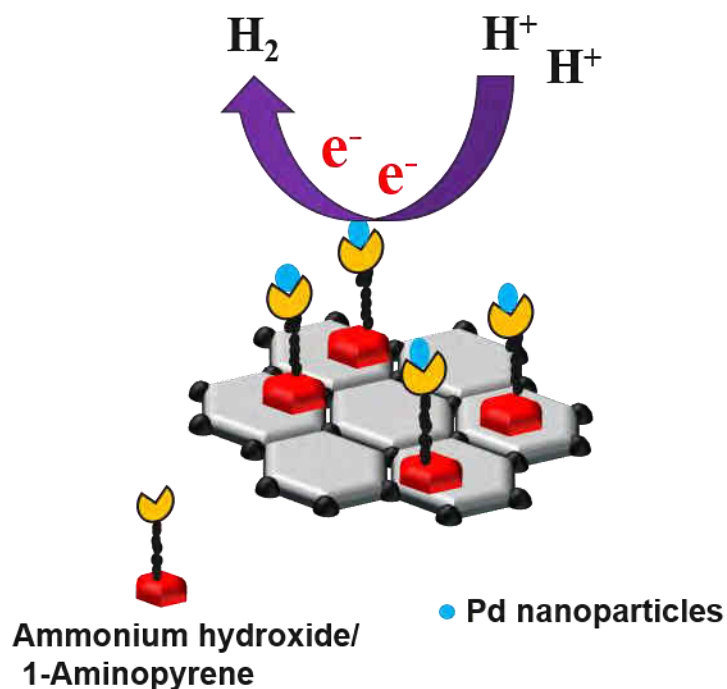
Figure 7. Schematic representation of hydrogen production via nanoparticle anchored N-doped graphene-based catalyst. Reproduced with permission from reference.[25] © 2022 Wiley-VCH GmbH.

For instance, variation in the synthesis strategies in electrocatalysts fabrication, with palladium (Pd) nanoparticle nucleation and varied nitrogen (N) dopants over reduced graphene oxide (RGO) is studied towards HER, and such studies are expected to aid towards designing application specific catalysts (Figure 7).[25] Newer approaches of integrating active materials with the advanced technologies such as 3D-printing for $H_2$ production is studied. Such integrations can be vital and interesting for the fabrication of cost-effective, on demand electrocatalysts for catalytic applications. For instance, surface modification via dip coating of active 2D MXene ($Ti_3C_2$), and TMDs such as molybdenum sulfide ($MoS_2$), tungsten sulfide ($WS_2$), molybdenum selenide ($MoSe_2$), and tungsten selenide ($WSe_2$), is carried out over 3D-printed carbon substrates for catalysis applications.[49] Also, works focusing on their parent

MAX phase remain critically low especially for electrocatalysis applications such as HER. Hence, multiple MAX phases constituting single ($Ti_2AlC$, $Ta_2AlC$, $Ti_2SnC$, $Ti_3SiC_2$, $V_2AlC$, $Cr_2AlC$ ) and dual transition metal ($Mo_2TiAlC_2$) phases were studied for HER, in order to understand the potential of MAX family for $H_2$ production.[18]

## 2.2 Nitrate reduction to ammonia

Electrochemical NRA can be considered as an interesting approach that inhibits several limitations accounting to conventional techniques such as Haber Bosch, and nitrogen reduction to ammonia.[103–106] The NRA also helps in strategically eradicating excess nitrate ions from the water bodies, and also a vital contributor to the energy sector by enhancing ammonia production.

Among transition metals, Cu is reported to be ideal for NRA applications,[107–109] and immense studies are reported in recent times using this material. Some of them also claim that copper oxide is very effective for the NRA, when compared to its metallic state. Also, in another recent study, electrolyte engineering of titanium electrodes for NRA was conducted, wherein the catalysts delivered 82% FE at −1 V vs reversible hydrogen electrode (RHE). Also the catalysts gave a partial current density to ammonia at around −22 mA cm$^{-2}$.[110] NRA using iron (Fe) based single atom catalysts was recently reported by a group of researchers, wherein the catalyst delivered ~75% FE at −0.66 V vs RHE and yield rate of ~20,000 µg h$^{-1}$ mgcat.$^{-1}$ at −0.85 V vs RHE.[111] Similarly, several other catalysts are fabricated and studied periodically to achieve catalysts with high FE, enhanced selectivity, sensitivity, and high surface area for ammonia production.

Interestingly, although there are reports on 2D materials and composites employed for NRA application,[112,113] still the studies are at a very early stage and require more optimizations for

fabrication of ideal catalysts. For instance, reports on metal organic frameworks (MOF) based materials for NRA are available in literature.[114–116] Also, most of the fabricated MOFs that serve as electrocatalysts for NRA result from anchoring, functionalizing, or doping of active components. Interestingly, in the current thesis, influence of thermal activation on Fe MOFs for ammonia synthesis is evaluated. Such studies could be an interesting for researchers to further understand the potential scope of the activating MOF based materials for NRA. The results and observation of such material enhancement are reported in the thesis, in chapter 5, section 5.1.3
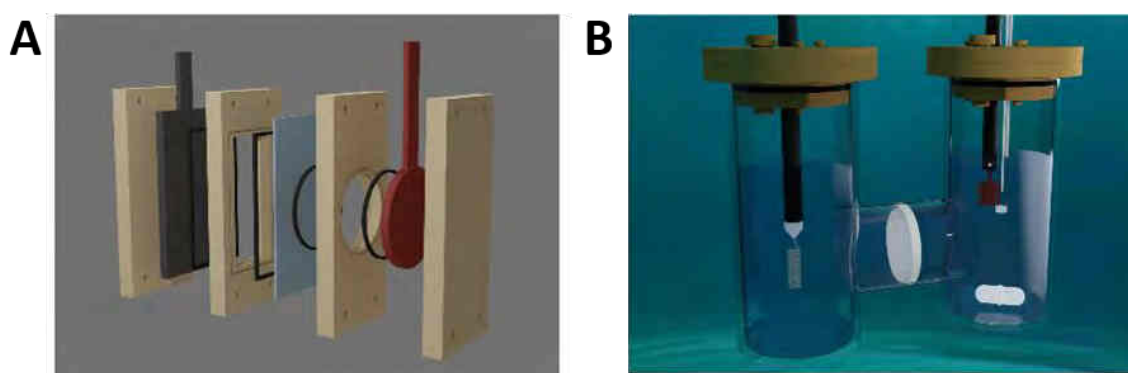


Figure 8. Integrated 3D-printed electrocatalysts and devices for ammonia synthesis A) electrolyzer B) H cell. Reproduced with permission from reference. [11] © 2023 The Authors. Advanced Materials Technologies published by Wiley-VCH GmbH.

Further, engineering electrocatalysts for NRA via employing technological advancements such as 3D-printing has started gaining attention. For instance, employing 3D printed carbon[117] and metal[82] based substrates for ammonia were recently reported. The key advantage of this technology accounts to the freedom of users in designing structures accounting to the experimental conditions. Further geometry, size, activation techniques, post-printing treatments such as nanostructuring of electrodes can also influence the electrocatalyst properties. Such customization can enhance the fabrication of efficient

electrocatalysts for ammonia production. The current thesis reports, the potential possibility of using 3D-printed Cu electrodes for NRA,[11] as a proof of concept which shall be discussed in the following sections chapter 5, section 5.3.1. Such reports can create a breakthrough in devising newer active materials for ammonia synthesis and can be integrated to various devices as shown in Figure 8.

## 2.3 CO₂ reduction and mitigation

Technologies associated with $CO_2$ reduction are coming up massively in recent times, as its increased level in the atmosphere can significantly affect the ecological balance.[60,118,119] Among various mitigation strategies, ERCO₂ continues to get attention owing to its mild operational conditions, and controllable reaction conditions, along with it being an economical and ecologically feasible technique together with renewable energy sources.[7] ERCO₂ related studies have been introduced since several decades. Several catalysts such as Cu,[120] silver (Ag)[118] and gold (Au), carbon-supported catalysts,[121] hybrid catalysts,[122] etc., have been investigated in recent time for this application. Devising ideal electrocatalysts is important as the catalytic reaction can lead to formation of various products accounting to its multi-proton multi-electron reaction mechanism (Figure 3). Interestingly, the 3D-printing community has become inquisitive about employing 3D-printed structures for CO₂ mitigation applications. In a report by Eva et al.,[80] Cu electroplated 3D-printed electrodes from PLA-carbon nanotube were employed as electrocatalyst for CO₂RR. Similarly, metal-based SLM 3D-printing was employed in another study, followed by an electrochemical dealloying approach resulting in 3D hierarchically porous CuAg bimetallic catalyst.[123] The catalyst was later employed for syngas production. Variations in the performance of catalysts subjected to variation in structure of electrocatalyst was evaluated and compared with other noble and non-

noble electrocatalyst. It was observed that 3D hierarchically porous CuAg catalyst exhibited an interesting mix of durability and syngas gas production rate, thus making 3D-printing technology interesting for $CO_2$ mitigation reaction.

## 2.4 Electrochemical sensing

3D-Printing technology towards devising electrocatalyst for energy conversion application has been well discussed in the above section. Interestingly, the possibilities of 3D-printing technology can also be employed and extended towards decentralize fabrication of non-enzymatic metal coated 3D-CE for sugar sensing.[33] Modifying the electrode surface can be crucial towards improving the property of the surface. Although, fabrication of electrocatalyst has opened up several possibilities, such as via atomic layer deposition (ALD) technique,[124] yet they face certain setbacks. For instance, techniques such as ALD require costly setup, skilled experts, and limited precursors.

Interestingly, electrodeposition of 3D-CE can be considered as a facile approach of devising active material substrates instead of relying on high-end high-cost equipment.[33] This could be considered as a excellence of this technology for developing cheaper conducting structures and employing a economical approach to modify 3D-CE substrate for non-enzymatic sugar (glucose and sucrose) sensing applications. Hence, a much simpler but effective metal electroplating technique could be employed over a 3D-CE, that would enhance the surface properties, conductivity of printed substrates, and eventually be active for desired applications.
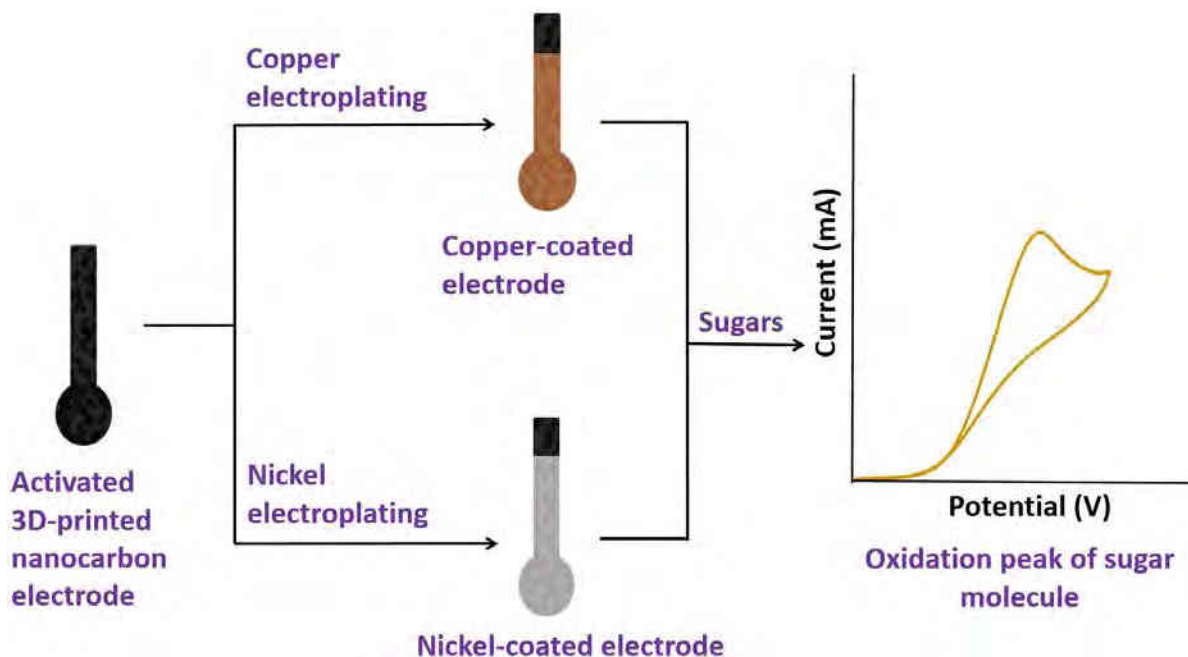
Figure 9. Schematic representation of metal plating 3D-printed carbon electrode for electrochemical sensing of sugars. Reproduced with permission from reference.[33] © 2020 The Author(s). Published by Elsevier B.V.

Several studies have been previously reported on employing nanoparticles, oxide or hydroxide of active material, serving as an active non-enzymatic catalytic site.[125,126] Also, employing metals such as Cu and nickel (Ni) has aided towards the fabrication of low cost electrocatalysts, rather than employing costly metals such as Pt, Au, Ag. The current study reported in thesis focuses on the metal plating of Cu and Ni over a 3D-CE to procure a metal plated 3D-printed non-enzymatic nanocarbon electrode substrate followed by employing them for sugar sensing applications (Figure 9).[33]

# Chapter 3

# 3. Aim of thesis

## 3.1 Objective

This doctoral thesis will be focused on systematically evaluating various 2D based materials, assessing their respective advantages and disadvantages in conjunction with potential applications such as hydrogen production and ammonia synthesis. This involves understanding the influence of material fabrication approaches, such as synthesis strategies, and material activation techniques in designing electrocatalysts for specific applications.

Additionally, we aim to optimize 3D-printing techniques for the purpose of electrochemical energy technologies, sensing, and for other potential applications. This includes discussion on the importance of nanostructuring of electrodes, the role of activation techniques/post-printing treatments in improving electrode surfaces for sensing/catalytic applications, and some potential scope of this technology for prospective future applications.

## 3.2 Hypothesis

To achieve the above objectives, the following strategies will be employed. Designing electrocatalysts via a suitable synthesis strategy and investigating the influence of activation-based techniques for enhancing material properties are expected to be vital for various electrocatalytic applications. Further, by integrating 2D and/or related materials with 3D-printing technology, and using the potential of 3D-printing technology alone, we hypothesize that the design of novel electrocatalysts will lead to significant advancements in mitigating electrocatalytic challenges in health and energy-related applications.

## 3.3 Organization/Structure of thesis

Overall, the thesis is divided into nine chapters, where chapter 1 introduces multiple topics covered in the thesis. Chapter 2 discusses the state-of-the-art related to electrocatalyst fabrication for electrocatalysis and sensing applications. Chapter 3 describes the aim of the thesis and Chapter 4 deals with the information related to electrode materials and experimental details in brief. Chapter 5 includes the results and discussion section associated with investigations carried out, and also a summary is provided in the following paragraph. Chapter 6, 7, and 8 includes conclusions, references, and a list of conferences attended/achievements of the author respectively. In Chapter 9 (appendix-A), a study on the critical evaluation of the origin of activity in layered $FePSe_3$ materials for $H_2$ production is done.

The work presented in the thesis focuses on designing electrocatalysts for energy conversion applications and patterning/modifying 3D-printed electrode surfaces for both energy conversion and electrochemical sensing applications. They are explained in detail in Chapter 5, Results and Discussions section. Chapter 5.1 discusses the importance of synthesis strategies and activation-based techniques for fabricating electrocatalysts for enhanced electrocatalytic application. Precisely, section A (5.1) deals with electrocatalysts fabrication for hydrogen production (5.1.1 & 5.1.2) and ammonia synthesis (5.1.3). Extending the electrocatalysts fabrication to newer technologies such as 3D-printing technology, section 5.2 discusses employing 3D-CE for $H_2$ production (5.2.1) and electrochemical sugar sensing (5.2.2) via surface modification of electrode surface, and section 5.3 covers the discussion on future prospects of employing 3D-printing technology for both energy (5.3.1 & 5.3.2) and emergency healthcare application (5.3.3). A brief outline of all sections and subsections of chapter 5 is given below:

**Section-A**

**5.1. Designing electrocatalysts towards hydrogen and ammonia production**

In this section, we discuss strategies of engineering electrocatalysts via various techniques for hydrogen production and ammonia synthesis. Initially in section 5.1.1, we evaluate the potential scope of synthesis techniques in fabricating two different Pd anchored N doped graphene-based materials, while 5.1.2 deals with the understanding of the potential of various layered MAX phases as electrocatalysts for HER applications. Electrocatalysts are also vital for ammonia synthesis, and the influence of temperature on PCN-250-Fe$_3$ MOF-based electrocatalysts for ammonia synthesis applications is evaluated in section 5.1.3. The following sections are categorized as follows:

5.1.1.  Grafting of Pd on N-doped graphene for HER

5.1.2.  Electrocatalytic activity of layered MAX phases for HER

5.1.3.  Fe-MOF electrocatalyst for nitrate to ammonia conversion

**Section-B**

**5.2 Employing 3D-printing technology towards novel electrocatalysts fabrication for energy and healthcare applications**

In this section, discussions on integrating 2D materials and/or related materials with 3D-printing technology via surface modification of 3D-CE will be carried out to understand the scope of this technology for energy and sensor-based applications. In section 5.2.1, surface modification of 3D-CE using 2D materials was carried out, and eventually studied for HER applications. Meanwhile, 5.2.2 put forth observations of surface modification of 3D-CE using metal nanoparticles for sugar sensing applications. The following sections are categorized as follows:

5.2.1.    2D materials patterned 3D-printed electrodes for HER

5.2.2.    Metal plated 3D-printed carbon electrodes for sugar sensing applications.

**Section-C**

**5.3. Future advancement of utilizing 3D-printing technology for energy and emergency healthcare application (Perspective reports)**

Beyond surface modification of 3D-printed structures (Section 5.2), there also are several other potential possibilities of using 3D-printing technology for diverse applications, especially accounting for its merits such as tunable geometry, porosity, size, customizations etc. In this section 5.3, the potential scope of 3D-printing technology towards diverse applications such as ammonia synthesis (5.3.1), $CO_2$ mitigation (5.3.2), and healthcare/emergency applications such as COVID-19 pandemic (5.3.3) are carried out. The following sections aim to motivate the researchers to understand the scope of utilizing this technology for future energy and healthcare applications. The following sections are categorized as follows:

5.3.1.    Advancements in 3D-printing towards ammonia synthesis

5.3.2.    3D-printing technology towards $CO_2$ reduction and capture

5.3.3.    3D-printing technology towards emergency healthcare application

# CHAPTER 4

## Chapter 4: Electrode materials and experimental details

# 4. Electrode materials and experimental details

The following section aim to provide a very brief overview of the materials employed in the current thesis along with catalyst fabrication approaches. The detailed reports of synthesis, analysis and experimentation conditions can be procured in chapter 5, section 5.1, 5.2, 5.3 and Appendix A.

## 4.1 Novel electrocatalysts material design

### 4.1.1 Graphene derivatives

Graphene is a sheet of single layer of carbon atoms that are tightly bound in a hexagonal honeycomb lattice. There has been a rapid increase in the employment of these types of materials,[127–129] since its discovery. Further, it is an allotrope of carbon, with $sp^2$ hybridized atoms. Graphene and its various derivatives is widely studied for electrochemical applications. Among them, RGO, is well known for catalysis applications owing to its superior conductivity, high surface area,[130,131] as anchoring agents, native defect sites, high adsorption capacity, etc. make them an interesting candidate for catalysis applications.[25] Techniques such as doping involves introduction of impurity/foreign atoms which can modify the properties of the base catalyst.[24,132,133] Among the dopants N, sulfur, phosphorous, boron are known be active participants for heteroatom doping, where addition can enhance the electrocatalytic effect, and in some cases retard the activity. Interestingly, N doping is known to increase the free charge carrier density of carbon based material and enhance their conductivity.[134,135] They also serve as anchoring sites for metal nanoparticles. In short, addition of external atoms to the carbon lattice is always correlated to the application that they would be employed for. In the current thesis, as detailed in section 5.1.1, two

different synthesis strategies (covalent and non-covalent based) will be employed for the fabrication of Pd anchored N-doped graphene electrocatalysts for hydrogen production.

### 4.1.2 MAX phases and MXenes

MAX phases are ternary transition metal carbides and nitrides with a formula ($M_{n+1}AX_n$), where M stands for an early transition metal, A is the element from IIIA, and IVA group, X is carbon (C) or N and n = 1, 2, or 3.[136,137] This class of materials show excellent properties owing to its good thermal and electrical conductivity, damage tolerance, high strength, high Young's modulus, low hardness, ready machinability, oxidation resistance etc. Interestingly, due to their layered structure and chemical bonding they show bifunctional properties of both metals and ceramics.[138] Stronger chemical bonding in MAX phase, calls for stronger etching conditions (to etch A layer) to procure an interesting set of 2D material called MXene, which is currently a very interesting field of study, especially for energy related applications. Although a number of studies on electrocatalytic properties of MXenes have been conducted, very few works are known that focus on using this set of material for catalytic applications. In the current study, electrocatalytic activity of a set of MAX is evaluated towards hydrogen production[18] as detailed in section 5.1.2.

Moving to another fascinating class of materials, MXene are transition metal carbides, nitrides, carbonitrides that have today expanded to a large family, where they are produced by etching of A element atom from their respective MAX ($M_{n+1}AX_n$) precursor material.[29,139,140] They possess a general formula of $M_{n+1}X_nT_x$, where M = early transition metal, X = C/N, and $T_x$ = −OH, −F, and −O−, and n = 1-4. Their family is continuing to expand and developing newer materials for various applications. Post graphene, this is one among the most discussed and anticipated class of materials by the researchers, owing to its

36

unique properties such as tunable structure, diverse chemical, electrical, optical and mechanical properties. MXenes have made significant contributions in the field of electrochemistry on account of its tunable surface and surface chemistry, making it promising both as an electrode material for energy storage and as catalysis applications. In the current study of the thesis, $Ti_3C_2T_x$ MXene will be used to modify the surfaces of 3D-CE and eventually the performance of the 3D-printed MXene based catalyst will be evaluated for HER (Section 5.2.1).

### 4.1.3 Transition metal dichalcogenides

Intriguing structural and electronic properties has made metal chalcogenides interesting for electrocatalysis applications.[141,142] Being a large family of materials, metal chalcogenides can be further classified into layered TMDs[49] and non-layered metal chalcogenides (NMCs) in their 2D form. This class of 2D TMD based electrocatalysts are found to be highly efficient towards developing cheap and high-performing electrode material for catalysis applications. Typically, they are semiconductors of $MX_2$ type, where M is a transition metal atom and X is a chalcogen atom. In the current study of the thesis, sulfides and selenides of Mo and W will be used to modify the surfaces of 3D-CE. The resultant electrodes will be eventually evaluated for HER (Section 5.2.1).

### 4.1.4 MOFs

MOFs are interesting class of crystalline materials with ultrahigh porosity, enormous internal surface areas, employed for wide range of applications. [143–145] In the current study, PCN-250-$Fe_3$ MOF was used as an active catalyst material that are known to be fabricated from precursor $Fe_3$-$\mu_3$-oxo metal cluster and tetratopic azobenzene-based ABTC linkers (ABTC =

3,3′,5,5′-azobenzenetetracarboxylate). [143,146,147] In the current study of the thesis, the influence of temperature on Fe based MOF materials for nitrate to ammonia was studied (Section 5.1.3).

### 4.1.5 Trichalcogenphosphites

Transition metal trichalcogenphosphites ($MPX_3$; M= transition metal, P= phosphor, and X= chalcogenide) are another interesting class of 2D materials gaining attention in the recent times towards electrocatalytic and photocatalytic properties. $FePSe_3$ is one such class of material belong to this family.[148] This layered crystal is held by van der Waals (vdW) interaction, and is a semiconductor with an optical band gap of 1.3 eV (bulk phase), while its monolayer band gap is still being investigated. The origin of activity of $FePSe_3$ layered materials for HER was evaluated and is detailed in chapter 9, appendix A.

## 4.2 Experimental Section

### 4.2.1 Preparation of Pd anchored N -doped electrocatalysts

Synthesis of Pd anchored covalently modified N-doped graphene (Pd@Amm.Hyd-(N)@RGO) and Pd anchored non-covalently modified N-doped graphene (Pd@Pyrene-(N)@RGO) catalyst fabrication for are detailed in reference[25] of our publication which is part of the thesis.

### 4.2.2 Fabrication of 3D-printed electrocatalysts

Autodesk Fusion 360 software was used to design the electrodes, and later the procured file is fed into the Prusa i3 MK3s printer. FFM/FDM based extrusion based 3D-printing of commercial graphene/PLA filament is carried out for the studies discussed in this thesis. The carbon based filaments are extruded down the nozzle at a temperature of 220 °C. The bed temperature during the process is around 60 °C. Post-printing techniques are employed to enhance the conductivity of the carbon substrates. The 3D-CE are then activated by immersing in DMF for a fixed interval of time. This is followed by rinsing the carbon electrodes with ethanol and water until the insulating PLA is removed from the surface. The 3D-CE are then dried in an oven at 65 °C for 120 min and further employed for respective studies.

### 4.2.3 Dip-coating 3D-CE

Patterning techniques such as spray, spin, dip coating helps in fabricating low cost, scalable, techniques to fabricate active material electrocatalysts. Owing to the lower complexity of the equipment required for modifying/fabricating electrodes, and less complications involved in slurry formulation, techniques such as dip coating becomes interesting for fabricating newer electrocatalysts. Active material of MXene ($Ti_3C_2T_x$) and TMDs ($MoS_2$, $MoSe_2$, $WS_2$, and

$WSe_2$) are dip coated over the 3D-printed electrode surfaces to modify the surface of the 3D-CE. [49] Slurries of sample in in DMF are prepared and sonicated for 0.5 h. Later the activated 3D-CE is dip coated using the prepared slurries for 3 h and allowed to dry overnight. Further, they are subjected to morphological and electrochemical studies.

### 4.2.4 Electroplating 3D-CE

Electroplating, electrochemical deposition or metal plating is a very well-known technique employed towards metal coating of active material over a solid substrate. Reduction of cations from the metal containing solution, on application of electric current results in a fine uniform coating of active material over the substrate. The protocol associated with the metal plating of activated 3D-CE using Cu and Ni electrolyte solution is detailed in reference,[33] of our publication which is part of the thesis.

# CHAPTER 5

## Chapter 5: Results and Discussions

**Section-A**

**Section-B**

**Section-C**

## 5.1. Designing electrocatalysts towards hydrogen and ammonia production

HER is vital for the future of renewable energy. However, finding newer electrocatalysts is important to minimize the overpotential required for efficient performance and hence calls for newer strategies of electrocatalyst fabrication to favor the reaction effectively with maximum efficiency. Evaluating the HER performance of fabricated electrocatalysts via various strategies is the central idea of one part of the following section. For instance, understanding the importance of synthesis strategy in fabricating Pd anchored N-doped graphene electrocatalysts for HER is detailed in 5.1.1. Meanwhile, section 5.1.2 covers the interesting behavior of single and double transition metal MAX carbide for HER applications. Thus, studies discussed in sections 5.1.1 and 5.1.2 revolve around evaluating the fabricated electrocatalyst for $H_2$ production. Further, as ammonia synthesis is another important electrocatalytic application, section 5.1.3 discusses strategies for enhancing the catalyst property via activating Fe-MOF electrocatalysts for ammonia synthesis. The discussion carried out in the section are published and the details are as follows:

### 5.1.1. Grafting of Pd on N-doped graphene for HER

<u>Akshay Kumar K. Padinjareveetil</u>, O. Alduhaish, S. F. Adil, Martin Pumera*, *Grafting of Pd on Covalently and Noncovalently Modified N-Doped Graphene for Electrocatalysis*, **Adv. Mater. Interfaces**, 2022, 2102317, doi.org/10.1002/admi.202102317, (IF=6.38).

### 5.1.2. Electrocatalytic activity of layered MAX phases for HER

<u>Akshay Kumar K. Padinjareveetil</u>, O. Alduhaish, Martin Pumera*, *Electrocatalytic*

*activity of layered MAX phases for the hydrogen evolution reaction,* **Electrochem. Commun**. 2021, 125, 106977, https://doi.org/10.1016/j.elecom.2021.106977, (IF=5.44).

### 5.1.3 Fe-MOF electrocatalyst for nitrate to ammonia conversion

<u>Akshay Kumar K. Padinjareveetil</u>, Juan V. Perales-Rondon, Dagmar Zaoralová, Michal Otyepka, Osamah Alduhaish, and Martin Pumera* *Fe-MOF Catalytic Nanoarchitectonic toward Electrochemical Ammonia Production*, **ACS Appl. Mater. Interfaces**, 2023, 15, 40, 47294–47306, https://doi.org/10.1021/acsami.3c12822, (IF: 9.5).

**5.1.1: Grafting of Pd on N-doped graphene for HER**

**Motivation**

Designing and fabrication of application-specific electrocatalysts are crucial for electrocatalysis, to minimize the overpotential for $H_2$ production. Interestingly, synthesis strategies can also play a vital role in designing efficient electrocatalysts. Thus, in the current study two different synthesis strategies are employed for the fabrication of electrocatalysts and evaluated for $H_2$ production.

**Objective**

Electrocatalysts were designed by anchoring Pd nanoparticles on the surface of N-doped RGO materials synthesized via two different approaches. Two different material fabrication technique was employed, wherein covalent and non-covalent attachment of N source to graphene is conducted, followed by nucleation of Pd nanoparticles. Morphological and physicochemical characteristic studies will be carried out and evaluated. Further, electrocatalytic activity of these fabricated catalysts toward HER will be evaluated using LSV.

**Outcome**

Pd anchored N covalently doped catalyst gave a better HER activity over the Pd anchored non-covalently N doped graphene electrocatalysts, thereby showcasing importance of synthesis techniques towards electrocatalyst fabrication for HER applications.

## Contribution

Investigation, methodology, conceptualization, formal analysis, data curation, characterizations, experimentation, validation, discussions, funding acquisition, writing (original draft, review and editing).

## Article

The article was published and the details of the article are as follows:

Akshay Kumar K. Padinjareveetil, O. Alduhaish, S. F. Adil, Martin Pumera*, *Grafting of Pd on Covalently and Noncovalently Modified N-Doped Graphene for Electrocatalysis*, **Adv. Mater. Interfaces**, 2022, 2102317, doi.org/10.1002/admi.202102317.

# Grafting of Pd on Covalently and Noncovalently Modified N-Doped Graphene for Electrocatalysis

*Kandambath Padinjareveetil Akshay Kumar, Osamah Alduhaish, Syed Farooq Adil, and Martin Pumera\**

Hydrogen evolution reaction (HER) is considered to be a fundamental solution for procuring clean energy. Palladium is one of the most catalytically active metals toward HER. Here, an electrocatalyst is designed where palladium nanoparticles (Pd NPs) are immobilized on the surface of nitrogen-doped reduced graphene oxide. A comparative study of two different nitrogen doping strategies is employed wherein covalent incorporation of nitrogen (N) source and noncovalent attachment of 1-aminopyrene to graphene lattice is carried out. The morphological and physicochemical characteristic studies confirmed that the doping is successful over the carbon lattice, followed by nucleation of Pd NPs over N sites. Electrocatalytic activity of these two different catalysts toward HER is examined using the linear sweep voltammetry technique. It is found that Pd anchored covalently N modified carbon outperforms the 1-aminopyrene based catalyst. These findings will have a profound impact upon the designing of application specific electrocatalysts.

## 1. Introduction

The urgency pertaining to control the rapid depletion of finite fossil fuels, and scarcity of energy resources calls for a quick and feasible solution with a long-term and sustained effect.[1–3] These intensifying sustainability issues are being periodically monitored and tackled to find possible solutions seeking

K. P. A. Kumar, M. Pumera
Future Energy and Innovation Laboratory
Central European Institute of Technology
Brno University of Technology
Purkyňova 123, Brno 61200, Czech Republic
E-mail: martin.pumera@ceitec.vutbr.cz

O. Alduhaish, S. F. Adil, M. Pumera
Chemistry Department P.O. Box 2455
College of Science King Saud University
Riyadh 11451, Saudi Arabia

M. Pumera
Energy Research Institute@NTU (ERI@N)
Research Techno Plaza
X-Frontier Block
Level 5
50 Nanyang Drive, Singapore 637553, Singapore

M. Pumera
Department of Medical Research
China Medical University Hospital
China Medical University
No. 91 Hsueh-Shih Road, Taichung 40402, Taiwan

clean, abundant, renewable, eco-friendly, and efficient strategies for energy related applications.[4–7] Among others, hydrogen ($H_2$) offers a significant solution to this global energy crisis and is presumed to be a potential successor of the conventional fossil fuels, in the future.[8,9] Though a technique centuries old, electrolysis of water, with its effective potential of combating the energy crisis is sought to be the most convenient source of clean energy carriers.[10,11] The prime significance of hydrogen energy production is its capacity to deliver high energy density and zero carbon emission.[12,13] Electrochemical water splitting ($2H_2O(l) \rightarrow 2H_2(g) + O_2(g)$) proceeds via two half-cell reactions where reduction of $H^+$ ions occurs at cathode (hydrogen evolution reaction, HER) and oxidation of water at the anode (oxygen evolution reaction, OER).[14–16] However, efficient splitting in aqueous media can get slightly retarded due to certain factors, and will require an additional potential to drive the reaction. This minimum thermodynamic potential to produce $H_2$ is called overpotential.[17,18] Thus, designing a clean, efficient, and cost-effective electrocatalyst that can help in lowering the overpotential of the system, and thereby result in increased hydrogen production become vital.

Conventionally, platinum (Pt) based electrocatalyst has been the most widely preferred catalyst due to its low overpotential and high energy density for HER.[19,20] However, its low abundance calls for an alternate solution which is inexpensive, durable, and efficient to mitigate the drawbacks associated with the former. Palladium (Pd), a member of the Pt family, is considered to be cheaper when compared to Pt. Also, its high affinity for hydrogen makes it an ideal catalyst for HER.[21–23] Several 2D materials have been identified as efficient conductive support material catalysts for water splitting.[13,24–28,29] Graphene and its derivatives are known to be most widely used for energy conversion applications.[30–33] Out of it, reduced graphene oxide (RGO) that exhibits properties similar to that of the graphene is well known for catalysis[34,35] owing to its high surface area. Furthermore, superior conductivity, high adsorption capacity, native defect sites, and the ability to act as ideal carbon support to metallic nanoparticles (NPs) or organic molecules are added advantages of using RGO.[36,37] Several approaches have been developed to fully exploit the catalytic activity of hybrid materials via incorporating metal NPs over carbon supports.[36,38–40]

**ADVANCED
SCIENCE NEWS**
www.advancedsciencenews.com

**ADVANCED
MATERIALS
INTERFACES**
www.advmatinterfaces.de

A systematic solution is sought by introducing the bridging ligands or heteroatoms that can integrate well with carbon support and hold the NPs. Known as doping,[41–44] this process involves the deliberate addition of foreign atoms which modifies the surface properties, alters the electronic properties and the elemental composition of the host matrix. Atoms of nitrogen (N), phosphorus (P), boron (B), and sulfur (S) are active participants for heteroatom doping.[45–47] Of them, N as a dopant is preferred to enhance the free charge carrier density of carbon material and increase its conductivity.[48,49] Modification of these nitrogen-doped carbon support with precious metals such as ruthenium,[50,51] cobalt,[52–54] nonprecious bimetallic Co-Cr nanostructures,[55] chromium nitride NPs,[56] etc., are well known in literature, wherein these catalysts showcased an enhanced catalytic activity. Also, in a study by Sarkar et al., galvanic electroless deposition of Pd on Ru nanocrystals were carried out on N-doped graphene (Pd–Ru@NG), wherein Pd leads to enhancement of the electrocatalytic performance of the catalyst towards HER.[57]

Interestingly, N sources help in preventing NP aggregation, formed during loading of Pd NPs over carbon supports, and assist in uniform nucleation of the NPs,[58,59] and thus acts as an anchoring hotspot. Among several nitrogen dopants available, nitrogen groups in both 1-aminopyrene and ammonium hydroxide are known to exhibit the aforementioned properties of anchoring and balancing the system to serve as an efficient electrocatalyst. 1-Aminopyrene, being a polycyclic aromatic hydrocarbon, induces a noncovalent π–π interaction with the conjugated basal planes of carbon lattice.[60–62] The protruding nitrogen of the amino group in this 1-aminopyrene, serves as specific binding sites for Pd NPs and helps in uniform nucleation.[36] Similarly, the usage of strong reducing agents such as ammonium hydroxide helps in the reduction of the functional groups over the carbon surface and also introduces N groups in the carbon lattice. This would enhance conductivity[63] along with introduction of N anchoring sites, that facilitate uniform dispersion of NPs.[40] Thus, although NPs, dopants, and substrates are important factors for designing an efficient and robust electrocatalyst, the synthesis strategy employed remains equally vital.

In this article, we investigated the ability of two different Pd immobilized nitrogen (N) dopant sources such as ammonium hydroxide (Pd@Amm.Hyd-(N)@RGO) and 1-aminopyrene (Pd@Pyrene-(N)@RGO) over RGO substrate for electrocatalytic application. Each of these nitrogen dopants acted in different ways, where the former catalyst was doped covalently, and the latter one noncovalently. The prepared catalysts were characterized using SEM, TEM, EDX, and BET analysis. ICP analysis gave information on the concentrations of elements within the sample and XPS gave information on the elemental composition and their respective oxidation states. Further, the electrochemical performance of the catalyst toward HER was studied using linear sweep voltammetry and also with other techniques in acidic medium.

## 2. Results and Discussions

The synthesis route of palladium (Pd) anchored covalently and noncovalently modified nitrogen-doped graphene (Pd@(N)@RGO) is depicted in detail in **Scheme 1**. Graphene oxide (GO) serves as a precursor material of RGO, which acts as a suitable carbon substrate for catalysis. Several defective sites are generated over the GO surface during the synthesis pathway from graphite which causes disruption in sp² states and affects conductivity.[64,65]

The conductivity of defective carbon surface is restored on treatment with reducing agents to obtain RGO. Aggregation of these carbon sheets are mitigated by doping nitrogen (N) sources into the carbon lattice, where eventually lone pairs of
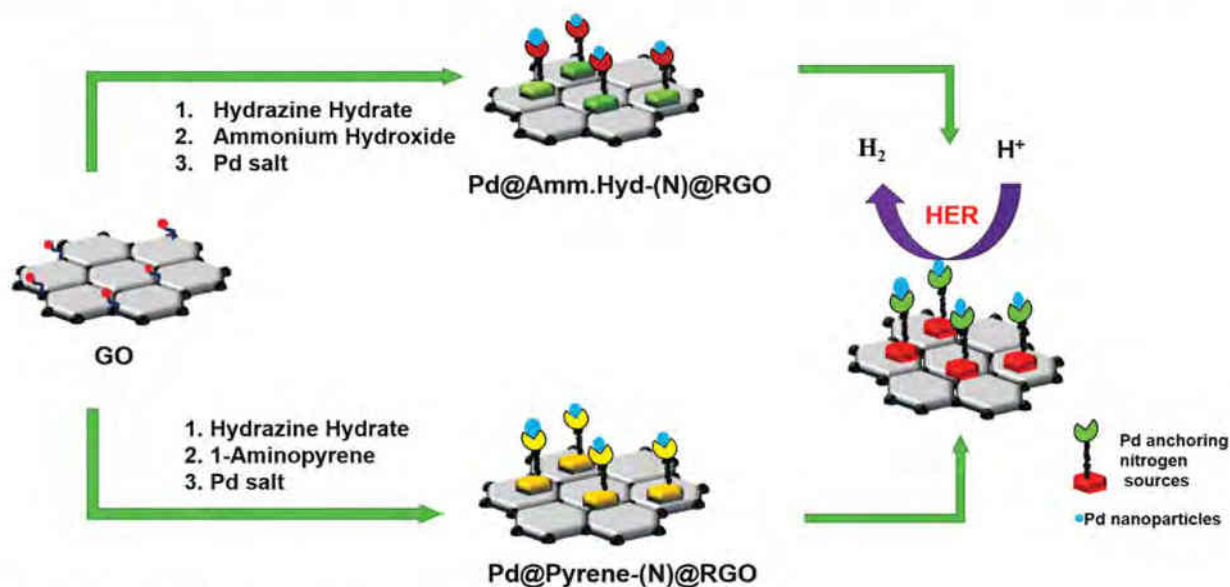


**Scheme 1.** Synthesis pathway adopted for preparing two different Pd@(N)@RGO catalysts.

**ADVANCED
SCIENCE NEWS**
www.advancedsciencenews.com

**ADVANCED
MATERIALS
INTERFACES**
www.advmatinterfaces.de
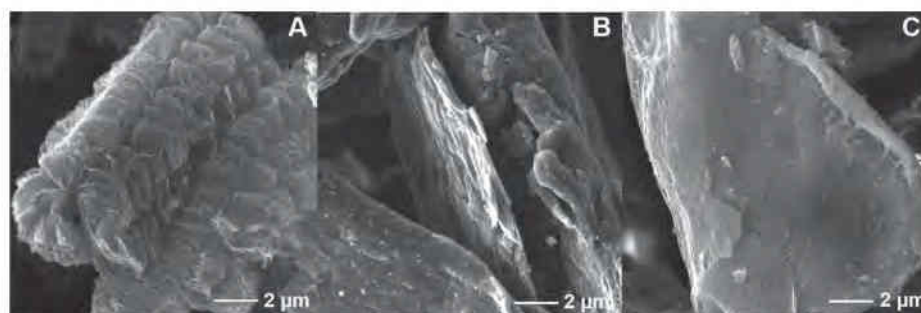
**Figure 1.** SEM images of A) RGO, B) Pd@Amm.Hyd-(N)@RGO, and C) Pd@Pyrene-(N)@RGO.

nitrogen conjugate with $\pi$ electrons of carbon. This process improves the properties of designed electrocatalysts.[66,67] Initially, morphological studies on the surface of synthesized samples were carried out using the scanning electron microscopy (SEM) technique. The black powdered RGO synthesized via the thermal treatment of GO, exhibited a fluffy and wrinkled structure as shown in **Figure 1**A. The changes on the surface of RGO were evident upon its subjection to doping of N in ammonium hydroxide (Figure 1B) and 1-aminopyrene (Figure 1C), followed by nucleation of Pd nanoparticles (NPs) on both surfaces. Both the doped samples showed 3D interconnected structures with stacked sheets.

Elemental distribution over the sample surface and composition were confirmed using the energy dispersive X-ray spectroscopy (EDX) technique. Uniform distribution of carbon and oxygen is seen throughout the RGO sample surface (**Figure 2**A) using EDX mapping. While other two samples, such as Pd@Amm.Hyd-(N)@RGO (Figure 2B) and Pd@Pyrene-(N)@RGO (Figure 2C) showed presence of C, O, N, and Pd elements over the catalyst surface. The presence of N and Pd elements in samples confirms the fact that doping and anchoring of NPs were successful. Also, the distribution of Pd NPs over (N)@RGO suggests an excellent ability of carbon support to act as

a catalytic substrate. The EDX spectral details of samples are depicted in Figure S1 (Supporting Information) where RGO (Figure S1A, Supporting Information) has shown a prominent carbon peak and oxygen peak. Both Pd@Amm.Hyd-(N)@RGO (Figures S1B, Supporting Information) and Pd@Pyrene-(N)@RGO (Figure S1C, Supporting Information) showed peaks of C, O, N, and Pd elements.

Further, TEM is done to understand the morphology and size of Pd NPs on the surface of the N-doped electrocatalysts. Based on the analysis of particles in Pd@Amm.Hyd-(N)@RGO electrocatalyst, spherically shaped uniform dispersion of Pd NPs was evident over crumpled sheets of (N)@RGO. The mean average particle size is about 30–40 nm in diameter (Figure S2A, Supporting Information). While, in the case of Pd@Pyrene-(N)@RGO electrocatalyst, Pd NPs with mean average particle size of 75–85 nm in diameter were evident over Pyrene-(N)@RGO surface (Figure S2B, Supporting Information). Thus, from TEM results it was evident that size of Pd NP is higher in Pd@Pyrene-(N)@RGO electrocatalyst than the Pd@Amm.Hyd-(N)@RGO electrocatalyst. X-ray photoelectron spectroscopy (XPS) was employed to perform compositional analyses, and to identify the chemical state and electronic structure of synthesized samples. The wide



**Figure 2.** SEM and EDX elemental maps of A) RGO, B) Pd@Amm.Hyd-(N)@RGO, and C) Pd@Pyrene-(N)@RGO.

**ADVANCED
SCIENCE NEWS**
www.advancedsciencenews.com

**ADVANCED
MATERIALS
INTERFACES**
www.advmatinterfaces.de

**Figure 3.** XPS survey spectrum of samples.

spectrum analysis of samples confirmed the successful doping over RGO, where distinguishable peaks of N were evident over both electrocatalyst surface (**Figure 3**).

The quantitative analysis of Pd@Amm.Hyd-(N)@RGO catalyst showed the presence of C 1s, Pd 3d, N 1s, and O 1s elements with atomic weights of 88.88%, 0.30%. 2.42%, and 8.40%, respectively. While in the Pd@Pyrene-N@RGO catalyst, the elements C 1s, Pd 3d, N 1s, and O 1s elements showed atomic weights of 90.12%, 0.64%, 3.14%, and 6.11%, respectively. RGO showed the presence of carbon and oxygen with 98.83% and 1.17%, respectively. A high-resolution Pd 3d spectra of the Pd@Amm.Hyd-(N)@RGO catalyst showed peaks at 335.2 and 335.9 eV corresponding to Pd $3d_{5/2}$, while peaks at binding energy of 340.5 and 341.3 eV corresponds to Pd $3d_{3/2}$ states (Figure S3A, Supporting Information).[40,68] Also, the shoulder peak at 338.1 eV and 343.1 eV is reported in literature.[40] The deconvoluted N 1s spectrum showed pyridinic, pyrrolic, and graphitic peaks at 398.9 eV (Peak a), 400.2 eV (Peak b), and 401.7 eV (Peak c), respectively, as shown in Figure S3A (Supporting Information).[69–71] The pyrrolic N at binding energy of 400.2 eV (Peak b) assists in donating their $\pi$ electrons, and the Pd metal is known to form a stable structure on binding with the pyrrolic N.[68,72] Further, the graphitic N peak at 401.7 eV (Peak c) affirms doping.[73,74] C 1s spectra in Figure S3A (Supporting Information) showed distinct peaks, where 284.6 eV (Peak a) represents the C—C bond with $sp^2$ hybridization, confirming the presence of graphite like carbon and peaks at 285 eV (Peak b) attributing to the $sp^2$ C=N bond.[40] Thus a strong covalent functionalization of N-$sp^2$ C bond is evident on the surface of carbon,[73,75] further enabling the nitrogen to serve as active sites for Pd nanoparticles. The shoulder peaks at 285.9 eV (Peak c), and 288 eV (Peak d), corresponds to C—O, and C=O groups. On further evaluation of O 1s spectra, four peaks were observed at 530.6 eV (—C=O) (Peak a), 531.9 eV (oxygen-bonded Pd (Pd—O)) (Peak b), 533.4 eV (—C—OH) (Peak c), as shown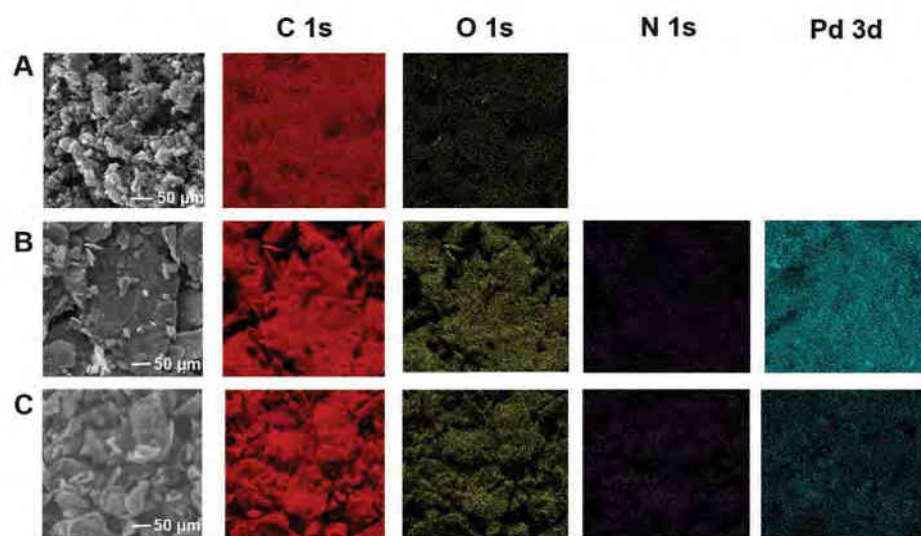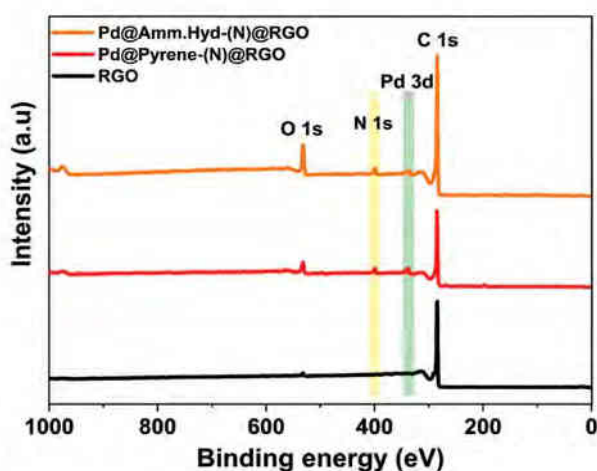 in the Figure S3A (Supporting Information). The peak at 535.8 eV (Peak d) could possibly be due to the chemisorbed oxygen (carboxylic groups), and/or water.[40,76]

Similarly, deconvoluted high-resolution spectra of Pd 3d in Pd@Pyrene-(N)@RGO gives peaks at 337.9 eV, and 343.1 eV corresponding to Pd $3d_{5/2}$ and Pd $3d_{3/2}$ states, as shown in Figure S3B (Supporting Information).[36] The difference in the binding energy of 5.2 eV further confirms the presence of Pd (0) or metallic Pd. The individual peaks of pyridinic, pyrrolic, and graphitic peaks from deconvoluted N 1s spectra at binding energies of 398.6 eV (Peak a), 399.7 eV (Peak b), and 401.2 eV (Peak c) are in accordance with the literature.[69,70] Non covalent functionalization of 1-aminopyrene group with carbon lattice via the $\pi$–$\pi$ interaction is confirmed from the binding energy of N 1s peak at 399.7 eV (Peak b).[77,78] The graphitic N peak at binding energy of 401.2 eV (Peak c) corresponds to the successful doping of C atoms in the hexagonal rings of the graphene lattice by N atoms. The C 1s spectra in Figure S3B (Supporting Information) gave signals at 284.6 eV (Peak a) and 285.3 eV (Peak b) corresponding to C—C, and C—O peaks. The peak at 288.1 eV (Peak c) corresponds to the —C—NH$_2$ bond which further confirms the noncovalent functionalization of 1-aminopyrene over the surface of highly reduced carbon lattice as ascribed in literature.[36] Thus, the above XPS results confirm successful reduction and noncovalent functionalization with carbon surface. Deconvolution of O 1s spectra gave two peaks at 531.8 and 533.6 eV, as shown in the S3B (Supporting Information).[40,76] Thus, the above XPS results are in good agreement, confirming successful reduction, doping of carbon surface and nucleation of Pd NPs.

Difference in the synthesis strategy of covalent and noncovalent bonding has resulted in variations in loading of Pd over the electrocatalyst. This was substantiated by the inductively coupled plasma (ICP) analysis, wherein the amount of Pd in Pd@Amm.Hyd-(N)@RGO was around 16.6 wt% while the Pd@Pyrene-(N)@RGO catalyst gave around 1.52 wt% of Pd. Thus, strong covalent bonding helps to increase loading of more Pd NPs in Pd@Amm.Hyd-(N)@RGO catalyst, while weaker noncovalent bonding in Pd@Pyrene-(N)@RGO results in lesser loading of Pd NPs. Further, BET studies were carried out in order to understand the surface area, and pore size of the material. The surface area of Pd@Amm.Hyd-(N)@RGO catalyst was found to be 355.39 m$^2$ g$^{-1}$, with a pore size around 25–45 nm. Based on the adsorption–desorption isotherms, the sample showcased Type IV isotherms, aligning to the mesoporous nature of the catalyst.[40] In Pd@Pyrene-(N)@RGO catalyst, they exhibited a higher surface area of 553.44 m$^2$ g$^{-1}$, and a pore size of around 20 nm. Also, these results accounts for the mesoporous nature of the catalyst.[36]

We further proceeded toward investigating the catalytic performance of these electrocatalysts. Electrocatalytic activity toward hydrogen evolution reaction (HER) was studied over an unmodified glassy carbon (GC) electrode surface via linear sweep voltammetry (LSV) technique. Commercial Pt/C was also used as a reference to evaluate the performance of other synthesized samples. The HER activity of Pd@Amm.Hyd-(N)@RGO, Pd@Pyrene-(N)@RGO, RGO, and Pt/C is shown in **Figure 4A**. To evaluate the performance of various catalysts, overpotentials at a current density of −10 mA cm$^{-2}$ were set as a reference indicator based on the solar constant, where a lower overpotential signifies better HER activity. Pt/C showed the lowest overpotential of −0.064 V versus RHE. Among Pd@(N)@RGO samples,

**ADVANCED
SCIENCE NEWS**
www.advancedsciencenews.com

**ADVANCED
MATERIALS
INTERFACES**
www.advmatinterfaces.de
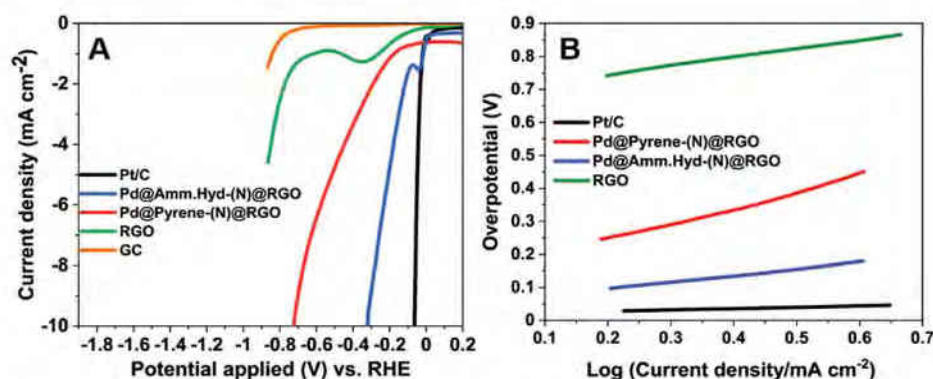
**Figure 4.** A) Linear sweep voltammograms of GC and synthesized samples at a scan rate of 5 mV s$^{-1}$ in 0.5 M H$_2$SO$_4$. B) Tafel plots of corresponding samples.

we found that Pd@Amm.Hyd-(N)@RGO (−0.324 V) showed lower onset potential over Pd@Pyrene-(N)@RGO samples (−0.727 V) at −10 mA cm$^{-2}$. On the other hand, the RGO exhibited a very high potential, as shown in Figure 4A.

The LSV experiments were repeated multiple times for both the electrocatalysts and the potential was measured and plotted based on the ability of catalysts to procure −10 mA cm$^{-2}$ (Figure S4, Supporting Information). A possible reason for the better catalytic activity of Pd@Amm.Hyd-(N)@RGO catalyst could be ascribed to the N source in the catalyst. Also, higher Pd loading owing to covalent synthesis strategy makes it a better electrocatalyst for HER. To further explain the mechanism of hydrogen evolution, the Tafel slope was calculated as shown in Figure 4B. Three major pathways are given below which describe the kinetics of catalyst in electrochemically converting proton in water media to hydrogen molecules, given as:

$$H_3O^+ + e^- \rightarrow H_{ads} + H_2O; \tag{1}$$
$b \approx 120 \text{ mV dec}^{-1} \left( \text{Adsorption; Volmer reaction} \right)$

$$H_3O^+ + H_{ads} + e^- \rightarrow H_2 + H_2O; \tag{2}$$
$b \approx 40 \text{ mV dec}^{-1} \left( \text{Desorption, Heyrovsky reaction} \right)$

$$H_{ads} + H_{ads} \rightarrow H_2; \tag{3}$$
$b \approx 30 \text{ mV dec}^{-1} \left( \text{Desorption, Tafel reaction} \right)$
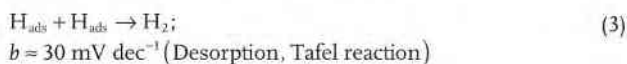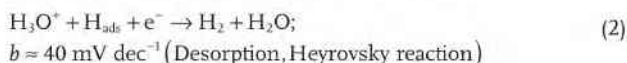
Tafel slope values ($b$) were obtained from the Tafel equation ($\eta = a + b \log |j|$), where $\eta$ is the overpotential, and $j$ is the current density. The Tafel slope values of Pt/C showed 40 mV dec$^{-1}$, and RGO showed around 258 mV dec$^{-1}$. Out of Pd@(N)@RGO catalysts, Pd@Amm.Hyd-(N)@RGO showed a Tafel slope of 201 mV dec$^{-1}$ while Pd@Pyrene-(N)@RGO showed a very high Tafel slope of 489 mV dec$^{-1}$. In short, Pd@Amm.Hyd-(N)@RGO exhibited a low overpotential value, and adsorption is observed to be the limiting step of this reaction. During the LSV measurements of Pd@Amm.Hyd-(N)@RGO samples, a reduction peak was clearly evident near −0.1 V versus RHE. To further understand the electrochemical behavior of the catalysts, cyclic voltammetry (CV) measurement was carried out at 50 mV s$^{-1}$ in 0.5 M H$_2$SO$_4$ solution (Figure S5, Supporting Information). In

Pd@Amm.Hyd-(N)@RGO catalyst, a cathodic and anodic peaks were observed, wherein reduction peak around −0.1 V accounts to the underpotential deposition of hydrogen (UPD-H$_{ads}$), owing to the adsorption of H on Pd surfaces (Figure S5, Supporting Information). The oxidation peak corresponds to the desorption of H from Pd surfaces. There are reports that substantiate this observation on the underpotential deposition of hydrogen (UPD) H$_{ads}$/H$_{des}$ shown by Pd systems.[23] Thus, in ammonium hydroxide samples, hydrogen intercalation peaks are evident owing to their strong covalent bonding and efficient nucleation of Pd nanoparticles. However, reduction peaks were not observed in Pd@Pyrene-(N)@RGO samples during CV measurements under similar conditions. This is possibly due to the low amount of Pd loading in Pd@Pyrene-(N)@RGO electrocatalyst, confirmed from ICP analysis. Low amount of Pd may result in the dilution of UPD-H$_{ads}$/UPD-H$_{des}$ signals in the background signals.

Durability test for both Pd@Amm.Hyd-(N)@RGO and Pd@Pyrene-(N)@RGO electrocatalyst were carried out via chronoamperometric technique at the potentials procured at −10 mA cm$^{-2}$. The experiments were conducted for 12 h, as shown in Figure S6 (Supporting Information). It was observed that although both the catalysts remained stable without any decline in the performance with time, Pd@Amm.Hyd-(N)@RGO was found to be better in terms of durability. The electrochemical active surface area (ECSA) (cm$^2$) of electrocatalyst was evaluated from the double layer capacitance[79] (the calculations are given in Section S7, Supporting Information). Further, electrochemical impedance spectroscopy (EIS) measurements were carried out for both the electrocatalysts using the three-electrode setup in 0.5 M H$_2$SO$_4$ solution. EIS spectra of both the electrocatalysts were recorded at the open-circuit potential and the plots are shown in Figure S8 (Supporting Information). It is very well evident that the $R_{ct}$ value of Pd@Pyrene-(N)@RGO catalyst is higher than the Pd@Amm.Hyd-(N)@RGO, affirming the higher conductive property of the latter catalyst. The turnover frequency (TOF), which is a measure of intrinsic activity of a catalyst, is also calculated for both electrocatalysts (the calculations are given in Section S9, Supporting Information). Post catalysis experiments, the catalysts were subjected to XPS characterizations, in order to

**ADVANCED
SCIENCE NEWS** _____
www.advancedsciencenews.com

**ADVANCED
MATERIALS
INTERFACES**
www.advmatinterfaces.de
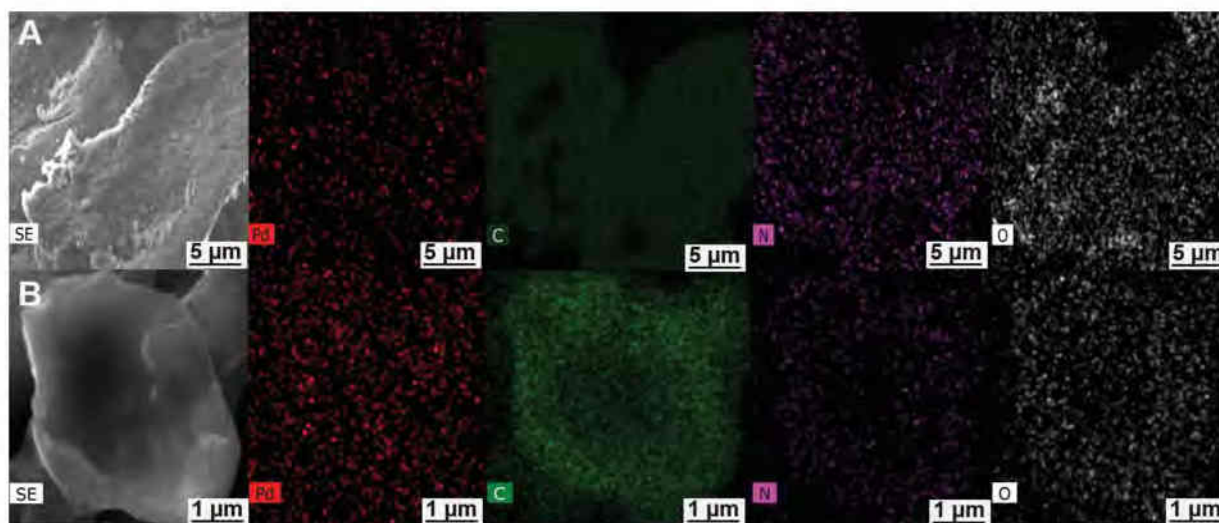
**Figure 5.** SEM and EDX elemental maps of A) Pd@Amm.Hyd-(N)@RGO and B) Pd@Pyrene-(N)@RGO post catalytic study.

identify if any difference in oxidation states had occurred in the course of the experiment. The Pd in Pd@Amm.Hyd-(N)@RGO retained the 0 and +2 oxidation states while Pd@Pyrene-(N)@ RGO retained 0 oxidation state (Figure S10, Supporting Information). More detailed information on the binding energies is given in Table S11 (Supporting Information). The deconvoluted Pd 3d XPS spectra of Pd@Amm.Hyd-(N)@RGO and Pd@ Pyrene-(N)@RGO electrocatalyst is given in the Figure S10 (Supporting Information) as well. In short, XPS analysis confirms that the catalyst has not undergone any major difference in the oxidation state in the course of the experiment.

Further, EDX mapping of electrocatalyst was carried out post stability measurements. The presence of Pd nanoparticles over the electrocatalyst surface has been confirmed for both the catalysts Pd@Amm.Hyd-(N)@RGO (**Figure** 5A) and Pd@Pyrene-(N)@RGO (Figure 5B), along with the presence of other elements such as C, N and O, elements.

## 3. Conclusions

In this study, reduced graphene oxide was successfully modified covalently and noncovalently using nitrogen sources that further facilitated nucleation of Pd NPs over its surface. Morphological studies gave an insight into these synthesized materials, and XPS measurements gave a better understanding of the composition and oxidation states of the catalysts. ICP analysis confirmed that covalently bonded electrocatalyst was successful in loading more Pd than the noncovalent electrocatalyst and TEM analysis confirmed that the size of Pd NPs in Pd@Amm.Hyd-(N)@RGO to be smaller than the Pd@Pyrene-(N)@RGO catalyst. Linear sweep measurements revealed that the Pd@Amm.Hyd-(N)@RGO showed lower overpotential and lower Tafel slope when compared to Pd@Pyrene-(N)@ RGO. The bifunctional property of ammonium hydroxide, both as a dopant and a strong reducing agent, is an added advantage to the fabricated catalyst to project high catalytic activity.

Further, covalent synthesis strategy employed using ammonium hydroxide also results in a higher loading of Pd NPs, making it active for HER. In short, the objective of anchoring more active Pd NPs over the catalyst surface is correlated to the differences in the synthesis strategy employed, wherein this technique could help in designing an ideal electrocatalyst for various catalytic applications. Thus, grafting of similar active nanoparticles over the catalyst surface could be an interesting approach toward designing application specific electrocatalyst.

## 4. Experimental Section

*Materials and Characterization*: Graphite powder (99.99%) was purchased from Alfa Aesar, USA. All other materials and organic solvents such as concentrated sulfuric acid ($H_2SO_4$, 98%), potassium permanganate ($KMnO_4$, 99%), sodium nitrate ($NaNO_3$, 99%) hydrogen peroxide ($H_2O_2$, 30 wt%), hydrazine hydrate ($N_2H_4$), ammonia hydroxide solution ($NH_4OH$), 1-aminopyrene (97%), and palladium (II) chloride ($PdCl_2$, 99.99%) were purchased from Sigma-Aldrich and used without further purification. The surface morphology was observed using a scanning electron microscopy (SEM, TESCAN LYRA 3) and MIRA3-XMU. The elemental analysis and mapping was carried out by energy-dispersive X-ray spectroscopy (EDX, MIRA). In addition, chemical compositional analyses were performed by XPS (Kratos AXIS Supra instrument) using a monochromatic Al K$\alpha$ (1486.7 eV) excitation source. The X-ray power was 225 W. The data were analyzed using Casa XPS software. The Pd amount in synthesized samples was analyzed using inductively coupled plasma optical emission spectrometry (IPC-OES, Arcos MV, SPECTRO Analytical Instruments, Kleve, Germany). Transmission electron microscopy was carried out using TEM, JEOL 7600F, Japan.

*Preparation of Graphene Oxide (GO)*: GO was synthesized from graphite powder using a modified Hummers method.[80,81] Initially, a mixture of graphite powder (0.5 g) and $NaNO_3$ (0.5 g) was added to conc. $H_2SO_4$ (23 mL) and stirred continuously for 10 min in an ice bath. Subsequently, $KMnO_4$ (3 g) was slowly added to the above mixture until it turned dark green. The mixture was later transferred to a water bath and heated to 35 – 40 °C for 1 h to obtain a thick paste. Afterward, deionized water (40 mL) was added to the above system and was stirred for 30 min at ≈90 °C. Next, about 100 ml of deionized water was added, followed

by slow addition of $H_2O_2$ (3 mL) which turns the dark brown mixture to yellowish. Post cooling, the mixture was filtered and washed thrice using deionized water. The thick brown paste obtained is dispersed in water (100 mL) and centrifuged for 2 min at 1000 rpm. The above step was repeated 4–5 times until all unsettled/floating particles were removed. Later they were centrifuged at a higher speed (8000 rpm) to remove smaller pieces of GO. Finally, the resultant paste was dispersed in water and sonicated well to obtain GO solution.

*Preparation of Palladium-Anchored Covalently Modified N-Doped Graphene (Pd@Amm.Hyd-(N)@RGO)*: In a typical procedure,[82] reduction of graphene oxide was carried out using a previously reported method. To procure graphene oxide (GO) sheets, initially, synthesized graphite oxide (200 mg) was dispersed in distilled water (40 mL) and sonicated for 30 min. The suspension obtained was transferred to an RB flask and simultaneously, hydrazine hydrate (4 mL), $NH_4OH$ (4 mL), $PdCl_2$ (100 mg) was added. The reaction flask contains a well-sealed condenser. The dispersion was stirred for 3 h in a water bath at 90 °C and allowed to cool down. The resultant black solid precipitate was collected, filtered and washed with DI water multiple times to remove excess hydrazine hydrate residues. The same was re-dispersed in water via sonication and the suspension was centrifuged at 4000 rpm for 30 min more. Finally, the product was collected using simple decantation and was then dried at 40 °C under vacuum.

*Preparation of Palladium-Anchored Noncovalently Modified N-Doped Graphene (Pd@Pyrene-(N)@RGO)*: Reduction of GO was carried out using a previously reported method.[82] Initially, GO (100 mg) was dispersed in water (30 mL) and sonicated for 30 min. This was followed first by the heating of the suspension obtained up to 100 °C and later, by the addition of hydrazine hydrate (3 mL). The suspension was subjected to a stirring of 24 h, after the temperature was lowered to 98 °C. The black powder obtained as a result, was filtered and the excess hydrazine was removed by washing it multiple times. The leftover bulk graphite was removed by centrifuging the suspension at a speed of 4000 rpm for 3–4 min. With further filtration and drying under vacuum, the final product was collected.

Next, a functionalized RGO with 1-aminopyrene was synthesized as previously reported.[36] Briefly, a dispersion of RGO (25 mg) was prepared in methanol (10 mL) via sonication for 30 min. The above dispersion is then added to a solution containing 1-aminopyrene (25 mg) in methanol (10 mL). Further, this mixture was stirred at room temperature for 48 h, followed by sonication for 6 h at 20 °C, and centrifugation of 3 h, for removing excess 1-aminopyrene from the reaction mixture. Further purification of unreacted 1-aminopyrene was carried out by re-dispersing black mixture in methanol (5 mL) and sonicating at 20 °C for 30 min. The resulting black suspension was subjected centrifugation for about 1 h and thus separated on decanting the acquired mixture. This procedure was duplicated several times till a colorless supernatant was obtained in the centrifuge tube and the product was then dried overnight under a vacuum.

The palladium-graphene composite (Pd@Pyrene-(N)@RGO) was then prepared by mixture of 5 mL dispersion of 1-aminopyrene functionalized RGO in ethanol (1 mg RGO/mL of ethanol), and 5 mL solution of $Na_2PdCl_4$ in ethanol (5 mg). After sonication for 1 h, the product was finally isolated by centrifugation (9000 rpm) and later re-dispersed in water (10 mL) for other purposes.

*Electrochemical Measurements*: The procured samples (2 mg mL$^{-1}$) were dispersed in a solution containing 400 uL isopropanol and distilled water in a ratio of 3:2, respectively. 16 µL of Nafion binder was added to the mixture and sonicated for 45 min. 10 µL of resultant sonicated sample was drop-casted over glassy carbon (GC) and dried. The experiment was carried out at room temperature using Ag/AgCl (1 M KCl) as the reference electrode and graphite rod as the counter electrode. Electrochemical measurements were conducted using a potentiostat (PGSTAT 204, Metrohm Autolab) operated by Nova 2.14 software. Hydrogen evolution reaction (HER) was investigated by linear sweep voltammetry (LSV) at a scan rate of 5 mV s$^{-1}$ in 0.5 M $H_2SO_4$. The reference electrode was calibrated versus the reversible hydrogen electrode (RHE), where $E_{RHE} = E_{Ag/AgCl} + E^0_{Ag/AgCl} + 0.059 \times pH$.

[1] G. Shaffer, S. M. Olsen, J. O. P. Pedersen, *Nat. Geosci.* **2009**, *2*, 105.
[2] N. E. Carpenter, *Chemistry of Sustainable Energy*, Chapman and Hall, New York **2014**.
[3] G. W. Crabtree, M. S. Dresselhaus, M. V. Buchanan, *Phys. Today* **2004**, *57*, 39.
[4] R. Gusmão, Z. Sofer, M. Pumera, *Adv. Funct. Mater.* **2019**, *29*, 1805975.
[5] A. Venkateshaiah, J. Y. Cheong, S. H. Shin, K. P. Akshaykumar, T. G. Yun, J. Bae, S. Wacławek, M. Černík, S. Agarwal, A. Greiner, V. V. T. Padil, I. D. Kim, R. S. Varma, *Green Chem.* **2020**, *22*, 1198.
[6] L. A. King, M. K. A. Hubert, C. Capuano, J. Manco, N. Danilovic, E. Valle, T. R. Hellstern, K. Ayers, T. F. Jaramillo, *Nat. Nanotechnol.* **2019**, *14*, 1071.
[7] Z. Yang, J. Ren, Z. Zhang, X. Chen, G. Guan, L. Qiu, Y. Zhang, H. Peng, *Chem. Rev.* **2015**, *115*, 5159.
[8] S. van Renssen, *Nat. Clim. Change* **2020**, *10*, 799.
[9] W. Lubitz, W. Tumas, *Chem. Rev.* **2007**, *107*, 3900.
[10] J. O. M. Bockris, *Int. J. Hydrogen Energy* **2002**, *27*, 731.
[11] M. A. Rosen, S. Koohi-Fayegh, *Energy Ecol. Environ.* **2016**, *1*, 10.
[12] Z. Wang, C. Li, K. Domen, *Chem. Soc. Rev.* **2019**, *48*, 2109.
[13] K. P. Akshay Kumar, O. Alduhaish, M. Pumera, *Electrochem. Commun.* **2021**, *125*, 106977.
[14] B. H. R. Suryanto, Y. Wang, R. K. Hocking, W. Adamson, C. Zhao, *Nat. Commun.* **2019**, *10*, 5599.

[15] C. C. L. McCrory, S. Jung, I. M. Ferrer, S. M. Chatman, J. C. Peters, T. F. Jaramillo, *J. Am. Chem. Soc.* **2015**, *137*, 4347.

[16] M. P. Browne, Z. Sofer, M. Pumera, *Energy Environ. Sci.* **2019**, *12*, 41.

[17] X. Chia, A. Ambrosi, Z. Sofer, J. Luxa, M. Pumera, *ACS Nano* **2015**, *9*, 5164.

[18] S. Niu, S. Li, Y. Du, X. Han, P. Xu, *ACS Energy Lett.* **2020**, *5*, 1083.

[19] N. Cheng, S. Stambula, D. Wang, M. N. Banis, J. Liu, A. Riese, B. Xiao, R. Li, T. K. Sham, L. M. Liu, G. A. Botton, X. Sun, *Nat. Commun.* **2016**, *7*, 13638.

[20] J. Zhang, Y. Zhao, X. Guo, C. Chen, C. L. Dong, R. S. Liu, C. P. Han, Y. Li, Y. Gogotsi, G. Wang, *Nat. Catal.* **2018**, *1*, 985.

[21] M. Liu, X. Wang, J. Liu, K. Wang, S. Jin, B. Tan, *ACS Appl. Mater. Interfaces* **2020**, *12*, 12774.

[22] E. Antolini, S. C. Zignani, S. F. Santos, E. R. Gonzalez, *Electrochim. Acta* **2011**, *56*, 2299.

[23] T. Bhowmik, M. K. Kundu, S. Barman, *ACS Catal.* **2016**, *6*, 1929.

[24] H. Jin, C. Guo, X. Liu, J. Liu, A. Vasileff, Y. Jiao, Y. Zheng, S. Z. Qiao, *Chem. Rev.* **2018**, *118*, 6337.

[25] Z. W. Seh, K. D. Fredrickson, B. Anasori, J. Kibsgaard, A. L. Strickler, M. R. Lukatskaya, Y. Gogotsi, T. F. Jaramillo, A. Vojvodic, *ACS Energy Lett.* **2016**, *1*, 589.

[26] K. P. Akshay Kumar, K. Ghosh, O. Alduhaish, M. Pumera, *Electrochem. Commun.* **2021**, *122*, 106890.

[27] M. Pumera, Z. Sofer, A. Ambrosi, *J. Mater. Chem. A* **2014**, *2*, 8981.

[28] K. Khan, A. K. Tareen, M. Aslam, Y. Zhang, R. Wang, Z. Ouyang, Z. Gou, H. Zhang, *Nanoscale* **2019**, *11*, 21622.

[29] V. V. T. Padil, K. P. Akshay Kumar, S. Murugesan, R. Torres-Mendieta, S. Wacławek, J. Y. Cheong, M. Černík, R. S. Varma, *Green Chem.* **2022**, *24*, 3081.

[30] A. Ali Tahir, H. Ullah, P. Sudhagar, M. Asri Mat Teridi, A. Devadoss, S. Sundaram, *Chem. Rec.* **2016**, *16*, 1591.

[31] M. Hu, Z. Yao, X. Wang, *Ind. Eng. Chem. Res.* **2017**, *56*, 3477.

[32] N. G. Sahoo, Y. Pan, L. Li, S. H. Chan, *Adv. Mater.* **2012**, *24*, 4203.

[33] X. Wang, G. Shi, *Energy Environ. Sci.* **2015**, *8*, 790.

[34] S. Choi, C. Kim, J. M. Suh, H. W. Jang, *Carbon Energy* **2019**, *1*, 85.

[35] H. W. Kim, M. B. Ross, N. Kornienko, L. Zhang, J. Guo, P. Yang, B. D. McCloskey, *Nat. Catal.* **2018**, *1*, 282.

[36] M. Khan, M. R. Shaik, S. F. Adil, M. Kuniyil, M. Ashraf, H. Frerichs, M. A. Sarif, M. R. H. Siddiqui, A. Al-Warthan, J. P. Labis, M. S. Islam, W. Tremel, M. N. Tahir, *Sci. Rep.* **2020**, *10*, 11728.

[37] S. Park, R. S. Ruoff, *Nat. Nanotechnol.* **2009**, *4*, 217.

[38] M. Liu, F. Hof, M. Moro, G. Valenti, F. Paolucci, A. Pénicaud, *Nanoscale* **2020**, *12*, 20165.

[39] K. P. A. Kumar, K. Ghosh, O. Alduhaish, M. Pumera, *Electrochem. Commun.* **2020**, *120*, 106827.

[40] M. Kuniyil, J. V. S. Kumar, S. F. Adil, M. R. Shaik, M. Khan, M. E. Assal, M. R. H. Siddiqui, A. Al-warthan, *Catalysts* **2019**, *9*, 469.

[41] Y. S. Yun, G. Yoon, M. Park, S. Y. Cho, H.-D. Lim, H. Kim, Y. W. Park, B. H. Kim, K. Kang, H.-J. Jin, *NPG Asia Mater.* **2016**, *8*, e338.

[42] L. Wang, Z. Sofer, M. Pumera, *ACS Nano* **2020**, *14*, 21.

[43] S. M. Tan, M. Pumera, *ACS Nano* **2019**, *13*, 2681.

[44] X. Li, Q. Zhao, X. Feng, L. Pan, Z. Wu, X. Wu, T. Ma, J. Liu, Y. Pan, Y. Song, M. Wu, *ChemSusChem* **2019**, *12*, 858.

[45] J. Duan, S. Chen, M. Jaroniec, S. Z. Qiao, *ACS Catal.* **2015**, *5*, 5207.

[46] B. R. Sathe, X. Zou, T. Asefa, *Catal. Sci. Technol.* **2014**, *4*, 2023.

[47] Z. Song, M. Wang, Z. Wang, Y. Wang, R. Li, Y. Zhang, C. Liu, Y. Liu, B. Xu, F. Qi, *Environ. Sci. Technol.* **2019**, *53*, 5337.

[48] S. Chen, S. Z. Qiao, *ACS Nano* **2013**, *7*, 10190.

[49] C. Li, Y. Hu, M. Yu, Z. Wang, W. Zhao, P. Liu, Y. Tong, X. Lu, *RSC Adv.* **2014**, *4*, 51878.

[50] B. Sarkar, D. Das, K. K. Nanda, *J. Mater. Chem. A* **2021**, *9*, 13958.

[51] Q. Zhi, S. Qin, W. Liu, R. Jiang, T. Sun, K. Wang, P. Jin, J. Jiang, *Catal. Sci. Technol.* **2021**, *11*, 3182.

[52] B. Sarkar, D. Das, K. K. Nanda, *Green Chem.* **2020**, *22*, 7884.

[53] H. Fei, Y. Yang, Z. Peng, G. Ruan, Q. Zhong, L. Li, E. L. G. Samuel, J. M. Tour, *ACS Appl. Mater. Interfaces* **2015**, *7*, 8083.

[54] P. Thakur, M. Yeddala, K. Alam, S. Pal, P. Sen, T. N. Narayanan, *ACS Appl. Energy Mater.* **2020**, *3*, 7813.

[55] B. Sarkar, B. K. Barman, K. K. Nanda, *ACS Appl. Energy Mater.* **2018**, *1*, 1116.

[56] B. Sarkar, A. Parui, A. K. Singh, K. K. Nanda, *J. Mater. Chem. A* **2021**, *9*, 16575.

[57] B. K. Barman, B. Sarkar, K. K. Nanda, *Chem. Commun.* **2019**, *55*, 13928.

[58] B. P. Vinayan, R. Nagar, S. Ramaprabhu, *J. Mater. Chem. A* **2013**, *1*, 11192.

[59] R. Arrigo, M. E. Schuster, Z. Xie, Y. Yi, G. Wowsnick, L. L. Sun, K. E. Hermann, M. Friedrich, P. Kast, M. Hävecker, A. Knop-Gericke, R. Schlögl, *ACS Catal.* **2015**, *5*, 2740.

[60] D. Liu, L. Yang, J. S. Huang, Q. H. Guo, T. Y. You, *RSC Adv.* **2014**, *4*, 13733.

[61] J. M. Fraile, J. I. García, J. A. Mayoral, *Chem. Rev.* **2009**, *109*, 360.

[62] S. Sabater, J. A. Mata, E. Peris, *Organometallics* **2015**, *34*, 1186.

[63] M. P. Kumar, T. Kesavan, G. Kalita, P. Ragupathy, T. N. Narayanan, D. K. Pattanayak, *RSC Adv.* **2014**, *4*, 38689.

[64] I. Jung, D. A. Dikin, R. D. Piner, R. S. Ruoff, *Nano Lett.* **2008**, *8*, 4283.

[65] A. Gholampour, M. Valizadeh Kiamahalleh, D. N. H. Tran, T. Ozbakkaloglu, D. Losic, *ACS Appl. Mater. Interfaces* **2017**, *9*, 43275.

[66] Y. Zhao, L. Yang, S. Chen, X. Wang, Y. Ma, Q. Wu, Y. Jiang, W. Qian, Z. Hu, *J. Am. Chem. Soc.* **2013**, *135*, 1201.

[67] S. Ratso, I. Kruusenberg, U. Joost, R. Saar, K. Tammeveski, *Int. J. Hydrogen Energy* **2016**, *41*, 22510.

[68] M. Narreddula, R. Balaji, K. Ramya, N. Rajalakshmi, A. Ramachandraiah, *Int. J. Hydrogen Energy* **2019**, *44*, 4582.

[69] M. Zhang, Y. Li, D. Pan, S. Yan, S. Meng, J. Xie, *RSC Adv.* **2016**, *6*, 33231.

[70] P. Lazar, R. Mach, M. Otyepka, *J. Phys. Chem. C* **2019**, *123*, 10695.

[71] K. Sandeep, K. Y. Gopika, M. R. Revathi, *Phys. Status Solidi RRL* **2019**, *13*, 1900387.

[72] C. Sen Liu, X. C. Liu, G. C. Wang, R. P. Liang, J. D. Qiu, *J. Electroanal. Chem.* **2014**, *728*, 41.

[73] L. Cui, X. Chen, B. Liu, K. Chen, Z. Chen, Y. Qi, H. Xie, F. Zhou, M. H. Rümmeli, Y. Zhang, Z. Liu, *ACS Appl. Mater. Interfaces* **2018**, *10*, 32622.

[74] C. Zhang, L. Fu, N. Liu, M. Liu, Y. Wang, Z. Liu, *Adv. Mater.* **2011**, *23*, 1020.

[75] R. Nandan, G. Raj, K. K. Nanda, *ACS Appl. Mater. Interfaces* **2022**, *14*, 16108.

[76] X. Chen, B. Chen, *Environ. Sci. Technol.* **2015**, *49*, 6181.

[77] X. H. Zhou, X. R. Huang, L. H. Liu, X. Bai, H. C. Shi, *RSC Adv.* **2013**, *3*, 18036.

[78] H. L. Pang, J. Liu, D. Hu, X. H. Zhang, J. H. Chen, *Electrochim. Acta* **2010**, *55*, 6611.

[79] L. L. Fang, Q. Tao, M. F. Li, L. W. Liao, D. Chen, Y. X. Chen, *Chin. J. Chem. Phys.* **2010**, *23*, 543.

[80] W. S. Hummers, R. E. Offeman, *J. Am. Chem. Soc.* **1958**, *80*, 1339.

[81] L. J. Cote, F. Kim, J. Huang, *J. Am. Chem. Soc.* **2009**, *131*, 1043.

[82] C. K. Chua, M. Pumera, *Chem. Commun.* **2016**, *52*, 72.

# Grafting of Pd on Covalently and Noncovalently Modified N-Doped Graphene for Electrocatalysis

*Kandambath Padinjareveetil Akshay Kumar, Osamah Alduhaish, Syed Farooq Adil, and Martin Pumera\**
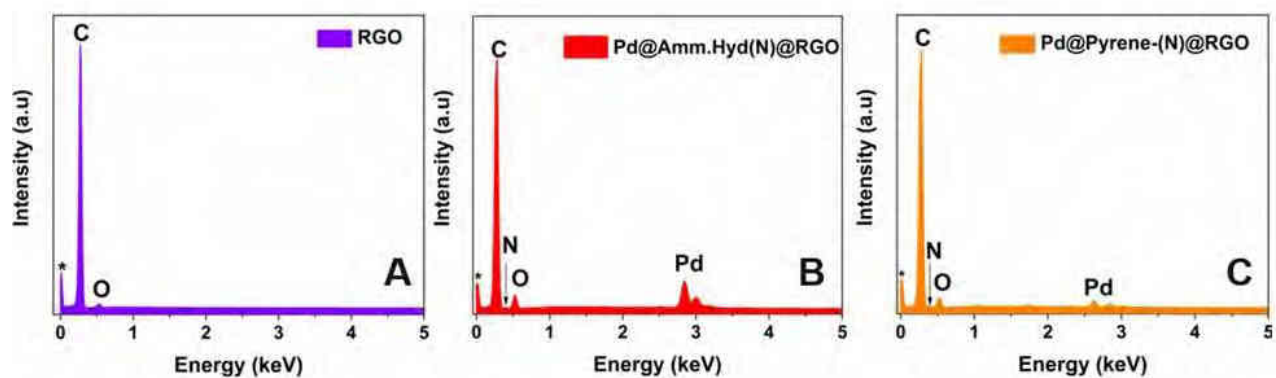
Figure S1. EDX spectral analysis of A) RGO B) Pd@Amm.Hyd-(N)@RGO C) Pd@Pyrene-(N)@RGO samples.
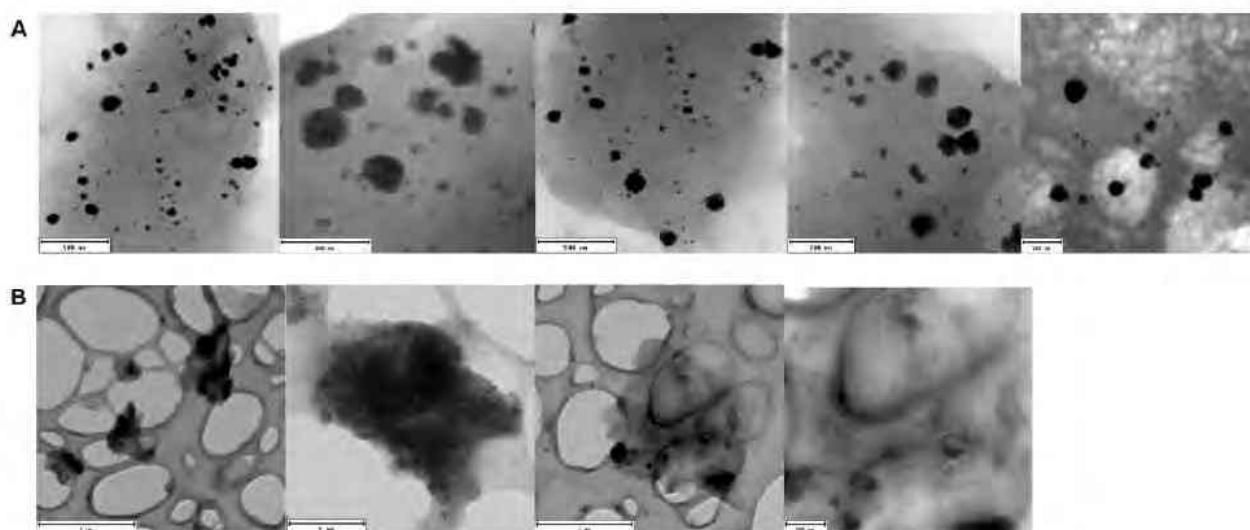


Figure S2. TEM images of A) Pd@Amm.Hyd-(N)@RGO B) Pd@Pyrene-(N)@RGO samples.
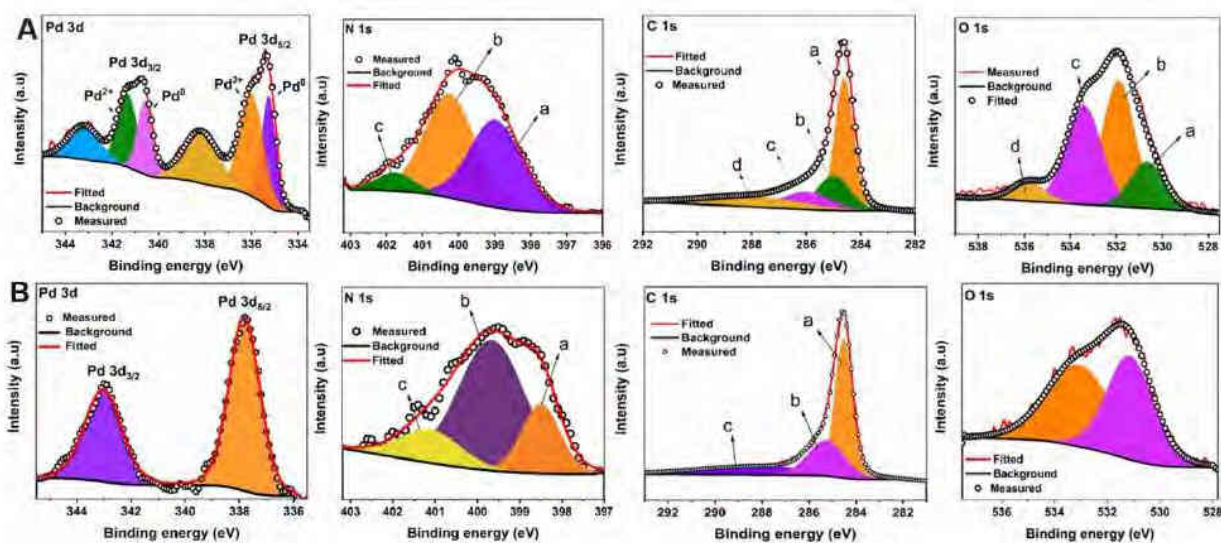
Figure S3. Deconvoluted XPS spectrum of A) Pd@Amm.Hyd-(N)@RGO B) Pd@Pyrene-(N)@RGO samples.
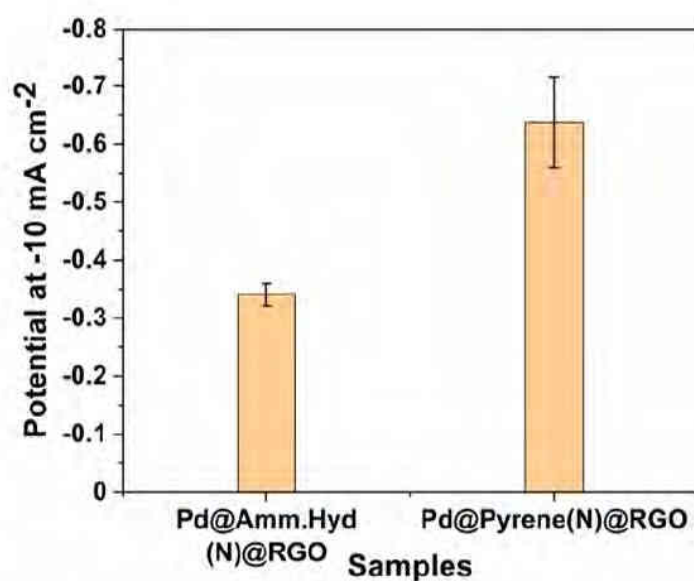


Figure S4. Potential procured by electrocatalysts in 0.5 M $H_2SO_4$ solution.
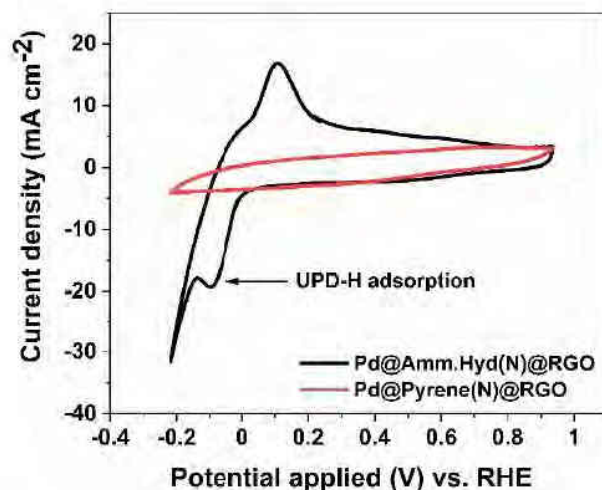
Figure S5. Cyclic voltammetry measurements of catalysts in 0.5 M $H_2SO_4$ solution.
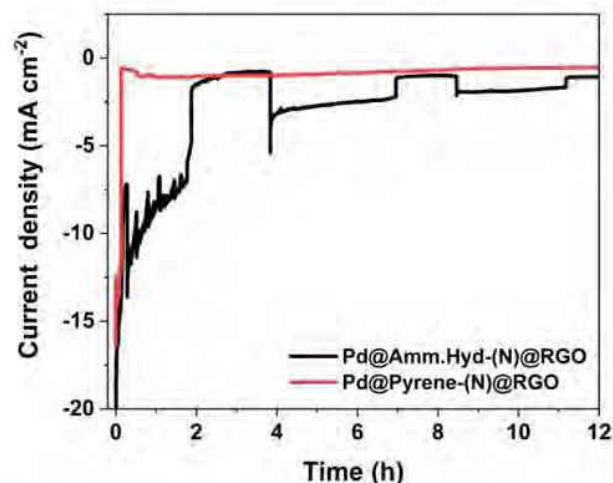


Figure S6. Chronoamperomety measurements of electrocatalysts in 0.5 M $H_2SO_4$ solutions

S7. Calculation of electrochemical surface area (ECSA)

ECSA of electrocatalysts were evaluated from the double layer capacitance given by the equation, ECSA= $C_{DL}/C_s$                                                  (1)[1]

where, $C_{DL}$ is the slope of anodic current in the non-faradaic region of the CV measurement and Cs is the specific capacitance of the active Pd electrode material (23.1 $\mu$F cm$^{-2}$) [2] under similar electrolyte conditions. CV measurements of both the electrocatalyst were carried out

57

in the non-faradaic region between 0.05 V and 0.25 V (vs. Ag/AgCl). The anodic current procured at the mid-point of the potential window was extracted and plotted against the scan rate to obtain the slope ($C_{DL}$) of each electrocatalyst. The $C_{DL}$ values for Pd@Amm.Hyd-(N)@RGO and Pd@Pyrene-(N)@RGO electrocatalyst was obtained around 2.73 mF and 1.73 mF giving an ECSA value of 118.18 cm$^2$ and 74.8 cm$^2$, respectively.
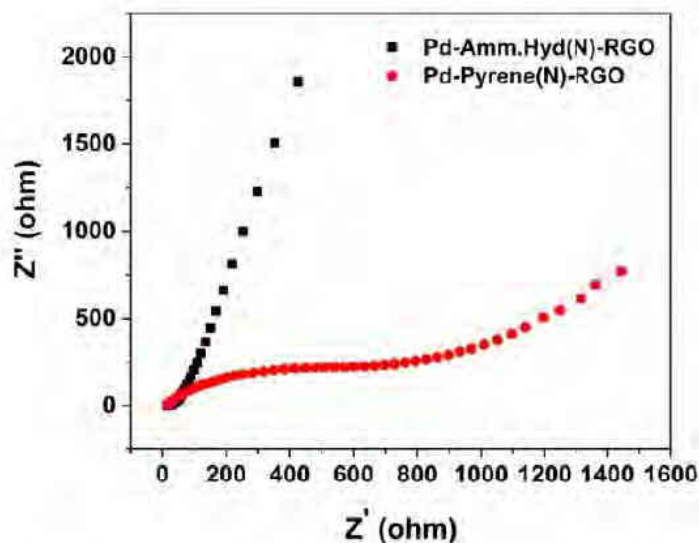


Figure S8. EIS measurements of electrocatalysts in 0.5 M H$_2$SO$_4$ solution.

S9. The TOF of the catalysts is calculated using the following formula (2)[3]

$$TOF = jS/2 * F * n \qquad \ldots\ldots\ldots\ldots\ldots \quad (2)$$

where j is the current density obtained at -0.15 V vs. RHE, S is the geometric surface area of working electrode, F is Faraday constant, and n is the number of moles of the active sites of the catalyst. The TOF value for Pd@Amm.Hyd-(N)@RGO came out to be around 0.015 s$^{-1}$ site$^{-1}$ for H$_2$ production and for Pd@Pyrene-(N)@RGO around 0.046 s$^{-1}$ site$^{-1}$.
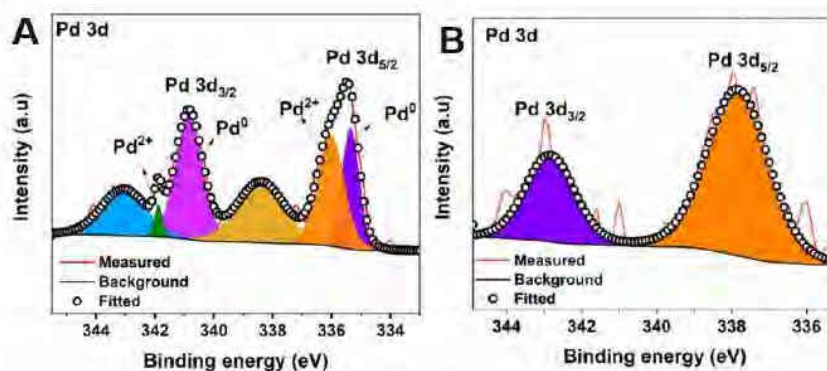
Figure S10. Deconvoluted XPS spectrum of Pd 3d samples post catalytic experiments A) Pd@Amm.Hyd-(N)@RGO B) Pd@Pyrene-(N)@RGO.

Table S11. Binding energy values of deconvoluted Pd 3d XPS spectrum of samples post catalytic experiments

| Samples | Pd 3d$_{5/2}$ | | Pd 3d$_{3/2}$ | |
|---|---|---|---|---|
| | 0 | +2 | 0 | +2 |
| Pd@Amm.Hyd-(N)@RGO | 335.3 eV | 336 eV | 340.8 eV | 341.8 eV |
| Pd@Pyrene-(N)@RGO | 337.8 eV | | 342.8 eV | |

References

[1]    G. R. Park, S. G. Jo, A. Varyambath, J. Kim, J. W. Lee, *Nanomaterials* **2021**, *11*.

[2]    L. L. Fang, Q. Tao, M. F. Li, L. W. Liao, D. Chen, Y. X. Chen, *Chinese J. Chem. Phys.* **2010**, *23*, 543.

[3]    P. Thakur, M. Yeddala, K. Alam, S. Pal, P. Sen, T. N. Narayanan, ACS Appl. Energy Mater. **2020**, 3, 7813.

**5.1.2: Electrocatalytic activity of layered MAX phases for HER**

**Motivation**

There has been curiosity to investigate new active materials for $H_2$ evolution. Interestingly, MAX phases exhibit an intermediate electrocatalytic performance towards $H_2$ generation and studies on this class of material remain unexplored. Hence, evaluating the performance of MAX phase catalysts can be interesting to device newer electrode materials, and further knowledge on the active MAX transition metal can be used as a foundation to synthesize their daughter MXenes for similar applications.

**Objective**

Morphological and electrochemical characterization of MAX ($Ti_2AlC$, $Ta_2AlC$, $Ti_2SnC$, $Ti_3SiC_2$, $V_2AlC$, and $Cr_2AlC$) and double transition metal carbide ($Mo_2TiAlC_2$,) will be carried out. LSV measurements of the catalysts would provide information on the catalyst that deliver lowest overpotential for $H_2$ production. Chronoamperometry measurements would provide information on the stability of electrocatalyst. Further, kinetics of these catalysts towards $H_2$ production will be evaluated using the Tafel slope analysis.

**Outcome**

$Mo_2TiAlC_2$ showed better HER activity over other MAX phases. Meanwhile, among single transition metal carbide, $V_2AlC$ gave the best HER activity, while $Ti_3SiC_2$ gave very high overpotential for $H_2$ production. Tafel slope analysis showcased that proton adsorption is the rate-limiting step in all studied electrocatalysts.

**Contribution**

Investigation, methodology, conceptualization, formal analysis, data curation, characterizations, experimentation, validation, discussions, writing (original draft, review and editing).

**Article**

The article was published and the details of the article are as follows:

Akshay Kumar K. Padinjareveetil, O. Alduhaish, Martin Pumera*, *Electrocatalytic activity of layered MAX phases for the hydrogen evolution reaction*, **Electrochem. Commun**. 2021, 125, 106977, https://doi.org/10.1016/j.elecom.2021.106977, (IF=5.44).

Short Communication

# Electrocatalytic activity of layered MAX phases for the hydrogen evolution reaction

K.P. Akshay Kumar [a,1], Osamah Alduhaish [b,2], Martin Pumera [a,b,c,d,*,3]

[a] Future Energy and Innovation Laboratory, Central European Institute of Technology, Brno University of Technology, Purkyňova 123, 61200 Brno, Czech Republic
[b] Chemistry Department P.O.Box 2455, College of Science King Saud University, Riyadh 11451, Saudi Arabia
[c] Department of Chemistry and Biochemistry, Mendel University in Brno, Zemedelska 1, CZ-613 00 Brno, Czech Republic
[d] Department of Medical Research, China Medical University Hospital, China Medical University, No. 91 Hsueh-Shih Road, Taichung 40402, Taiwan

ARTICLE INFO

ABSTRACT

The hydrogen evolution reaction (HER) is important for the advancement of next-generation electrochemical energy devices. The search for an alternative inexpensive catalyst for energy conversion to replace expensive and rare noble metals is of high priority. There has been a significant push to investigate electrocatalysis of various layered materials for hydrogen evolution. However, the electrocatalytic activity of layered MAX phases remains largely unexplored. Herein, electrocatalytic activity studies of MAX ($Ti_2AlC$, $Ta_2AlC$, $Ti_2SnC$, $Ti_3SiC_2$, $V_2AlC$, $Mo_2TiAlC_2$, and $Cr_2AlC$) phases are conducted. Material and electrochemical characterization are carried out to understand the morphology and catalytic activity, respectively. From Tafel slope analysis, it was found that proton adsorption is the rate-limiting step for all the MAX phases studied. Double transition-metal MAX carbides ($Mo_2TiAlC_2$) showed better catalytic activity for HER than single transition-metal MAX carbides.

## 1. Introduction

Exploring clean, renewable, and efficient strategies for energy production is a major challenge in the present situation. Natural resources are being depleted at an alarming rate and the use of sustainable energy sources is encouraged [1–4]. Among the available sustainable energy sources, electrochemical energy is an ideal and efficient method to address the present energy crisis. Hydrogen energy is attracting immense attention due to its zero carbon emission and high energy density [5]. Electrochemical splitting of water to generate hydrogen via the hydrogen evolution reaction (HER) is an ideal step towards efficient electrocatalysis [3,6–8]. Noble metal catalysts such as platinum are considered to be the most efficient catalysts for HER, but face major disadvantages for large-scale hydrogen production due to their scarcity, and high cost [9]. Thus, dependence on expensive noble metals has been significantly reduced while the use of alternative inexpensive catalysts has been encouraged [3,10].

In addition, a number of two-dimensional (2D) materials such as

graphene [11,12], transition metal dichalcogenides (TMDs) [13-16], transition metal phosphides [17,18], and heavy pnictogens [19] such as As, Sb, and Bi have been shown to be promising electrocatalysts. Although 2D nanomaterials have been extensively used for energy conversion applications, some have faced a setback due to their poor intrinsic activity, low density of active sites, or weak conductivity [20]. These nanomaterials have been tuned to improve their properties for fast catalytic reaction kinetics. Beyond this, there is another class of layered materials known as MAX phases that remain largely unexplored for hydrogen evolution applications.

About 150 MAX phases are known and the family continues to expand [21,22]. MAX phases are layered carbides and nitrides with the general formula $M_{n+1}AX_n$ where $n = 1–3$, M represents an early transition metal, A is an element of group 13–14 and X is carbon or nitrogen [23-25]. Studies have also shown the successful synthesis of ($M'$, $M''$)$_{n+1}AlC_n$ ordered phases, where two $M'$ layers sandwich one or two $M''$ layers [26,27]. MAX phases show the properties of both ceramics and metals due to their layered structure and the intrinsic nature of their

* Corresponding author at: Future Energy and Innovation Laboratory, Central European Institute of Technology, Brno University of Technology, Purkyňova 123, 61200 Brno, Czech Republic.
E-mail addresses: oalduhaish@ksu.edu.sa (O. Alduhaish), pumera.research@gmail.com (M. Pumera).
[1] orcid.org/0000-0001-9039-4637.
[2] orcid.org/0000-0001-5344-9459.
[3] orcid.org/0000-0001-5846-2951.

chemical bonding. They exhibit good electrical and thermal conductivity, have a high elastic modulus, thermal shock resistance, damage tolerance, are readily machinable, and resistant to both oxidation and corrosion [21,28–31]. The bonding of layers in MAX phases is stronger and requires a stronger etching and exfoliation method to convert them to another set of interesting materials called MXenes [32,33]. They are presently a hot topic in the scientific community and in industry due to their energy-related applications [1,34–36].

We have studied the electrocatalytic activity of a set of MAX phases for their possible energy conversion applications as these have not yet been investigated. Morphological studies were carried out using a scanning electron microscopy (SEM) and the elemental composition was confirmed from EDX spectra. The distribution of constituent elements was analyzed using EDX mapping. Linear sweep voltammetry (LSV) was carried out to study the catalytic properties of the material towards HER. Herein, we add new candidates to the existing list of known layered materials for electrochemical and electrocatalytic applications.

## 2. Experimental section

### 2.1. Materials and characterization

MAX phases (Ti$_2$AlC, Ta$_2$AlC, Ti$_2$SnC, Ti$_3$SiC$_2$, V$_2$AlC, Mo$_2$TiAlC$_2$, and Cr$_2$AlC) were purchased from Laizhou Kai Kai Ceramic Materials Co., Ltd, China. Sulfuric acid (H$_2$SO$_4$) of analytical grade, isopropanol, and Nafion were procured from Sigma Aldrich, Germany. The surface morphology of the MAX phases was observed using a scanning electron microscopy (SEM, TESCAN LYRA 3). The elemental analysis and mapping were carried out with an energy-dispersive X-ray (EDX) detector (BRUKER XFlash 5010) within the SEM.

### 2.2. Electrochemical measurements

MAX phases (5 mg mL$^{-1}$) were dispersed in a solution containing isopropanol and distilled water in a ratio of 3:2, respectively. 40 μL of Nafion binder was added to the mixture. Prior to drop-casting the mixture over glassy carbon (GC), the mixture was subjected to ultrasonication for 60 min to obtain a well-dispersed suspension. 10 μL of the suspension was then drop-casted over GC electrode and left to dry at room temperature. Voltammetry measurements were conducted using a potentiostat (PGSTAT 204, Metrohm Auto lab) operated by Nova 2.14 software. The hydrogen evolution reaction (HER) was investigated by linear sweep voltammetry (LSV) at a scan rate of 5 mV s$^{-1}$ in 0.5 M H$_2$SO$_4$. The measurements were carried out at room temperature with Ag/AgCl (1 M KCl) as the reference electrode (RE) and platinum wire as the counter electrode (CE). The reference electrode was calibrated versus the reversible hydrogen electrode (RHE), where $E_{RHE} = E_{Ag/AgCl} + E^0_{Ag/AgCl} + 0.059 \times$ pH. Chronoamperometry measurements were carried out using a rotating disk electrode (RDE) in 0.5 M H$_2$SO$_4$ solution.

## 3. Results and discussion

The morphology of the MAX phases was analyzed using a scanning electron microscopy (SEM) as shown in Fig. 1. The Ti$_2$AlC, V$_2$AlC, Ta$_2$AlC, and Cr$_2$AlC MAX phases show stacked configurations with sheet-like layers, whereas other sets of MAX phases such as Ti$_2$SnC, Ti$_3$SiC$_2$ and Mo$_2$TiAlC$_2$ exhibited structures that were round and clumpy. The EDX spectral analysis confirmed the presence of the constituent elements (Fig. 1) and the elemental ratios calculated from atomic percentage followed the stoichiometry of the samples (Table S1).

The EDX elemental maps confirmed the uniform distribution of elements over the sample surface (Fig. S1). After analysis of the morphology and elemental compositions of the MAX phases, we further explored the properties of the materials as catalysts for the electrochemical splitting of water. Previous studies show that MAX/MAB
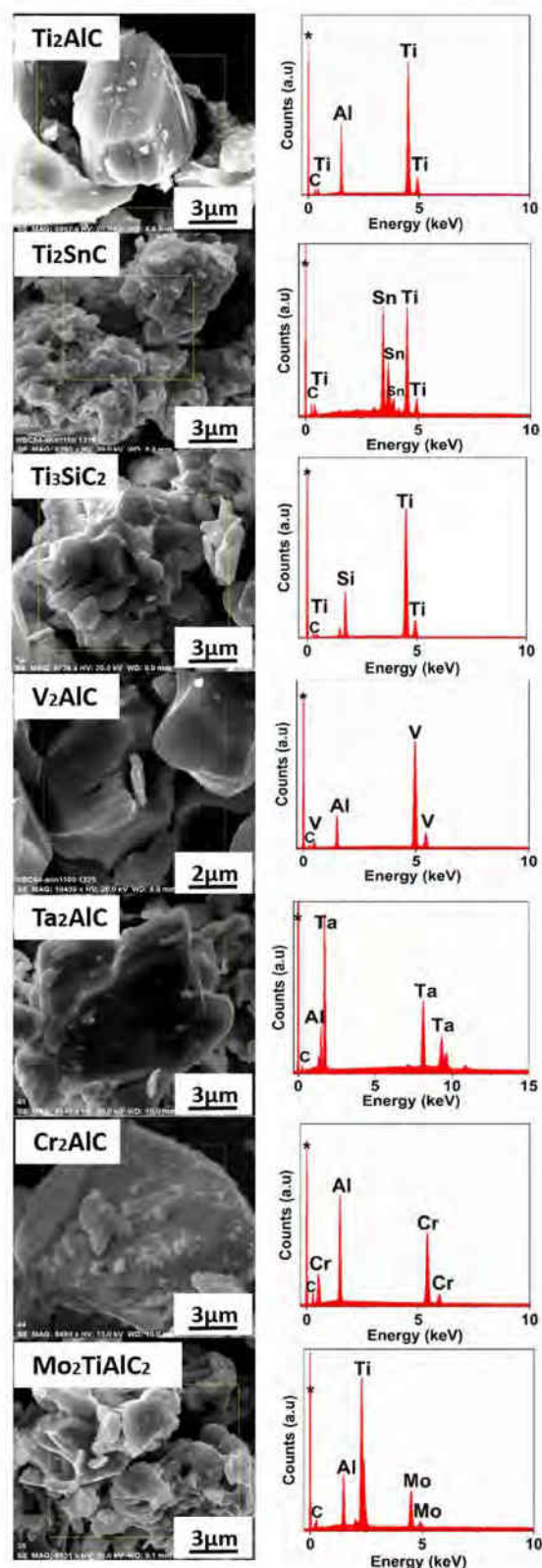


Fig. 1. SEM and EDX spectra of MAX phases.

phases possess catalytically active basal planes that make them ideal for electrochemical applications [25,37]. Linear sweep voltammetry (LSV) measurements were used to study the electrocatalytic performance of the MAX phase. Unmodified glassy carbon (GC) was used as a reference to evaluate the electrocatalytic performance of the materials. Overpotential at a current density of $-1$ mA cm$^{-2}$ was used for comparison of the different phases, where a lower overpotential signifies better HER activity. LSV measurements of drop-casted MAX phases over GC electrode are shown in Fig. 2A, where the measured overpotentials of the MAX phases (Ti$_2$AlC, V$_2$AlC, Ta$_2$AlC, Cr$_2$AlC, Ti$_2$SnC, Mo$_2$TiAlC$_2$) were lower than GC, with the exception of Ti$_3$SiC$_2$ ($-0.85$ V vs. RHE).

The difference in the electrochemical behavior of the materials is related to the surface atoms. In Mo$_2$TiAlC$_2$, the Ti atoms are sandwiched between two molybdenum (Mo) layers that, in turn, are adjacent to the aluminum (Al) planes. This results in a Mo-Ti-Mo-Al-Mo-Ti-Mo stacking order with carbon atoms retaining their positions in the octahedral sites between the M layers [26]. The presence of Mo atoms over the outer layers of the M sites in Mo$_2$TiAlC$_2$ results in different surface properties compared to regular Ti-Alcontaining solid solutions [38] such as Ti$_2$AlC. Thus, in Fig. 2A, we observe that Ti$_2$AlC has a higher overpotential ($-0.76$ V vs. RHE) and Mo$_2$TiAlC$_2$ a low overpotential ($-0.57$ V vs. RHE). In a study conducted by Anasori et al. on the ordered double-transition metal MXene, it was found that the electrochemical response of Mo$_2$TiC$_2$T$_x$ was dominated by the surface Mo layers [39]. The HER mechanism involved in these measurements was analyzed using the Tafel equation $\eta = b \log |j| + a$ (Fig. 2B), where $\eta$ is the overpotential, $j$ is the current density and $b$ is the Tafel slope. Tafel slopes are determined by the rate-limiting steps of HER as follows [40-42]:

Adsorption (Volmer step):

$$H_3O^+ + e^- \rightarrow H_{ads} + H_2O; b \approx 120 \text{ mV dec}^{-1} \tag{1}$$

Desorption (Heyrovsky step):

$$H_{ads} + H_3O^+ + e^- \rightarrow H_2 + H_2O; b \approx 40 \text{ mV dec}^{-1} \tag{2}$$
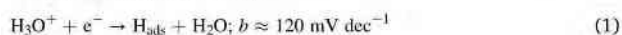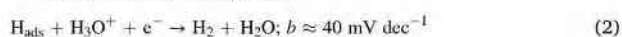
Desorption (Tafel step):

$$H_{ads} + H_{ads} \rightarrow H_2; b \approx 30 \text{ mV dec}^{-1} \tag{3}$$

Ti$_2$SnC showed the lowest Tafel slope of 104 mV dec$^{-1}$ while Ti$_3$SiC$_2$ had the highest Tafel slope value of 186 mV dec$^{-1}$. The Tafel slope values of the other MAX phases Mo$_2$TiAlC$_2$, V$_2$AlC, Cr$_2$AlC, Ta$_2$AlC, Ti$_2$AlC are 127, 127, 129, 129, and 138 mV dec$^{-1}$ respectively. Thus, it could be inferred from the Tafel slope values that the rate-determining step of MAX phases is due to the Volmer adsorption process as the slope is around/more than 120 mV dec$^{-1}$.

The stability of the electrodes was evaluated using the chronoamperometry technique, where a constant potential needed to obtain $-1$ mA cm$^{-2}$ of current density was applied based on LSV measurements in 0.5 M H$_2$SO$_4$. A rotating disk electrode (RDE) with a rotation speed of 600 rpm was used to measure the current continuously for 120 min to monitor the stability of the catalyst. The use of RDE involved continuous rotation of the working electrode to prevent blocking of the catalyst surface by the evolved gas bubbles. However, as the measurement proceeded the bubbles continued to hinder the active area, leading to a rapid decay in the current [43]. The fluctuations in current are observed when the bubbles are removed/formed during the reaction (Fig. S2A–C). For the analyzed MAX phases, the catalyst was found to be stable only for a very short time. In general, the above observations suggest that the MAX phases possess intermediate electrocatalytic performance compared to other reported layered materials.

## 4. Conclusions

In summary, various combinations of elements from the periodic table result in changes to the electronic structure of the material and in
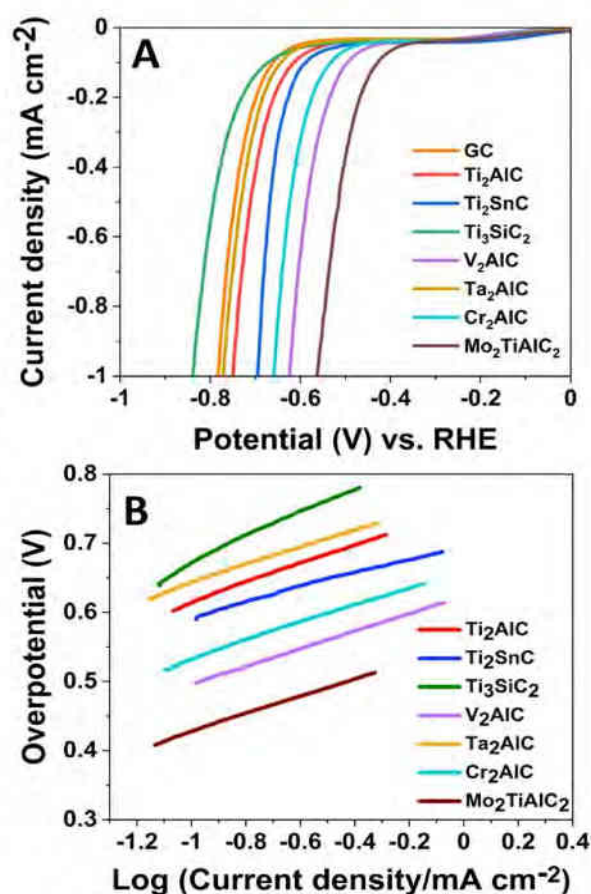


**Fig. 2.** (A) Linear sweep voltammograms of GC, MAX phases at a scan rate of 5 mV s$^{-1}$. (B) Tafel plots of MAX phases.

turn alter its catalytic and electrochemical properties. Morphological analysis of these layered materials using SEM provided an overview of the material. The electrocatalytic activity of MAX phases (Ti$_2$AlC, V$_2$AlC, Ta$_2$AlC, Cr$_2$AlC, Ti$_2$SnC, Mo$_2$TiAlC$_2$, and Ti$_3$SiC$_2$) was successfully analysed using linear sweep voltammetry (LSV). Molybdenum containing layered ternary carbide (Mo$_2$TiAlC$_2$) showed a low overpotential at a current density of $-1$ mA cm$^{-2}$ while Ti$_3$SiC$_2$ showed a high overpotential. New materials will play a vital role in the development of novel, low-cost and efficient electrocatalysts for HER to fuel a sustainable energy system in the future.

## CRediT authorship contribution statement

**K.P. Akshay Kumar:** Investigation, Methodology, Formal analysis, Data curation, Validation, Writing - original draft. **Osamah Alduhaish:** Conceptualization, Analysis, Discussion. **Martin Pumera:** Conceptualization, Resources, Supervision.

## Declaration of Competing Interest

The authors declare that they have no known competing financial interests or personal relationships that could have appeared to influence the work reported in this paper.

## Acknowledgement

## Appendix A. Supplementary data

Supplementary data to this article can be found online at https://doi.org/10.1016/j.elecom.2021.106977.

## References

[1] J. Pang, R.G. Mendes, A. Bachmatiuk, L. Zhao, H.Q. Ta, T. Gemming, H. Liu, Z. Liu, M.H. Rummeli, Applications of 2D MXenes in energy conversion and storage systems, Chem. Soc. Rev. 48 (1) (2019) 72–133, https://doi.org/10.1039/C8CS00324F.

[2] Z. Wang, C. Li, K. Domen, Recent developments in heterogeneous photocatalysts for solar-driven overall water splitting, Chem. Soc. Rev. 48 (7) (2019) 2109–2125, https://doi.org/10.1039/C8CS00542G.

[3] X. Chia, M. Pumera, Characteristics and performance of two-dimensional materials for electrocatalysis, Nat. Catal. 1 (12) (2018) 909–921, https://doi.org/10.1038/s41929-018-0181-7.

[4] A. Venkateshaiah, J.Y. Cheong, S.-H. Shin, K.P. Akshaykumar, T.G. Yun, J. Bae, S. Wacławek, M. Černík, S. Agarwal, A. Greiner, V.V.T. Padil, I.-D. Kim, R. S. Varma, Recycling non-food-grade tree gum wastes into nanoporous carbon for sustainable energy harvesting, Green Chem. 22 (4) (2020) 1198–1208, https://doi.org/10.1039/C9GC04310A.

[5] Z. Ge, B. Fu, J. Zhao, X. Li, B.o. Ma, Y. Chen, A review of the electrocatalysts on hydrogen evolution reaction with an emphasis on Fe, Co and Ni-based phosphides, J. Mater. Sci. 55 (29) (2020) 14081–14104, https://doi.org/10.1007/s10853-020-05010-w.

[6] N. Dubouis, A. Grimaud, The hydrogen evolution reaction: From material to interfacial descriptors, Chem. Sci. 10 (2019) 9165–9181, https://doi.org/10.1039/c9sc03831k.

[7] M.P. Browne, Z. Sofer, M. Pumera, Layered and two dimensional metal oxides for electrochemical energy conversion, Energy Environ. Sci. 12 (1) (2019) 41–58, https://doi.org/10.1039/C8EE02495B.

[8] J. Zhu, L. Hu, P. Zhao, L.Y.S. Lee, K.-Y. Wong, Recent advances in electrocatalytic hydrogen evolution using nanoparticles, Chem. Rev. 120 (2) (2020) 851–918, https://doi.org/10.1021/acs.chemrev.9b00248.

[9] S. Shiva Kumar, V. Himabindu, Hydrogen production by PEM water electrolysis - a review, Mater. Sci. Energy Technol. 2 (2019) 442–454, https://doi.org/10.1016/j.mset.2019.03.002.

[10] J. Zhu, Z.C. Wang, H. Dai, Q. Wang, R. Yang, H. Yu, M. Liao, J. Zhang, W. Chen, Z. Wei, N. Li, L. Du, D. Shi, W. Wang, L. Zhang, Y. Jiang, G. Zhang, Boundary activated hydrogen evolution reaction on monolayer MoS2, Nat. Commun. 10 (2019) 1–7, https://doi.org/10.1038/s41467-019-09269-9.

[11] Y. Jiao, Y. Zheng, K. Davey, S.Z. Qiao, Activity origin and catalyst design principles for electrocatalytic hydrogen evolution on heteroatom-doped graphene, Nat. Energy 1 (2016) 16130, https://doi.org/10.1038/nenergy.2016.130.

[12] L.u. Wang, Z. Sofer, M. Pumera, Will any crap we put into graphene increase its electrocatalytic effect? ACS Nano 14 (1) (2020) 21–25, https://doi.org/10.1021/acsnano.9b00184.

[13] X. Chia, A.Y.S. Eng, A. Ambrosi, S.M. Tan, M. Pumera, Electrochemistry of nanostructured layered transition-metal dichalcogenides, Chem. Rev. 115 (21) (2015) 11941–11966, https://doi.org/10.1021/acs.chemrev.5b00287.

[14] X. Chia, A. Adriano, P. Lazar, Z. Sofer, J. Luxa, M. Pumera, Layered platinum dichalcogenides (PtS2, PtSe2, and PtTe2) electrocatalysis: monotonic dependence on the chalcogen size, Adv. Funct. Mater. 26 (24) (2016) 4306–4318, https://doi.org/10.1002/adfm.201505402.

[15] J. Yang, H.S. Shin, Recent advances in layered transition metal dichalcogenides for hydrogen evolution reaction, J. Mater. Chem. A 2 (17) (2014) 5979–5985, https://doi.org/10.1039/C3TA14151A.

[16] C.(. Zhu, D. Gao, J. Ding, D. Chao, J. Wang, TMD-based highly efficient electrocatalysts developed by combined computational and experimental approaches, Chem. Soc. Rev. 47 (12) (2018) 4332–4356, https://doi.org/10.1039/C7CS00705A.

[17] Y. Wang, B. Kong, D. Zhao, H. Wang, C. Selomulya, Strategies for developing transition metal phosphides as heterogeneous electrocatalysts for water splitting, Nano Today 15 (2017) 26–55, https://doi.org/10.1016/j.nantod.2017.06.006.

[18] H. Zhang, A.W. Maijenburg, X. Li, S.L. Schweizer, R.B. Wehrspohn, Bifunctional heterostructured transition metal phosphides for efficient electrochemical water splitting, Adv. Funct. Mater. 30 (2020) 2003261, https://doi.org/10.1002/adfm.202003261.

[19] R. Gusmão, Z. Sofer, D. Bouša, M. Pumera, Pnictogen (As, Sb, Bi) nanosheets for electrochemical applications are produced by shear exfoliation using kitchen blenders, Angew. Chem. Int. Ed. 56 (46) (2017) 14417–14422, https://doi.org/10.1002/anie.201706389.

[20] Y. Chen, G. Zhao, W. Sun, Strategies of engineering 2D nanomaterial-based electrocatalysts toward hydrogen evolution reaction, Mater. Renewable Sustainable Energy 9 (2020) 1–11, https://doi.org/10.1007/s40243-020-00170-w.

[21] M. Radovic, M.W. Barsoum, MAX phases: Bridging the gap between metals and ceramics, Am. Ceram. Soc. Bull. 92 (2013) 20–27.

[22] M. Sokol, V. Natu, S. Kota, M.W. Barsoum, On the chemical diversity of the MAX phases, Trends Chem. 1 (2) (2019) 210–223, https://doi.org/10.1016/j.trechm.2019.02.016.

[23] Z. Sun, D. Music, R. Ahuja, S. Li, J.M. Schneider, Bonding and classification of nanolayered ternary carbides, Phys. Rev. B - Condens. Matter Mater. Phys. 70 (2004) 1–3, https://doi.org/10.1103/PhysRevB.70.092102.

[24] P. Eklund, J. Rosen, P.O.Å. Persson, Layered ternary Mn+1AXn phases and their 2D derivative MXene: An overview from a thin-film perspective, J. Phys. D Appl. Phys. 50 (11) (2017) 113001, https://doi.org/10.1088/1361-6463/aa57bc.

[25] N.F. Rosli, M.Z.M. Nasir, N. Antonatos, Z. Sofer, A. Dash, J. Gonzalez-Julian, A. C. Fisher, R.D. Webster, M. Pumera, MAX and MAB phases: two-dimensional layered carbide and boride nanomaterials for electrochemical applications, ACS Appl. Nano Mater. 2 (2019) 6010–6021, https://doi.org/10.1021/acsanm.9b01526.

[26] B. Anasori, M. Dahlqvist, J. Halim, E.J. Moon, J. Lu, B.C. Hosler, E.N. Caspi, S. J. May, L. Hultman, P. Eklund, Experimental and theoretical characterization of ordered MAX phases, J. Appl. Phys. 118 (2015) 094304, https://doi.org/10.1063/1.4929640.

[27] Z. Liu, L. Zheng, L. Sun, Y. Qian, J. Wang, M. Li, (Cr2/3Ti1/3)3AlC2 and (Cr5/8Ti3/8)4AlC3: New MAX-phase compounds in Ti-Cr-Al-C system, J. Am. Ceram. Soc. 97 (2014) 67–69, https://doi.org/10.1111/jace.12731.

[28] Z.M. Sun, Progress in research and development on MAX phases: a family of layered ternary compounds, Int. Mater. Rev. 56 (2011) 143–166, https://doi.org/10.1179/1743280410Y.0000000001.

[29] M. Ade, H. Hillebrecht, Ternary borides Cr2AlB2, Cr3AlB4, and Cr4AlB6: the first members of the series (CrB2)nCrAl with n = 1, 2, 3 and a unifying concept for ternary borides as MAB-phases, Inorg. Chem. 54 (2015) 6122–6135, https://doi.org/10.1021/acs.inorgchem.5b00049.

[30] X.H. Wang, Y.C. Zhou, Layered machinable and electrically conductive Ti 2 AlC and Ti 3 AlC 2 ceramics : a review, J. Mater. Sci. Technol. 26 (2010) 385–416, https://doi.org/10.1016/S1005-0302(10)60064-3.

[31] M. Magnuson, M. Mattesini, Chemical bonding and electronic-structure in MAX phases as viewed by X-ray spectroscopy and density functional theory, Thin Solid Films 621 (2017) 108–130, https://doi.org/10.1016/j.tsf.2016.11.005.

[32] M. Khazaei, A. Ranjbar, K. Esfarjani, D. Bogdanovski, R. Dronskowski, S. Yunoki, Insights into exfoliation possibility of MAX phases to MXenes, Phys. Chem. Chem. Phys. 20 (13) (2018) 8579–8592, https://doi.org/10.1039/C7CP08645H.

[33] Y. Gogotsi, B. Anasori, The rise of MXenes, ACS Nano 13 (8) (2019) 8491–8494, https://doi.org/10.1021/acsnano.9b06394.

[34] G. Gao, A.P. O'Mullane, A. Du, 2D MXenes: a new family of promising catalysts for the hydrogen evolution reaction, ACS Catal. 7 (2017) 494–500, https://doi.org/10.1021/acscatal.6b02754.

[35] Z.W. Seh, K.D. Fredrickson, B. Anasori, J. Kibsgaard, A.L. Strickler, M. R. Lukatskaya, Y. Gogotsi, T.F. Jaramillo, A. Vojvodic, Two-dimensional molybdenum carbide (MXene) as an efficient electrocatalyst for hydrogen evolution, ACS Energy Lett. 1 (3) (2016) 589–594, https://doi.org/10.1021/acsenergylett.6b00247.

[36] K.P.A. Kumar, K. Ghosh, O. Alduhaish, M. Pumera, Dip-coating of MXene and transition metal dichalcogenides on 3D-printed nanocarbon electrodes for the hydrogen evolution reaction, Electrochem. Commun. 122 (2020), 106890, https://doi.org/10.1016/j.elecom.2020.106890.

[37] L.T. Alameda, C.F. Holder, J.L. Fenton, R.E. Schaak, Partial etching of Al from MoAlB single crystals to expose catalytically active basal planes for the hydrogen evolution reaction, Chem. Mater. 29 (21) (2017) 8953–8957, https://doi.org/10.1021/acs.chemmater.7b02511.

[38] B. Anasori, J. Halim, J. Lu, C.A. Voigt, L. Hultman, M.W. Barsoum, Mo2TiAlC2: A new ordered layered ternary carbide, Scr. Mater. 101 (2015) 5–7, https://doi.org/10.1016/j.scriptamat.2014.12.024.

[39] B. Anasori, Y. Xie, M. Beidaghi, J. Lu, B.C. Hosler, L. Hultman, P.R.C. Kent, Y. Gogotsi, M.W. Barsoum, Transition metals carbides (MXenes), ACS Nano 9 (2015) 9507–9516, https://doi.org/10.1021/acsnano.5b03591.

[40] C.G. Morales-Guio, L.A. Stern, X. Hu, Nanostructured hydrotreating catalysts for electrochemical hydrogen evolution, Chem. Soc. Rev. 43 (2014) 6555–6569, https://doi.org/10.1039/c3cs60468c.

[41] Y. Li, H. Wang, L. Xie, Y. Liang, G. Hong, H. Dai, MoS2 nanoparticles grown on graphene: an advanced catalyst for the hydrogen evolution reaction, J. Am. Chem. Soc. 133 (2011) 7296–7299, https://doi.org/10.1021/ja201269b.

[42] M. Zeng, Y. Li, Recent advances in heterogeneous electrocatalysts for the hydrogen evolution reaction, J. Mater. Chem. A 3 (29) (2015) 14942–14962, https://doi.org/10.1039/C5TA02974K.

[43] S.K. Singh, D. Kumar, V.M. Dhavale, S. Pal, S. Kurungot, Strategic preparation of efficient and durable NiCo alloy supported N-doped porous graphene as an oxygen evolution electrocatalyst: a theoretical and experimental investigation, Adv. Mater. Interfaces 3 (2016) 1–14, https://doi.org/10.1002/admi.201600532.

# Supplementary data

## Electrocatalytic activity of Layered MAX Phases for Hydrogen Evolution Reaction

K P Akshay Kumar[a], Osamah Alduhaish[b] and Martin Pumera[a, b, c, d*]

[a]Future Energy and Innovation Laboratory, Central European Institute of Technology, Brno University of Technology, Purkyňova 123, 61200 Brno, Czech Republic

[b]Chemistry Department P.O.Box 2455, College of Science King Saud University Riyadh 11451, Saudi Arabia

[c]Department of Chemistry and Biochemistry, Mendel University in Brno, Zemedelska 1, CZ-613 00, Brno, Czech Republic

[d]Department of Medical Research, China Medical University Hospital, China Medical University, No. 91 Hsueh-Shih Road, Taichung 40402, Taiwan

Email: pumera.research@gmail.com
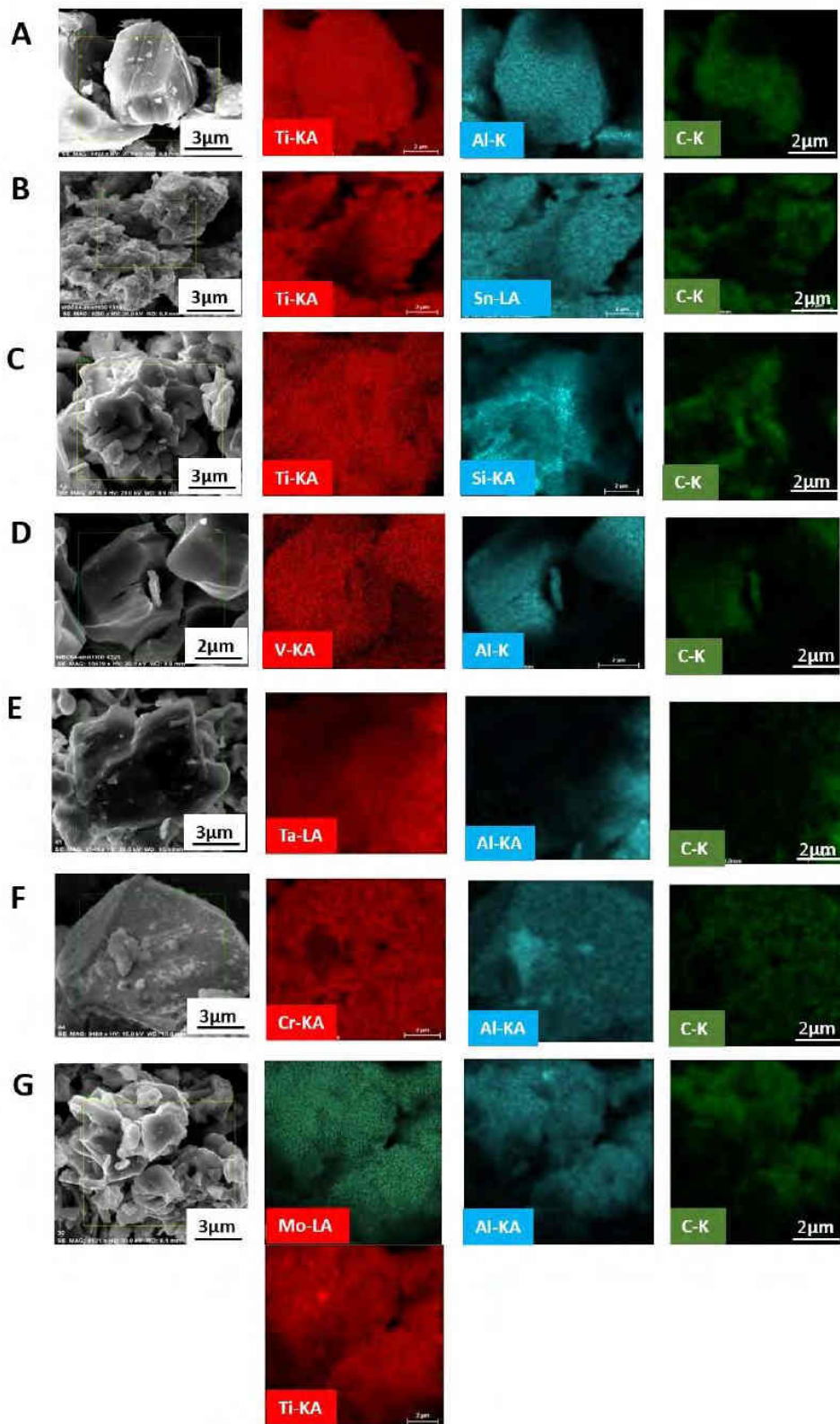
Fig. S1. SEM, EDX mapping of MAX phases (A) Ti$_2$AlC (B) Ti$_2$SnC (C) Ti$_3$SiC$_2$ (D) V$_2$AlC (E) Ta$_2$AlC (F) Cr$_2$AlC (G) Mo$_2$TiAlC$_2$

Table S1. Atomic percentage of MAX phases from EDX spectral analysis

| MAX | M (%) | A (%) | X (%) |
|---|---|---|---|
| $Ti_2AlC$ | 49.97 | 23.73 | 21.74 |
| $Ti_2SnC$ | 49.43 | 23.14 | 27.43 |
| $Ti_3SiC_2$ | 57.95 | 19.23 | 18.02 |
| $V_2AlC$ | 49.50 | 24.08 | 26.43 |
| $Ta_2AlC$ | 52.58 | 23.01 | 23.41 |
| $Cr_2AlC$ | 44.96 | 27.68 | 27.36 |
| $Mo_2TiAlC_2$ | 26.63 (Mo) / 12.91 (Ti) | 11.84 | 48.63 |
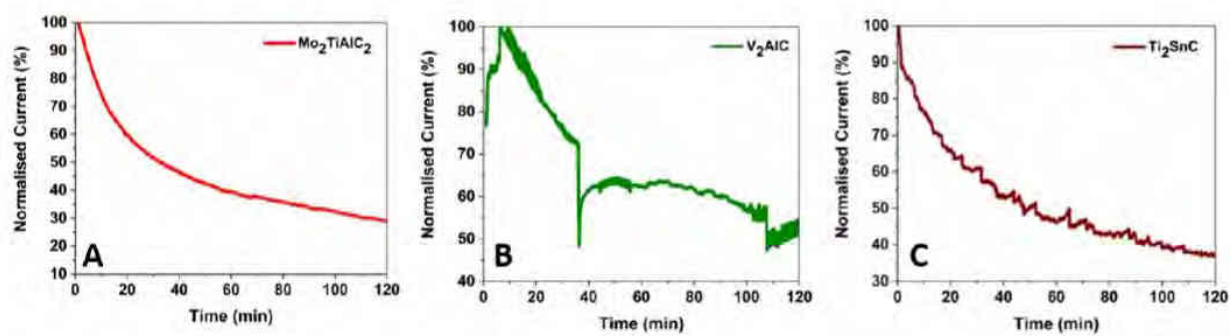


Fig. S2. Chronoamperometric measurements of MAX phase over GC for 120 minutes in 0.5 M $H_2SO_4$.

68

### 5.1.3 Fe-MOF electrocatalyst for nitrate to ammonia conversion

**Motivation**

With the search for newer electrocatalyst material for catalytic applications, MOF has emerged as an active electrode material in recent times. Merits such as enhanced structural, compositional integrity along with enhanced activity during catalytic reduction makes them desirable for catalytic applications. Evaluating the performance of MOF electrocatalyst upon subjection to thermal activation could be interesting for ammonia production.

**Objective**

Pristine and thermally activated PCN-250-Fe$_3$ MOF will be examined for electrocatalytic NRA. As a part of this study, cyclic stability, MOF stability in solvents, NRA at various concentrations, and theoretical studies will be carried out for both catalysts.

**Outcome**

Employing newer and simpler strategies such as thermal activation of MOF samples was shown to enhance ammonia production. Such approaches are vital for enhancing the material properties, especially towards electrocatalysis, rather than relying on time consuming material modification approaches. In short, the following studies open newer possibilities to tailor catalyst surfaces for catalytic applications such as ammonia synthesis.

**Contribution**

Investigation, methodology, conceptualization, formal analysis, data curation, characterizations, experimentation, validation, discussions, funding acquisition, writing (original draft, review and editing).

**Article**

The article was published and the details of the article are as follows:

Akshay Kumar K. Padinjareveetil, Juan V. Perales-Rondon, Dagmar Zaoralová, Michal Otyepka, Osamah Alduhaish, and Martin Pumera* *Fe-MOF Catalytic Nanoarchitectonic toward Electrochemical Ammonia Production*, **ACS Appl. Mater. Interfaces**, 2023, 15, 40, 47294–47306, https://doi.org/10.1021/acsami.3c12822, (IF: 9.5).

# Fe-MOF Catalytic Nanoarchitectonic toward Electrochemical Ammonia Production

Akshay Kumar K. Padinjareveetil, Juan V. Perales-Rondon, Dagmar Zaoralová, Michal Otyepka, Osamah Alduhaish, and Martin Pumera*

Read Online

ACCESS | 📊 Metrics & More | 📰 Article Recommendations | 🆂ℹ Supporting Information
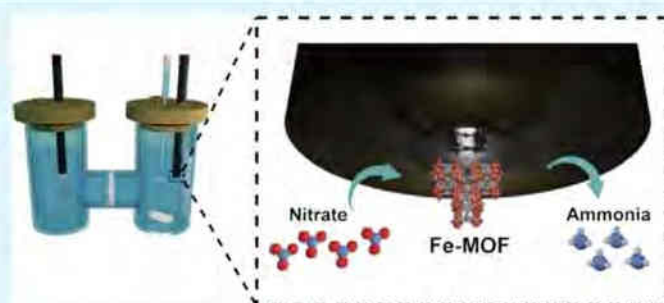
**ABSTRACT:** Electrochemical reduction of nitrate into ammonia has lately been identified as one among the promising solutions to address the challenges triggered by the growing global energy demand. Exploring newer electrocatalyst materials is vital to make this process effective and feasible. Recently, metal–organic framework (MOF)-based catalysts are being well investigated for electrocatalytic ammonia synthesis, accounting for their enhanced structural and compositional integrity during catalytic reduction reactions. In this study, we investigate the ability of the PCN-250-Fe$_3$ MOF toward ammonia production in its pristine and activated forms. The activated MOF catalyst delivered a faradaic efficiency of about 90% at −1 V vs RHE and a yield rate of $2.5 \times 10^{-4}$ mol cm$^{-2}$ h$^{-1}$, while the pristine catalyst delivered a 60% faradaic efficiency at the same potential. Theoretical studies further provide insights into the nitrate reduction reaction mechanism catalyzed by the PCN-250-Fe$_3$ MOF catalyst. In short, simpler and cost-effective strategies such as pretreatment of electrocatalysts have an upper hand in aggravating the intrinsic material properties, for catalytic applications, when compared to conventional material modification approaches.

**KEYWORDS:** metal–organic framework, PCN-250-Fe$_3$, ammonia synthesis, thermal activation, electrochemical nitrate reduction, electrocatalysts

## 1. INTRODUCTION

The exponential growth in the global population has led to a significant decline in the availability of fossil fuels and increased energy demands, especially in a low-carbon economy. Exploring clean, secure, and renewable energy sources therefore has become a matter of serious concern for the scientific community across the world.[1–5] Studies have shown ammonia to be a potential carbon-free candidate to mitigate the growing energy demand, owing to its high gravimetric energy density (3 kWh kg$^{-1}$) and high hydrogen capacity (17.65 wt %), facilitating ease in storage and transportation, along with clean emissions.[6–9] Along with being a green hydrogen-rich fuel, ammonia is also fundamental to the production of fertilizers in modern agricultural sectors and finds diverse applications in fields such as pharmaceuticals, textiles, refrigeration, etc. The conventional strategy employed for the large-scale production of ammonia is the Haber–Bosch

process,[10,11] where both nitrogen and hydrogen are subjected to high-temperature (400–500 °C) and high-pressure (150–300 atm) conditions in the presence of a heterogeneous iron (Fe)-based catalyst. However, being an energy intensive process, involving large emissions of carbon dioxide (CO$_2$), there have been rigorous attempts in finding alternatives to this method.[12–16] Electrochemical ammonia synthesis has emerged as a suitable technique for ammonia production, with nitrogen reduction reaction being the most extended and studied method.[17–20] Although the process has evolved with time, yet

A

limitations such as low solubility, high bond dissociation energy of N≡N (941 kJ mol$^{-1}$), low selectivity at high current densities, modest faradaic efficiency (FE), low yield rate, competitive hydrogen evolution reaction (HER), and sluggish kinetic hamper its frequent use.[21−23] The limitations therefore invite further improvements and newer techniques for enabling large-scale production under mild conditions.

Alternative techniques such as nitrate reduction into ammonia (NRA) have gained momentum for ammonia synthesis, addressing several limitations faced by the aforementioned techniques.[24−26] Recognizing the extensive presence of nitrate ions, in the environment, especially as a pollutant in waters, it has been considered as a perfect alternative nitrogen source for ammonia synthesis as well.[27,28] Designing a strategy to eradicate a water pollutant like nitrate, which also brings a serious threat to human health, represents an advantage in terms of both energy production and addressing environmental issues. Thus, the nitrate electro-reduction can be considered as an eco-friendly and efficient approach of converting aqueous waste nitrate into ammonia under favorable operating conditions.[29] The conversion of nitrate to ammonia involves an eight-electron transfer that proceeds through multiple reaction pathways at a definite potential region[30,31] However, side reactions such as HER can also occur in this region and result in the consumption of electrons for hydrogen generation and eventually in decreased FE and selectivity. Thus, the necessity for designing specific electrocatalysts is of utmost importance, which dismisses both N≡N bond formation and competitive HER, and also efficiently reducing nitrate into ammonia is of utmost importance. Electrocatalysts such as transition metals,[31,32] their oxides,[33] metal single-atom catalysts,[34] or alloys[24] have been studied for ammonia production from nitrate. Tailoring the surface of the electrocatalysts is also another strategy to enhance the properties of the catalyst. For instance, surface modifications of electrocatalysts with negatively charged species are known to suppress the HER interference during the reaction, resulting in enhanced activity and selectivity for NRA applications.[35] In another study, 2D Ti$_3$C$_2$T$_x$ MXene was also used as a suitable substrate to disperse and anchor copper (Cu) over it, resulting in molecular Cu@MXene catalysts.[36] The catalyst gave around a 94% ammonia selectivity and 90.5% nitrate conversion rate, thereby opening up newer strategies to develop electrocatalysts for NRA.

From the past two decades, metal−organic frameworks (MOFs) have gained significant recognition owing to their porous nature, crystalline structure, tunable functionality, and high surface area within the single entity of the material.[37,38] The members of this emerging group are synthesized by self-assembling of organic ligands with desired metal centers, having several potential applications.[39] Previously, MOFs have been well studied for gas storage, separation, energy storage, and multiple other applications. However, only fewer studies have been reported on MOFs for the ammonia production via NRA. In a recent study, a MOF-derived cobalt (Co)-doped Fe/Fe$_2$O$_3$ catalyst has been reported by Zhang et al. for electrochemical nitrate reduction.[40] The electronic structure of the Fe d band center was tuned via Co doping, resulting in the modulation of adsorption energy of intermediates and inhibiting hydrogen formation. This Co-doped Fe/Fe$_2$O$_3$ MOF electrocatalyst resulted in a 99% ammonia selectivity, an FE of 85.2%, and a high nitrate removal capacity of 100.8 mg N/g$_{cat}$ h. In another recent work by Qin et al., Ru$_x$O$_y$

clusters anchored on nickel (Ni) MOFs (RuNi-MOFs) were studied for electrocatalytic NRA.[41] The catalyst achieved an FE of 73% at −1.2 V vs Ag/AgCl for NH$_4^+$ and NH$_4^+$−N yield rates of 274 μg h$^{-1}$ mg$_{cat}^{-1}$ at −1.7 V vs Ag/AgCl.

The above works clearly discuss the possibility of engineering MOFs via heteroatom doping and anchoring molecular catalysts for efficient electrocatalytic NRA. However, since this study is still in its infancy, exploring the further possibility of modifying MOFs without any doping or anchoring of active components becomes relevant to understand the real potential of MOFs in this field. For instance, studies on the differences in the intrinsic material property when subjected to thermal activation have never been undertaken before, especially for electrocatalytic applications such as ammonia production. Such observations can be vital, especially in enabling direct enhancement of material toward ammonia synthesis, without any additional and time-consuming techniques such as doping, substitution, functionalization, etc.

In this study, an Fe metal center-based MOF, known as the PCN-250-Fe$_3$ MOF, has been examined for electrocatalytic NRA in both its pristine and activated forms. The activated material gave a substantial improvement in FE (~90% at −1.0 V vs reversible hydrogen electrode (RHE)) when compared to its pristine form. Cyclic stability and MOF stability in solvents with time are also assessed as a part of this study. The thermodynamic feasibility of the PCN-250-Fe$_3$ MOF catalyst toward NRA is corroborated by density functional theory (DFT) calculations as well. This study is a breakthrough in NRA using MOF materials, especially in understanding the importance of material pretreatments for catalytic applications.

## 2. EXPERIMENTAL SECTION

**2.1. Reagents and Materials.** All chemical reagents, such as potassium nitrate (KNO$_3$), sodium sulfate (Na$_2$SO$_4$), hydrochloric acid (HCl), sulfamic acid (H$_3$NSO$_3$), p-aminobenzenesulfonamide (H$_2$NC$_6$H$_4$SO$_2$NH$_2$), N-(1-naphthyl)ethylenediamine dihydrochloride (C$_{10}$H$_7$NHCH$_2$CH$_2$NH$_2$·2HCl), phosphoric acid (H$_3$PO$_4$), sodium hydroxide (NaOH), ammonium chloride (NH$_4$Cl), citric acid (HOC(COOH)(CH$_2$COOH)$_2$), salicylic acid (2-(HO)-C$_6$H$_4$CO$_2$H), sodium hypochlorite solution (NaClO, 6−14%), sodium nitroferricyanide (Na$_2$[Fe(CN)$_5$NO]), and sodium nitrite (NaNO$_2$), were used as received from Merck and Sigma-Aldrich Co., Ltd., without further purification. The PCN-250-Fe$_3$ MOF also was procured from commercial sources, called framergy. All solutions were prepared by using ultrapure water (18.2 MΩ cm resistivity at 25 °C).

**2.2. Characterization.** The scanning electron microscopy (SEM) images were obtained from a LYRA 3 SEM (TESCAN) and Verios 460L (Thermo Fisher Scientific, USA). The energy-dispersive X-ray spectroscopy (EDS) images were obtained with a Bruker XFlash 5010 detector attached with the LYRA. X-ray photoelectron spectroscopy (XPS) was measured using a Kratos AXIS Supra instrument with monochromatized Al K$_α$ excitation (1486.7 eV), and the data were analyzed using CasaXPS software. The X-ray diffraction (XRD) measurements were conducted with a diffractometer (SmartLab 3 kW, Rigaku) with a Bragg−Brentano geometry (Cu K$_α$ radiation; λ = 0.15418 nm) operated at a voltage of 40 kV and a current of 30 mA. The ultraviolet−visible (UV−vis) absorbance spectra from the wavelength range 190 to 900 nm were measured on a double-beam Jasco Co. Model V-750. $^1$H NMR experiments were conducted using a 500 MHz Bruker, ADVANCE NEO 4500 de.

**2.3. Sample Preparation.** The MOF samples were activated using a vacuum oven at 150 °C for 3 h. Further, the MOF samples were measured to obtain a 1 mg·mL$^{-1}$ concentration in 10 mL of distilled water. To obtain an optimal dispersion, the solution was sonicated using an ultrasonic homogenizer probe for 30 min at an amplitude of 70%, 20 s of sonication, and 10 s of resting. To this

**Scheme 1. (A, B) Chemical Structure of the ABTC Linker with the $Fe_3$-$(\mu_3$-O)(COO)$_6$ Node. (C) Crystallographic Structure of the PCN-250-Fe$_3$ MOF (Carbon Atoms Are Gray, Oxygen Red, Nitrogen Blue, Hydrogen White, and Iron Orange). (D) Schematic Representation of Thermal Activation of the MOF**
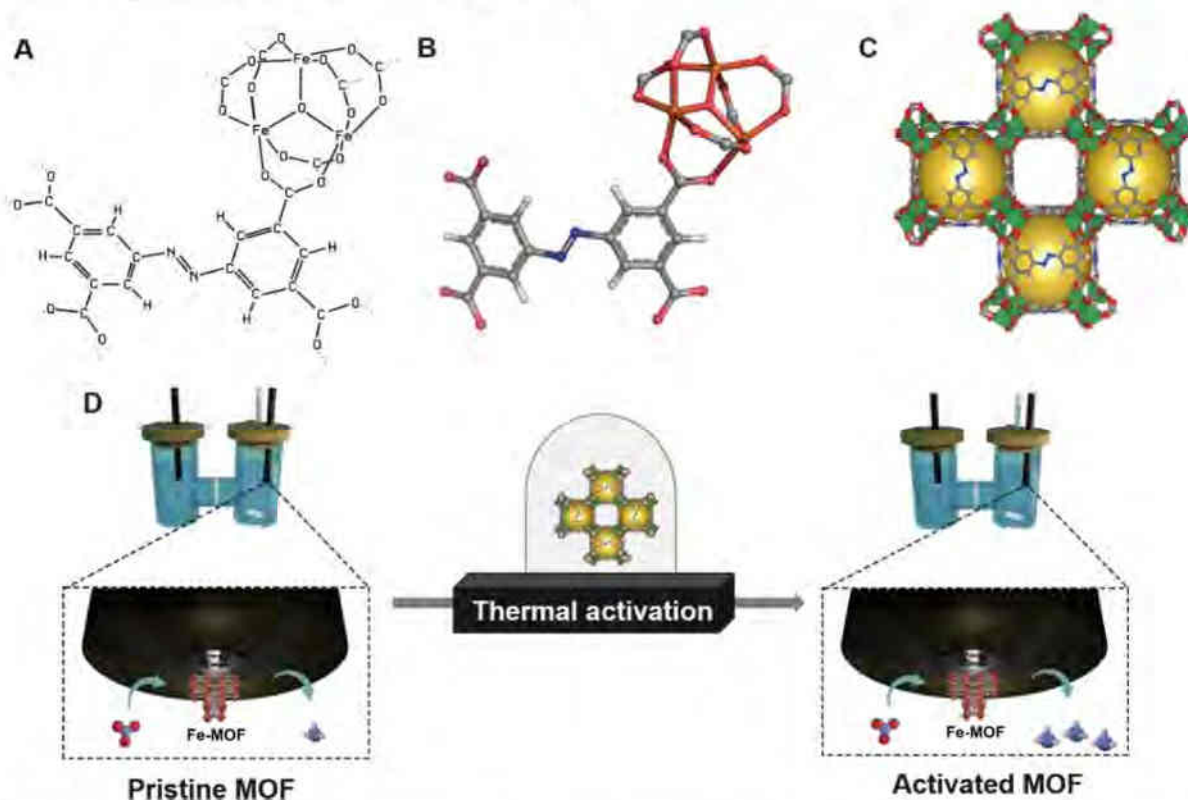


dispersion, 40 μL of Nafion binder (∼5% in a mixture of lower aliphatic alcohols and water) is added and sonicated well. From the stock solution, 10 μL of sample is drop-casted over the glassy carbon (GC) electrode and dried prior to assembling it in the H cell. Studies on pristine/nonactivated samples were carried out by direct sonication of MOF samples in the similarly ascribed concentration range and further analyzed for NRA.

**2.4. Electrochemical Measurements.** The electrochemical measurements were carried out using an Autolab PGSTAT204 (Metrohm) operated by Nova 2.14 software. The electrolysis experiments were conducted in an H-type electrolytic cell with a frit separation. The PCN-250-Fe$_3$ MOF over GC served as the working electrode at the cathodic end of the H cell along with commercial Ag/AgCl reference electrode, while platinum wire served as the counter electrode at the anodic end. The electrolytic experiments were conducted at multiple potentials (−0.6 to −1.4 V vs RHE), with each experiment carried out for 1 h with a constant magnetic stirring rate (100 rpm). All potentials were recorded against the RHE. The conversion of Ag/AgCl to RHE is carried out via the following equation: $E_{RHE} = E_{Ag/AgCl} + 0.0591 \text{ pH} + 0.199$.

**2.5. Colorimetric Determination of Ion Concentrations.** Quantification of the ion concentration of different products was carried out using well-known colorimetric methods. A UV−vis spectrophotometer was used to detect the concentration of different reagents/products of pre- and post-electrolysis experiments.

**2.6. Determination of Ammonia.** Ammonia (NH$_3$) concentration after electrolysis was determined by the well-known indophenol blue method.[34] Once the electrolytic experiment was performed, an aliquot of the electrolyte was taken out from the cell, and a proper dilution to 600 μL of solution was done. Subsequently, 600 μL of a 3 M NaOH solution containing 10 wt % salicylic acid and

10 wt % sodium citrate was added to the solution. After that, 300 μL of 0.20 M NaClO and 60 μL of 2.0 wt % C$_5$FeN$_6$Na$_2$O (sodium nitroferricyanide) solution was also added to the solution. The resulting solution was allowed to rest for 2 h, after which the UV−vis absorption spectrum was taken. NH$_3$ concentration was determined by the formation of the indophenol blue product that was quantified using the absorbance at a wavelength of 655 nm. The corresponding calibration curve was obtained using standard solutions of ammonium chloride.

**2.7. Determination of Nitrite.** A previously reported quantitative protocol was used to carry out nitrite (NO$_2^-$) determination.[42,43] To do so, a color reagent containing p-aminobenzenesulfonamide (0.4 g), N-(1-naphthyl)ethylenediamine dihydrochloride (0.02 g), ultrapure water (5 mL), and phosphoric acid (1 mL, $\rho$ = 1.70 g/mL) was prepared. Post electrolysis, a certain volume of electrolyte was taken out from the cell and diluted to 1.5 mL to the detection range. After that, 50 μL of the color reagent was added into the 1.5 mL solution, followed by the addition of 100 μL of phosphoric acid ($\rho$ = 1.70 g/mL), and mixed uniformly. The absorption intensity at a wavelength of 540 nm was recorded after the solution rested for 20 min. The calibration curve concentration−absorbance was carried out by using a series of standard sodium nitrite solutions.

**2.8. Determination of Ammonia by the $^1$H NMR Quantitative Method and Isotopic Labeling Experiment.** Post electrolysis, an aliquot of the electrolyte was collected from the H cell. Concentrated H$_2$SO$_4$ (250 μL) was added to 5 mL of electrolyte to ensure a high acidic condition that is ideal to be quantified by $^1$H NMR and using maleic acid as an internal standard. The calibration curve was carried out as follows: a series of standard solutions of known concentrations of $^{14}$NH$_4^+$ (50, 100, 150, 200, and 250 ppm) were prepared in 0.5 M Na$_2$SO$_4$ + 0.1 M KNO$_3$. Next, 5 mL of each
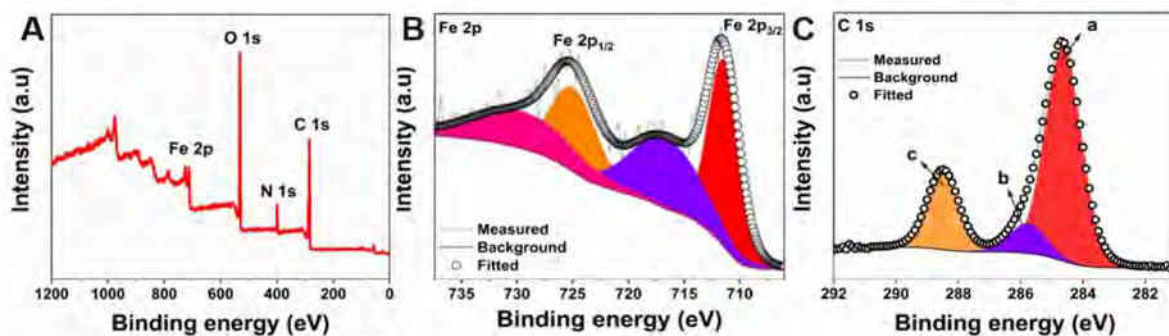
**Figure 1.** (A) XPS survey spectrum of the pristine PCN-250-Fe$_3$ MOF phase. Deconvoluted XPS spectrum for (B) Fe 2p and (C) C 1s.
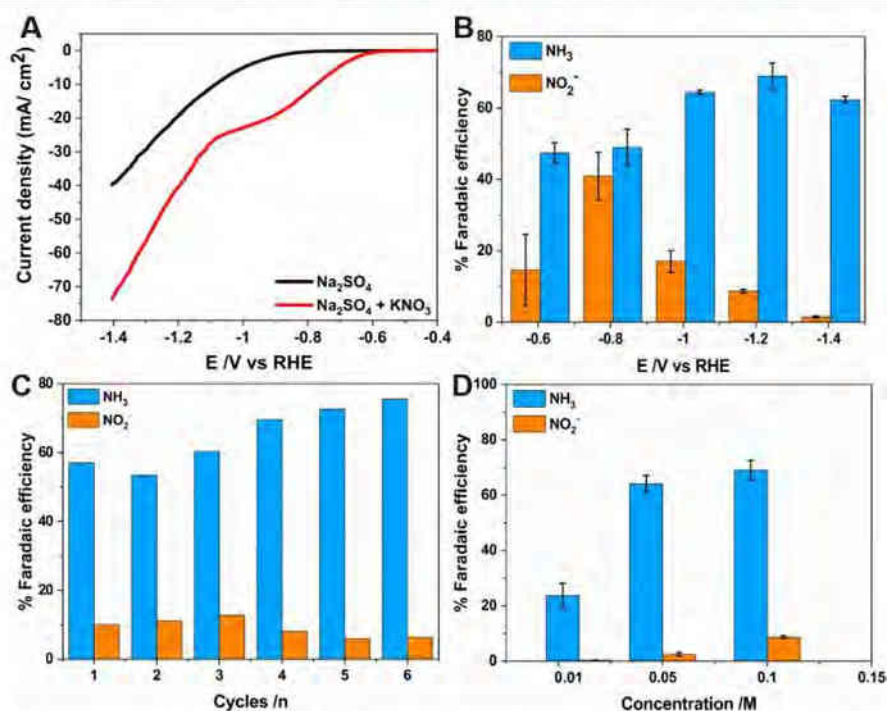


**Figure 2.** Electrocatalytic experiments of the pristine PCN-250-Fe$_3$ MOF. (A) LSV curves in the Na$_2$SO$_4$ 0.5 M electrolyte with and without KNO$_3$ 0.1 M. The experiment was conducted at a scan rate of 20 mV s$^{-1}$. (B) Potential-dependent FE plots of NH$_3$ and NO$_2^-$. (C) FE of NH$_3$ and NO$_2^-$ on consecutive cycling electrolytic tests at −1.2 V vs RHE (the electrolyte used was Na$_2$SO$_4$ 0.5 M + KNO$_3$ 0.1 M). (D) FEs of the nonactivated pristine Fe-based MOF sample toward NH$_3$ and NO$_2^-$ at different concentrations of KNO$_3$.

solution was mixed with 0.002 g of maleic acid. To carry out the measurement, 500 μL of this solution was placed in an NMR tube, and 50 μL of deuterium oxide (D$_2$O) was added to it for the NMR detection. The calibration curve was achieved by using the peak area ratio between $^{14}$NH$_4^+$ and maleic acid.

### 2.9. Calculation of Different Parameters to Evaluate the Performance of the Electrocatalysts.

$$\text{Faradaic efficiency} = \frac{nFn_{\text{NH}_3\text{orNO}_2^-}}{Q} \times 100\% \qquad (1)$$

$$\text{Yield rate} = \frac{n_{\text{NH}_3}}{tA} \qquad (2)$$

where $F$ is the faradaic constant (96485 C mol$^{-1}$), $n_{\text{NH}_3 \text{ or NO}_2^-}$ is the number of mol of NH$_3$ or NO$_2^-$, $n$ is the number of electrons

involved in the electrochemical reaction (8 for NH$_3$ and 2 for NO$_2^-$), $t$ is the electrolysis time (1 h), $A$ is the area of the electrode, and $Q$ is the total charge measured during the electrolytic experiment.

### 2.10. Computational Study Details.
Ground state structures of all investigated species were optimized by the M06-L method[44] in combination with the Def2TZVP basis set[45] utilizing the Gaussian 16 software.[46] The M06-L functional is recommended for calculations of transition metal complexes and inorganic and organometallic systems.[44] It displayed also a good performance in calculations of hydrocarbon adsorption on Fe-MOF-74[47] and alkane oxidative dehydrogenation by Fe$_2$Me MOF nodes.[48] The spin-unrestricted formalism was applied in all calculations. The solvent effects were considered by applying the universal continuum model based on electron density.[49] The computational hydrogen electrode method[50,51] was applied to calculate reaction energies assuming that the chemical potential of electron−proton pair ($\mu_{H^+ + e^-}$) is equal to the
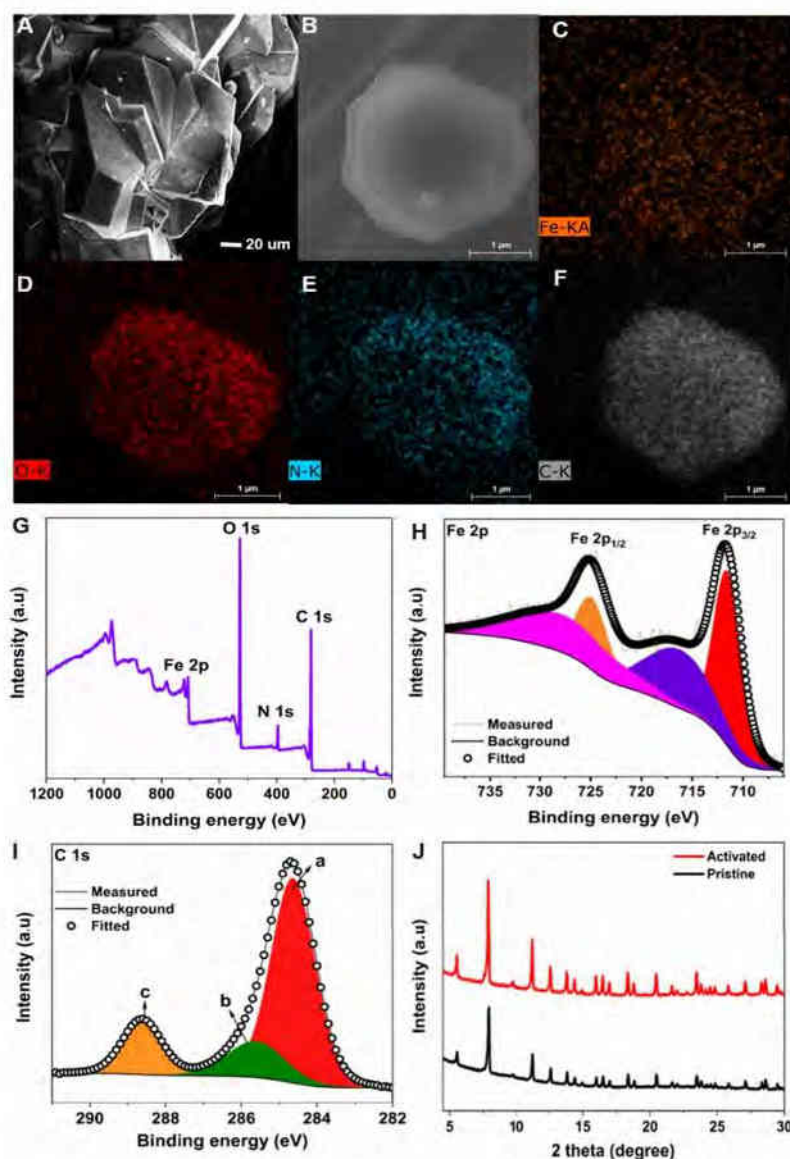
**Figure 3.** Activated PCN-250-Fe$_3$ MOF (A, B) SEM image; (C−F) EDS mapping of elements (scale bar 1 $\mu$m); (G) XPS survey spectrum. Deconvoluted XPS spectrum of (H) Fe 2p and (I) C 1s; (J) XRD pattern of both activated and pristine MOF samples.

chemical potential of 1/2 H$_2$ ($\mu_{1/2H_2}$). The structure of PCN-250 consists of trimetallic nodes bridged by ABTC linkers (ABTC = 3,3′,5,5′-azobenzenetetracarboxylate; Scheme 1A,B). A cluster model of the Fe$_3$-($\mu_3$-O)(COO)$_6$ node with ABTC linkers replaced by formate ions was utilized in all calculations (Figure S4). This cluster model was found to give results with a sufficient accuracy.[48] The trimetallic node consists either of three Fe(III) centers (Fe$_3$(III)OH model; Figure S4A) or of two Fe(III) and one Fe(II) center (Fe$_2$(III)Fe(II); Figure S4B).[48,52] In the former case, to maintain neutrality of the network, counterions such as OH$^-$ (considered here), F$^-$, and Cl$^-$ are usually added to one of the Fe(III) atoms. The spin multiplicity 16 of the Fe$_3$(III) model and spin multiplicity 15 of the Fe$_2$(III)Fe(II) model were considered according to ref 48.

## 3. RESULTS AND DISCUSSION

**Pristine MOF toward Ammonia Synthesis.** The PCN-250-Fe$_3$ MOF was used as a base catalyst.[53−56] This Fe-based MOF is formulated as an outcome of the reaction between precursor Fe$_3$-$\mu_3$-oxo metal cluster and tetratopic azobenzene-based ABTC linkers (ABTC = 3,3′,5,5′-azobenzenetetracarboxylate). The orange crystals of the PCN-250-Fe$_3$ MOF constitute three Fe(III) octahedra atoms that share one oxygen atom ($\mu_3$-oxo) with each other, subsequently connected by six ABTC ligands (Scheme 1A−C).

Scheme 1D showcases the overall outline of this study in employing Fe-based MOF electrocatalysts for the ammonia production. The morphology of the material was primarily
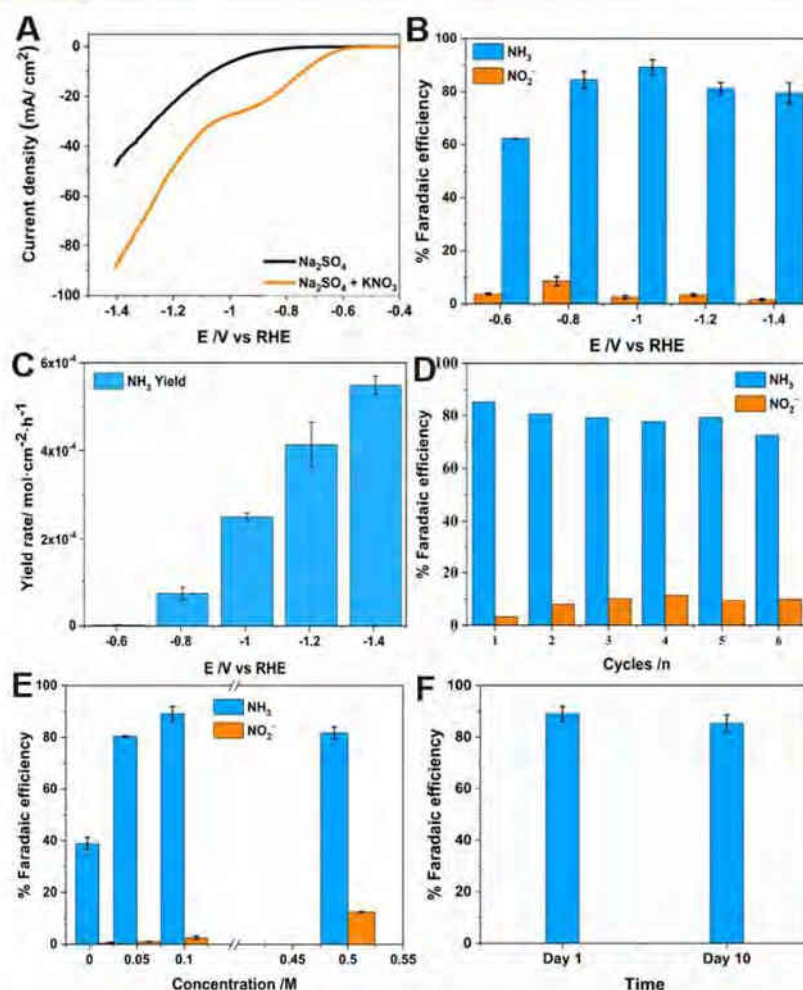
**Figure 4.** (A) LSV measurements of the activated PCN-250-Fe₃ MOF in the Na₂SO₄ 0.5 M electrolyte with and without KNO₃ 0.1 M. The experiment was conducted at a scan rate of 20 mV s⁻¹. Electrocatalytic experiments of the activated PCN-250-Fe₃ MOF (B) FE and (C) NH₃ yield rate at various potentials. (D) FE of NH₃ and NO₂⁻ at consecutive cycling electrolytic tests at −1 V vs RHE (all electrolysis experiments from Figure 4B−D were carried out in the Na₂SO₄ 0.5 M + KNO₃ 0.1 M electrolyte). (E) FEs of electrocatalysts toward NH₃ and NO₂⁻ at different concentrations of 0.01, 0.05, 0.1, and 0.5 M KNO₃. (F) Stability assessments of activated MOF electrocatalysts toward NH₃ production (FE) with time (electrolysis experiments carried out in the Na₂SO₄ 0.5 M + KNO₃ 0.1 M electrolyte).

assessed by SEM (Figure S1A), and EDS mapping confirms the presence of Fe, carbon (C), nitrogen (N), and oxygen (O) elements over the material surface, as shown in Figure S1B−E.

XPS was conducted on a pristine PCN-250-Fe₃ MOF catalyst. The survey spectrum showed prominent sharp peaks of Fe 2p, C 1s, N 1s, and O 1s at their respective binding energies of 710, 284.6, 399.7, and 531.7 eV upon analysis from 0 to 1200 eV (Figure 1A). The quantitative analysis of the catalyst showed the presence of Fe 2p, C 1s, N 1s, and O 1s elements in the atomic percentage (at.%) of 2.14, 65.32, 6.09, and 26.45%, respectively. On deconvolution of the Fe 2p spectrum, the two peaks at 711.4 and 724.9 eV were obtained, which correspond to the Fe $2p_{3/2}$ and $2p_{1/2}$ states, respectively (Figure 1B). This clearly attributes to the +3 oxidation state of Fe centers in the PCN-250-Fe₃ MOF catalyst. The satellite

peaks of Fe $2p_{3/2}$ and $2p_{1/2}$ are also observed in the deconvoluted spectra at 716.6 and 729.4 eV.[57,58] The C 1s spectra also gave three peaks at 284.6, 285.7, and 288.4 eV, which correspond to the C=O (peak a), C−N (peak b), and C=C/C−C (peak c), respectively (Figure 1C). The O 1s spectra also show the Fe−O (peak a) and O−H (peak b) bonding peaks as well shown in Figure S2. The XPS results of pristine/nonactivated MOF samples well match with literature data as well.[58]

Electrocatalytic activity of the pristine PCN-250-Fe₃ MOF toward NRA was primarily investigated using the linear sweep voltammetry (LSV) technique. The experiments were carried out with and without KNO₃ in a 0.5 M Na₂SO₄ electrolyte. The electrocatalytic performance of these MOFs was studied in a three-electrode setup by drop-casting the MOF over GC,

which served as the working electrode substrate. From the LSV curves, it is evident that the MOF electrocatalysts can reduce the $NO_3^-$ ions in the electrolyte, owing to the low onset potential and high current density, in comparison to electrolyte systems without $NO_3^-$ (Figure 2A). The current has been normalized with the geometrical surface area of the electrode. The area of the electrode was calculated using the equation $\Pi r^2$, where $r = 1.5$ mm. The obtained current value via experimentation was divided by the area of the electrode surface. The major objective of the study is to track the behavior of the catalyst toward NRA via electrolysis in the proposed working potential range and to identify the peak potential that delivers the maximum FE in the procured volcano-shaped curve. The electrolysis measurements were executed in a H-type electrolytic cell with the cathodic and anodic compartments well separated by a frit. At the cathodic compartment of the cell, the electrocatalyst PCN-250-Fe$_3$ MOF drop-casted over the GC serves as the working electrode, along with the reference electrode, while the counter electrodes were held at the anodic compartment. Each electrolytic experiment was carried out for 1 h at room temperature with continuous magnetic stirring (100 rpm) at the potential range previously mentioned. Post electrolysis, solution samples from the cathodic part were collected and quantified for ammonia and nitrite using the standard colorimetric method.[34,42,43]

Upon identifying the interesting behavior of the Fe-based MOF from the LSV measurements, NRA was performed sequentially via electrolysis in an H-type cell at potentials ranging from −0.6 to −1.4 V vs RHE. The concentration of $NH_3$ and $NO_2^-$ was then analyzed using the colorimetric assay to calculate the FE of the catalyst toward these compounds. The results are plotted in Figure 2B. The nonactivated pristine MOF samples gave a maximum FE of 65% at −1.2 V vs RHE, and the FE was much lower at other measured potentials. Moreover, the stability of the electrocatalysts was assessed using six continuous chronoamperometry experiments for 1 h each, where no obvious decay in FE was seen (Figure 2C). Experiments were also repeated at different nitrate concentrations, using the nonactivated pristine MOF samples at −1.2 V vs RHE, as shown in Figure 2D. A decrease in FE was observed when the concentration of $KNO_3$ reaches lower values (0.01 M), while 0.1 and 0.05 showcased a reasonable FE.

**Activated MOF toward Ammonia Synthesis.** The MOFs were thermally activated in vacuum at 150 °C for 3 h and used for the subsequent characterization and electrocatalytic studies. Morphological and structural analysis of the activated PCN-250-Fe$_3$ MOF material was carried out using SEM, EDS, XPS, and XRD studies and compared with the nonactivated pristine MOF to confirm if the structural integrity remains intact, as suggested by previous studies. The morphology of the material was primarily assessed by SEM, where dodecahedral-shaped crystals could be clearly identified, as shown in Figure 3A. A further magnified structure of the PCN-250-Fe$_3$ MOF is given in Figure 3B. Elemental distribution over the sample surface was carried out by using EDS elemental mapping, where Fe, O, N, and C showed a uniform distribution over the sample surface (Figure 3C−F).

XPS was conducted for detailed elemental analysis of the activated PCN-250-Fe$_3$ MOF for a better understanding of the electronic structure of the material and chemical states of the atoms in the material. The survey spectrum was measured for the elemental identification in the range of 0 to 1200 eV. Prominent sharp peaks of Fe 2p, C 1s, N 1s, and O 1s were observed at their respective binding energies, as shown in Figure 3G. The at. % Fe 2p, C 1s, N 1s, and O 1s elements were procured in the order of 3.93, 65.01, 5.06, and 26%, respectively. The deconvoluted Fe 2p spectrum displayed two peaks at 711.53 and 724.9 eV for Fe $2p_{3/2}$ and $2p_{1/2}$, respectively (Figure 3H). The satellite peaks are also evident in the deconvoluted Fe 2p spectra.[57,58] The C 1s spectrum depicts three peaks at 284.6, 285.6, and 288.6 eV, which correspond to the C=O (peak a), C−N (peak b), and C=C/C−C (peak c), respectively (Figure 3I). The XPS results are in compliance with those previously reported in the literature.[58] Further, XRD measurements were carried out for understanding the crystal structure and lattice arrangements of the material. The XRD patterns obtained from the activated PCN-250-Fe$_3$ MOF material exhibited a crystalline nature, as shown in Figure 3J. The activated MOFs were further compared with the pristine form to identify if the former has undergone any possible alteration upon thermal activation. Based on this result, it is inferred that the activation has not brought any major changes to the material, in terms of its structural integrity, and has also retained the framework of the PCN-250-Fe$_3$ MOF.[54,58,59] Thus, the above characterization results showed that the structure of the material remains intact and is further evaluated by using the electrochemical experiments.

As in the case of the nonactivated pristine sample, the NRA of activated samples was preliminarily analyzed using the LSV technique. Figure 4A illustrates the electrochemical activity of the activated MOFs with and without nitrate in electrolyte systems containing 0.5 M $Na_2SO_4$. A difference in LSV measurements could be identified between the activated and pristine samples (Figure 2A), where the thermally activated samples exhibit a slightly lower overpotential over pristine samples. Further, we extend our studies toward NRA via a couple of experimental demonstrations to understand the performance of the activated PCN-250-Fe$_3$ MOF electrocatalyst. This typically includes understanding the relevance of activation of the MOF prior to its use as an electrocatalyst for ammonia synthesis. Upon analysis, it was interesting to note that the activated catalyst delivered an FE of about 90% for ammonia at −1 V vs RHE and around 80% for ammonia production at the potential range between −0.8 and −1.4 V vs RHE, as shown in Figure 4B. Thus, the ability of the electrocatalyst to produce a reasonably high FE, via thermal activation, enables the potential of engineering and modifying multiple other MOF or similar materials for ammonia production. In addition, post electrolysis, morphological analysis of the activated Fe-based MOF catalyst was conducted to evaluate differences in the material structure. SEM and EDS mapping of the activated Fe-MOF electrocatalyst structure was carried out. The Fe-MOF catalyst retained its structure (Figure S3A) postcatalytic activity and further exhibited a uniform distribution of Fe, C, O, and N elements throughout the sample surface (Figure S3B−E). Figure 4C represents the yield rate, where a clear and proportional increase in the ammonia production with respect to the cathodic potential is observed, which is also expected.

Chronoamperometry tests were also conducted via continuous electrolysis cycles for 6 h at −1 V vs RHE to evaluate the stability of the electrocatalyst toward NRA. Ammonia and nitrite concentrations were measured, and FEs for all these samples were calculated. Figure 4D depicts the electrocatalytic
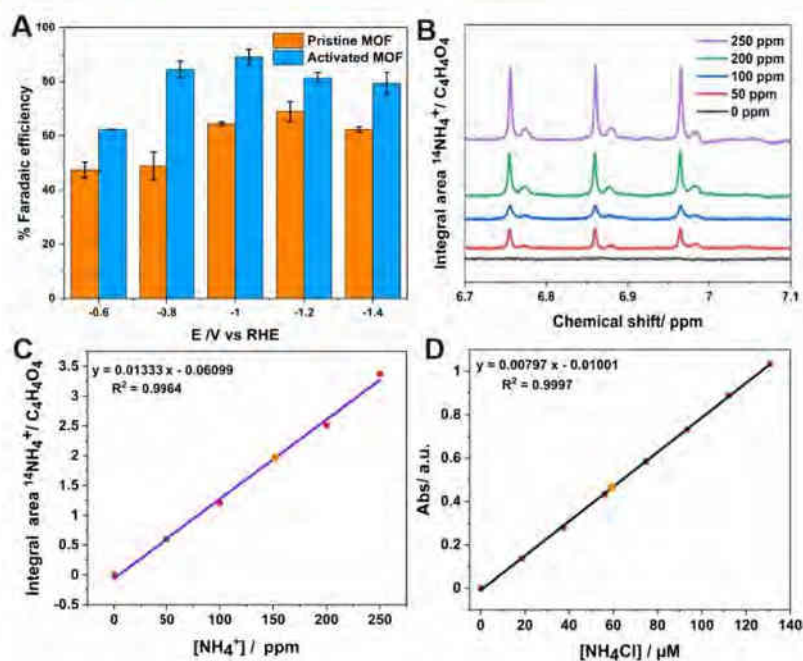
**Figure 5.** (A) Comparison of the FE of pristine and activated MOFs, respectively. (B) $^{1}$H NMR spectra at various concentrations corresponding to a calibration curve. (C) Calibration curve for ammonia determination using the $^{1}$H NMR method (the measured sample is depicted in orange). (D) UV calibration curve for ammonia determination using the colorimetric indophenol blue method (the measured sample is depicted in orange).

stability of the PCN-250-Fe$_3$ MOF electrocatalyst, where no obvious decay in FE after six cycles is seen. This further demonstrates the potential of the PCN-250-Fe$_3$ MOF for real applications such as for NRA. The above results of the PCN-250-Fe$_3$ MOF delivering maximum FE at −1 V vs RHE in 0.1 M KNO$_3$ have prompted us to carry out experiments at various nitrate concentrations such as 0.5, 0.05, and 0.01 M to further evaluate the efficiency of the electrocatalyst toward NRA (Figure 4E). It was observed that the FE of the electrocatalyst at 0.5 and 0.05 M was slightly lower than 0.1 M; however, they are within the error range of FE at 0.1 M. Notably, at a higher concentration of nitrate (0.5 M), the FE of NO$_2^-$ is found to be high compared with 0.1 and 0.05 M. This could be possibly due to the fact that in concentrated nitrate solution, hydrogen adsorption is hindered[60] due to excessive amounts of nitrate, resulting in an increased FE of NO$_2^-$ when compared to other systems. However, in the case of NH$_3$, the FE remains almost the same or slightly decreased when compared to 0.1 M. On the other hand, a severe decline in FE for NH$_3$ was obtained at 0.01 M, most probably due to the competitive adsorption of the supporting electrolyte (SO$_4^{2-}$). As described in the case of other metals, the mechanism of the reaction is influenced by the presence of strong adsorbates such as sulfate.[60] When the nitrate concentration is 0.01 M or lower, sulfate acts as a competitive anion for active sites with a consequent decrease in FE for both NH$_3$ and NO$_2^-$ at the optimal potential. This result accords with other observations in the literature.[40] Furthermore, stability assessment of activated MOF samples was carried out by analyzing their FE toward ammonia production after storing them for 10 days under room temperature in aqueous media. No major difference in the FE of MOF electrocatalysts was observed during its storage for

the ascribed duration (Figure 4F), confirming the stability of the activated sample.

**Evaluating Fe MOFs for Ammonia Production.** The literature has often emphasized on the importance of activating MOFs via multiple techniques (conventional heating and vacuum, solvent-exchange, supercritical CO$_2$ exchange, freeze-drying, chemical treatment, etc.) for their enhanced performance, owing to its increased porosity and surface area.[61−63] Activation involves the removal of guest molecules such as volatile solvents or trapped entities from the MOF without affecting the structural integrity of the active material. Interestingly, the literature suggests that subjecting the Fe-MOF to varying pressures and temperatures can aid in enhancing its properties for targeted applications. A pressure-induced sequential phase transformation of the MOF was studied by Yuan et al., and the implications for MOF densification were analyzed, which showed a significant increase in the volumetric CH$_4$ uptake (by 21%).[54] Another interesting study was conducted by Day et al., where variation in activation temperature played a vital role in improving the MOF properties.[64] In the above study, the thermal activation of the MOF carried out at 150 and 250 °C was employed toward acetylene adsorption. Notable observations put forward by the group include the removal of guest molecules such as volatile solvents from the MOF at 150 °C and decarboxylation of the ligand in open metal site formation at 250 °C, along with the formation of the mixed valent state of Fe(II/III) in the latter. This mixed valence can also aid in the enhancement of the gas adsorption performance. Hence, such investigations can play a vital role in improving the MOF properties and fabrication of application-specific catalysts.

On analyzing the FE of MOF samples, a clear increase in FE was observed in activated samples, compared to the pristine

nonactivated MOF, at every corresponding potential (Figure 5A). In other words, the nonactivated pristine MOF samples gave a maximum FE of 65% at −1.2 V vs RHE, while the potential of activated samples that delivered maximum FE was much lower (−1 V vs RHE) and delivered around 90% FE. Also, an evident increase in FE was observed at each corresponding potential of the activated MOF compared to the pristine samples. Thus, the observation on FE emphasizes the improvement in MOF properties upon activation, indicating this approach to be ideal for enhancing the material property. The possibility of enhancement in the PCN-250-Fe₃ MOF via the mixed valence state of Fe(II/III) is expected at very high temperatures.[64] Thus, without subjecting the Fe-MOF sample to a very high temperature of 250 °C, there was an increment in FE via the removal of volatile solvent molecules/guest molecules. In short, from an electrocatalytic point of view, the activation of samples is speculated to result in the exposure of more active Fe sites that are accessible for the nitrate ions in the electrolyte for ammonia production. The presence of the highly charged trivalent Fe(III) metal cation aids toward a strong metal−ligand coordination bond, eventually enhancing the thermostable properties of the Fe-MOF. With 650 °C known to be its decomposition temperature, the activation was employed only to 150 °C (around 1/4 of its decomposition temp), yet an enhancement in FE was evident in the studied MOF samples. Thermogravimetric studies on PCN-250-Fe₃ MOF molecules also confirm that below 100 °C, the sharp weight loss could be attributed to the removal of surface-adsorbed water molecules,[65−67] and/or subsequent heating, which aid toward removal of trapped entities, owing to the synthesis conditions. Thus, thermal activation is expected to remove the trapped entities on the pores, eventually exposing the catalytically active sites that are accessible for electrolyte ions for ammonia production. In principle, the activation of the MOF can modify the porosity of the material by increasing the active sites[68,69] and thus creating more room for electrolyte accessibility for ammonia production.

Such activation-based approaches are evident toward carbon dioxide (CO₂) based-reaction as well. For instance, some recent works emphasize the role of the microenvironments in the modulation of activity of different catalysts for relevant energy-related reactions such as CO₂ reduction reaction.[70−73] In fact, one of the factors relevant in the microenvironment's modulation is the porosity of the material, wherein engineering the electrocatalyst structure appropriately can tailor the selectivity toward a specific C₁ or C₂ product.[71] Likewise, the thermal activation of the MOF can enhance the efficiency of the material toward ammonia production. In short, although there are studies explaining the importance of activation, a better clarity can be brought via such experimental demonstrations that shall be helpful in understanding the potential of the electrocatalyst involved in the study. Carrying out such conclusive studies can also be beneficial in designing newer electrocatalysts by paying special attention to the careful activation of pristine materials for similar applications and/or for other interesting applications in the future. Furthermore, a comparison of various Fe-based catalyst systems has been detailed in Table S1, constituting their experimental conditions, FE, and yield rate in reducing nitrate to ammonia. To further confirm the reliability of colorimetric methods in determining the ammonia content, ¹H NMR experiments were conducted. Figure 5B shows the ¹H NMR spectra at various

NH₄Cl concentrations (ppm), delivering a typical triplet corresponding to the ¹H NMR signal of the equivalent H in ¹⁴NH₄⁺. Figure 5C depicts a calibration curve obtained by plotting the area of the ¹H signal divided by the area of the signal corresponding to maleic acid (internal standard) as a function of the NH₄Cl concentration. On comparing the calibration curve with the one procured using the colorimetric indophenol method (Figure 5D), a similar concentration value was obtained (59.52 $\mu$M for the colorimetric method and 58.72 $\mu$M for ¹H NMR) with an error percentage of 1.4%. It was observed that the ammonia content, determined by two different methods, yielded a similar value (orange symbol in both calibration curves), providing additional confirmation of the accuracy of the colorimetric method used for ammonia quantification.

**Theoretical Studies.** To obtain a deeper understanding of the NRA reaction mechanism catalyzed by the PCN-250-Fe₃ MOF, step-by-step geometry optimizations of NO₃⁻, NH₃, and all intermediate species adsorbed on a cluster model of the PCN-250 catalyst were performed using DFT methods. Since the unit cell of PCN-250 consists of 416 atoms and calculations of the whole unit cell would be computationally ineffective, a cluster model of the Fe₃-($\mu$3-O)(COO)₆ node with ABTC linkers replaced by formate ions was utilized in all calculations (Figure S4).

The trimetallic node consisted of three Fe centers either all in oxidation state III (Fe₃(III)OH model; Figure S4A) or two in oxidation state III and one in II (Fe₂(III)Fe(II); Figure S4B) following the methodology of similar studies.[48,52] In the former case, to maintain neutrality of the network, the OH⁻ counterion is usually placed close to one of the Fe(III) atoms.

Using the Fe₃(III)OH model, we have evaluated the energy profiles of different reaction routes that lead either to the formation of the desired NH₃ or to the formation of other products (NO₂, NO, N₂O, N₂, and HNO₂; Figure S5). Considered reaction routes were based on the study of Wu et al.[34] The most probable reaction mechanism of the NRA reaction (Figure 6) was calculated both in the gas phase and in the aqueous environment, which corresponded more to the used experimental conditions. It was initiated by a solution-mediated proton transfer to the NO₃⁻ to form HNO₃ (reaction energy $\Delta E_R = 0.67$ eV in the gas phase and 1.35 eV in water; Figure 6B, step 0). The reaction then proceeded through eight-proton and eight-electron transfers (Figure 6A,B and Figure S6A,B, steps 1−8). Generally, all reaction steps were more favorable in the aqueous environment, which indicates that the presence of a solvent with a certain polarity facilitated the electron transfer and thus promoted the NRA reaction. It is worth noting that similar results were obtained by using the Fe₂(III)Fe(II) model of the PCN-250 MOF (Figure S6) with one exception in step 4, which was slightly endothermic in the gas phase ($\Delta E_R = 0.27$ eV). In short, these DFT results substantiate the feasibility of the NRA reaction mechanism of the studied reaction system.

## 4. CONCLUSIONS

In this study, we investigated the potential ability of PCN-250-Fe₃ MOF electrocatalysts toward enhanced ammonia production via thermal activation. The activated MOF catalyst was successful in delivering a high FE of 90% at −1 V vs RHE, while pristine samples gave about 60% at the same potential. A clear enhancement in FE was observed for activated PCN-250-Fe₃ MOF catalysts over the pristine material at every
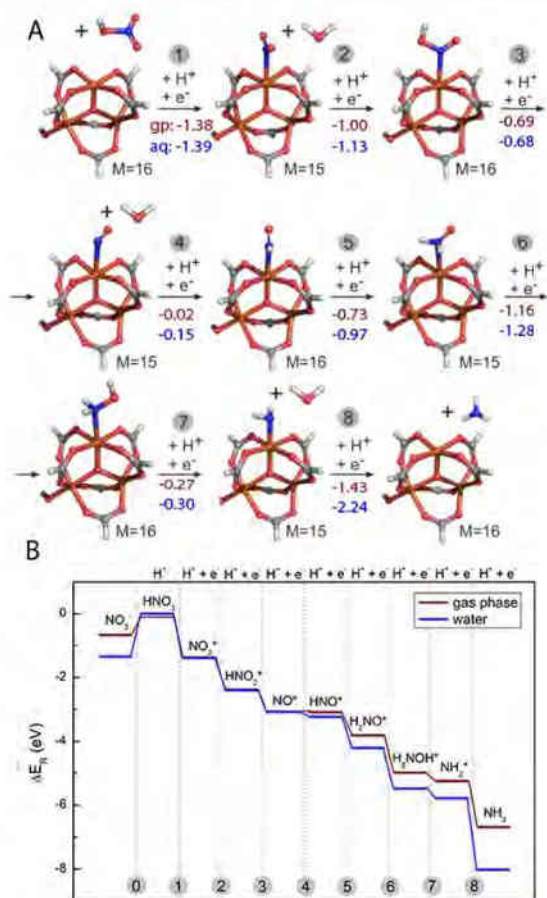
**Figure 6.** (A) Reaction mechanism of NRA catalyzed by PCN-250 (Fe$_3$(III)OH model). The brown values are the reaction energies ($\Delta E_R$) in the gas phase, and the blue values are in water. The multiplicities ($M$) of all species are also reported. The carbon atoms are gray, oxygen red, nitrogen blue, iron orange, and hydrogen white. (B) Diagram of the NRA reaction energies for the reaction steps in the gas phase and water.

corresponding potential. The theoretical results are also in good accordance with the experimental results toward NRA by the PCN-250-Fe$_3$ MOF electrocatalysts. Further, the stability of the activated material with time was also assessed for understanding the potential of the material. Thus, the above studies and observation can open up possibilities for researchers to tailor or surface engineer catalyst surfaces for fabricating the desired electrocatalyst for catalytic applications.

## ■ ASSOCIATED CONTENT

### ⑤ Supporting Information

The Supporting Information is available free of charge at https://pubs.acs.org/doi/10.1021/acsami.3c12822.

> SEM and EDS mapping of the pristine PCN-250-Fe$_3$ MOF sample, deconvoluted O 1s XPS spectra of the pristine MOF sample, SEM and EDS mapping of the Fe-MOF catalyst post catalysis, cluster models of the PCN-250-Fe$_3$ MOF, and reaction pathways (PDF)

## ■ AUTHOR INFORMATION

### Corresponding Author

**Martin Pumera** − *Future Energy and Innovation Laboratory, Central European Institute of Technology, Brno University of Technology, Brno 612 00, Czech Republic; Chemistry Department, College of Science, King Saud University, Riyadh 11451, Saudi Arabia; Faculty of Electrical Engineering and Computer Science, VSB - Technical University of Ostrava, Ostrava 708 00, Czech Republic; Department of Paediatrics and Inherited Metabolic Disorders, First Faculty of Medicine, Charles University Prague, Prague 128 08, Czech Republic; Department of Medical Research, China Medical University Hospital, China Medical University, Taichung 40402, Taiwan;* orcid.org/0000-0001-5846-2951; Email: martin.pumera@ceitec.vutbr.cz

### Authors

**Akshay Kumar K. Padinjareveetil** − *Future Energy and Innovation Laboratory, Central European Institute of Technology, Brno University of Technology, Brno 612 00, Czech Republic*

**Juan V. Perales-Rondon** − *Future Energy and Innovation Laboratory, Central European Institute of Technology, Brno University of Technology, Brno 612 00, Czech Republic;* orcid.org/0000-0001-7182-6289

**Dagmar Zaoralová** − *IT4Innovations, VŠB − Technical University of Ostrava, Ostrava-Poruba 708 00, Czech Republic*

**Michal Otyepka** − *IT4Innovations, VŠB − Technical University of Ostrava, Ostrava-Poruba 708 00, Czech Republic; Regional Centre of Advanced Technologies and Materials, Czech Advanced Technology and Research Institute (CATRIN), Palacký University Olomouc, Olomouc 783 71, Czech Republic;* orcid.org/0000-0002-1066-5677

**Osamah Alduhaish** − *Chemistry Department, College of Science, King Saud University, Riyadh 11451, Saudi Arabia;* orcid.org/0000-0001-5344-9459

Complete contact information is available at:
https://pubs.acs.org/10.1021/acsami.3c12822

### Author Contributions

A.K.K.P.: investigation, methodology, conceptualization, formal analysis, data curation, characterizations, experimentation, validation, discussions, funding acquisition, writing (original draft), and writing (review and editing). J.V.P.-R.: investigation, methodology, conceptualization, formal analysis, data curation, validation, and writing (review and editing). D.Z. and M.O.: theoretical calculations, formal analysis, discussions, methodology, funding acquisition, and writing (review and editing). O.A.: discussions and writing (review and editing). M.P.: supervision, methodology, funding acquisition, and writing (review and editing).

### Notes

The authors declare no competing financial interest.

## ■ REFERENCES

(1) Chu, S.; Majumdar, A. Opportunities and Challenges for a Sustainable Energy Future. *Nature* 2012, 488 (7411), 294−303.

(2) Dresselhaus, M. S.; Thomas, I. L. Alternative Energy Technologies. *Nature* 2001, 414, 332−337.

(3) Si, X.; Lu, R.; Zhao, Z.; Yang, X.; Wang, F.; Jiang, H.; Luo, X.; Wang, A.; Feng, Z.; Xu, J.; Lu, F. Catalytic Production of Low-Carbon Footprint Sustainable Natural Gas. *Nat. Commun.* 2022, 13 (1), 258.

(4) Akshay Kumar, K. P.; Ghosh, K.; Alduhaish, O.; Pumera, M. Dip-Coating of MXene and Transition Metal Dichalcogenides on 3D-Printed Nanocarbon Electrodes for the Hydrogen Evolution Reaction. *Electrochem. commun.* 2021, 122, 106890.

(5) Akshay Kumar, K. P.; Alduhaish, O.; Pumera, M. Electrocatalytic activity of layered MAX phases for the hydrogen evolution reaction. *Electrochem. commun.* 2021, 125, 106977.

(6) Li, L.; Tang, C.; Xia, B.; Jin, H.; Zheng, Y.; Qiao, S. Z. Two-Dimensional Mosaic Bismuth Nanosheets for Highly Selective Ambient Electrocatalytic Nitrogen Reduction. *ACS Catal.* 2019, 9 (4), 2902−2908.

(7) Wang, S.; Ichihara, F.; Pang, H.; Chen, H.; Ye, J. Nitrogen Fixation Reaction Derived from Nanostructured Catalytic Materials. *Adv. Funct. Mater.* 2018, 28 (50), 1−26.

(8) Schlögl, R. Catalytic Synthesis of Ammonia—A "Never-Ending Story"? *Angew. Chemie - Int. Ed.* 2003, 42 (18), 2004−2008.

(9) Christensen, C. H.; Johannessen, T.; Sørensen, R. Z.; Nørskov, J. K. Towards an Ammonia-Mediated Hydrogen Economy? *Catal. Today* 2006, 111 (1−2), 140−144.

(10) Humphreys, J.; Lan, R.; Tao, S. Development and Recent Progress on Ammonia Synthesis Catalysts for Haber−Bosch Process. *Adv. Energy Sustain. Res.* 2021, 2 (1), 2000043.

(11) Bernthsen, H. A. The Synthesis of Ammonia from Its Elements-II. *Sci. Am.* 1912, 74 (1930), 410−411.

(12) Soloveichik, G. Electrochemical Synthesis of Ammonia as a Potential Alternative to the Haber−Bosch Process. *Nat. Catal.* 2019, 2 (5), 377−380.

(13) Wan, Y.; Xu, J.; Lv, R. Heterogeneous Electrocatalysts Design for Nitrogen Reduction Reaction under Ambient Conditions. *Mater. Today* 2019, 27 (August), 69−90.

(14) Guo, C.; Ran, J.; Vasileff, A.; Qiao, S.-Z. Rational Design of Electrocatalysts and Photo(Electro)Catalysts for Nitrogen Reduction to Ammonia (NH3) under Ambient Conditions. *Energy Environ. Sci.* 2018, 11 (1), 45−56.

(15) Kitano, M.; Inoue, Y.; Yamazaki, Y.; Hayashi, F.; Kanbara, S.; Matsuishi, S.; Yokoyama, T.; Kim, S. W.; Hara, M.; Hosono, H. Ammonia Synthesis Using a Stable Electride as an Electron Donor and Reversible Hydrogen Store. *Nat. Chem.* 2012, 4 (11), 934−940.

(16) Van Der Ham, C. J. M.; Koper, M. T. M.; Hetterscheid, D. G. H. Challenges in Reduction of Dinitrogen by Proton and Electron Transfer. *Chem. Soc. Rev.* 2014, 43 (15), 5183−5191.

(17) Zhang, L.; Ji, X.; Ren, X.; Ma, Y.; Shi, X.; Tian, Z.; Asiri, A. M.; Chen, L.; Tang, B.; Sun, X. Electrochemical Ammonia Synthesis via Nitrogen Reduction Reaction on a MoS2 Catalyst: Theoretical and Experimental Studies. *Adv. Mater.* 2018, 30, 1800191.

(18) Chen, G. F.; Cao, X.; Wu, S.; Zeng, X.; Ding, L. X.; Zhu, M.; Wang, H. Ammonia Electrosynthesis with High Selectivity under Ambient Conditions via a Li+ Incorporation Strategy. *J. Am. Chem. Soc.* 2017, 139 (29), 9771−9774.

(19) Qiu, W.; Xie, X. Y.; Qiu, J.; Fang, W. H.; Liang, R.; Ren, X.; Ji, X.; Cui, G.; Asiri, A. M.; Cui, G.; Tang, B.; Sun, X.; et al. High-Performance Artificial Nitrogen Fixation at Ambient Conditions Using a Metal-Free electrocatalyst. *Nat. Commun.* 2018, 9 (1), 1−8.

(20) Yu, X.; Han, P.; Wei, Z.; Huang, L.; Gu, Z.; Peng, S.; Ma, J.; Zheng, G. Boron-Doped Graphene for Electrocatalytic N2 Reduction. *Joule* 2018, 2 (8), 1610−1622.

(21) Geng, Z.; Liu, Y.; Kong, X.; Li, P.; Li, K.; Liu, Z.; Du, J.; Shu, M.; Si, R.; Zeng, J. Achieving a Record-High Yield Rate of 120.9 MgNH3mgcat.−1h−1 for N2 Electrochemical Reduction over Ru Single-Atom Catalysts. *Adv. Mater.* 2018, 30 (40), 2−7.

(22) Wang, Y.; Yu, L.; Hu, L.; Chen, G.; Xin, H.; Feng, X. Ambient Ammonia Synthesis via Palladium-Catalyzed Electrohydrogenation of Dinitrogen at Low Overpotential. *Nat. Commun.* 2018, 9 (1), 1795 DOI: 10.1038/s41467-018-04213-9.

(23) Cui, X.; Tang, C.; Zhang, Q. A Review of Electrocatalytic Reduction of Dinitrogen to Ammonia under Ambient Conditions. *Adv. Energy Mater.* 2018, 8 (22), 1−25.

(24) Wang, Y.; Xu, A.; Wang, Z.; Huang, L.; Li, J.; Li, F.; Wicks, J.; Luo, M.; Nam, D. H.; Tan, C. S.; Ding, Y.; Wu, J.; Lum, Y.; Dinh, C. T.; Sinton, D.; Zheng, G.; Sargent, E. H.; et al. Enhanced Nitrate-to-Ammonia Activity on Copper-Nickel Alloys via Tuning of Intermediate Adsorption. *J. Am. Chem. Soc.* 2020, 142 (12), 5702−5708.

(25) van Langevelde, P. H.; Katsounaros, I.; Koper, M. T. M. Electrocatalytic Nitrate Reduction for Sustainable Ammonia Production. *Joule* 2021, 5 (2), 290−294.

(26) Lu, X.; Song, H.; Cai, J.; Lu, S. Recent Development of Electrochemical Nitrate Reduction to Ammonia: A Mini Review. *Electrochem. commun.* 2021, 129, 107094.

(27) Duca, M.; Koper, M. T. M. Powering Denitrification: The Perspectives of Electrocatalytic Nitrate Reduction. *Energy Environ. Sci.* 2012, 5 (12), 9726−9742.

(28) Scheidler, A.; Nixon, S.; Lack, T. J.; Thyssen, N.EEA. *Groundwater Quality and Quantity in Europe.* Office for Official Publications of the European Communities Environmental Assessment Report No 3 1999.

(29) Padinjareveetil, A. K. K.; Perales-Rondon, J. V.; Pumera, M. Engineering 3D Printed Structures Towards Electrochemically Driven Green Ammonia Synthesis: A Perspective. *Adv. Mater. Technol.* 2023, 8 (13), 2202080.

(30) Pérez-Gallent, E.; Figueiredo, M. C.; Katsounaros, I.; Koper, M. T. M. Electrocatalytic Reduction of Nitrate on Copper Single Crystals in Acidic and Alkaline Solutions. *Electrochim. Acta* 2017, 227, 77−84.

(31) Chen, G. F.; Yuan, Y.; Jiang, H.; Ren, S. Y.; Ding, L. X.; Ma, L.; Wu, T.; Lu, J.; Wang, H. Electrochemical Reduction of Nitrate to Ammonia via Direct Eight-Electron Transfer Using a Copper−Molecular Solid Catalyst. *Nat. Energy* 2020, 5 (8), 605−613.

(32) Liu, J. X.; Richards, D.; Singh, N.; Goldsmith, B. R. Activity and Selectivity Trends in Electrocatalytic Nitrate Reduction on Transition Metals. *ACS Catal.* 2019, 9 (8), 7052−7064.

(33) Wang, C.; Ye, F.; Shen, J.; Xue, K. H.; Zhu, Y.; Li, C. In Situ Loading of Cu2O Active Sites on Island-like Copper for Efficient Electrochemical Reduction of Nitrate to Ammonia. *ACS Appl. Mater. Interfaces* 2022, 14 (5), 6680−6688.

(34) Wu, Z. Y.; Karamad, M.; Yong, X.; Huang, Q.; Cullen, D. A.; Zhu, P.; Xia, C.; Xiao, Q.; Shakouri, M.; Chen, F. Y.; Kim, J. Y.; Xia, Y.; Heck, K.; Hu, Y.; Wong, M. S.; Li, Q.; Gates, I.; Siahrostami, S.; Wang, H. Electrochemical Ammonia Synthesis via Nitrate Reduction on Fe Single Atom Catalyst. *Nat. Commun.* 2021, 12 (1), 1−10.

(35) Wang, J.; Cai, C.; Wang, Y.; Yang, X.; Wu, D.; Zhu, Y.; Li, M.; Gu, M.; Shao, M. Electrocatalytic Reduction of Nitrate to Ammonia on Low-Cost Ultrathin CoOx Nanosheets. *ACS Catal.* 2021, 11 (24), 15135−15140.

(36) Li, L. X.; Sun, W. J.; Zhang, H. Y.; Wei, J. L.; Wang, S. X.; He, J. H.; Li, N. J.; Xu, Q. F.; Chen, D. Y.; Li, H.; Lu, J. M. Highly Efficient and Selective Nitrate Electroreduction to Ammonia Catalyzed by Molecular Copper Catalyst@Ti3C2TxMXene. *J. Mater. Chem. A* 2021, 9 (38), 21771−21778.

(37) Wang, Q.; Astruc, D. State of the Art and Prospects in Metal-Organic Framework (MOF)-Based and MOF-Derived Nanocatalysis. *Chem. Rev.* **2020**, *120* (2), 1438−1511.

(38) Moosavi, S. M.; Nandy, A.; Jablonka, K. M.; Ongari, D.; Janet, J. P.; Boyd, P. G.; Lee, Y.; Smit, B.; Kulik, H. J. Understanding the Diversity of the Metal-Organic Framework Ecosystem. *Nat. Commun.* **2020**, *11* (1), 1−10.

(39) Sakamaki, Y.; Tsuji, M.; Heidrick, Z.; Watson, O.; Durchman, J.; Salmon, C.; Burgin, S. R.; Beyzavi, H. Preparation and Applications of Metal-Organic Frameworks (MOFs): A Laboratory Activity and Demonstration for High School and/or Undergraduate Students. *J. Chem. Educ.* **2020**, *97* (4), 1109−1116.

(40) Zhang, S.; Li, M.; Li, J.; Song, Q.; Liu, X. High-Ammonia Selective Metal − Organic Framework − Derived Co-Doped Fe/Fe 2 O 3 Catalysts for Electrochemical Nitrate Reduction. *Proc. Natl. Acad. Sci.* **2022**, *119* (6), e2115504119 DOI: 10.1073/pnas.2115504119.

(41) Qin, J.; Wu, K.; Chen, L.; Wang, X.; Zhao, Q.; Liu, B.; Ye, Z. Achieving High Selectivity for Nitrate Electrochemical Reduction to Ammonia over MOF-Supported RuxOyclusters. *J. Mater. Chem. A* **2022**, *10* (8), 3963−3969.

(42) Wang, Y.; Yu, Y.; Jia, R.; Zhang, C.; Zhang, B. Electrochemical Synthesis of Nitric Acid from Air and Ammonia through Waste Utilization. *Natl. Sci. Rev.* **2019**, *6* (4), 730−738.

(43) Wang, Y.; Zhou, W.; Jia, R.; Yu, Y.; Zhang, B. Unveiling the Activity Origin of a Copper-Based electrocatalyst for Selective Nitrate Reduction to Ammonia. *Angew. Chemie - Int. Ed.* **2020**, *59* (13), 5350−5354.

(44) Zhao, Y.; Truhlar, D. G. A New Local Density Functional for Main-Group Thermochemistry, Transition Metal Bonding, Thermochemical Kinetics, and Noncovalent Interactions. *J. Chem. Phys.* **2006**, *125* (19), 194101 DOI: 10.1063/1.2370993.

(45) Schäfer, A.; Horn, H.; Ahlrichs, R. Fully Optimized Contracted Gaussian Basis Sets for Atoms Li to Kr. *J. Chem. Phys.* **1992**, *97* (4), 2571−2577.

(46) Glendening, E. D.; Reed, A. E.; Carpenter, J. E.; Weinhold, F. A.03 Citation, NBO Version 3.1 https://gaussian.com/citation_a03/

(47) Verma, P.; Xu, X.; Truhlar, D. G. Adsorption on Fe-MOF-74 for C1-C3 Hydrocarbon Separation. *J. Phys. Chem. C* **2013**, *117* (24), 12648−12660.

(48) Barona, M.; Ahn, S.; Morris, W.; Hoover, W.; Notestein, J. M.; Farha, O. K.; Snurr, R. Q. Computational Predictions and Experimental Validation of Alkane Oxidative Dehydrogenation by Fe2M MOF Nodes. *ACS Catal.* **2020**, *10* (2), 1460−1469.

(49) Marenich, A. V.; Cramer, C. J.; Truhlar, D. G. Universal Solvation Model Based on Solute Electron Density and on a Continuum Model of the Solvent Defined by the Bulk Dielectric Constant and Atomic Surface Tensions. *J. Phys. Chem. B* **2009**, *113* (18), 6378−6396.

(50) Nørskov, J. K.; Rossmeisl, J.; Logadottir, A.; Lindqvist, L.; Kitchin, J. R.; Bligaard, T.; Jónsson, H. Origin of the Overpotential for Oxygen Reduction at a Fuel-Cell Cathode. *J. Phys. Chem. B* **2004**, *108* (46), 17886−17892.

(51) Dattila, F.; Seemakurthi, R. R.; Zhou, Y.; López, N. Modeling Operando Electrochemical CO2Reduction. *Chem. Rev.* **2022**, *122*, 11085−11130, DOI: 10.1021/acs.chemrev.1c00690.

(52) Gopalsamy, K.; Babarao, R. Heterometallic Metal Organic Frameworks for Air Separation: A Computational Study. *Ind. Eng. Chem. Res.* **2020**, *59* (35), 15718−15731.

(53) Feng, D.; Wang, K.; Wei, Z.; Chen, Y.-P.; Simon, C. M.; Arvapally, R. K.; Martin, R. L.; Bosch, M.; Liu, T.-F.; Fordham, S.; Yuan, D.; Omary, M. A.; Haranczyk, M.; Smit, B.; Zhou, H.-C. Kinetically Tuned Dimensional Augmentation as a Versatile Synthetic Route towards Robust Metal-Organic Frameworks. *Nat. Commun.* **2014**, *5*, 5723.

(54) Yuan, S.; Sun, X.; Pang, J.; Lollar, C.; Qin, J. S.; Perry, Z.; Joseph, E.; Wang, X.; Fang, Y.; Bosch, M.; Sun, D.; Liu, D.; Zhong, H.-C. PCN-250 under Pressure: Sequential Phase Transformation

and the Implications for MOF Densification. *Joule* **2017**, *1* (4), 806−815.

(55) Kirchon, A.; Li, J.; Xia, F.; Day, G. S.; Becker, B.; Chen, W.; Sue, H. J.; Fang, Y.; Zhou, H. C. Modulation versus Templating: Fine-Tuning of Hierarchally Porous PCN-250 Using Fatty Acids To Engineer Guest Adsorption. *Angew. Chemie - Int. Ed.* **2019**, *58* (36), 12425−12430.

(56) Honig, E. S.Metal Organic Frameworks and Ligands for MOF Synthesis. Strem Chem. Inc. 2018.

(57) Yamashita, T.; Hayes, P. Analysis of XPS spectra of Fe2+ and Fe3+ ions in oxide materials. *Appl. Surf. Sci.* **2008**, *254* (8), 2441−2449.

(58) An, J. R.; Wang, Y.; Dong, W. W.; Gao, X. J.; Yang, O. Y.; Liu, Y. L.; Zhao, J.; Li, D. S. Efficient Visible-Light Photoreduction of CO2 to CH4 over an Fe-Based Metal-Organic Framework (PCN-250-Fe3) in a Solid-Gas Mode. *ACS Appl. Energy Mater.* **2022**, *5* (2), 2384−2390.

(59) Chen, Y.; Qiao, Z.; Wu, H.; Lv, D.; Shi, R.; Xia, Q.; Zhou, J.; Li, Z. An Ethane-Trapping MOF PCN-250 for Highly Selective Adsorption of Ethane over Ethylene. *Chem. Eng. Sci.* **2018**, *175*, 110−117.

(60) De Groot, M. T.; Koper, M. T. M. The Influence of Nitrate Concentration and Acidity on the Electrocatalytic Reduction of Nitrate on Platinum. *J. Electroanal. Chem.* **2004**, *562* (1), 81−94.

(61) Mondloch, J. E.; Karagiaridi, O.; Farha, O. K.; Hupp, J. T. Activation of Metal-Organic Framework Materials. *CrystEngComm* **2013**, *15* (45), 9258−9264.

(62) Howarth, A. J.; Peters, A. W.; Vermeulen, N. A.; Wang, T. C.; Hupp, J. T.; Farha, O. K. Best Practices for the Synthesis, Activation, and Characterization of Metal−Organic Frameworks. *Chem. Mater.* **2017**, *29*, 26−39.

(63) Drake, H. F.; Day, G. S.; Vali, S. W.; Xiao, Z.; Banerjee, S.; Li, J.; Joseph, E. A.; Kuszynski, J. E.; Perry, Z. T.; Kirchon, A.; Ozdemir, O. K.; Lindahl, P. A.; Zhou, H.-C. The Thermally Induced Decarboxylation Mechanism of a Mixed-Oxidation State Carboxylate-Based Iron Metal-Organic Framework. *Chem. Commun.* **2019**, *55* (85), 12769−12772.

(64) Day, G. S.; Rowe, G. T.; Ybanez, C.; Ozdemir, R. O.; Ornstein, J. Evaluation of Iron-Based Metal−Organic Framework Activation Temperatures in Acetylene Adsorption. *Inorg. Chem.* **2022**, *61*, 9242−9250.

(65) Drake, H. F.; Xiao, Z.; Day, G. S.; Vali, S. W.; Chen, W.; Wang, Q.; Huang, Y.; Yan, T. H.; Kuszynski, J. E.; Lindahl, P. A.; Ryder, M. R.; Zhou, H. C. Thermal decarboxylation for the generation of hierarchical porosity in isostructural metal−organic frameworks containing open metal sites. *Mater. Adv.* **2021**, *2*, 5487−5493.

(66) Chen, Y.; Qiao, Z.; Huang, J.; Wu, H.; Xiao, J.; Xia, Q.; Xi, H.; Hu, J.; Zhou, J.; Li, Z. Unusual Moisture-Enhanced CO 2 Capture within Microporous PCN- 250 Frameworks. *ACS Appl. Mater. Interfaces* **2018**, *10*, 38638−38647.

(67) Kirchon, A.; Day, G. S.; Fang, Y.; Banerjee, S.; Ozdemir, O. K.; Zhou, H. C. Suspension Processing of Microporous Metal-Organic Frameworks: A Scalable Route to High-Quality Adsorbents. *Iscience* **2018**, *5*, 30−37.

(68) Clayson, I. G.; Hewitt, D.; Hutereau, M.; Pope, T.; Slater, B. High Throughput Methods in the Synthesis, Characterization, and Optimization of Porous Materials. *Adv. Mater.* **2020**, *32* (44), 2002780 DOI: 10.1002/adma.202002780.

(69) Al Amery, N.; Abid, H. R.; Al-Saadi, S.; Wang, S.; Liu, S. Facile Directions for Synthesis, Modification and Activation of MOFs. *Mater. Today Chem.* **2020**, *17*, 100343.

(70) Li, F.; Thevenon, A.; Rosas-Hernández, A.; Wang, Z.; Li, Y.; Gabardo, C. M.; Ozden, A.; Dinh, C. T.; Li, J.; Wang, Y.; Edwards, J. P.; Xu, Y.; McCallum, C.; Tao, L.; Liang, Z. Q.; Luo, M.; Wang, X.; Li, H.; O'Brien, C. P.; Tan, C. S.; Nam, D. H.; Quintero-Bermudez, R.; Zhuang, T. T.; Li, Y. C.; Han, Z.; Britt, R. D.; Sinton, D.; Agapie, T.; Peters, J. C.; Sargent, E. H. Molecular Tuning of CO2-to-Ethylene Conversion. *Nature* **2020**, *577* (7791), 509−513.

(71) Yang, K. D.; Ko, W. R.; Lee, J. H.; Kim, S. J.; Lee, H.; Lee, M. H.; Nam, K. T. Morphology-Directed Selective Production of Ethylene or Ethane from CO 2 on a Cu Mesopore Electrode. *Angew. Chem.* **2017**, *129* (3), 814−818.

(72) Li, C. W.; Ciston, J.; Kanan, M. W. Electroreduction of Carbon Monoxide to Liquid Fuel on Oxide-Derived Nanocrystalline Copper. *Nature* **2014**, *508* (7497), 504−507.

(73) Hahn, C.; Jaramillo, T. F. Using Microenvironments to Control Reactivity in CO2 Electrocatalysis. *Joule* **2020**, *4* (2), 292−294.

# Supporting information

## Fe-MOF Catalytic Nanoarchitectonic toward Electrochemical Ammonia Production

Akshay Kumar K. Padinjareveetil,[a] Juan V. Perales-Rondon,[a] Dagmar Zaoralová,[b] Michal Otyepka,[b,c] Osamah Alduhaish,[d] Martin Pumera[a,d,e f,g*]

[a] Future Energy and Innovation Laboratory, Central European Institute of Technology, Brno University of Technology, Purkyňova 123, 61200 Brno, Czech Republic

[b] IT4Innovations, VŠB – Technical University of Ostrava, 708 00 Ostrava-Poruba, Czech Republic

[c] Regional Centre of Advanced Technologies and Materials, Czech Advanced Technology and Research Institute (CATRIN), Palacký University Olomouc, 783 71 Olomouc, Czech Republic

[d] Chemistry Department P.O.Box 2455, College of Science King Saud University, Riyadh, 11451 Saudi Arabia

[e] Faculty of Electrical Engineering and Computer Science, VSB - Technical University of Ostrava, 17. listopadu 2172/15, 70800 Ostrava, Czech Republic

[f] Department of Paediatrics and Inherited Metabolic Disorders, First Faculty of Medicine, Charles University, Prague, Ke Karlovu 2, 128 08 Prague, Czech Republic

[g] Department of Medical Research, China Medical University Hospital, China Medical University, No. 91 Hsueh-Shih Road, Taichung 40402, Taiwan

* Author for correspondence; pumera.research@gmail.com
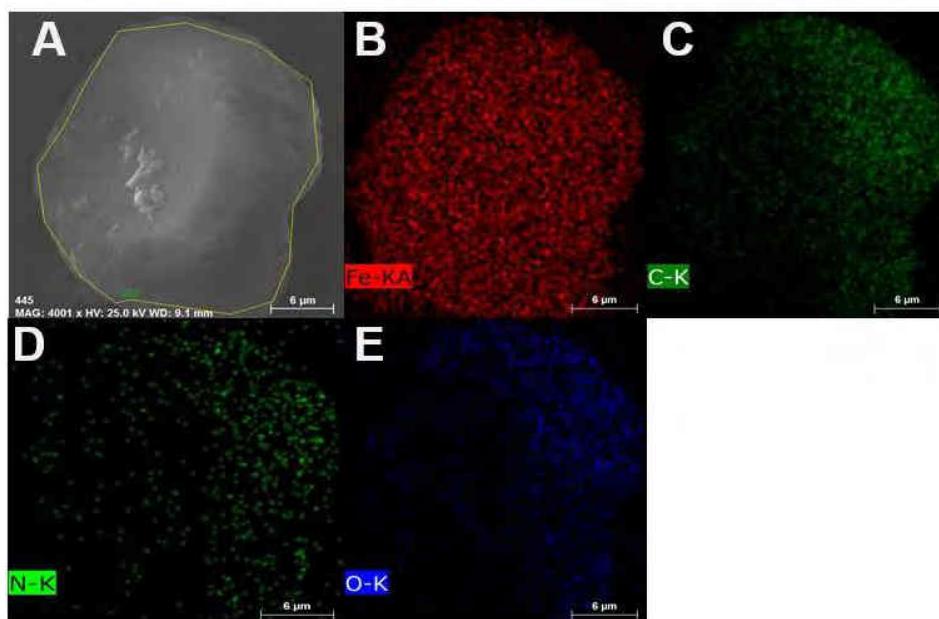
Figure S1. (A) SEM image of pristine PCN-250-Fe₃ MOF sample. (B-E) EDS mapping of elements.
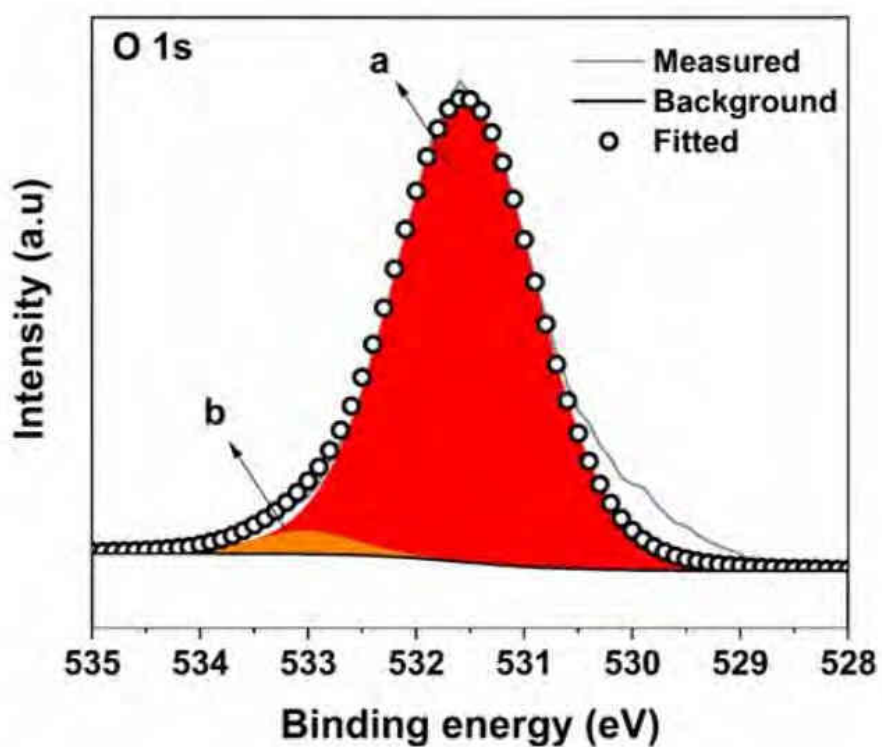


Figure S2. Deconvoluted O 1s XPS spectra of pristine PCN-250-Fe₃ MOF sample.
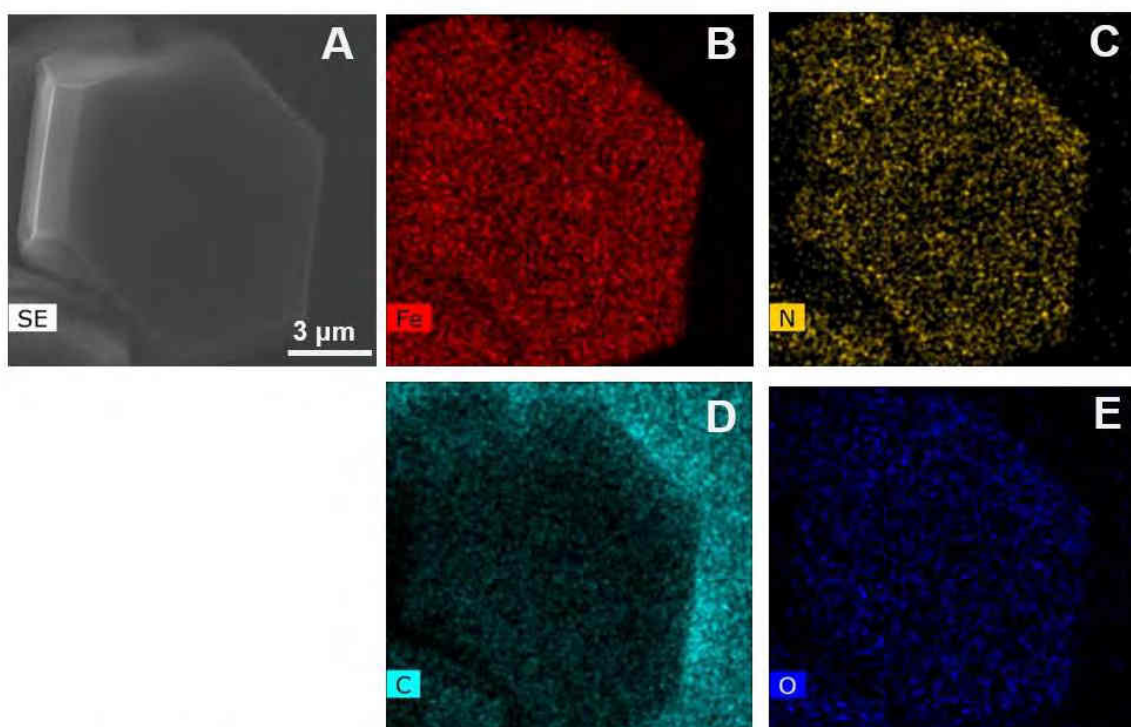
Figure S3. (A) SEM image of Fe MOF catalyst post electrocatalytic experiments. EDS

mapping of (B) Fe, (C) N, (D) C, (E) O elements.

**Table S1**. Nitrate to ammonia conversion results using various Fe based catalysts.

| Material | NH$_3$ FE / Potential | Yield rate | Electrolyte conditions | Reference |
|---|---|---|---|---|
| Fe single-atom catalysts (Fe-PPy SACs) | ~100% at −0.7 V vs RHE | 2.75 mg$_{NH3}$ h$^{-1}$ cm$^{-2}$ at −0.7 V vs RHE | 0.1 M KOH/ 0.1 M KNO$_3$ | 1 |
| 2D Fe-based cyano-coordination polymer nanosheets (Fe-cyano NSs) | ~90.4% at −0.5 V vs RHE | 42.1 mg h$^{-1}$mg$_{cat}^{-1}$ at −0.5 V vs RHE | 1 M KOH/ 0.1 M KNO$_3$ | 2 |
| Fe-doped Co$_3$O$_4$ nanoarray | 95.5% at −0.7 V vs RHE | 0.624 mg mg$_{cat.}^{-1}$ h$^{-1}$ at −0.7 V vs RHE | 0.1 M PBS/ 50 mM NO$_3^-$ | 3 |
| Atomically dispersed FeMo-N-C SAC catalyst | 94.7% at −0.45 V vs RHE | 18.0 μmol cm$^{-2}$ h$^{-1}$ | 0.05 M PBS/ 0.16 M KNO$_3$ | 4 |
| Fe$_1$/NC at 900 ℃ | 86% at −0.7 V vs RHE | 18.8 mg$_{NH3}$ h$^{-1}$ mg$_{cat}^{-1}$ at −0.9 V | 0.1 M K$_2$SO$_4$ / 0.5 M KNO$_3$ | 5 |
| Single-atom Fe-doped V$_2$O$_5$ | 97.1% at −0.7 V vs RHE | 12.5 mg h$^{-1}$ cm$^{-2}$ at −0.7 V | 1 M KOH/ 0.1 M KNO$_3$ | 6 |
| Cu-Fe bimetallic catalysts (Cu$_5$Fe$_5$/OMC) | ~70% at −0.5 V vs RHE | 365.9 μg h$^{-1}$mg$_{cat}^{-1}$ at −0.8 V vs RHE | 0.1 M PBS/ 500 ppm KNO$_3$ | 7 |
| Fe single atom catalyst | ~75% at −0.66 V vs RHE | ~20,000 μg h$^{-1}$ mg$_{cat.}^{-1}$ at −0.85 V vs RHE | 0.5 M KNO$_3$/ 0.10 M K$_2$SO$_4$ | 8 |
| Co-doped Fe/Fe$_2$O$_3$ | 85.2 ± 0.6% at −0.75 V vs RHE | 1,505.9 ± 130.5 μg h$^{-1}$ cm$^{-2}$ at −0.95 V vs. RHE | 0.1 M Na$_2$SO$_4$ with NaNO$_3$ | 9 |
| PCN-250-Fe$_3$ MOF (Activated) | ~90% at − 1 V vs. RHE | 2.5 x 10$^{-4}$ mol cm$^{-2}$ h$^{-1}$ at −1 V vs. RHE | 0.5 M Na$_2$SO$_4$/ 0.1 M KNO$_3$ | This work |
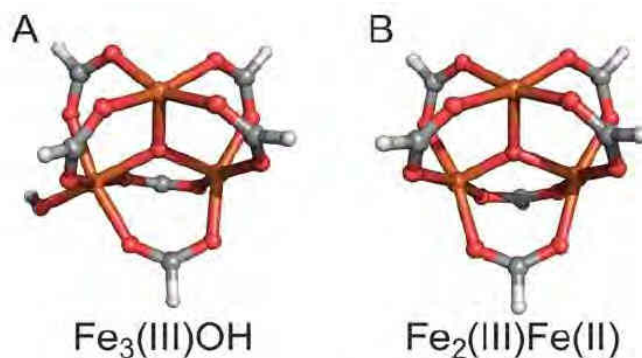
Figure S4. Cluster models of PCN-250. A) Model with all three Fe atoms in oxidation state +III. The OH⁻ group is added to maintain the system neutral. B) Model with two Fe atoms in oxidation state +III and one Fe atom in oxidation state +II. Carbon atoms are grey, oxygen red, iron orange and hydrogen white.
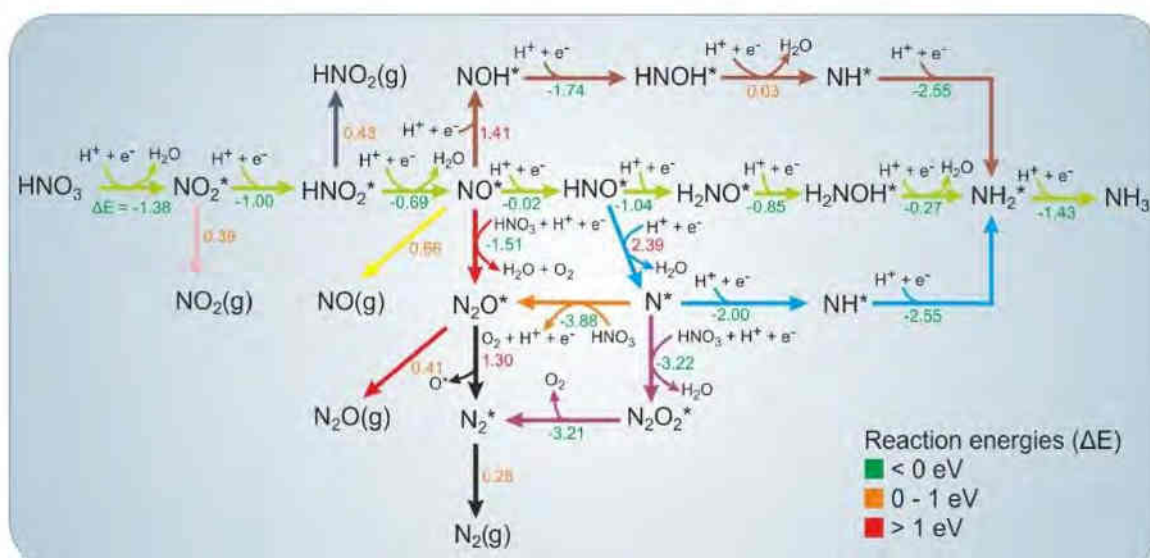


Figure S5. Possible reaction pathways of the $NO_3^-$ reduction reaction based on the study of Wu et al.[34] catalyzed by PCN-250 represented as a $Fe_3(III)OH$ model (Figure S4A) in the gas phase. Numbers under/next to arrows are reaction energies (ΔE) in eV. Reaction pathway marked by green arrows is depicted in Figure 6 and discussed in the main text.
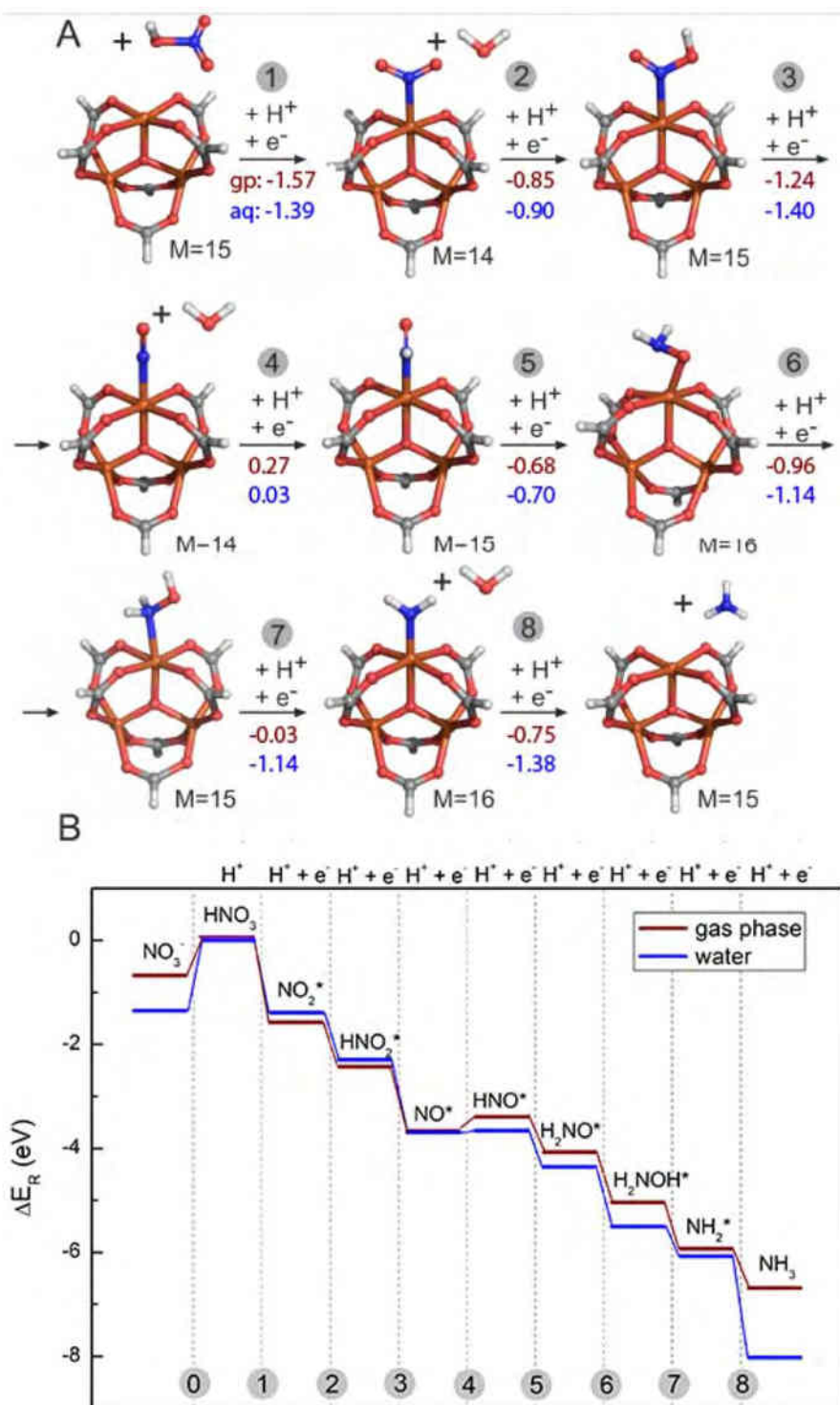
Figure S6. A) The reaction mechanism of the NRA catalyzed by the PCN-250 ($Fe_2$(III)Fe(II) model). Brown values are reaction energies ($\Delta E_R$) in the gas phase, blue values in water. B) Diagram of the NRA reaction energies. The multiplicities (M) of species are also reported. Carbon atoms are grey, oxygen red, nitrogen blue, iron orange and hydrogen white.

# References

(1) Li, P.; Jin, Z.; Fang, Z.; Yu, G. A Single-Site Iron Catalyst with Preoccupied Active Centers That Achieves Selective Ammonia Electrosynthesis from Nitrate. *Energy Environ. Sci.* **2021**, *14* (6), 3522–3531. https://doi.org/10.1039/d1ee00545f.

(2) Fang, Z.; Jin, Z.; Tang, S.; Li, P.; Wu, P.; Yu, G. Porous Two-Dimensional Iron-Cyano Nanosheets for High-Rate Electrochemical Nitrate Reduction. *ACS Nano* **2022**, *16* (1), 1072–1081. https://doi.org/10.1021/acsnano.1c08814.

(3) Wei, P.; Liang, J.; Liu, Q.; Xie, L.; Tong, X.; Ren, Y.; Li, T.; Luo, Y.; Li, N.; Tang, B.; et al. Iron-Doped Cobalt Oxide Nanoarray for Efficient Electrocatalytic Nitrate-to-Ammonia Conversion. *J. Colloid Interface Sci.* **2022**, *615* (February), 636–642. https://doi.org/10.1016/j.jcis.2022.01.186.

(4) Murphy, E.; Liu, Y.; Matanovic, I.; Guo, S.; Tieu, P.; Huang, Y.; Ly, A.; Das, S.; Zenyuk, I.; Pan, X.; et al. Highly Durable and Selective Fe- and Mo-Based Atomically Dispersed Electrocatalysts for Nitrate Reduction to Ammonia via Distinct and Synergized NO2-Pathways. *ACS Catal.* **2022**, *12* (11), 6651–6662. https://doi.org/10.1021/acscatal.2c01367.

(5) Liu, L.; Xiao, T.; Fu, H.; Chen, Z.; Qu, X.; Zheng, S. Construction and Identification of Highly Active Single-Atom Fe1-NC Catalytic Site for Electrocatalytic Nitrate Reduction. *Appl. Catal. B Environ.* **2023**, *323*, 122181. https://doi.org/10.1016/j.apcatb.2022.122181.

(6) Zhang, N.; Zhang, G.; Shen, P.; Zhang, H.; Ma, D.; Chu, K. Lewis Acid Fe-V Pairs Promote Nitrate Electroreduction to Ammonia. *Adv. Funct. Mater.* **2023**. https://doi.org/10.1002/adfm.202211537.

(7) Zhao, J.; Liu, L.; Yang, Y.; Liu, D.; Peng, X.; Liang, S.; Jiang, L. Insights into Electrocatalytic Nitrate Reduction to Ammonia via Cu-Based Bimetallic Catalysts. *ACS Sustain. Chem. Eng.* **2023**, *11* (6), 2468–2475. https://doi.org/10.1021/acssuschemeng.2c06498.

(8) Wu, Z. Y.; Karamad, M.; Yong, X.; Huang, Q.; Cullen, D. A.; Zhu, P.; Xia, C.; Xiao, Q.; Shakouri, M.; Chen, F. Y.; et al. Electrochemical Ammonia Synthesis via Nitrate Reduction on Fe Single Atom Catalyst. *Nat. Commun.* **2021**, *12* (1), 1–10. https://doi.org/10.1038/s41467-021-23115-x.

(9) Zhang, S.; Li, M.; Li, J.; Song, Q.; Liu, X. High-Ammonia Selective Metal-Organic Framework-Derived Co-Doped Fe/Fe2O3 Catalysts for Electrochemical Nitrate Reduction. *Proc. Natl. Acad. Sci. U. S. A.* **2022**, *119* (6). https://doi.org/10.1073/pnas.2115504119.

## 5.2 Employing 3D-printing technology towards novel electrocatalysts fabrication for energy and healthcare applications

This section evaluates strategies for employing 3D-printed electrode materials for energy and healthcare applications. 3D-printing technology is advancing accounting to its easiness in catalyst fabrication, customizations, and it provides the user with the freedom of fabricating structures based on the targeted applications. Thus, the study on fabricating 3D-printed 2D material substrates for HER is discussed in 5.2.1. Employing a dip coating strategy of modifying 3D-CE surfaces has enhanced the possibilities of rapid, quick electrode fabrication for $H_2$ production. Also, 3D-printing technology has significantly advanced in various domains beyond energy. 5.2.2 discusses evaluating the scope of 3D-printing technology in fabricating electrode material for sugar sensing applications via modifying the surface of 3D-CE with a metal plating approach. The idea revolves around the electrochemical detection of carbohydrates via modifying 3D-printed electrodes using electrodeposition of Cu and Ni nanoparticles. In short, the following studies have shown strategies for electrode modification of 3D-CE, eventually making them ideal for HER and sugar sensing applications. The discussion carried out in the section are published and the details are as follows:

### 5.2.1. 2D materials patterned 3D-printed electrodes for HER

Akshay Kumar K. Padinjareveetil, K. Ghosh, O. Alduhaish, Martin Pumera*, *Dip-coating of MXene and transition metal dichalcogenides on 3D-printed nanocarbon electrodes for the hydrogen evolution reaction*, **Electrochem. Commun**. 2021, 122, 106890 doi.org/10.1016/j.elecom.2020.106890, (IF=5.44).

### 5.2.2. Metal plated 3D-printed carbon electrodes for sugar sensing applications

Akshay Kumar K. Padinjareveetil, Ghosh, O. Alduhaish, Martin Pumera*, *Metal-plated 3D-printed electrode for electrochemical detection of carbohydrates*, **Electrochem. Commun**. 2020, 120, 106827, https://doi.org/10.1016/j.elecom.2020.106827, (IF=5.44).

## 5.2.1 2D materials patterned 3D-printed electrodes for HER

**Motivation**

Pristine/activated 3D-CE are not ideal for catalysis. Employing material coating/patterning techniques such as dip coating of 3D-printed electrodes is expected to deliver a new rapid and cost-effective approach of fabricating electrocatalysts for catalytic applications such as $H_2$ production.

**Objective**

Electrocatalytic active materials such as TMDs ($MoS_2$, $MoSe_2$, $WS_2$, and $WSe_2$) and MXene ($Ti_3C_2$) were used for the modification of 3D-CE via dip coating. Morphological characterization of electrode surface is carried to confirm the coating of active material over 3D-CE. LSV was carried to evaluate the $H_2$ production ability of patterned 3D-CE and kinetics were evaluated using the Tafel slope analysis.

**Outcome**

2D material patterned 3D-CE gave a higher HER activity over pristine 3D-CE, affirming the surface modification of 3D-CE to be successful. MXene coated electrode gave a better HER activity over TMDs. Thus, a facile, cost-effective, binder-free approach of modifying 3D-CE is demonstrated for catalysis-based application.

**Contribution**

Investigation, methodology, conceptualization, formal analysis, data curation, characterizations, experimentation, validation, discussions, funding acquisition, writing (original draft, review and editing).

**Article**

The article was published and the details of the article are as follows:

Akshay Kumar K. Padinjareveetil, K. Ghosh, O. Alduhaish, Martin Pumera*, *Dip-coating of MXene and transition metal dichalcogenides on 3D-printed nanocarbon electrodes for the hydrogen evolution reaction*, **Electrochem. Commun**. 2021, 122, 106890 doi.org/10.1016/j.elecom.2020.106890, (IF=5.44).

Contents lists available at ScienceDirect

# Electrochemistry Communications

journal homepage: www.elsevier.com/locate/elecom

# Dip-coating of MXene and transition metal dichalcogenides on 3D-printed nanocarbon electrodes for the hydrogen evolution reaction

K.P. Akshay Kumar [a], Kalyan Ghosh [a], Osamah Alduhaish [b,2], Martin Pumera [a,b,c,d,1,*]

[a] Future Energy and Innovation Laboratory, Central European Institute of Technology, Brno University of Technology, Purkyňova 123, 61200 Brno, Czech Republic
[b] Chemistry Department P.O. Box 2455, College of Science King Saud University, Riyadh 11451, Saudi Arabia
[c] Department of Chemistry and Biochemistry, Mendel University in Brno, Zemedelska 1, CZ-613 00, Brno, Czech Republic
[d] Department of Medical Research, China Medical University Hospital, China Medical University, No. 91 Hsueh-Shih Road, Taichung 40402, Taiwan

## ARTICLE INFO

## ABSTRACT

3D-printing technology is widely accepted as a scalable and advanced manufacturing procedure for the fabrication of electrodes for electrochemical applications. 3D-printed carbon-based electrodes can be used for electrochemical analysis, replacing conventional carbon electrodes. However, a bare 3D-printed carbon electrode exhibits poor electrochemical performance. Herein, a post-treatment of 3D-printed electrodes was carried out using catalytically active materials to improve their electrochemical performance. We used a dip-coating technique which is a more universal, facile, and cost-effective approach compared with other conventionally used techniques such as atomic layer deposition or electrodeposition. The 3D-printed nanocarbon electrodes were dip-coated with MXene ($Ti_3C_2T_x$) and different transition metal dichalcogenides such as $MoS_2$, $MoSe_2$, $WS_2$, and $WSe_2$ to study their catalytic activity towards the hydrogen evolution reaction (HER). This study demonstrates a simple method of improving the catalytic surface properties of 3D-printed nanocarbon electrodes for energy conversion applications.

## 1. Introduction

3D-printing or additive manufacturing is attracting significant attention because it facilitates customized fabrication and rapid prototyping with high accuracy [1,2]. Fused deposition modeling (FDM) or fused filament modeling (FFM) is a 3D-printing approach in which thermoplastic filaments are extruded down the nozzle to print structures in a layer-by-layer manner [3,4]. Recently, a commercial conductive nanocarbon/polylactic acid (PLA) filament has been widely used for FDM 3D-printing and then for electrochemical applications [5–7]. The carbon surface of 3D-printed electrodes possesses poor electrocatalytic properties. Several methods of depositing catalysts over 3D-printed electrodes have been developed, including atomic layer deposition (ALD) [8], electrodeposition [9] and spray coating [10]. ALD requires specialized and expensive equipment, and is not suitable for rapid, low-cost manufacturing of 3D-printed electrodes. In addition, precursors for ALD deposition are limited, and thus not all required materials can be deposited on ALD electrodes. Electrodeposition of catalysts again requires precursor materials [9], which in many cases are not available. We thus turned to a proven technique of modifying surfaces with any electrocatalytic material, which is dip-coating [11,12].

Herein, we report the facile, cost-effective, binder-free dip-coating of a 3D-printed nanocarbon electrode in a slurry of MXene ($Ti_3C_2T_x$) and transition metal dichalcogenides ($MoS_2$, $MoSe_2$, $WS_2$, and $WSe_2$) for the hydrogen evolution reaction (HER). The modified electrodes are characterized by scanning electron microscopy (SEM), energy dispersive X-ray (EDX) spectroscopy, and the electrocatalytic activity of the dip-coated 3D-printed nanocarbon electrodes is assessed via linear sweep voltammetry (LSV) and chronoamperometry measurements. This dip-coating of electrocatalytic active materials over 3D-printed nanocarbon electrodes represents a simple and user-friendly approach towards energy conversion applications.

* Corresponding author at: Future Energy and Innovation Laboratory, Central European Institute of Technology, Brno University of Technology, Purkyňova 123, 61200 Brno, Czech Republic.
  E-mail addresses: oalduhaish@ksu.edu.sa (O. Alduhaish), pumera.research@gmail.com (M. Pumera).
[1] Orcid: 0000-0001-5846-2951.
[2] Orcid: 0000-0001-5344-9459.

## 2. Experimental section

### 2.1. Materials and methods

*N,N*-Dimethylformamide (DMF), ethanol, sulfuric acid ($H_2SO_4$), molybdenum sulfide ($MoS_2$), molybdenum selenide ($MoSe_2$), tungsten sulfide ($WS_2$), and tungsten selenide ($WSe_2$) were purchased from Sigma-Aldrich, Germany. MXene ($Ti_3C_2$) ceramic aqueous paste was purchased from Y-carbon, Ukraine. All chemicals were of analytical grade and used as received. The conductive graphene/polylactic acid (PLA) filament was procured from Graphene Laboratories Inc., New York, USA.

### 2.2. Preparation of 3D-printed electrodes

The electrodes were designed using Autodesk Fusion 360 software and then printed using a Prusa i3 MK3s printer (Prusa Research, Czech Republic). The commercial graphene/PLA filament was extruded down the nozzle (Olsson Ruby-tipped 0.6 mm, 3DVerkstan, Sweden) at a temperature of 220 °C with a bed temperature of 60 °C. The 3D-printed electrodes were then activated to improve their conductivity by immersing in DMF for 4 h and rinsed with ethanol and water to remove the insulating PLA [13–16]. The electrodes were then dried in an oven at 65 °C for 2 h and used for dip-coating.

### 2.3. Dip-coating of 3D-printed nanocarbon electrodes

Initially, slurries of MXene ($Ti_3C_2T_x$) and the TMDs ($MoS_2$, $MoSe_2$, $WS_2$, and $WSe_2$) were prepared by adding 50 mg of the sample to 200 µL of DMF and bath sonicating for 30 min. The activated 3D-printed nanocarbon electrodes (3D-CEs) were then dipped into the respective slurry at room temperature for 3 h, as depicted in Scheme 1. The final electrodes were dried and subjected to morphological and electrochemical characterization. These dip-coated 3D-printed electrodes are referred to as $Ti_3C_2T_x$@3D-CE, $MoS_2$@3D-CE, $MoSe_2$@3D-CE, $WS_2$@3D-CE, and $WSe_2$@3D-CE in later sections.

### 2.4. Characterization

The surface morphology of the dip-coated activated 3D-printed nanocarbon electrodes was studied using SEM, TESCAN LYRA 3. The elemental composition and mapping were examined using an EDX detector (BRUKER XFlash 5010) attached to the SEM. The electrochemical measurements were carried out using a potentiostat (PGSTAT 204,
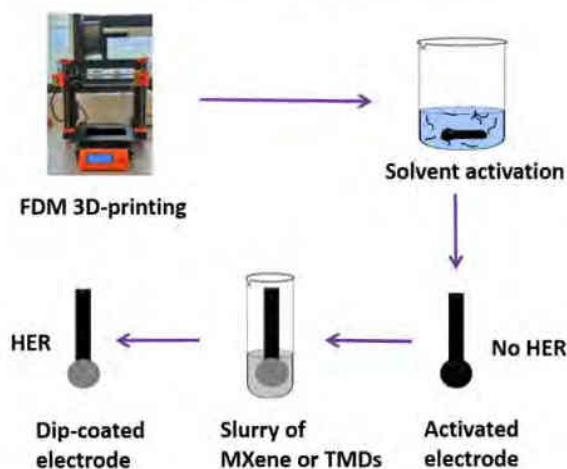
Metrohm Autolab, Netherlands) operated by NOVA 2.1 software, where the dip-coated 3D-printed nanocarbon electrode (activated) was used as the working electrode (WE), with a platinum wire as the counter electrode (CE), and Ag/AgCl (1 M KCl) as the reference electrode (RE) in 0.5 M $H_2SO_4$ electrolyte. The specific current (mA/g) was calculated by dividing the current (mA) by the amount of active material (in grams) deposited on the electrode surface. The mass of the deposited material was calculated by measuring the mass of the nanocarbon electrodes before and after the dip-coating. All electrochemical measurements were carried out at ambient conditions in the open air and no other special conditions were used.

## 3. Results and discussion

The FDM technique was employed to fabricate a 3D-printed nanocarbon electrode using a commercial graphene/PLA filament followed by surface activation using DMF to improve the conductivity of the electrode surface [13,16,17,22]. The activated electrodes were then dip-coated in a slurry of layered materials as shown in Scheme 1.

A SEM image of the solvent-activated 3D-printed nanocarbon electrodes, which were subsequently used as substrates for dip coating, is shown in Fig. S1. The dip-coating method enables a binder-free coating of active materials to be achieved, due to the physisorption of layered materials on the surface of the 3D-printed electrode. An SEM micrograph and EDX spectrum of $Ti_3C_2T_x$@3D-CE are shown in Fig. 1A and B, respectively. It was found that the surface of the dip-coated 3D-printed nanocarbon electrode was attached with $Ti_3C_2T_x$ layers. . The EDX spectral analysis confirms the presence of titanium, carbon, oxygen, aluminum, fluorine, and chlorine with atomic percentages of 39.96, 23.65, 18.46, 9.57, 7.70, and 0.67%, respectively, over the surface of the dip-coated electrode (Fig. 1B). The presence of F and O on the electrode surface was ascribed to surface terminations (–F and –OH) from the processing of the original MAX phase to MXene [18–20]. The EDX mapping images shown in Fig. 1(C–H), further confirm the presence of the constituent elements Ti, C, O, F, Al, and Cl.

SEM micrographs of the dip-coated nanocarbon electrodes $MoS_2$@3D-CE, $MoSe_2$@3D-CE, $WS_2$@3D-CE, and $WSe_2$@3D-CE are shown in Fig. 2A–D, respectively. It was found that the microparticles are deposited on top of the electrode surfaces in each type of electrode. A



**Scheme 1.** Schematic representation of the dip-coating of activated 3D-printed nanocarbon electrode in a slurry of MXene or TMDs.
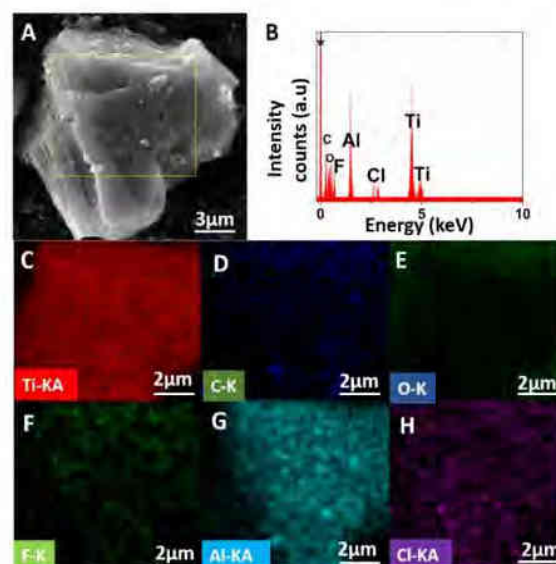


**Fig. 1.** (A) SEM, (B) EDX spectra of dip-coated MXene ($Ti_3C_2T_x$) on the 3D-printed nanocarbon electrode surface (* background peak), (C–H) EDX mapping of the individual elements Ti, C, O, F, Al, and Cl.
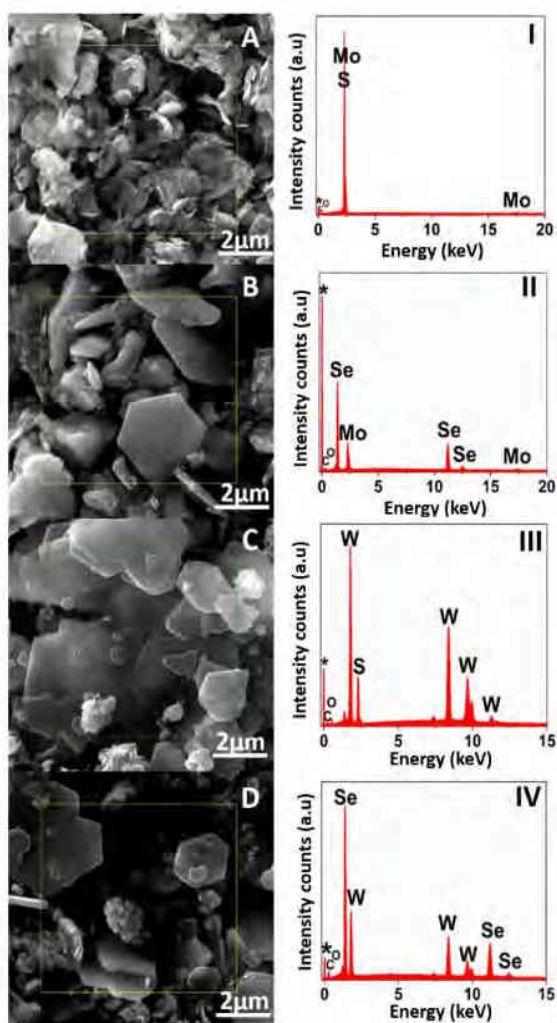
Fig. 2. SEM and EDX spectra of dip-coated electrodes (A, I) MoS$_2$@3D-CE; (B, II) MoSe$_2$@3D-CE; (C, III) WS$_2$@3D-CE; (D, IV) WSe$_2$@3D-CE; (* background peak).



Fig. 3. LSV measurements using the various dip-coated electrodes.

spectral analysis was conducted to investigate the surface composition of the dip-coated nanocarbon electrodes using EDX spectroscopy for MoS$_2$@3D-CE, MoSe$_2$@3D-CE, WS$_2$@3D-CE, and WSe$_2$@3D-CE surfaces as depicted in Fig. 2I, II, III, and IV, respectively. The elemental compositions of the dip-coated electrodes are shown in Table S1.

Linear sweep voltammetry (LSV) was used to study the catalytic activity of the dip-coated 3D-printed nanocarbon electrodes through the hydrogen evolution reaction (HER) in acidic medium (0.5 M H$_2$SO$_4$), as shown in Fig. 3. The measurements were carried out in a potential range of 0 to −1.1 V at a scan rate of 5 mV s$^{-1}$ to study the HER. The bare 3D-CE tends to be a poor catalyst for the HER, as shown in Fig. 3.

The activated dip-coated nanocarbon electrodes showed improved catalytic performance. It was found that for Ti$_3$C$_2$T$_x$@3D-CE, the potential required to attain a current density of −200 mA g$^{-1}$ was −0.481 V. In the case of the TMD-based active catalysts, to reach −200 mA g$^{-1}$ of current density the required potential was −0.620 and −0.496 V for MoS$_2$@3D-CE and MoSe$_2$@3D-CE, respectively, while for WS$_2$@3D-CE and WSe$_2$@3D-CE the required potential was −0.622 and −0.496 V, respectively. This demonstrates that dip-coating MXene (Ti$_3$C$_2$T$_x$) and TMD (MoS$_2$, MoSe$_2$, WS$_2$, and WSe$_2$) over 3D-CE modifies the electrode in such a way that it acts as an active catalyst material. The HER

measurements of the modified 3D-CEs were analyzed using the Tafel equation $\eta = b \log|j| + a$, where $\eta$ is the overpotential, $j$ is the specific current and $b$ is the Tafel slope [21]. Tafel slopes determine rate-limiting steps of the HER measurements. The Tafel slope values were found to be 316 mV dec$^{-1}$ for MXene@3D-CE and 335 and 260 mV dec$^{-1}$ for MoSe$_2$@3D-CE and WSe$_2$@3D-CE, respectively. In the case of MoS$_2$@3D-CE and WS$_2$@3D-CE, very high Tafel slopes of 647 and 970 mV dec$^{-1}$, respectively, were attained (Fig. S2). In short, MXene-coated 3D-CE exhibits a low overpotential compared to the TMDs taken for analysis. Dip-coating of 3D-CEs with sulfide-based transition metals (MoS$_2$ and WS$_2$) produced high overpotentials and very high Tafel slope values when compared to the selenides of Mo and W. Furthermore, the stability of the electrodes was evaluated using the chronoamperometry measurement continuously for 2.5 h in 0.5 M H$_2$SO$_4$. Using the data obtained from the LSV measurement, a constant potential was applied to the electrodes based on the potential observed at the specific current of −200 mA g$^{-1}$. From the chronoamperometry measurement, the specific current versus time plot is drawn for all the electrodes up to 150 min, leaving an initial stability time of 5 min. (Fig. S3). The electrodes were found to be stable throughout the test while MoS$_2$@3D-CE showed some degradation which is in line with results previously reported by our group [10]. The small fluctuations in the specific current may be due to the detachment of H$_2$ gas from the surface of the electrode and not the materials themselves. The electrode performance is stable and the material is present on the electrode surface even after the electrochemical reactions, confirming a good affinity between the active material and the activated electrode (Fig. S4). This technique is shown to be a simple and scalable prototype method for catalytically activating the nanocarbon electrode surface using active layered and 2D materials for energy conversion purposes.

## 4. Conclusions

In summary, we have demonstrated a universal, fast, cost-effective approach for developing binder/surfactant-free modified 3D-printed electrodes for electrochemical applications. Dip-coating of activated 3D-printed nanocarbon electrodes in a slurry of titanium carbide (MXene) and transition metal dichalcogenides (TMDs) improved the catalytic property of the electrodes, as demonstrated for the hydrogen evolution reaction (HER). This method of fabricating a catalytically active 3D-printed nanocarbon electrode surface can be used to coat a variety of substrates, and may be adopted for various electrochemical applications in the future.

## CRediT authorship contribution statement

**K.P. Akshay Kumar:** Investigation, Methodology, Formal analysis, Data curation, Validation, Writing - original draft. **Kalyan Ghosh:** Investigation, Writing - review & editing. **Osamah Alduhaish:** Funding acquisition. **Martin Pumera:** Conceptualization, Resources, Supervision, Writing - review & editing.

## Declaration of Competing Interest

The authors declare that they have no known competing financial interests or personal relationships that could have appeared to influence the work reported in this paper.

## Acknowledgment

## Appendix A. Supplementary data

Supplementary data to this article can be found online at https://doi.org/10.1016/j.elecom.2020.106890.

## References

[1] A. Ambrosi, M. Pumera, 3D-printing technologies for electrochemical applications, Chem. Soc. Rev. 45 (2016) 2740–2755, https://doi.org/10.1039/c5cs00714c.

[2] L.A. Verhoef, B.W. Budde, C. Chockalingam, B. García Nodar, A.J.M. van Wijk, The effect of additive manufacturing on global energy demand: an assessment using a bottom-up approach, Energy Policy 112 (2018) 349–360, https://doi.org/10.1016/j.enpol.2017.10.034.

[3] G.I.J. Salentijn, P.E. Oomen, M. Grajewski, E. Verpoorte, Fused deposition modeling 3D printing for (bio)analytical device fabrication: procedures, materials, and applications, Anal. Chem. 89 (2017) 7053–7061, https://doi.org/10.1021/acs.analchem.7b00828.

[4] M.R. Hartings, Z. Ahmed, Chemistry from 3D printed objects, Nat. Rev. Chem. 3 (2019) 305–314, https://doi.org/10.1038/s41570-019-0097-z.

[5] M.P. Browne, E. Redondo, M. Pumera, 3D-printing for electrochemical energy applications, Chem. Rev. 120 (2020) 2783–2810, https://doi.org/10.1021/acs.chemrev.9b00783.

[6] C. Zhu, T. Liu, F. Qian, W. Chen, S. Chandrasekaran, B. Yao, Y. Song, E.B. Duoss, J.D. Kuntz, C.M. Spadaccini, M.A. Worsley, Y. Li, 3D printed functional nanomaterials for electrochemical energy storage, Nano Today 15 (2017) 107–120, https://doi.org/10.1016/j.nantod.2017.06.007.

[7] P.L. dos Santos, S.J. Rowley-Neale, A.G.M. Ferrari, J.A. Bonacin, C.E. Banks, Ni–Fe (oxy)hydroxide modified graphene additive manufactured (3D-printed) electrochemical platforms as an efficient electrocatalyst for the oxygen evolution reaction, ChemElectroChem 6 (2019) 5633–5641, https://doi.org/10.1002/celc.201901541.

[8] M.P. Browne, J. Plutnar, A.M. Pourrahimi, Z. Sofer, M. Pumera, Atomic layer deposition as a general method turns any 3D-printed electrode into a desired catalyst: case study in photoelectrochemistry, Adv. Energy Mater. 9 (2019) 1–10, https://doi.org/10.1002/aenm.201900994.

[9] C. Iffelsberger, S. Ng, M. Pumera, Catalyst coating of 3D printed structures via electrochemical deposition: case of the transition metal chalcogenide MoS$_x$ for hydrogen evolution reaction, Appl. Mater. Today 20 (2020) 100654, https://doi.org/10.1016/j.apmt.2020.100654.

[10] R. Gusmão, Z. Sofer, P. Marvan, M. Pumera, MoS$_2$ versatile spray-coating of 3D electrodes for the hydrogen evolution reaction, Nanoscale 11 (2019) 9888–9895, https://doi.org/10.1039/c9nr01876j.

[11] B. Cui, H. Lin, J.B. Li, X. Li, J. Yang, J. Tao, Core-ring structured NiCo$_2$O$_4$ nanoplatelets: synthesis, characterization, and electrocatalytic applications, Adv. Funct. Mater. 18 (2008) 1440–1447, https://doi.org/10.1002/adfm.200700982.

[12] Z. Ge, Z. He, An effective dipping method for coating activated carbon catalyst on the cathode electrodes of microbial fuel cells, RSC Adv. 5 (2015) 36933–36937, https://doi.org/10.1039/c5ra05543a.

[13] M.P. Browne, F. Novotný, Z. Sofer, M. Pumera, 3D printed graphene electrodes' electrochemical activation, ACS Appl. Mater. Interfaces 10 (2018) 40294–40301, https://doi.org/10.1021/acsami.8b14701.

[14] D.M. Wirth, M.J. Sheaff, J.V. Waldman, M.P. Symcox, H.D. Whitehead, J.D. Sharp, J.R. Doerfler, A.A. Lamar, G. Leblanc, Electrolysis activation of fused-filament-fabrication 3D-printed electrodes for electrochemical and spectroelectrochemical analysis, Anal. Chem. 91 (2019) 5553–5557, https://doi.org/10.1021/acs.analchem.9b01331.

[15] F. Novotný, V. Urbanová, J. Plutnar, M. Pumera, Preserving fine structure details and dramatically enhancing electron transfer rates in graphene 3D-printed electrodes via thermal annealing: toward nitroaromatic explosives sensing, ACS Appl. Mater. Interfaces 11 (2019) 35371–35375, https://doi.org/10.1021/acsami.9b06683.

[16] R. Gusmão, M.P. Browne, Z. Sofer, M. Pumera, The capacitance and electron transfer of 3D-printed graphene electrodes are dramatically influenced by the type of solvent used for pre-treatment, Electrochem. Commun. 102 (2019) 83–88, https://doi.org/10.1016/j.elecom.2019.04.004.

[17] C.L. Manzanares Palenzuela, F. Novotný, P. Krupička, Z. Sofer, M. Pumera, 3D-printed graphene/polylactic acid electrodes promise high sensitivity in electroanalysis, Anal. Chem. 90 (2018) 5753–5757, https://doi.org/10.1021/acs.analchem.8b00083.

[18] P. Srimuk, F. Kaasik, B. Krüner, A. Tolosa, S. Fleischmann, N. Jäckel, M.C. Tekeli, M. Aslan, M.E. Suss, V. Presser, MXene as a novel intercalation-type pseudocapacitive cathode and anode for capacitive deionization, J. Mater. Chem. A 4 (2016) 18265–18271, https://doi.org/10.1039/c6ta07833h.

[19] Y. Huang, H. Yang, Y. Zhang, Y. Zhang, Y. Wu, M. Tian, P. Chen, R. Trout, Y. Ma, T.H. Wu, Y. Wu, N. Liu, A safe and fast-charging lithium-ion battery anode using MXene supported Li$_3$VO$_4$, J. Mater. Chem. A 7 (2019) 11250–11256, https://doi.org/10.1039/c9ta02037c.

[20] N.M. Caffrey, Effect of mixed surface terminations on the structural and electrochemical properties of two-dimensional Ti$_3$C$_2$T$_2$ and V$_2$CT$_2$ MXenes multilayers, Nanoscale 10 (2018) 13520–13530, https://doi.org/10.1039/c8nr03221a.

[21] N.F. Rosli, M.Z.M. Nasir, N. Antonatos, Z. Sofer, A. Dash, J. Gonzalez-Julian, A.C. Fisher, R.D. Webster, M. Pumera, MAX and MAB phases: two-dimensional layered carbide and boride nanomaterials for electrochemical applications, ACS Appl. Nano Mater. (2019) 6010–6021, https://doi.org/10.1021/acsanm.9b01526.

[22] K.P. Akshay Kumar, Kalyan Ghosh, Osamah Alduhaish, Martin Pumera, Metal-plated 3D-printed electrode for electrochemical detection of carbohydrates, Electrochem. Commun. 120 (2020) 1–7, https://doi.org/10.1016/j.elecom.2020.106827, 106827.

# Supplementary information

# MXene and transition metal dichalcogenides dip-coating on 3D-printed nanocarbon electrode for hydrogen evolution reaction

K P Akshay Kumar[a], Kalyan Ghosh[a], Osamah Alduhaish[b] and Martin Pumera[a, c, d, e*]

[a]Future Energy and Innovation Laboratory, Central European Institute of Technology, Brno University of Technology, Purkyňova 123, 61200 Brno, Czech Republic

[b]Chemistry Department P.O.Box 2455, College of Science King Saud University Riyadh 11451, Saudi Arabia

[c]Center for Advanced Functional Nanorobots, Department of Inorganic Chemistry, Faculty of Chemical Technology, University of Chemistry and Technology Prague, Technická 5, 16628 Prague, Czech Republic

[d]Department of Chemical and Biomolecular Engineering, Yonsei University, 50 Yonsei-ro, Seodaemun-gu, Seoul 03722, Korea

[e]Department of Medical Research, China Medical University Hospital, China Medical University, No. 91 Hsueh-Shih Road, Taichung 40402, Taiwan

*Corresponding author

E-mail: pumera.research@gmail.com
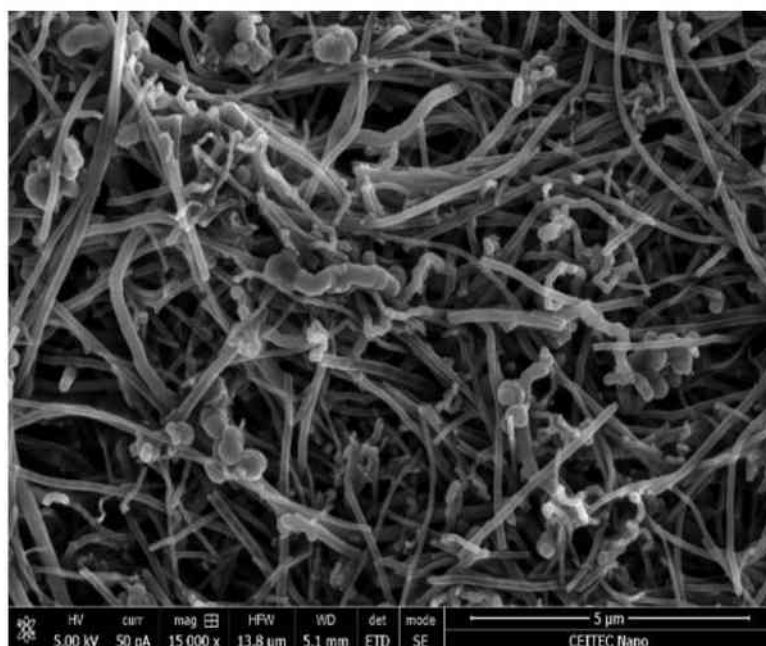
Fig. S1. Scanning electron microscopy image of the activated 3D-printed nanocarbon electrode surface.

Table S1. EDX spectral details of transition metal dichalcogenides (A) MoS$_2$@3D-CE (B) MoSe$_2$@3D-CE (C) WS$_2$@3D-CE (D) WSe$_2$@3D-CE

| dip-coated electrode | atomic (%) | | | |
|---|---|---|---|---|
| MoS$_2$@3D-CE | **Mo** | **S** | **C** | **O** |
| | 24.2 | 48.74 | 25.09 | 1.06 |
| MoSe$_2$@3D-CE | **Mo** | **Se** | **C** | **O** |
| | 19.73 | 44.67 | 31.37 | 4.23 |
| WS$_2$@3D-CE | **W** | **S** | **C** | **O** |
| | 26.06 | 43.00 | 17.72 | 13.22 |
| WSe$_2$@3D-CE | **W** | **Se** | **C** | **O** |
| | 23.95 | 46.27 | 27.14 | 2.64 |
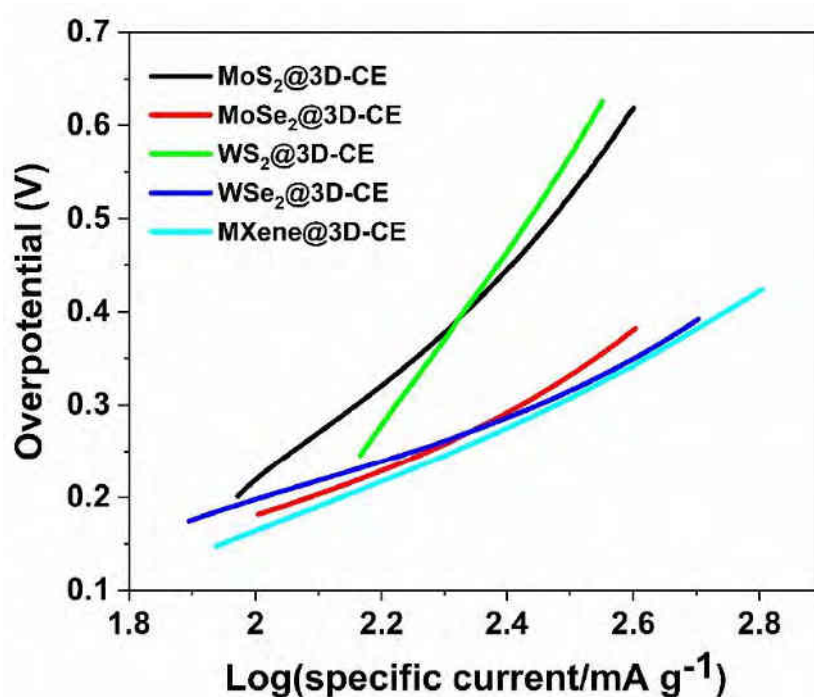


Fig. S2. Tafel slopes of the various dip-coated electrodes.
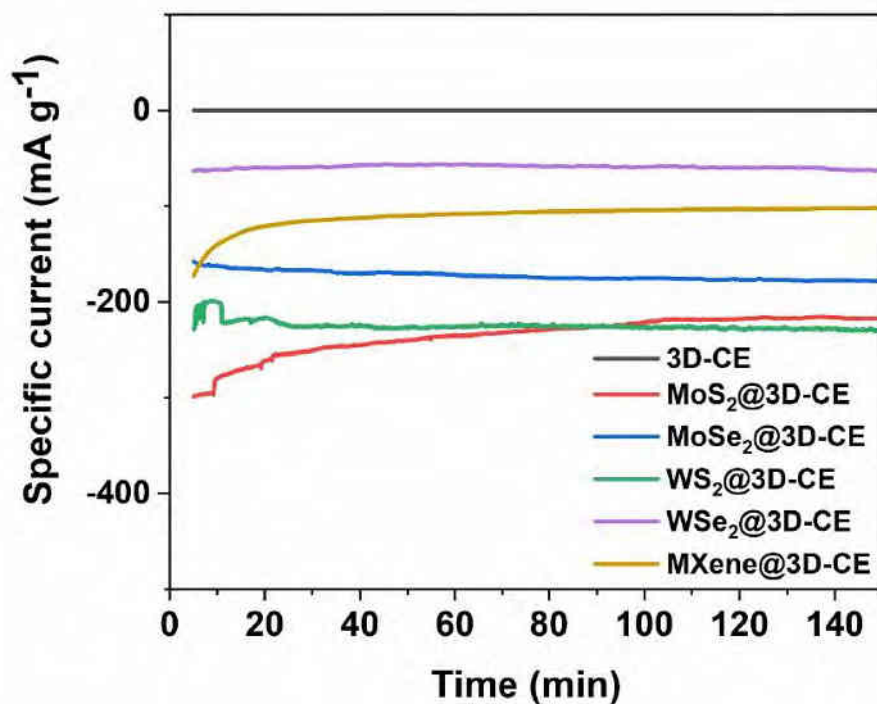
Fig. S3. Chronoamperometry measurements of the various dip-coated electrodes in 0.5 M $H_2SO_4$ for 150 minutes.
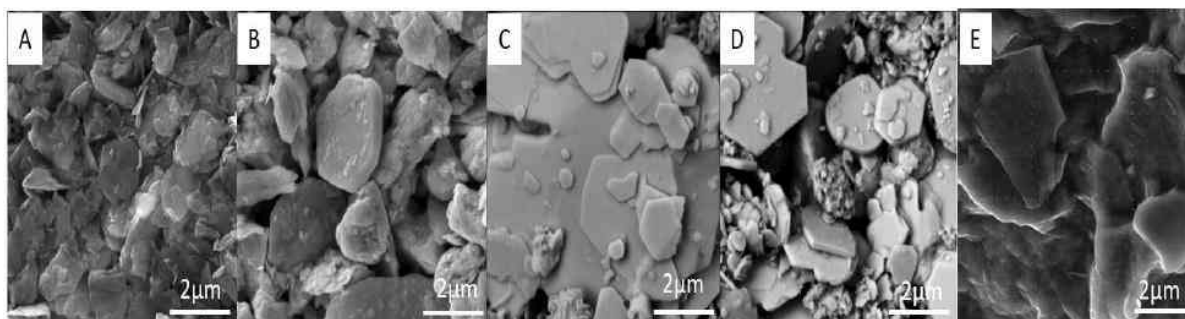


Fig. S4. Scanning electron microscopy images of dip-coated nanocarbon electrode surface after electrochemical measurements (A) $MoS_2$@3D-CE, (B) $MoSe_2$@3D-CE, (C) $WS_2$@3D-CE, (D) $WSe_2$@3D-CE and (E) $Ti_3C_2T_x$@3D-CE.

101

## 5.2.2 Metal plated 3D-printed carbon electrodes for sugar sensing applications

**Motivation**

3D-printed electrode are not catalytically active to targeted analytes. Employing ideal modification approaches to fabricate 3D-printed active electrodes can aid towards on-demand decentralized sensors.

**Objective**

A non-enzymatic 3D-CE is fabricated via metal plating of Cu and Ni, to detect carbohydrates. Morphology analysis was employed to confirm distribution of metal nanoparticles over electrode surface. Electrochemical characterization via cyclic voltammetry and chronoamperometry will be employed to confirmed sugar sensing ability of metal plated 3D-printed electrode.

**Outcome**

Metal plated 3D-CE was successful for carbohydrate sensing. The studies aid towards enhancing the possibilities of employing 3D-CE for successful sensing of specific targeted products.

**Contribution**

Investigation, methodology, conceptualization, formal analysis, data curation, characterizations, experimentation, validation, discussions, writing (original draft, review and editing).

**Article**

The article was published and the details of the article are as follows:

Akshay Kumar K. Padinjareveetil, Ghosh, O. Alduhaish, Martin Pumera*, *Metal-plated 3D-printed electrode for electrochemical detection of carbohydrates*, **Electrochem. Commun**. 2020, 120, 106827, https://doi.org/10.1016/j.elecom.2020.106827, (IF=5.44).

# Metal-plated 3D-printed electrode for electrochemical detection of carbohydrates

K.P. Akshay Kumar[a], Kalyan Ghosh[a], Osamah Alduhaish[b], Martin Pumera[a,b,c,d,*]

[a] Future Energy and Innovation Laboratory, Central European Institute of Technology, Brno University of Technology, Purkyňova 123, 61200 Brno, Czech Republic
[b] Chemistry Department P.O. Box 2455, College of Science, King Saud University, Riyadh 11451, Saudi Arabia
[c] Department of Chemical and Biomolecular Engineering, Yonsei University, 50 Yonsei-ro, Seodaemun-gu, Seoul 03722, Republic of Korea
[d] Department of Medical Research, China Medical University Hospital, China Medical University, No. 91 Hsueh-Shih Road, Taichung 40402, Taiwan

## ARTICLE INFO

## ABSTRACT

The decentralized fabrication of sensors using 3D-printing technology and low power requirements of electrochemical detection promise to revolutionize point-of-care sensing. One of the obstacles is that the 3D-printed devices are often not catalytic to the target analytes. Here, we develop a non-enzymatic printed nanocarbon electrode sensor to detect sugars (glucose and sucrose) via copper and nickel electroplating over a 3D-printed conducting electrode. The morphological and spectroscopic characterizations of copper-plated and nickel-plated 3D-printed carbon electrodes were performed. Scanning electron micrographs show the formation of metal nanoparticles over the surface of a 3D-printed nanocarbon electrode. X-ray photoelectron spectroscopy reveals the composition and chemical states of the metal coating. Electrochemical characterization via cyclic voltammetry and chronoamperometry was carried out, and glucose and sucrose sensing were performed. This method of on-demand decentralized sensor fabrication and modifications should find broad applications.

## 1. Introduction

Additive manufacturing or 3D-printing is a new fabrication approach of developing a structure with any shape through the layer-by-layer deposition of materials through a computer-controlled program [1]. The 3D-printing technique benefits to rapid prototyping, customized design with minimal waste, and large scale manufacturing [2,3]. 3D-printing techniques have been potentially used for fabricating a novel electrode for electrochemical sensing devices [4]. Fused deposition modeling (FDM) is a common method for fabricating an electrode substrate, where a thermoplastic filament is extruded down the nozzle and a desired shaped object is printed [5,6]. However, such surfaces often do not have the desired catalytic properties to enable sensing applications. Improving the surface properties of these electrodes for electrochemical applications is the current challenge [7]. Atomic layer deposition has been used to modify metal electrodes for electrocatalytic purposes [8]; however, it requires high-end cleanroom equipment and is not feasible for decentralized low-cost electrode fabrication. Gold modification of iron 3D-printed electrodes was shown by us previously for DNA detection [9]. The electrodeposition method is facile; however, metallic 3D printing requires high-end high-cost equipment. We

recently introduced a procedure to electrochemically coat low-cost FDM electrodes with transition metal dichalcogenides for hydrogen evolution reaction [10]. Transition metal nanoparticles of copper/nickel and their oxide/hydroxide serve as an active non-enzymatic catalytic site [11–16]. The above observations and importance of 3D-printing technology and active metal sites lead us to the inspiration of coating 3D-printed conducting electrodes by electrodeposition of copper and nickel for sugar sensing [17–25]. Electroplating of non-precious metals such as copper and nickel offers a low-cost alternative to using costly metals such as gold, silver, and platinum. This is the main attraction of the proposed non-enzymatic biosensor material [26,27] using a 3D-printed structure. The 3D-printed substrate after activation serves as an active site for sensing due to porous structure and high surface area. Metal electroplating on 3D-printed porous structure helps to improve the surface properties and eliminates the kinetic barrier [15]. Further, the presence of carbon support also improves the conduction path of electrons between the analyte and electrode surface [22].

Diabetes mellitus, or diabetes, is a chronic disorder caused by an increased concentration of sugar in the blood, which may lead to stroke, heart disease, and damage to the eyes, nerves, and kidneys [28,29]
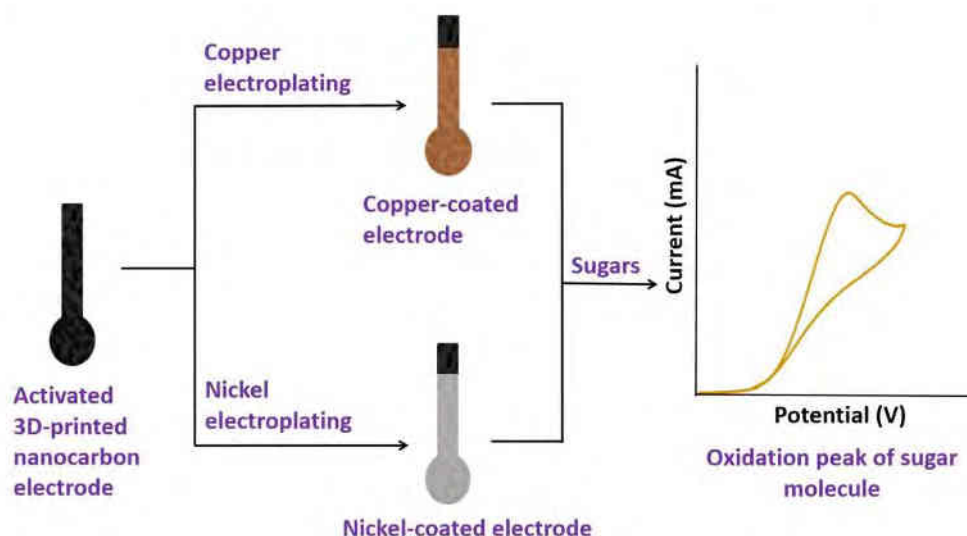
**Scheme 1.** Schematic representation of the copper and nickel electroplating of an activated 3D-printed nanocarbon electrode and its electrochemical sensing of sugars.
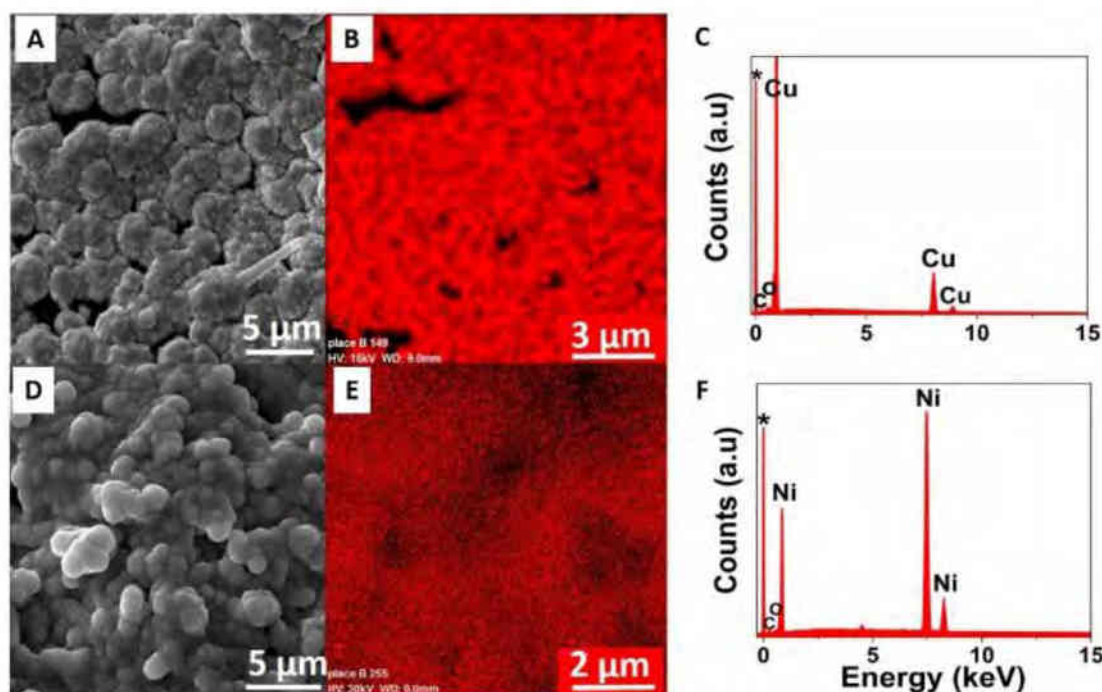


**Fig. 1.** (A) Scanning electron microscopy (SEM) image of Cu@3D-CE, (B)-(C) Energy-dispersive X-ray spectroscopy (EDX) mapping and EDX spectral analysis of Cu@3D-CE, (D) SEM image of Ni@3D-CE, (E)-(F) EDX mapping and EDX Spectral analysis of Ni@3D-CE (* background peak).

Around 693 million people are expected to be diabetic by 2045 [30]. The amount of glucose in the blood for non-diabetic patients is in the range of 3.9–6.2 mM [29]. Traditionally, there are many devices for detecting blood sugar levels [31]. However, the challenge is to develop a sensor that is time-accurate, quick, low-cost, and easily monitor sugar level in the blood. Hence, the concept of non-enzymatic sensors came to light due to the advantages of being faster, reliable, and precise compared with enzymatic sensors [13,32–35].

We have fabricated the sugar-sensing electrode by employing a simple and scalable technique. The electrode was fabricated using a low-cost conducting substrate and a cost-effective method to electroplate 3D-printed nanocarbon electrode for non-enzymatic sugar sensing, specifically glucose and sucrose.

## 2. Experimental section

### 2.1. Materials and methods

Copper sulfate pentahydrate ($CuSO_4 \cdot 5H_2O$), sodium hydroxide (NaOH), glucose, sucrose, dimethylformamide (DMF), nickel sulphate
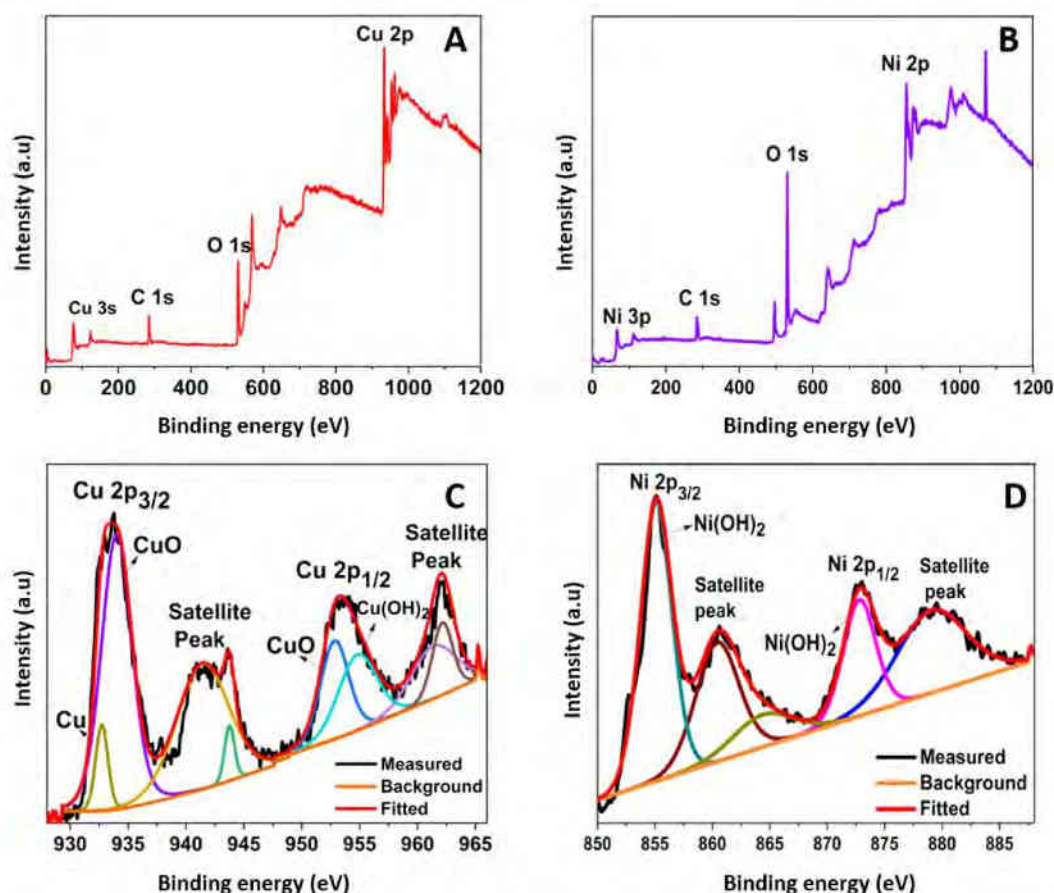
**Fig. 2.** X-ray photoelectron spectroscopy (XPS) survey spectrum of (A) copper electroplated 3D-printed nanocarbon electrode (Cu@3D-CE). (B) Nickel electroplated 3D-printed nanocarbon electrode (Ni@3D-CE); deconvoluted spectra of (C) Cu 2p of Cu@3D-CE, and (D) Ni 2p of Ni@3D-CE samples.

hexahydrate ($NiSO_4 \cdot 6H_2O$), boric acid ($H_3BO_3$), ethanol, and sulphuric acid ($H_2SO_4$) were purchased from Sigma-Aldrich, Germany. All chemicals were of analytical grade and used as received. Commercially available filament, conductive graphene/ polylactic acid (PLA) filament (Graphene Supermarket, USA) was used for 3D printing of the electrodes. All stock solutions were prepared with ultra-pure water purified by a Millipore-Q System, having resistivity not less than 18.2 M$\Omega$ cm$^{-1}$. A fresh solution of desired sugar (either glucose or sucrose) was prepared daily prior to analysis.

### 2.2. 3D-printing of carbon electrodes using graphene/PLA filament

3D-printing via FDM [1,36,37] was done to print structures based on the input design assigned to the printer (Prusa I3 MK3 printer, Prusa Research, Czech Republic) with an Olsson ruby-tipped 0.4 mm nozzle (3DVerkstan, Sweden). Graphene/PLA filament is extruded down the nozzle at a temperature of 220 °C and bed temperature around 60 °C. The 3D-printed electrode consists of a hybridized composition of conductive graphene and non-conductive PLA polymer. To improve the conductivity of these electrodes, solvent activation was carried out by immersing the printed nanocarbon electrodes in DMF for four hours. The electrodes were washed with ethanol and water to remove PLA and then dried in the oven at 65 °C for two hours [5]. The activated 3D-printed nanocarbon electrode are denoted as 3D-CE in the following sections.

### 2.3. Electroplating of carbon electrodes

The dried 3D-printed electrode was electroplated with the respective electrolyte solution. Briefly, the activated 3D-printed carbon electrode was used as a working electrode (WE), platinum as a counter electrode (CE), and Ag/AgCl (1 M KCl) with a salt bridge (0.1 M KCl) as a reference electrode (RE).

**Copper Plating.** Chronoamperometric measurements were carried out at a constant potential of −0.5 V for electroplating the carbon electrode using a mixture of 0.1 M copper(II) sulfate pentahydrate and 0.5 M sulfuric acid solution for 10 min (Fig. S1). With the application of constant reduction potential, a fine layer of copper metal is deposited over the surface of the printed nanocarbon electrode. A change in color of the electrode (black to brown) was observed. The electrode was allowed to dry at room temperature [14,38].

**Nickel Plating.** The electrodeposition of metallic nickel on the nanocarbon electrode was carried out in an electrolyte mixture of 0.1 M nickel sulphate hexahydrate and 0.5 M boric acid [17]. Cyclic voltammetry (CV) was performed in a potential scan range of 0.0 to −2 V at a scan rate of 50 mV s$^{-1}$ (Fig. S2). To ensure complete formation of the nickel hydroxide layer, the electrode was transferred to a 0.1 M NaOH solution and cycled 20 times in a potential range of 0.9 to −0.9 V at the scan rate of 100 mV s$^{-1}$ (Fig. S3).

### 2.4. Materials characterization

The surface morphology of the metal (copper/nickel) electroplated
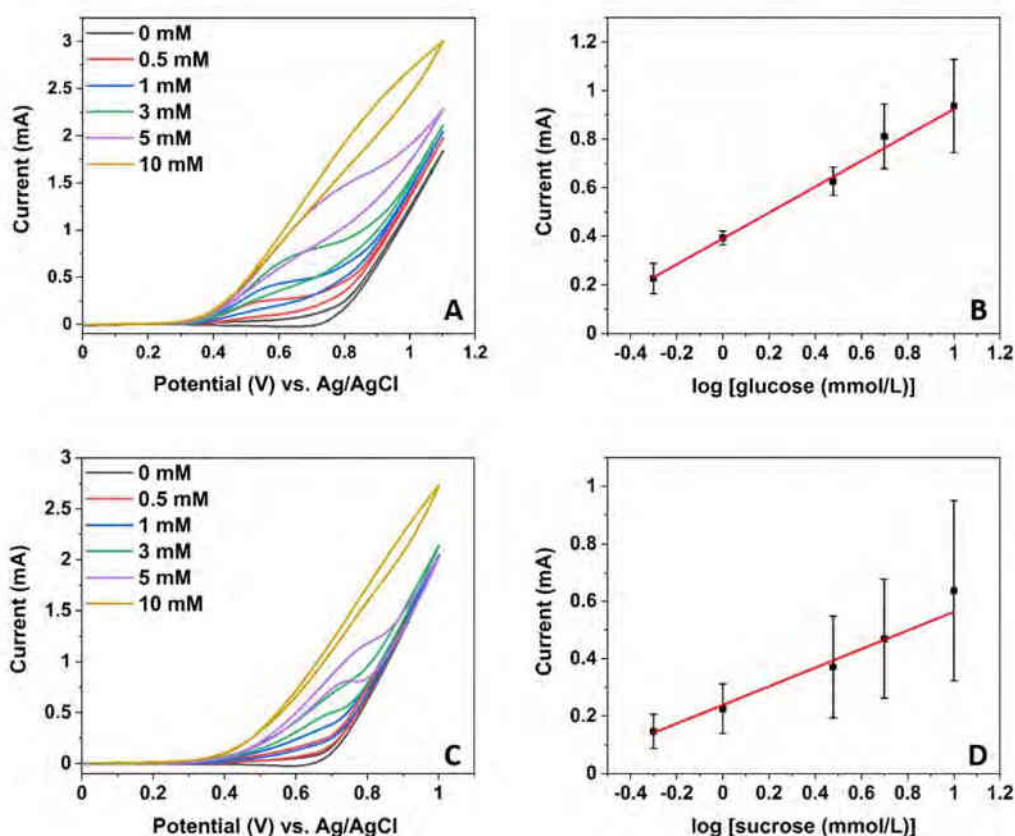
**Fig. 3.** (A) Cyclic voltammograms of increasing glucose concentrations in 0.1 M NaOH solution using Cu@3D-CE at scan rate 20 mV s$^{-1}$. (B) Analysis of peak current versus glucose concentration at +0.6 V. (C) Cyclic voltammograms of increasing sucrose concentrations in 0.1 M NaOH solution using a Cu@3D-CE at scan rate 20 mV s$^{-1}$. (D) Analysis of peak current versus sucrose concentration at +0.65 V.

3D-printed nanocarbon electrode was observed using a scanning electron microscopy (SEM, TESCAN LYRA 3). The elemental analysis was carried out by energy-dispersive X-ray spectroscopy (EDX). In addition, chemical compositional analyses were performed by XPS (Kratos AXIS Supra instrument) using a monochromatic Al Kα (1486.7 eV) excitation source. The X-ray power was 225 W. The data were analyzed using Casa XPS software.

### 2.5. Electrochemical measurements

Cyclic voltammetric and chronoamperometric measurements were conducted using a potentiostat (PGSTAT 204, Metrohm Autolab) operated by Nova 2.14 software. The measurements were carried out at room temperature using Ag/AgCl (1 M KCl) with a salt bridge (0.1 M KCl) as the reference electrode and platinum wire as the counter electrode. The electrolyte comprises varying concentrations of sugar solution (0.5–10 mM) in 0.1 M NaOH.

### 3. Results and discussion

We have fabricated a 3D-printed electrode from a graphene/PLA filament and its surface was activated by dimethylformamide [3,5]. From the SEM image, it was observed that the 3D-printed electrode contains nanofiber shaped carbon/graphene having a diameter of 80–150 nm and a few micrometers in length. The SEM image is depicted in the supplementary information (Fig. S4). To improve the electrocatalytic activity of the 3D-printed nanocarbon electrode for glucose and sucrose detection, we have electroplated it with non-precious metals: copper and nickel. The schematic presentation of sugar sensing using an electroplated 3D-printed carbon electrode is presented in Scheme 1.

The ensued metal electroplated 3D-printed carbon electrode (M@3D-CE) was characterized before the sugar detection tests. The morphology of the resulting copper (Fig. 1A) and nickel (Fig. 1D) deposition is characterized using SEM imaging, where the formation of nanoparticles is evident over the surface of the 3D-printed nanocarbon electrode. From the size distribution profile, the average particle size was found to be 2.31 and 1.4 μm for Cu@3D-CE and Ni@3D-CE, respectively shown in (Fig. S5).

The EDX analysis was used to study the type of elements present in the material and their distribution. The formation of copper nanoparticles over the surface of the carbon electrode is evident from EDX mapping (Fig. 1B). The EDX spectral analysis of copper electroplated 3D-printed nanocarbon electrode (Cu@3D-CE) confirmed the presence of Cu, C, and O with their atomic percentage as 88.00, 9.31, and 2.69%, respectively (Fig. 1C). Coverage by these copper nanoparticles on the 3D-printed nanocarbon electrode enhances the electrocatalytic efficiency of the electrode toward sugar sensing. Similarly, the presence of nickel nanoparticles over the surface of nickel electroplated 3D-printed nanocarbon electrode (Ni@3D-CE) can be observed from the SEM image (Fig. 1D) and EDX mapping (Fig. 1E). The EDX spectral analysis confirmed the presence of Ni, C, and O with their atomic percentage as 75.33, 24.02, and 0.45%, respectively (Fig. 1F).

XPS analysis of M@3D-CE was conducted to confirm the composition and chemical states of the material. Fig. 2A shows the XPS survey spectrum of copper electroplated 3D-printed nanocarbon electrode

(Cu@3D-CE) after electroplating. From the wide scan spectrum, the peaks at 285, 530, and 934 eV are corresponding to C 1s, O 1s and Cu 2p, respectively. The wide spectral analysis showed the atomic % of copper, carbon and oxygen are 15.00, 40.28, 44.57%, respectively. The high-resolution Cu 2p core level spectrum shows two characteristic peaks at the binding energy (BE) of 933.6 and 953.3 eV corresponding to Cu 2p3/2 and Cu 2p1/2, respectively, (Fig. 2C) of Cu(II) state which is arising most likely from CuO or $Cu(OH)_2$ [20]. The strong presence of $Cu^{2+}$ was further confirmed from the peaks observed at 941.6 and 962.2 eV which are sake-up satellite peaks corresponding to the characteristic $d^9$ ground state configuration [21–23,39]. In addition, the small peaks that appeared at 932.7 and 952.8 eV correspond to the Cu 2p3/2 and Cu 2p1/2, respectively which can be assigned to Cu(0) or Cu (I) state. However, the Cu(0) state can be separated from Cu(I) state in XPS analysis due to their overlapping peaks. The possible presence of Cu(I) is most likely due to the formation of small quantity of $Cu_2O$ [40].

Fig. 2B depicts the wide spectral analysis of (Ni@3D-CE), showing the presence of Ni 2p, C 1s and O 1s peaks. The high-resolution core level Ni 2p spectrum shows the peak appeared at 855.0 and 872.8 eV corresponding to the Ni 2p3/2 and Ni 2p1/2, respectively acquainting a spin–orbit peak separation of 17.8 eV, which can be assigned to $Ni^{2+}$ (Fig. 2D). The presence of $Ni^{2+}$ state is possibly due to the formation of nickel hydroxide [$Ni(OH)_2$] after electrodeposition [24,25,39].

After confirming the electrochemically deposited metal coating on the 3D-printed electrodes, we have investigated the electrochemical response of enzyme-free sugar sensing of M@3D-CE. The CV analyses of glucose and sucrose sensing (0.5–10 mM) using Cu@3D-CE are shown in Fig. 3A and C, respectively. A quantifiable peak is observed on increasing concentration of sugar. From the observed peak current in the sugar oxidation CV analysis, the current at oxidation potentials of 0.6 V for glucose and 0.65 V for sucrose were plotted with a range of sugar concentration from 0.5 to 10 mM, as depicted in Fig. 3B and D, respectively. Fig. 3B displays the calibration curve of linearity ($R^2 = 0.9937$) over a range of concentrations from 0.5 to 10 mM with a slope of 0.532 $mol^{-1}$ L A. Fig. 3D displays the linear response ($R^2 = 0.9807$) over a range of concentrations from 0.5 to 10 mM with a slope of 0.324 $mol^{-1}$ L A. The obtained plot gives us a clear relation of concentration and sensitivity of the electrode.

It is well-known that the reactivity of glucose is higher than sucrose towards Cu(II) [19]. This can be evidenced from the more prominent oxidation peak as observed from the cyclic voltammograms of glucose and sucrose at the concentration from 0.5 to 5 mM (Fig. 3A, C). This difference reactivity of glucose and sucrose towards Cu(II) can be explained considering the chemical structures of the glucose and sucrose which are shown in (Fig. S6). The glucose being a monosaccharide is easy to oxidize while the sucrose which is a disaccharide, constitutes glucose and fructose, is less susceptible to oxidize [41]. The electrocatalytic process for glucose oxidation is mediated by the Cu(II)/Cu(III) redox couple in the alkaline solution, where Cu(III) species acted as an electron transfer mediator [42]. The mechanism of glucose sensing towards Cu(II) can be explained by formation and decomposition of intermediate charge transfer complex which is stated as follows [13,42].

$$CuO + OH^- \rightarrow CuOOH + e^- \tag{1}$$

$$Cu(II) \rightarrow Cu(III) + e^- \tag{2}$$

$$Cu(III) + glucose + e^- \rightarrow Cu(II) + gluconolactone \tag{3}$$

Hence, at a particular potential, the Cu(III) on electrode surface oxidize glucose to gluconolactone and then again return to its initial state Cu(II). As the glucose unit of sucrose only show the reactivity towards Cu(II), the overall sensitivity of sucrose decreased.

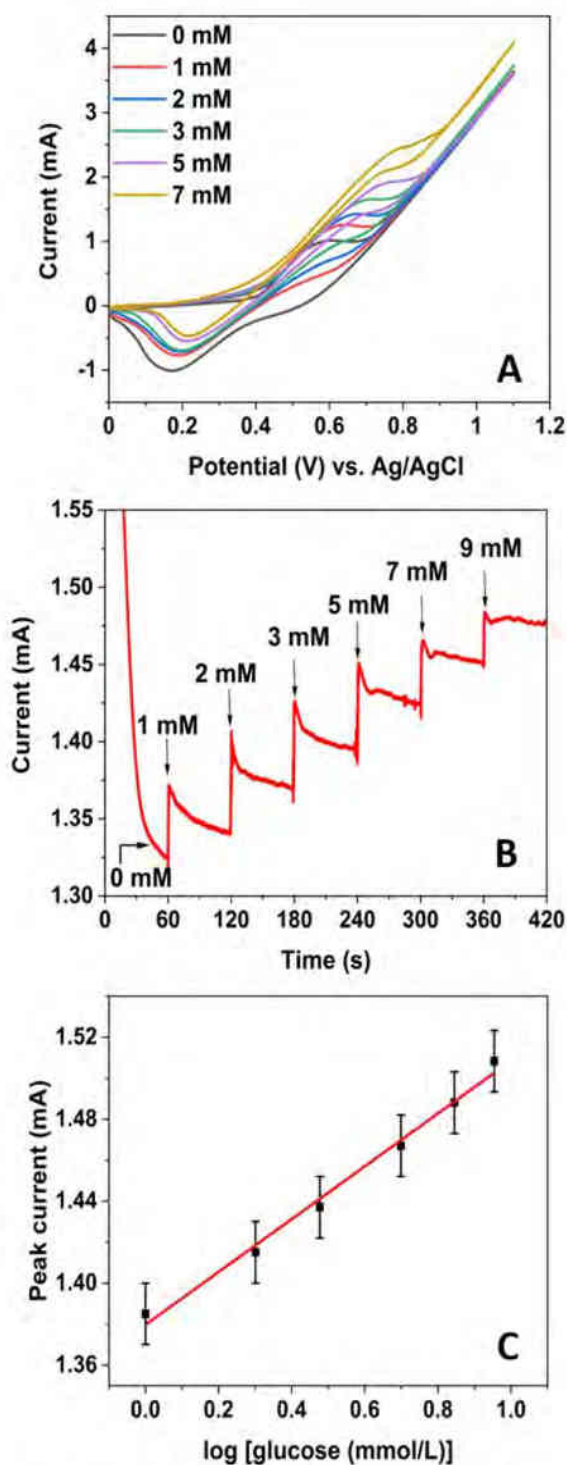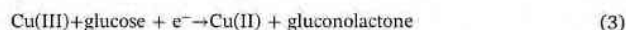**Fig. 4.** (A) Cyclic voltammograms of nickel electroplated 3D-printed nanocarbon electrode with increasing glucose concentration in a 0.1 M NaOH solution at a scan rate of 20 mV $s^{-1}$. (B) Chronoamperometric measurements obtained by sequential addition of 500 μL. of glucose with increasing concentration every 60 s at +0.85 V vs. (Ag/AgCl). (C) Chronoamperometric peak current versus concentration of glucose at +0.85 V.

We further extended our studies on Ni@3D-CE by carrying out CV measurements at a potential scan range from 0.0 to 1.1 V at a scan rate of 20 mV s$^{-1}$ (Fig. 4A). Chronoamperometric measurements of Ni@3D-CE were carried out where a sharp increase in current was measured on successive addition of 500 μL glucose in 0.1 M NaOH. The glucose was added every 60 s from 1 to 9 mM concentration at a potential of + 0.85 V (Fig. 4B). Fig. 4C displays the calibration curve ($R^2$ = 0.9909) over a range of concentrations from 1 to 9 mM with a slope of 0.128 mol$^{-1}$ L A.

It was found that the Cu@3D-CE was sensitive for glucose and sucrose, while the Ni@3D-CE was sensitive only to glucose. Here, for Ni@3D-CE, the oxygen atoms on nickel hydroxide [NiO(OH)] easily interact with the hydroxyl groups of glucose, promoting their dehydrogenation and conversion of glucose to gluconolactone in alkaline solution [25]. The reactions are stated as follows:

$$NiO + H_2O \rightarrow NiOOH \qquad (4)$$

$$NiOOH + glucose \rightarrow NiO + H_2O_2 + gluconolactone \qquad (5)$$

$$Gluconolactone \rightarrow gluconic\ acid \qquad (6)$$

$$Gluconic\ acid + H_2O \rightarrow gluconate^- + H^+$$
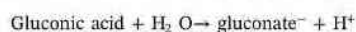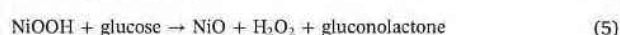
To evaluate the glucose-sensing of Ni@3D-CE we carried out cyclic voltammetric measurements which showed a shift of oxidation potential of ~ 0.2 V over the range of glucose concentration used. Hence, we followed a more sensitive approach of chronoamperometric technique to confirm the glucose-sensing using Ni@3D-CE. The chronoamperometric technique being a more precise and sensitive method showed better linearity and identical error bar throughout the concentration range. Unfortunately, Ni@3D-CE was not sensitive to sucrose. The electrode did not show any significant oxidation peak in the range of sucrose concentration from 1 to 10 mM in the CV measurement. This result is also in agreement with the previously reported work [43,44].

## 4. Conclusions

We have demonstrated, for the first time, metal plating of 3D-printed nanocarbon electrodes for carbohydrate sensing. Thus, this approach would suggest an easy modification of 3D-printed nanocarbon substrate as functional electrodes for successful sensing of desired molecular targets. The metal ions deposited over the active sites of nanocarbon substrate which can improve the surface properties and eliminate the kinetic barrier followed by improved sensing between metal oxides/hydroxides and carbohydrates. The 3D-printing approach enable to fabricate any customized shaped electrodes as needed. We believe the employed approach of decentralized electrode fabrication and the non-precious metal coating is expected to find broad use in various electrochemical applications such as oxygen evolution reaction (OER), hydrogen evolution reaction (HER), ammonia reduction, etc.

## Declaration of Competing Interest

The authors declare that they have no known competing financial interests or personal relationships that could have appeared to influence the work reported in this paper.

## Acknowledgments

## Appendix A. Supplementary data

Supplementary data to this article can be found online at https://doi.org/10.1016/j.elecom.2020.106827.

## References

[1] A. Ambrosi, M. Pumera, 3D-printing technologies for electrochemical applications, Chem. Soc. Rev. 45 (10) (2016) 2740–2755, https://doi.org/10.1039/c5cs00714c.

[2] M.P. Browne, E. Redondo, M. Pumera, 3D printing for electrochemical energy applications, Chem. Rev. 120 (5) (2020) 2783–2810, https://doi.org/10.1021/acs.chemrev.9b00783.

[3] C.L. Manzanares Palenzuela, F. Novotný, P. Krupička, Z. Sofer, M. Pumera, 3D-printed graphene/polylactic acid electrodes promise high sensitivity in electroanalysis, Anal. Chem. 90 (9) (2018) 5753–5757, https://doi.org/10.1021/acs.analchem.8b00083.

[4] J. Muñoz, M. Pumera, Accounts in 3D-printed electrochemical sensors: towards monitoring of environmental pollutants, ChemElectroChem 7 (16) (2020) 3404–3413, https://doi.org/10.1002/celc.202000601.

[5] M.P. Browne, F. Novotný, Z. Sofer, M. Pumera, 3D printed graphene electrodes' electrochemical activation, ACS Appl. Mater. Interfaces 10 (46) (2018) 40294–40301, https://doi.org/10.1021/acsami.8b14701.

[6] M.P. Browne, M. Pumera, Impurities in graphene/PLA 3D-printing filaments dramatically influence the electrochemical properties of the devices, Chem. Commun. 55 (58) (2019) 8374–8377, https://doi.org/10.1039/C9CC03774H.

[7] D.W. Hwang, S. Lee, M. Seo, T.D. Chung, Recent advances in electrochemical non-enzymatic glucose sensors – a review, Anal. Chim. Acta 1033 (2018) 1–34, https://doi.org/10.1016/j.aca.2018.05.051.

[8] M.P. Browne, J. Plutnar, A.M. Pourrahimi, Z. Sofer, M. Pumera, Atomic layer deposition as a general method turns any 3D-printed electrode into a desired catalyst: case study in photoelectrochemisty, Adv. Energy Mater. 9 (26) (2019) 1900994, https://doi.org/10.1002/aenm.201900994.

[9] A.H. Loo, C.K. Chua, M. Pumera, DNA biosensing with 3D printing technology, Analyst 142 (2) (2017) 279–283, https://doi.org/10.1039/c6an02038k.

[10] C. Iffelsberger, S. Ng, M. Pumera, Catalyst coating of 3D printed structures via electrochemical deposition: case of the transition metal chalcogenide MoSx for hydrogen evolution reaction, Appl. Mater. Today 20 (2020) 100654, , https://doi.org/10.1016/j.apmt.2020.100654.

[11] R. Madhu, V. Veeramani, S.M. Chen, A. Manikandan, A.Y. Lo, Y.L. Chueh, Honeycomb-like porous carbon-cobalt oxide nanocomposite for high-performance enzymeless glucose sensor and supercapacitor applications, ACS Appl. Mater. Interfaces 7 (29) (2015) 15812–15820, https://doi.org/10.1021/acsami.5b04132.

[12] H. Liu, X. Wu, B. Yang, Z. Li, L. Lei, X. Zhang, Three-dimensional porous NiO nanosheets vertically grown on graphite disks for enhanced performance non-enzymatic glucose sensor, Electrochim. Acta 174 (2015) 745–752, https://doi.org/10.1016/j.electacta.2015.06.062.

[13] H. Zhu, L. Li, W. Zhou, Z. Shao, X. Chen, Advances in non-enzymatic glucose sensors based on metal oxides, J. Mater. Chem. B 4 (46) (2016) 7333–7349, https://doi.org/10.1039/C6TB02037B.

[14] J.W. Dini, D.D. Snyder, Electrodeposition of copper, in: Modern Electroplating, fifth ed., 2011, pp. 33–78. doi: 10.1002/9780470602638.ch2.

[15] E. Vaněčková, et al., Copper electroplating of 3D printed composite electrodes, J. Electroanal. Chem. 858 (2020) 113763, , https://doi.org/10.1016/j.jelechem.2019.113763.

[16] P.C. Andricacos, C. Uzoh, J.O. Dukovic, J. Horkans, H. Deligianni, Damascene copper electroplating for chip interconnections, IBM J. Res. Dev. 42 (5) (1998) 567–573, https://doi.org/10.1147/rd.425.0567.

[17] S.M. Janjan, F. Nasirpouri, M.G. Hosseini, Electrodeposition mechanism of nickel films on polycrystalline copper from dilute simple sulphate solutions, Russ. J. Electrochem. 47 (7) (2011) 787–792, https://doi.org/10.1134/S1023193511070159.

[18] R.E. Hummel, R.J. Smith, E.D. Verink, The passivation of nickel in aqueous solutions—I. The identification of insoluble corrosion products on nickel electrodes using optical and ESCA techniques, Corros. Sci. 27 (8) (1987) 803–813, https://doi.org/10.1016/0010-938X(87)90038-2.

[19] N.A. Choudhry, D.K. Kampouris, R.O. Kadara, N. Jenkinson, C.E. Banks, Next generation screen printed electrochemical platforms: non-enzymatic sensing of carbohydrates using copper(ii) oxide screen printed electrodes, Anal. Methods 1 (3) (2009) 183–187, https://doi.org/10.1039/b9ay00095j.

[20] Q. Wang, Q. Wang, M. Li, S. Szunerits, R. Boukherroub, Preparation of reduced graphene oxide/Cu nanoparticle composites through electrophoretic deposition: application for nonenzymatic glucose sensing, RSC Adv. 5 (21) (2015) 15861–15869, https://doi.org/10.1039/C4RA14132F.

[21] G. He, L. Wang, One-step preparation of ultra-thin copper oxide nanowire arrays/copper wire electrode for non-enzymatic glucose sensor, Ionics (Kiel) 24 (10) (2018) 3167–3175, https://doi.org/10.1007/s11581-018-2513-7.

[22] H. Maaoui, et al., Copper oxide supported on three-dimensional ammonia-doped porous reduced graphene oxide prepared through electrophoretic deposition for non-enzymatic glucose sensing, Electrochim. Acta 224 (2017) 346–354, https://doi.org/10.1016/j.electacta.2016.12.078.

[23] H. Chen, et al., A portable micro glucose sensor based on copper-based nanocomposite structure, New J. Chem. 43 (20) (2019) 7806–7813, https://doi.org/10.1039/c9nj00888h.

[24] A.N. Mansour, C.A. Melendres, Characterization of α-Ni(OH)$_2$ by XPS, Surf. Sci. Spectra 3 (3) (1994) 255–262, https://doi.org/10.1116/1.1247754.

[25] S. Mishra, P. Yogi, P.R. Sagdeo, R. Kumar, Mesoporous nickel oxide (NiO) nanopetals for ultrasensitive glucose sensing, Nanoscale Res. Lett. 13 (2018) 16, https://doi.org/10.1186/s11671-018-2435-3.

[26] F.J. Garcia-Garcia, P. Salazar, F. Yubero, A.R. González-Elipe, Non-enzymatic glucose electrochemical sensor made of porous NiO thin films prepared by reactive

magnetron sputtering at oblique angles, Electrochim. Acta 201 (2016) 38–44, https://doi.org/10.1016/j.electacta.2016.03.193.

[27] E. Zhang, Y. Xie, S. Ci, J. Jia, Z. Wen, Porous Co$_3$O$_4$ hollow nanododecahedra for nonenzymatic glucose biosensor and biofuel cell, Biosens. Bioelectron. 81 (2016) 46–53, https://doi.org/10.1016/j.bios.2016.02.027.

[28] Y. Su, B. Luo, J.Z. Zhang, Controllable cobalt oxide/Au hierarchically nanostructured electrode for nonenzymatic glucose sensing, Anal. Chem. 88 (3) (2016) 1617–1624, https://doi.org/10.1021/acs.analchem.5b03396.

[29] C. Chen, et al., Recent advances in electrochemical glucose biosensors: a review, RSC Adv. 3 (14) (2013) 4473–4491, https://doi.org/10.1039/c2ra22351a.

[30] N.H. Cho, et al., IDF diabetes atlas: global estimates of diabetes prevalence for 2017 and projections for 2045, Diabetes Res. Clin. Pract. 138 (2018) 271–281, https://doi.org/10.1016/j.diabres.2018.02.023.

[31] H.C. Wang, A.R. Lee, Recent developments in blood glucose sensors, J. Food Drug Anal. 23 (2) (2015) 191–200, https://doi.org/10.1016/j.jfda.2014.12.001.

[32] D.-W. Hwang, S. Lee, M. Seo, T.D. Chung, Recent advances in electrochemical non-enzymatic glucose sensors – a review, Anal. Chim. Acta 1033 (2018) (2018) 1–34, https://doi.org/10.1016/j.aca.2018.05.051.

[33] X. Niu, X. Li, J. Pan, Y. He, F. Qiu, Y. Yan, Recent advances in non-enzymatic electrochemical glucose sensors based on non-precious transition metal materials: opportunities and challenges, RSC Adv. 6 (88) (2016) 84893–84905, https://doi.org/10.1039/C6RA12506A.

[34] X. Chen, G. Wu, Z. Cai, M. Oyama, X. Chen, Advances in enzyme-free electrochemical sensors for hydrogen peroxide, glucose, and uric acid, Microchim. Acta 181 (7–8) (2014) 689–705, https://doi.org/10.1007/s00604-013-1098-0.

[35] E. Sehit, Z. Altintas, Significance of nanomaterials in electrochemical glucose sensors: An updated review (2016–2020), Biosens. Bioelectron. 159 (2020) 112165, , https://doi.org/10.1016/j.bios.2020.112165.

[36] R. Singh, H.K. Garg, Fused Deposition Modeling – A State of Art Review and Future

Applications. Reference Module in Materials Science and Materials Engineering, Elsevier Ltd., 2016. doi:10.1016/B978-0-12-803581-8.04037-6.

[37] S.C. Daminabo, S. Goel, S.A. Grammatikos, H.Y. Nezhad, V.K. Thakur, Fused deposition modeling-based additive manufacturing (3D printing): techniques for polymer material systems, Mater. Today Chem. 16 (2020) 100248, , https://doi.org/10.1016/j.mtchem.2020.100248.

[38] M.J. Kim, et al., One-step electrodeposition of copper on conductive 3D printed objects, Addit. Manuf. 27 (2019) 318–326, https://doi.org/10.1016/j.addma.2019.03.016.

[39] X. Wang, et al., Super-light Cu@Ni nanowires/graphene oxide composites for significantly enhanced microwave absorption performance, Sci. Rep. 7 (1) (2017) 1584, https://doi.org/10.1038/s41598-017-01529-2.

[40] H. Maaoui, et al., Non-enzymatic glucose sensing using carbon quantum dots decorated with copper oxide nanoparticles, Sensors 16 (10) (2016) 1720, https://doi.org/10.3390/s16101720.

[41] K.E. Toghill, R.G. Compton, Electrochemical non-enzymatic glucose sensors: a perspective and an evaluation, Int. J. Electrochem. Sci. 5 (9) (2010) 1246–1301.

[42] F.C.U. Santos, L.L. Paim, J. Luiz da Silva, N.R. Stradiotto, Electrochemical determination of total reducing sugars from bioethanol production using glassy carbon electrode modified with graphene oxide containing copper nanoparticles, Fuel 163 (2016) 112–121, https://doi.org/10.1016/j.fuel.2015.09.046.

[43] X. Gao, et al., Nickel catalysts supported on acetylene black for high-efficient electrochemical oxidation and sensitive detection of glucose, Nanoscale Res. Lett. 15 (1) (2020) 23, https://doi.org/10.1186/s11671-019-3218-1.

[44] X. Gao, X. Du, D. Liu, H. Gao, P. Wang, J. Yang, Core-shell gold-nickel nanostructures as highly selective and stable nonenzymatic glucose sensor for fermentation process, Sci. Rep. 10 (1) (2020) 1365, https://doi.org/10.1038/s41598-020-58403-x.

# Supplementary information

## Metal-plated 3D-printed electrode for electrochemical detection of carbohydrates

K P Akshay Kumar [a], Kalyan Ghosh[a], Osamah Alduhaish[b] and Martin Pumera[a,b,c,d*]

[a]Future Energy and Innovation Laboratory, Central European Institute of Technology, Brno University of Technology, Purkyňova 123, 61200 Brno, Czech Republic

[b]Chemistry Department, College of Science, King Saud University, Riyadh 11451, Saudi Arabia

[c]Department of Chemical and Biomolecular Engineering, Yonsei University, 50 Yonsei-ro, Seodaemun-gu, Seoul 03722, Korea

[d]Department of Medical Research, China Medical University Hospital, China Medical University, No. 91 Hsueh-Shih Road, Taichung 40402, Taiwan
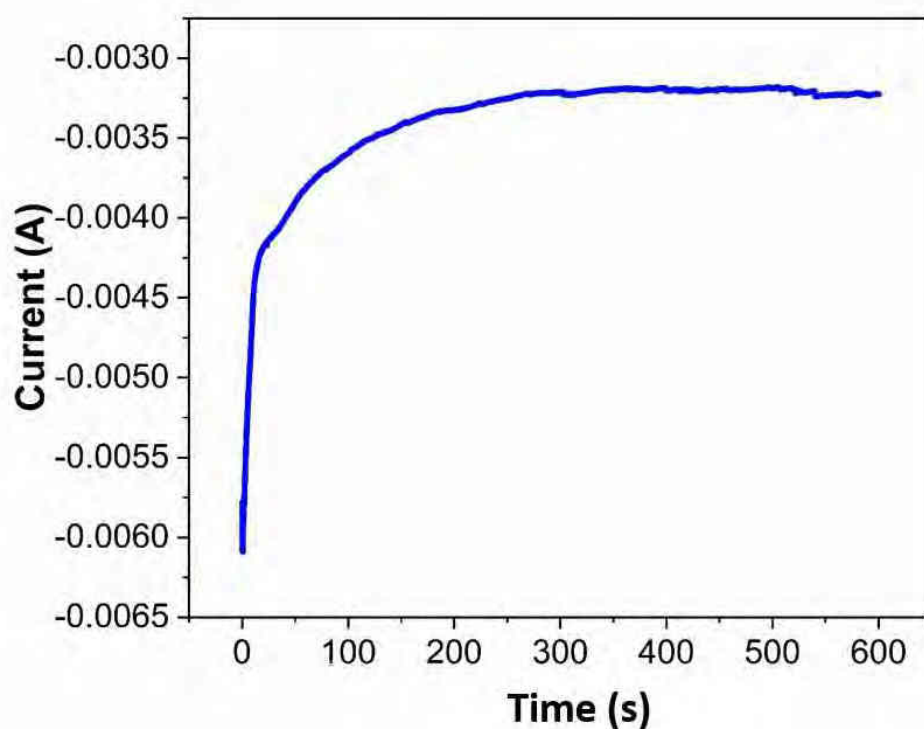
**Fig. S1.** Chronoamperometric deposition of copper over the surface of activated nanocarbon electrode for 10 min using 0.1 M $CuSO_4.5H_2O$ and 0.5 M $H_2SO_4$.
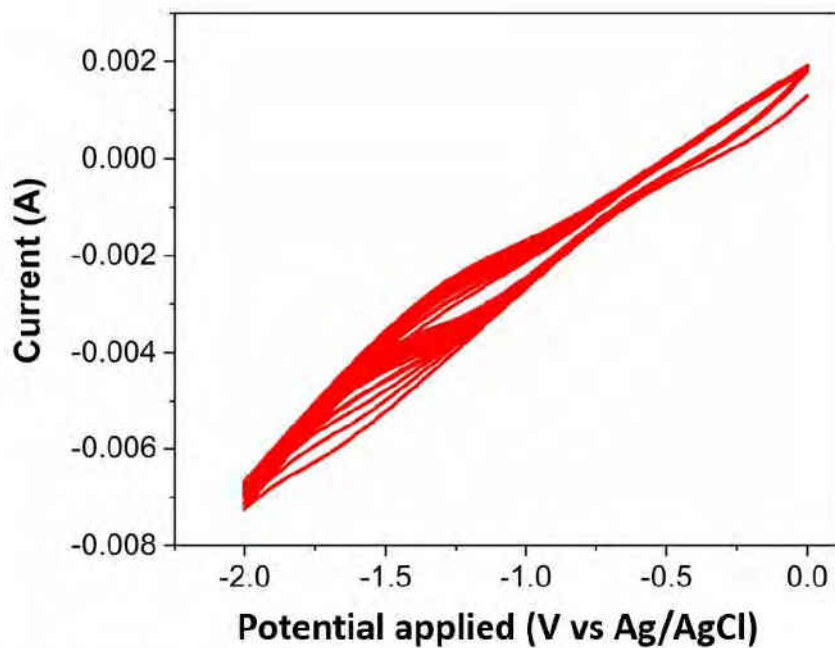
**Fig. S2.** Cyclic voltammograms of electroplating activated 3D-printed nanocarbon electrodes using 0.1 M NiSO$_4$.6H$_2$O and 0.5 M H$_3$BO$_3$ at a scan rate of 50 mV s$^{-1}$.
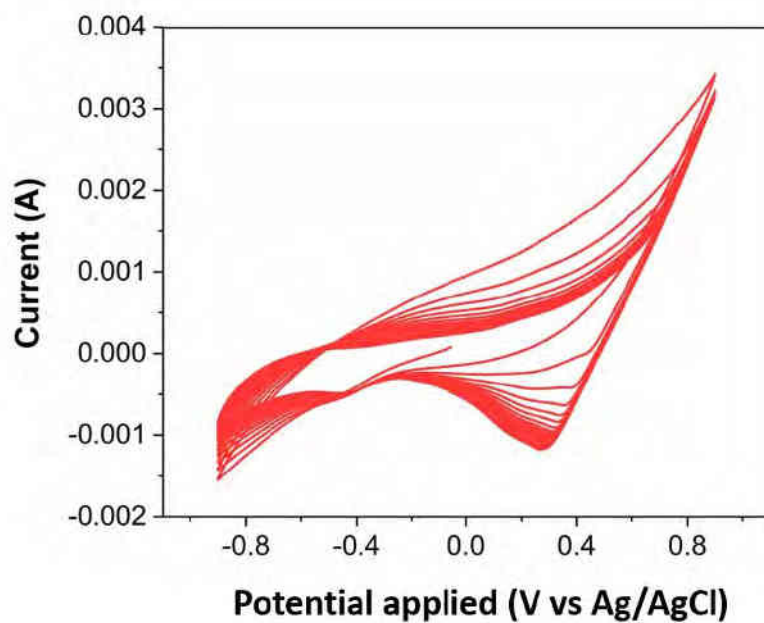


**Fig. S3.** Cyclic voltammograms of nickel plated nanocarbon electrode from -0.9 V to 0.9 V in 0.1 M NaOH for complete formation of nickel hydroxide layer at a scan rate of 100 mV s$^{-1}$.
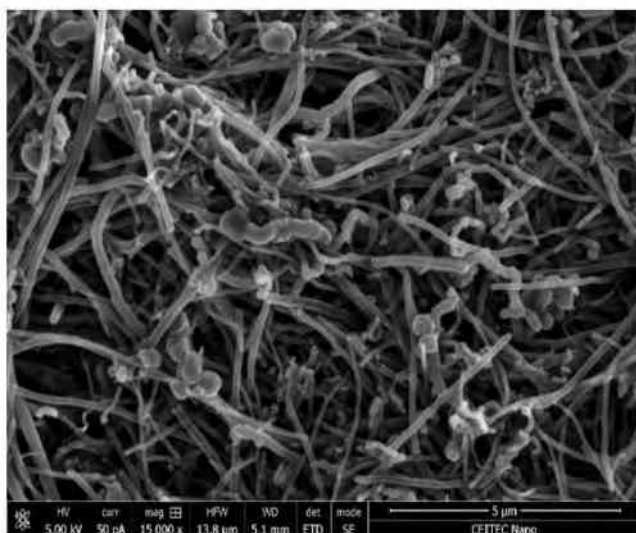
**Fig. S4.** SEM image of 3D-printed nanocarbon electrode
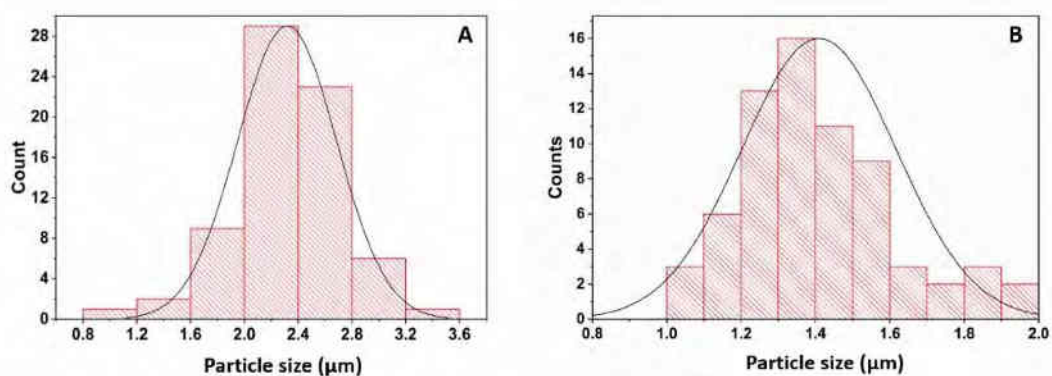


**Fig. S5.** Average particle size distribution profile from the SEM images A) Cu@3D-CE (B) Ni@3D-CE.
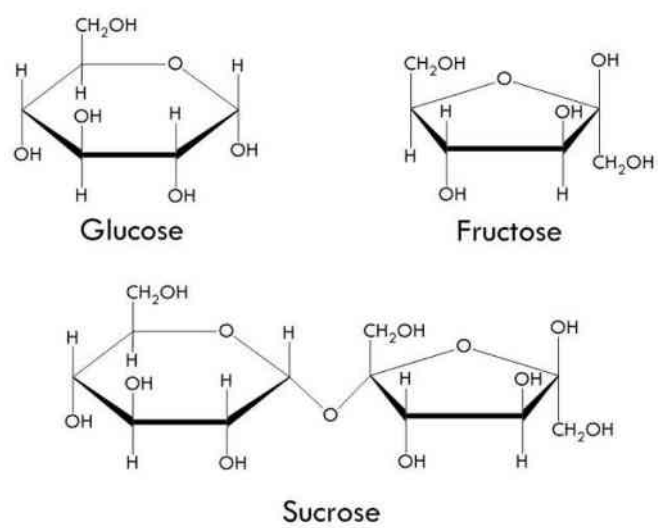
**Fig. S6.** Chemical structure of glucose and sucrose molecule

## 5.3. Future advancement of utilizing 3D-printing technology for energy and emergency healthcare application (Perspective reports)

The inclining energy crisis, along with rising global temperature and environmental imbalances, has significantly triggered the scientific community to find alternate sources. Electrocatalysts can play a key role in addressing these concerns by minimizing the excessive potential for respective applications. Eventually, fabrication of these electrocatalysts via 3D-printing technology would be an interesting domain to mitigate associated concerns, and such reports could be interesting for researchers working closely on these disciplines. Thus, Section-C, 5.3 deals with strategies employed in engineering electrocatalysts towards ammonia synthesis (5.3.1) and $CO_2$ mitigation (5.3.2). Precisely, section 5.3.1 extensively covers a discussion on the fabrication of 3D-printed structures towards NRA, along with an experimental demonstration of 3D-printed Cu electrodes for ammonia synthesis. Further, rising $CO_2$ levels are major concerns in the present global context. Section 5.3.2 discusses the advances in 3D-printing technology towards $CO_2$ mitigation via selective conversion of them to specific products and some interesting $CO_2$ capture techniques. Further, section 5.3.3 discusses the role played by 3D-printing technology during health emergency situations such as the COVID-19 pandemic. The discussion carried out in the section are published and the details are as follows:

### 5.3.1 Advancements in 3D-printing towards ammonia synthesis

Akshay Kumar K. Padinjareveetil, Martin Pumera*, *Engineering 3D Printed Structures Towards Electrochemically Driven Green Ammonia Synthesis: A Perspective*, **Adv.**

**Mater. Technologies**, 2023 ,10, 8, 2201734, https://doi.org/10.1002/admt.202202080, (IF=8.8).


### 5.3.2 3D-printing technology towards CO₂ reduction and capture

<u>Akshay Kumar K. Padinjareveetil</u>, Martin Pumera*, *Advances in Designing 3D-Printed Systems for CO₂ Reduction,* **Adv. Mater. Interfaces**, 2023, 10, 8, 2201734 https://doi.org/10.1002/admi.202201734, (IF=6.38).


### 5.3.3 3D-printing technology towards emergency healthcare application

<u>Akshay Kumar K. Padinjareveetil</u>, Martin Pumera*, *3D-Printing to Mitigate COVID-19 Pandemic*, **Adv. Funct. Mater**. 2021, 31, doi.org/10.1002/adfm.202100450, (IF=19.9).

### 5.3.1 Advancements in 3D-printing towards ammonia synthesis

**Motivation**

3D-printing technology has received massive attention for various electrocatalytic applications such as $H_2$, and $O_2$ production. Interestingly, the field has stepped into a new domain of employing 3D-printing structures for ammonia synthesis. Thus, a perspective article constituting the potential possibilities of this field will be interesting to researchers venturing into this field.

**Objective**

The article discusses the scope of employing 3D-printing technology for fabrication of electrocatalyst with enhanced activity, along with techniques and approaches of catalyst designing, modification, post-printing treatments, and catalytic mechanism. Further, the role of 3D-printed metal based, carbon based, alloys, 2D materials composites as catalyst for nitrate to ammonia conversion will be carried out. Further, an experimental demonstration of employing 3D-printed metal structures towards ammonia synthesis will be done for the first time, to analyse the potential of this field.

**Contribution**

Writing (original draft, review and editing).

**Outcome**

The article has broadly discussed the factors influencing the electrocatalyst fabrication towards ammonia synthesis such as shape, size, composition, morphology, post-printing

treatments. Further, experimental demonstration has showed the real potential of 3D-printed electrocatalyst for ammonia synthesis, thereby setting up a foundation for further exploration in this field.

**Article**

The article was published and the details of the article are as follows:

Akshay Kumar K. Padinjareveetil, Martin Pumera*, *Engineering 3D Printed Structures Towards Electrochemically Driven Green Ammonia Synthesis: A Perspective* , **Adv. Mater. Technologies**, 2023 ,10, 8, 2201734, https://doi.org/10.1002/admt.202202080, (IF=8.8).

# Engineering 3D Printed Structures Towards Electrochemically Driven Green Ammonia Synthesis: A Perspective

*Akshay Kumar K. Padinjareveetil, Juan V. Perales-Rondon, and Martin Pumera**

Broadening scope of 3D printing technology is recently identified as a potential strategy to mitigate concerns in the light of rising energy crisis and environmental imbalances. The importance of ammonia as a hydrogen carrier is well known and, in the context of 3D printing, designing and fabrication of electrode substrates for ammonia synthesis from nitrate sources will present a twofold advantage toward addressing the energy crisis and also limiting the harmful effect of excessive nitrate from the environment. Studies in the direction of employing 3D printed catalysts or reactors for ammonia production have been rarely reported. Thus, in this perspective article, the possibilities of engineering several 3D printed electrocatalysts for nitrate reduction to ammonia via various techniques are discussed and experimental demonstrations to substantiate the potential of 3D printed electrocatalysts toward ammonia production are provided, for the first time. In addition, postfabrication treatments, modification, and patterned coating of 3D printed substrates using active materials are also discussed along with the possibilities of fabricating catalysts for ammonia synthesis via nitrogen reduction reaction. Certain limitations and possible solutions of this printing technology for ammonia production are discussed along with the future outlook. Such timely discussions will be interesting for researchers and scientists for enhancing further possibilities toward broadening this field and toward other catalytic applications.

## 1. Introduction

The consistent decline in the availability of fossil fuels along with a rapidly growing population has resulted in a severe energy crisis in most parts of the world today. Several efforts have been carried out by the global scientific community to derive renewable and sustainable energy sources to meet these growing demands.[1–4] The synthesis of ammonia at an industrial scale is considered to be one of the most impactful discoveries of the last century[5] and its importance is manifold with applications in agricultural sectors, pharmaceuticals, textiles, refrigeration, and so on. Being a "green" hydrogen-rich molecule, ammonia is known to be an important next-generation energy carrier due to its high hydrogen content (17.65 wt%) and high gravimetric energy density (3 kWh kg$^{-1}$), which assists in convenient storage and transportation along with clean emissions.[6–11] Hence, its production requires critical attention, especially for combatting the increasing energy shortage. Owing to the environmental concerns, and high set-up cost for ammonia production via traditional techniques such as the Haber–Bosch process, researchers are now focusing on simple, efficient, and alternative approaches for ammonia synthesis.

Interestingly, studies focusing on nitrate ions have recently gained momentum as a new area of research where they are known to be a potential source for ammonia production. The electrochemical reduction of nitrate ($NO_3^-$) into ammonia ($NH_3$), abbreviated as NRA, involves an eight-electron and nine-proton transfer reaction proceeding through multiple reaction pathways/intermediate steps.[12,13] NRA has a reaction potential lower than hydrogen evolution reaction (HER). Furthermore, HER can be an interfering and competitive process during NRA, where electrons can be consumed for hydrogen generation, which can significantly limit the Faradaic efficiency (FE) and selectivity of the reaction system. Hence, the fabrication of catalysts becomes a key step in addressing the challenges associated with NRA, by limiting the N≡N bond formation and competitive HER, aiding selective reduction, and delivering appreciable FE necessary for practical applications. Although several fabrication

A. K. K. Padinjareveetil, J. V. Perales-Rondon, M. Pumera
Future Energy and Innovation Laboratory
Central European Institute of Technology
Brno University of Technology
Purkyňova 123, Brno 61200, Czech Republic
E-mail: martin.pumera@ceitec.vutbr.cz
M. Pumera
Department of Chemical and Biomolecular Engineering
Yonsei University
50 Yonsei-ro, Seodaemun-gu, Seoul South Korea, 03722
M. Pumera
Faculty of Electrical Engineering and Computer Science
VSB – Technical University of Ostrava
17. listopadu 2172/15 Ostrava 70800, Czech Republic

**ADVANCED
SCIENCE NEWS**
www.advancedsciencenews.com

**ADVANCED
MATERIALS
TECHNOLOGIES**
www.advmattechnol.de

techniques for catalysts have already been reported.[14–17] the demand for newer alternative strategies is increasing.

From the fabrication point of view, traditional formative manufacturing techniques such as injection moulding, and subtractive manufacturing techniques such as drilling, cutting, and milling, although practiced, have several limitations.[18,19] For instance, complexity associated in device and electrode fabrication, along with time consumption and high cost, has slowed the pace toward fabricating state-of-the-art catalysts. Also, poor selectivity, stability, activity, and mass transfer limitations associated with the catalysts limit their usage for catalytic applications directly. Thus, the need for simpler fabrication approaches that can easily modulate the internal structure, and print complex geometries, has increased dramatically. Furthermore, the complexity associated with traditional techniques, along with high fabrication time, the need for skilled users, excessive resource wastage, and the need for advanced operational facilities for material fabrication has led to further distress.

Advancements like 3D printing technology (known as "additive manufacturing" technique) have revolutionized the material fabrication technique, accounting for its rapid prototyping ability, and flexibility in designing and printing.[20–23] In addition, this innovative technique has the potential to deliver structures with myriad geometries, better rigidity, tunable porosity, and size, thereby mitigating the multiple limitations associated with conventional fabrication techniques. Modifying designs using computer-assisted design (CAD) software is relatively simple; therefore, materials can be easily formulated and examined on the basis of targeted products and experimental conditions. Nanostructuring of these 3D printed structures in the micrometer (μm) resolution can induce porosity and enhance the surface area, delivering nanometric features that can efficiently escalate and favor the catalytic reaction.[23–25] Engineering 3D printed structures can result in varied geometric morphologies, enhancing the chances of fabricating active catalyst structures for ammonia production.

Other advantages such as its user-friendly nature, rapid and flexible customization, and possibility to formulate and fabricate complex structures using different catalytic materials, make 3D printing a highly desirable technology for NRA. Also, this would be a breakthrough in the design of materials that can be easily integrated into an electrolyzer, with a consequent easiness in scalability and manufacturing. In other words, the flexible nature of 3D printing technology favors rapid material production, facilitating the easy optimization of designs to obtain higher yields.

In short, this perspective article discusses the scope of devising 3D printed materials with enhanced activity, selectivity, and considerable yield for ammonia production. This accounts for the fact that proper formulation, engineering, and postfabrication treatments of the 3D printed substrates could render active sites capable of performing NRA, and consequently improve ammonia production. Further, we discuss various strategies for designing 3D printed electrocatalysts, an overview of the catalytic reaction mechanisms, experimentation using 3D printed electrocatalysts toward ammonia production as a proof of concept, key challenges, and a future outlook of this field. The above discussion is anticipated to provide researchers working in this area with relevant ideas on designing newer electrode materials for ammonia

synthesis by exploiting the possible benefits of 3D printing technology.

## 2. Nutshell on 3D Printing Technology

A bottom-up technique, 3D printing classified under the category of automated manufacturing processes that has the potential to fabricate desired 3D objects by depositing active material in a layer-by-layer manner.[21,22,26] Right from its inception in the 1980s, this field of study has made remarkable progress in terms of providing complete autonomy for designing and printing customized products.[27,28] Fundamental advantages of this technology emanate from its features like immediate prototyping ability, scalability, repeatability, flexibility in structural design, the capacity of manufacturing complex designs, and minimal waste generation.[19,22] The technology today has come a long way from its initial usage of generating prototypes to a full-fledged 3D printing industry based across regions. The principles of 3D printing techniques have evolved with time based on the precursor materials used, setup cost, and targeted applications. The diverse prospects associated with 3D printing make it a reliable technique for fabricating various industrial tools and its popularity can be measured in terms of its shrinking cost, increasing purchase rates, and its application has broadened to multiple domains such food,[29] biosensing,[27] biomedical,[25,30] health emergency,[22] electrochemistry,[20,23,31–33] and beyond. Interestingly, today it is also expanding to educational[34] and domestic circles.

The printing process begins with modeling 3D structures using CAD 3D modeling software, a 3D scanner, or photogrammetry.[22,23] After successful modeling of the design (**Figure 1**A), it is converted to stereolithography file format (STL), which is the standard format file, followed by slicing using another software. Postslicing, the final output is obtained in the form of a G-code file that contains geometrical information of the modeled design, commands, extrusion and bed temperature details, number and density of layers, and so on (Figure 1B). The G-code file can be later transferred to the 3D printer for final printing. While printing, the 2D layers of active/precursor material are aligned on top of each other sequentially, resulting in the desired 3D structure (Figure 1C). 3D printing techniques and precursor materials, such as metal filaments/powders, thermoplastics, carbon based filaments, composites, and ceramics, offer multiple possibilities for a diverse range of applications. Certain techniques associated with the technology are discussed below since a proper understanding of these printing strategies is indeed necessary for designing application-specific devices/electrodes for targeted applications.[20,35,36]

### 2.1. Extrusion-Based Printing

Fused deposition modeling (FDM) or "fused filament fabrication" (FFF) involves the extrusion of active filaments down the printer nozzle to obtain a rigid 3D printed structure as shown in **Figure 2**A.[25,31] This printing technique is in high demand owing to its low cost and flexibility in using different materials. Each filament has its specific extrusion temperature capable of melting desired filaments down the printer

**ADVANCED
SCIENCE NEWS**
www.advancedsciencenews.com

**ADVANCED
MATERIALS
TECHNOLOGIES**
www.advmattechnol.de
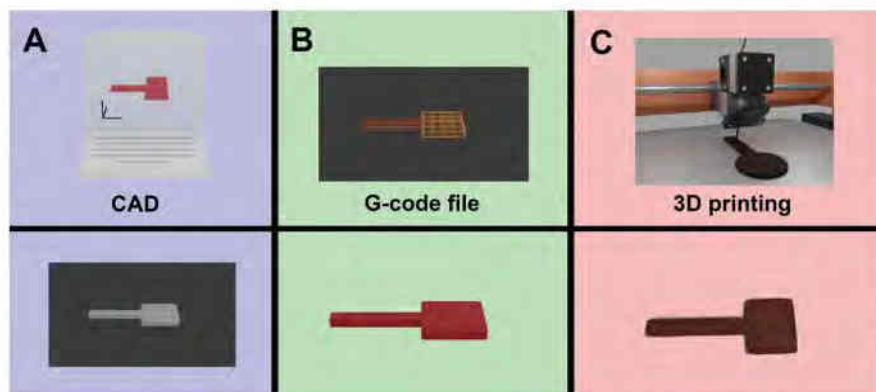
**Figure 1.** Schematic representations of steps involved in designing and fabrication of 3D structures. A) designing, B) slicing of modeled structure, and C) 3D printing.
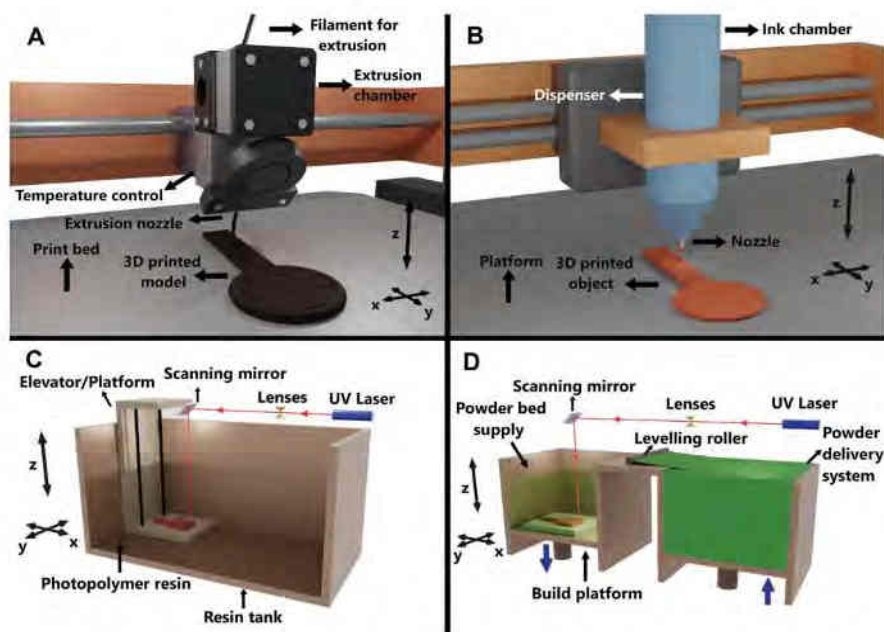


**Figure 2.** Schematic representations of 3D printing techniques: A) fused deposition modeling, B) direct ink writing, C) stereolithography, and D) selective laser sintering.

nozzle to the print bed platform. The precursor material includes graphene/polylactic acid (PLA) filaments (also known as "black magic"),[25] carbon-black/PLA (protopasta), metal/PLA filaments[37,38] (where metal = copper [Cu], bronze, stainless steel [SS], titanium [Ti], iron [Fe], aluminum [Al], etc.), PLA, acrylonitrile butadiene styrene (ABS), customized filaments, and so on. The directly printed materials are often subjected to post-fabrication protocols to make them conductive electrode/support for desired applications. Interestingly, studies on 3D printed graphene/PLA filament[31] and metal/PLA filaments[37] have been reported recently, as ideal electrode substrate for catalytic applications.

Furthermore, another interesting extrusion-based technique commonly used is direct ink writing (DIW, Figure 2B) where liquid-phase "ink" is dispensed out of the nozzle and deposited on the underlying printed layers to fabricate 3D structures.[39,40] Typically, the inks are electrochemically active materials of interest in suspension or solution form. Ink formulation is a key aspect of this printing technique, where electroactive materials along with additives, binders, solvents, and so on, are optimized based on their rheological properties in order to develop an ideal ink capable of extruding down the nozzle. This printing technology has expanded in terms of printing various materials[41] that are difficult to practically realize using FDM techniques,

**ADVANCED
SCIENCE NEWS**

www.advancedsciencenews.com

**ADVANCED
MATERIALS
TECHNOLOGIES**

www.advmattechnol.de

thus improving its scope for wider applications. Low cost, easy operation, and highly functional products are other advantages of this technology.[18]

## 2.2. Photopolymerization

Developed in the 1980s, this technique involves the selective curing of liquid photopolymer (resin) sequentially using a specific light source to fabricate active structures. This technique can be further categorized into stereolithography (SLA, Figure 2C)[42] and digital light processing, where in the former, a thin film of photopolymer resin is solidified using UV light to obtain a 3D printed structure while the latter uses a digital light source.[43] Good accuracy and resolution, versatility, multicolor, and multimaterial printing are added advantages of this technique.[18,19]

## 2.3. Powder Bed Fusion

Selective laser sintering (SLS, Figure 2D)[22,44] uses thermal energy or high-powered lasers to sinter finely powdered material together to procure a final solid structure. This method is highly advantageous as it can function without any external aid, has high accuracy, and constitutes a wide range of materials facilitating the easy production of complex structures. However, its operation requires better expertise and is also expensive in terms of equipment and maintenance costs.

Selective laser melting (SLM), on the other hand, uses precursor materials like metal powders, which are heated until the melting point is achieved.[42,44] Upon heating, the metal powder particles become fused to procure the 3D printed structure , often a conductive metal or metal alloy. Electron beam melting (EBM) is yet another quick 3D printing technique, where a computer-controlled electron gun is used to fabricate 3D structures from active metal powder in high vacuum conditions.[19,45] Precious metals and alloys are active materials employed for printing via this technique. Low cost, faster printing with high build speed, and reduced waste generation are some notable advantages of this technique.[18]

In short, the above techniques can effectively aid in the design and fabrication of 3D substrates for a broad spectrum of applications. Furthermore, these 3D printed structures, upon appropriate tailoring or postprinting treatments,[46,47] can serve as conductive catalyst substrates and/or catalyst support for electrocatalytic applications. It is, however, the user's choice regarding the type of material and printing technique that will be paramount in designing substrates. Apart from that, further advancements in this technology can be advantageous in the designing and fabrication of reactor vessels, along with multiple components in an electrolyzer cell. Thus, research in this direction can make this technology efficient in devising a complete electrochemical setup by itself, thus reducing the production cost significantly. In the following sections, multiple approaches toward designing 3D printed substrates for ammonia production will be discussed.

## 2.4. 3D Printing versus Conventional Techniques

3D printing differs from the traditional manufacturing technique such as "subtractive manufacturing," where, in the case of the latter, the expected final structures are carved out of a bulk material via drilling, milling, sawing, broaching, and so on.[18,19,23] The excess waste generated during preparation, immense time consumption involved in designing complex structure, the requirement of extensive human effort, expensive instrumental setups, and the inability to alter the volumetric density of the building material are a few of the drawbacks associated with subtractive manufacturing.[22] Debates on the efficiency of 3D printing and conventional techniques are ongoing. However, more than a replacement of established conventional techniques, 3D printing expects to enhance the existing ones for various applications. However, in the case of 3D printed substrates for catalytic applications, this technology has an upper hand over other techniques, especially due to its ability to fabricate custom-made catalysts with versatile structures, different shapes, and geometry of the 3D printed electrodes, subjected to the experimental condition.[20,23] For the NRA application, 3D printing can be an advantageous option to fabricate the required 3D printed electrodes, especially to design a substrate using active materials, already known for ammonia production. Such possible prototyping and modifications in 3D printing technology make it more advanced than other traditional printing techniques. 3D printing industries are also expected to witness a massive hike in designing and printing complete electrolyzer cells or catalytic reactors soon. The precursor materials employed are expected to possess high chemical resistance toward the electrolytes often used for electrolysis, making this technology highly promising for designing reactor vessels. However, other advanced printing techniques, such as SLA, SLS, SLM, and so on, are expected to be efficient technologies for fabricating better reactors for ammonia production as well. Thus, by mitigating the issues of intensive energy or labor involved in traditional techniques, 3D printing can serve as an alternative that is capable of simultaneously 3D printing an electrolyzer cell comprising both active electrocatalysts and a reactor vessel. Finally, it is also worth highlighting the advantages of 3D printing in the field of electrolyzer development in terms of less time consumption and ease of iteration of different cell designs for prototype optimization.

In general, prototype cell development processes involve a cycle of steps such as design, built, and testing in real conditions to evaluate performance and to identify the limitations and modify the subsequent designs until an optimized electrolyzer is obtained according to the requirements of the system under study. The entire process can be enhanced through the use of 3D printing technology as prototyping and simulation are simpler and more automated, allowing an optimal construction of devices in a smaller number of iterations. In other words, it can bypass the excessive time taken for optimization.

## 2.5. Summarized 3D Printing Techniques

For a better understanding and appropriate technique selection, 3D printing techniques (discussed so far), associated precursor
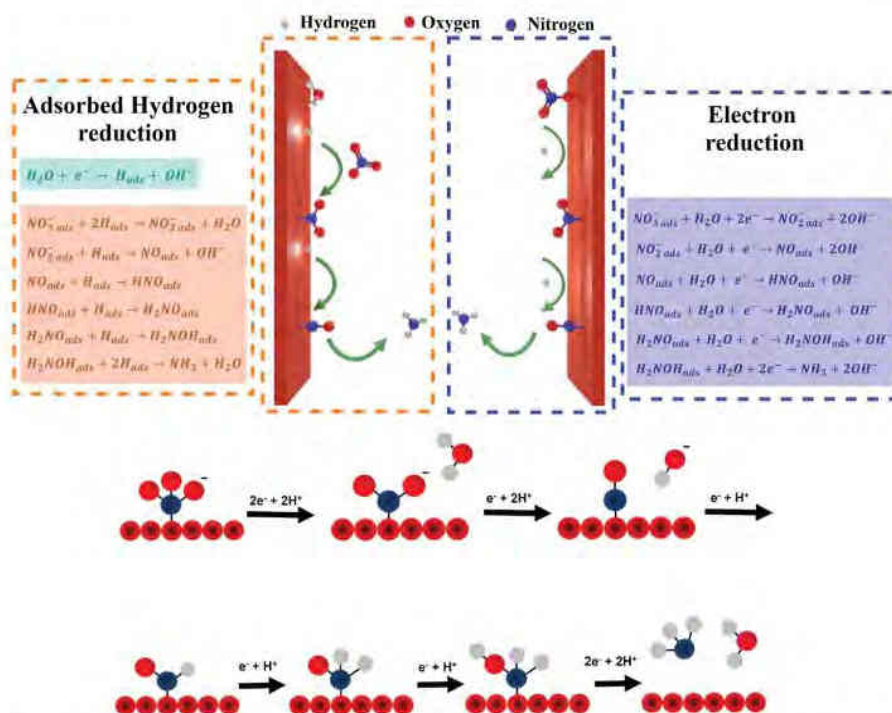
**Figure 3.** Representation of the reaction mechanism proposed for NRA. Top: The two main mechanisms that explain this reaction taking place at the surface of a cathode electrode, namely, the adsorbed hydrogen reduction (left) and the electron reduction (right). The reaction mechanism has been simplified to understand better. Bottom: Schematic of the step-by-step reaction mechanism (electron reduction) with a ball-type structure. Adapted with permission.[68] Copyright 2021, Royal Society of Chemistry.

materials, advantages, and limitations associated with each technique are presented in Table 1.

## 3. Insights toward NRA and Benchmarking Protocol

### 3.1. Significance of NRA

Haber–Bosch is a very well-established method known for large-scale ammonia production,[55,56] but is an energy-intensive process that involves considerable emission of $CO_2$ and harsh operating conditions. The limitations of this method invite immediate and alternative solutions for ammonia synthesis. One such strategy involves the electrochemical nitrogen reduction reaction (NRR) which operates under mild conditions compared to the Haber–Bosch.[57–60] However, the significantly high energy consumed during the breakage of N≡N , along with the competitive HER, low FE, and selectivity, has compelled researchers to come up with newer experimental approaches, although studies on NRR continue on a vast scale. NRA is one such emerging approaches toward ammonia production which is being extensively studied by researchers currently.[13,61–65] Discussions on the advantages of these approaches over conventional techniques are provided in the Introduction. In the present section, we attempt to explain the reported reaction mechanism associated with the NRA. Further examination has revealed that nitrogen ($N_2$) containing sources such as $NO_3^-$ ions are present in abundance as major water contaminants, especially in surface-to-ground-level

water bodies.[66,67] This method, interestingly, bypasses several limitations possessed by previous techniques for ammonia synthesis, and also strategically eradicates the negative effect of nitrate ions in the environment, making it a significant contributor to the energy sector as well.

### 3.2. Reaction Mechanism

The mechanism of NRA involves a complex eight-electron transfer process that proceeds through a series of complex pathways.[12] Equation (1) explains the mechanism involved in the nitrate reduction reaction and the respective potential procured with respect to standard hydrogen electrode (SHE)

$$NO_3^- + 9H^+ + 8e^- \rightarrow NH_3 + 3H_2O, E^0 = -0.12 \text{ V vs SHE} \quad (1)$$
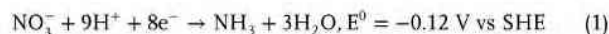
The mechanism of nitrate electroreduction[69–74] proceeds via direct electrocatalytic reduction, which includes two main pathways. The first one is regulated by the active adsorbed hydrogen atom ($H_{ads}$), called hydrogen adsorption reduction, and the second one comprises the electron reduction from the cathode, known as the electron reduction pathway. These two main pathways are illustrated in **Figure 3**, where the equations of both electrochemical processes are listed.[68] In the $H_{ads}$ mediated pathway (Figure 3, top left), the water molecule is reductively adsorbed on the electrode surface ($H_{ads}$). Furthermore, nitrate is reduced directly into $NH_3$ by $H_{ads}$ species through a step-by-step

**ADVANCED
SCIENCE NEWS**
www.advancedsciencenews.com

**ADVANCED
MATERIALS
TECHNOLOGIES**
www.advmattechnol.de

**Table 1.** Summary of 3D printing techniques for devising 3D structures for catalytic applications.

| 3D printing technique | Precursor materials | Layer thickness | Advantages | Disadvantages | Refs. |
|---|---|---|---|---|---|
| FDM (Solid based) | Carbon black/PLA, Graphene/PLA, Carbon black/ABS, Graphene/ABS, PLA, ABS Thermoplastic filaments, etc. | 50–300 µm | • Cheap, scalable, rapid, and easy prototyping<br>• Easy maintenance, controllable extrusion conditions and nonlaser technique<br>• Multiple postfabrication approaches for enhancing printed surface<br>• (E.g., solvent activation, chemical activation, electrochemical activation, enzymatic, etc.)<br>• Ideal substrate for functionalizing and patterned coating approaches to modify electrode surface<br>• Fabrication of electrochemical cells and reaction wares | • Unoptimized extrusion temperature can result in extruder clogging and bad printing<br>• Time-consuming functionalization and modification approaches<br>• Active materials restricted to filament form<br>• Exposure to highly corrosive aqueous electrolytes can degrade the polymer counterparts (e.g., PLA) | [19,42,48,49] |
| | Metal/ PLA: Cu/PLA, Ti/PLA, Fe/PLA, stainless steel, etc. | 50–300 µm | • Direct fabrication of metal substrates, a possible replacement to costly conventional metal fabrication techniques<br>• Robust, low cost, higher thermal conductivity, and active electrocatalytic surfaces<br>• Resilience to bending<br>• Tunable porosity and properties upon subjection to ideal postfabrication treatments (e.g., sintering) | • High sintering temperature and time-consuming optimization conditions<br>• Solvent-based activation techniques not ideal for polymer removal | [50,37] |
| | Multi-material printing: (composites of Metal/PLA, Graphene/PLA filaments, PLA, etc.) | 50–300 µm | • Combining multimaterial features to enhance the material property<br>• Possibilities of obtaining alloy like structures<br>• Great possibilities for automatizing the design and preparation of multiple components for electrolyzer device | • Complex integration of multiple filaments in the printing protocol<br>• Complex postfabrication protocols<br>• Size limitations<br>• Unoptimized conditions increase chances of nozzle clogging | [19,51] |
| | Customized FDM printing (2D materials filaments, nanomaterial/polymers composites, etc.) | 50–300 µm | • High chance of customization of materials<br>• Tunable properties and reduces the possibilities of foreign impurities<br>• Application-specific devices/catalyst with loading subjected to user's need | • Time consuming<br>• Tedious optimization procedures | [19,52] |
| DIW (Solid based) | Conductive extrudable inks (nanomaterials, glass, metals, etc.) obeying ideal rheological property | 50–300 µm | • Low cost, simple, easy processibility, and varied choices<br>• Tunable composition with multimaterial fabrication facility | • Restacking of active material<br>• Unoptimized rheology aid in clogging and incomplete prints<br>• Poor mechanical properties and low resolution | [18,20,53] |
| SLA (liquid based) | Photopolymer-based materials | 1–50 µm | • Easy, quick, and fine printing with accuracy and good resolution<br>• No need for support material | • Time-consuming protocols<br>• Expensive precursors and lack of conductive materials<br>• Much more complex integration for electrode fabrication | [19,42] |
| SLS (Powder based) | Metals, ceramics, thermoplastics, low temperature metal alloys | 20–150 µm | • Laser-based technique with high accuracy and broad range of material availability<br>• No need for additional support material | • High cost of instrumentation<br>• Time consuming and limited scalability<br>• Poor mechanical properties and surface finishing | [18,19,42] |
| SLM (Powder based) | Metal and/or metal alloy powders (stainless steel, Ti-based, Ag-based, Cu-based) | 20–150 µm | • Highly conductive 3D structures<br>• Decreased electrolyte resistance<br>• Highly desirable for material modification | • Limited precursor availability<br>• Costly instrumentation setup<br>• Time consuming | [19,42,54] |

**ADVANCED
SCIENCE NEWS**
www.advancedsciencenews.com

**ADVANCED
MATERIALS
TECHNOLOGIES**
www.advmattechnol.de

mechanism using a variety of intermediates such as $NO_2^-{}_{ads}$, $NO_{ads}$, $N_{ads}$, $NH_{ads}$, $NH_{2ads}$, and so on.[68]

On the other hand, in the electron reduction pathway (Figure 3, top right), a similar mechanism occurs without the intermediation of $H_{ads}$, but the direct cathodic reduction on the electrode surface.[68] Schematic representation of the electron transfer mechanism taking place during the electron reduction pathway is given in Figure 3, bottom. Also, during this reaction pathway, two intermediate $N_{ads}$ recombine to form the most stable $N_2$. Based on theoretical calculations, the migration barrier of $N_{ads}$ (0.75 eV) is found to be higher than that of $H_{ads}$ (0.10 eV). This fact, along with the less feasibility of N–N bond formation over the N–H bond, enhances the possibility of ammonia formation over the catalyst surface by the $H_{ads}$. In short, the $H_{ads}$-mediated pathway could greatly enhance ammonia production via the adsorption of H on the electrode surface. In the electron-mediated pathway, $NO_3^-$ is initially reduced into $NO_2^-$ on the electrode surface and then reduced into $NO_{ads}$. This intermediate can further result in the formation of either $N_2$ or $NH_3$ via multiple complex intermediates such as $N_2O_{ads}$, $HNO_{ads}$, $H_2NO_{ads}$, or $NH_2OH_{ads}$, wherein $NH_3$ is procured as a final product. In both cases, the most possible stable products are $N_2$ and $NH_3$. However, their prevalence is mainly based on the electrolytic conditions as well as the electrode material selected. For this reason, the careful and rational selection of electrocatalysts should be done in order to favor the mechanism toward $NH_3$ formation over $N_2$. In addition, although HER is usually perceived as a competing reaction, its total suppression could hinder ammonia production because $H_{ads}$ is relevant for the reaction to proceed. Therefore, catalyst materials exhibiting balanced H and $NO_3^-$ adsorption capabilities are desirable.

### 3.3. Experimentation and Quantification

To understand and further compare the performance of a catalyst toward ammonia production, a suitable benchmarking protocol should be followed. As a general approach, the first step consists of conducting an electrolytic experiment followed by quantifying the products generated during an electrolytic experiment. Thus, the classical method to carry out NRA experiments is via amperometry electrolytic experiments in specific experimental cells. Typically, at a laboratory scale, two-compartment H-type three-electrodes cells are employed. The electrocatalyst fabricated (here 3D printed electrodes) serves as a working electrode on the cathodic side along with the Ag/AgCl reference electrode while platinum mesh or wire acts as a counter electrode assembled at the anodic side.

Postelectrolysis, the quantification of products is carried out, where in general, the most common products determined in the reaction are $NH_3$ and nitrite ($NO_2^-$).[75] In addition, $NO_3^-$ content is also determined to track the ability of the electrocatalyst to effectively reduce nitrate. Techniques other than UV–vis spectroscopy have also been proposed in the literature to carry out these quantifications.[76] However, the colorimetric technique has gained considerable popularity owing to its ease of usage, low cost, higher accessibility for instrumentation, and accuracy.

Ammonia is quantified using indophenol blue method, where its presence is confirmed via quantification of a blue complex that results in a slightly green solution with maximum absorbance at the wavelength of 655 nm.[17] Nitrite, on the other hand, is determined by another colorimetric assay where the addition of appropriate reagents results in the formation of a complex red-colored compound measured for its absorbance at 540 nm.[75,76] These compounds are determined to further calculate FE, considering the charge measured during the electrolytic experiment. FE, being a very important parameter to differentiate between several catalytic materials, is frequently used to benchmark electrocatalysts in this field. In addition, selectivity is also an important parameter in the screening of electrocatalysts and evaluating the performance of a material toward ammonia production. Measuring the nitrate concentration is necessary to calculate selectivity. Similar to the quantification approach adopted in ammonia and nitrite, nitrate concentration is measured using a colorimetric method using appropriate reagents, and the absorbance of nitrate is directly measured at 220 nm (subtracting double of absorbance at 275 nm previously).[75] All these methods are used to obtain the important parameters for understanding the role of the catalyst and, ultimately, provide a rational strategy to unequivocally select the best catalytic material to enhance NRA.

## 4. Scope of 3D Printing Technology for Ammonia Production

3D printing technology has garnered significant recognition in recent years for its multidimensional possibilities, and escalating scientific advancement toward electrocatalytic applications.[20,24,31,32,77,78] However, 3D printed electrodes—an ever-expanding domain with great possibilities—have been surprisingly overlooked for ammonia production although they have been well explored for HER,[31,79] oxygen evolution reaction (OER),[80,81] carbon dioxide reduction reactions ($CO_2RR$),[19,32] and $CO_2$ capture.[19] In short, the primary objective of this section is to understand the feasibility of the available 3D printing technology to fabricate 3D printed structures for NRA efficiently. Owing to its immense multidisciplinary aspects, 3D printing technology can flourish in both industry and academia in the near future, for diverse applications (**Scheme 1**).

Geometry optimization is a very crucial parameter for fabricating ideal substrates as they can both facilitate as well as hinder the evolution and detachment of gaseous products from the electrode surface.[19,82] For instance, a lack of proper geometric optimization or poor design of the substrates can accumulate gaseous products over the electrode surface, resulting in the passivation of the active electrode and a significant drop in the catalytic response. Interestingly, 3D printing technology can be beneficial for resolving the aforementioned concerns and is expected to be promising for the fabrication of active functional electrocatalysts with better accuracy and enhanced performance.

**Figure 4** shows 3D printed electrodes/devices of varying configurations employed for electrochemical applications.[51,84] These differing complex structures/shapes can be mesh shaped, basket shaped, ribbon shaped, square shaped, circular electrodes with void shapes and varying sizes, etc. Hence, similar adoption and strict optimization can aid in fabricating 3D printed electrocatalysts for NRA, thereby mitigating the limitations faced in fabrication of active catalysts to an extent. Porosity and surface area of 3D structures are also critical aspects for ammonia production.

**ADVANCED**
**SCIENCE NEWS**

www.advancedsciencenews.com

**ADVANCED**
**MATERIALS**
TECHNOLOGIES

www.advmattechnol.de
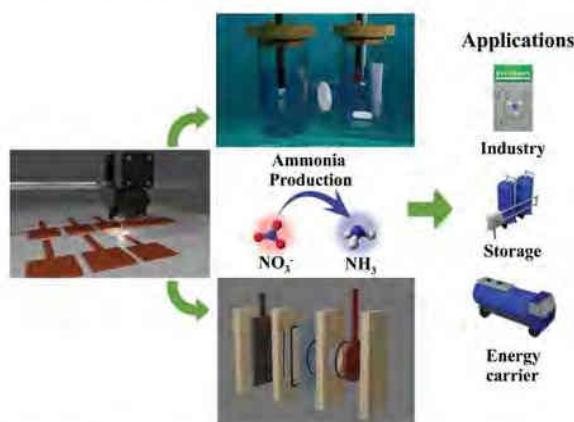
**Scheme 1.** Multidimensional applications of 3D printed structures toward ammonia production.
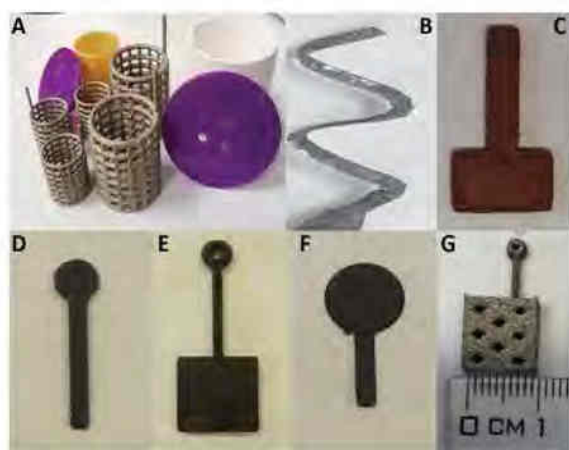


**Figure 4.** 3D printed electrodes and electrochemical cells of various size and geometry. A) Selective laser melting 3D printed stainless steel gauze-shaped and fused deposition modeling 3D printed polylactic acid based electrochemical cells. Reproduced with permission.[83] Copyright 2017, Wiley-VCH. B) Helical-shaped 3D printed steel electrode. Reproduced with permission.[84] Copyright 2015, Wiley-VCH. C) Square-shaped 3D printed copper electrode. D–F) 3D carbon electrodes of various shape and size. C–F) Adapted with permission under the term of CC-BY license.[19] Copyright 2023, The Authors, Advanced Materials Interfaces published by Wiley-VCH. G) Square shaped electrode. Adapted with permission,[85] Copyright 2019, Wiley-VCH.

The advancements in technology can render enhanced surface area for ammonia production via techniques such as sintering, solvent activation, chemical activation, and patterning, a detailed evaluation of which shall be provided in the subsequent sections.

Electrochemical studies on 3D printed electrodes in various electrolyte systems are available in the literature.[25,86,24] Although the degradation of polymers such as PLA in acidic and alkaline electrolytes is known, a timely improvement in the fabrication of newer metal/polymer and carbon/polymer composites may help to overcome this. Masking 3D printed substrates to mitigate degradation toward harsh electrolyte conditions could be other possible strategies.[19] Employing customized filament fabrication techniques or other metal 3D printing techniques can serve

as an immediate solution to this. However, with progress in the technology, this is expected to be used in designing functional electrocatalysts and reactors among others. Furthermore, the following sections and critical discussions provide a broader understanding of the feasibility of 3D printing technology for ammonia production.

## 4.1. Fused Deposition Modeling

Extrusion-based FDM printing is considered one of the fundamental strategies for 3D printing electrodes/devices. In the FDM technique, active materials, typically filaments, are extruded out of the hot end of the nozzle to obtain a 3D printed structure (detailed in Section 2).[25] At laboratory scale, Original Prusa i3 MK3S+ 3D printer with a nozzle thickness of 0.4/0.6 mm is employed, which can extrude various filaments of carbon/polymer, metal/polymer, and customized 2D material filaments, via FDM technique (**Figure 5**A). The choice of filaments is often application-specific and undergoes specific postprinting treatments to improve the properties of the printed structures. Although several established works using 3D printed electrode substrates via the FDM technique for various electrocatalytic applications have been reported,[20,31,87] ammonia production using 3D printed electrodes is a relatively unexplored domain.

In FDM, the filament materials constitute insulating polymer components along with conductive active fillers. Postprinting, the 3D printed substrates are further subjected to certain modification techniques to remove the nonconductive PLA/ABS polymer components and eventually expose more catalytically active sites over the electrode surface.[33,88] In addition, sputtering, coatings, and patterning can result in modifying the electrode surfaces for desired catalytic applications as explained in detail in Section 5.

### 4.1.1. 3D Printed Carbon/Polymer Electrodes

Carbon materials are interesting catalytic materials owing to their good electrical conductivity, high surface area, and chemical stability. Interestingly, modifications[89–91] via heteroatom doping, size, morphology and vacancy engineering, crystal facet regulation, and so on can also render carbon materials active for catalytic applications as well. Multiple studies have been put forth regarding modifications and surface engineering strategies over carbon-based substrates for efficient ammonia production.[92,93] These studies show that suitably modified carbon/graphene substrates are ideal for ammonia production and the scope of availing carbon/graphene filaments in the context of 3D printing ensures a huge advancement in the field of 3D printing technology for ammonia production. In short, fabricating 3D printed carbon-based macro/microstructures using carbon-based filaments presents new possibilities in devising electrocatalysts and/or substrates for catalytic applications. Graphene/PLA filament (Figure 5B)[31,94] and carbon-black/PLA ( Figure 5C) are two types of commercial 3D printable filament material that are used for printing carbon electrode substrates. Several works have demonstrated the possibility of easy modification of these activated 3D printed carbon surfaces for enhanced catalytic

**ADVANCED
SCIENCE NEWS**
www.advancedsciencenews.com

**ADVANCED
MATERIALS
TECHNOLOGIES**
www.advmattechnol.de
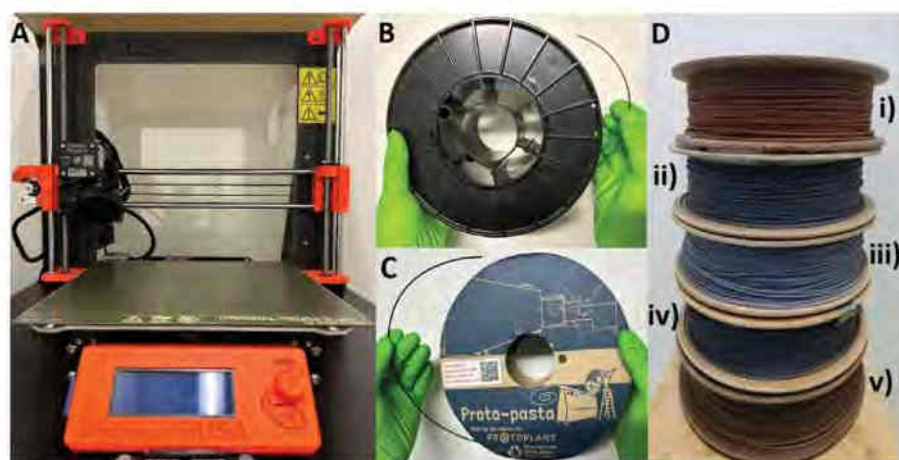
**Figure 5.** A) Prusa FDM 3D printer capable of extruding filaments to 3D structures. B) Spool of graphene/PLA filament. C) Spool of carbon black/PLA filament. D) Commercial 3D printable filaments of i) copper, ii) titanium, iii) aluminum, iv) stainless steel, and v) bronze.

properties.[25,85] Speculating that although direct 3D printed carbon electrodes may not deliver very high performance like the conventionally well-known catalyst, they can serve as good substrate material for ammonia production.

For instance, in a study by our group, 3D printed carbon substrates were evaluated for NRA.[95] The two filament substrates of 0D carbon black (Protopasta), and 1D carbon nanotubes (graphene/PLA) were evaluated systematically. **Figure 6**A shows linear sweep voltammetry (LSV) profile of 0D carbon black and 1D carbon nanotubes in electrolyte solution of $Na_2SO_4$ (with and without nitrate), conducted at scan rate of 5 mV s$^{-1}$. It was observed that 0D was inactive, while 1D exhibited nitrate reduction ability, upon preliminary analysis. Second, electrolysis measurements of the 3D printed carbon 1D catalyst at multiple potentials were done, and the quantitative measurements revealed that the electrocatalysts showed an increasing yield rate of from 6.8 to 364.5 µg h$^{-1}$ cm$^{-2}$ and more than 50% FE at potentials beyond −1.21 V versus RHE (Figure 6B). Cyclic stability assessments at −1.21 V showed a roughly constant performance of 3D printed 1D carbon catalyst in terms of both FE and yield rate (Figure 6C), thereby aiding in devising a cost-effective 3D printed carbon catalyst for NRA application. Furthermore, the role of metal oxide impurities ($TiO_2$ and $Fe_3O_4$), carbon defects (basal plane, edge plane), and active sites in 3D printed 1D carbon catalyst was further elucidated in the study. The studies affirmed that a synergistic effect of intrinsic surface features of defective carbon nanotubes and metallic impurities can enhance the NRA performance (Figure 6D). Because commercially procured carbon filaments may have varying inherent impurities ($TiO_2$ and $Fe_3O_4$) that could influence catalytic activities, the researchers have further employed uniform deposition of manganese oxides (MnOx) over 3D printed carbon substrates via atomic layer deposition (ALD) technique to procure functionalized carbon frameworks. LSV was initially employed for a preliminary analysis, wherein the ALD-coated layer exhibited a better nitrate reduction ability over the pristine 3D carbon substrate (Figure 6E). Quantification of products postelectrolysis shows that the yield rate (435.9 µg h$^{-1}$ cm$^{-2}$ at −1.21 V; Figure 6F) and FE (64.8%

at −1.21 V; Figure 6G) of ALD-coated 3D carbon substrate (300 cycles) catalyst showed a clear dominance over the pristine 3D printed carbon substrate. Furthermore, it was observed that the FE and yield progressively increased with increasing ALD cycles (Figure 6H), thus displaying the potential of ALD-coated MnOx layers to modify the surface chemistry of 3D printed carbon frameworks for catalytic applications such as NRA.

Thus, it can be assured that these commercially available or customized carbon substrates will be a benchmark for the 3D printing industry, specifically for ammonia production. Multiple studies recommend the modification of 3D printed electrodes via electrodeposition[25] and patterned coating of active material[96] in order to achieve better performance. This is explained in Section 5 with a major focus on ammonia production. Therefore, exploiting 3D printed carbon surfaces via appropriate modification techniques and optimization can make them ideal electrocatalysts for ammonia production and open up further application possibilities.

### 4.1.2. 3D Printed Metal/Polymer Electrodes

With the progress in technology, newer, cost-effective, and scalable techniques with high build speed have also been devised to fabricate 3D printed metal structures.[19] For instance, FDM can be used to extrude metal/PLA filaments, which is also a possible replacement for SLA/SLM. However, there is still a long way to go. The 3D printing hubs have given immense possibility to procure various metal/polymer filaments of Cu, Ti, Al, SS, and bronze, leaving users with extensive choices for fabricating application-specific catalysts (Figure 5D).

Cu/PLA: Among the FDM printable metal/polymer filaments, Cu/PLA is a well-known commercial filament used for 3D printing Cu substrates.[37,38] Interestingly, from the catalysis point of view and previous reports, among transition metals, Cu (CuO or $Cu_2O$) is considered to be a highly desirable material for ammonia production owing to its high catalytic activity, selectivity, and high FE. Also, the fact that Cu 3D printed metal electrodes have

**ADVANCED
SCIENCE NEWS**

www.advancedsciencenews.com

**ADVANCED
MATERIALS
TECHNOLOGIES**

www.advmattechnol.de
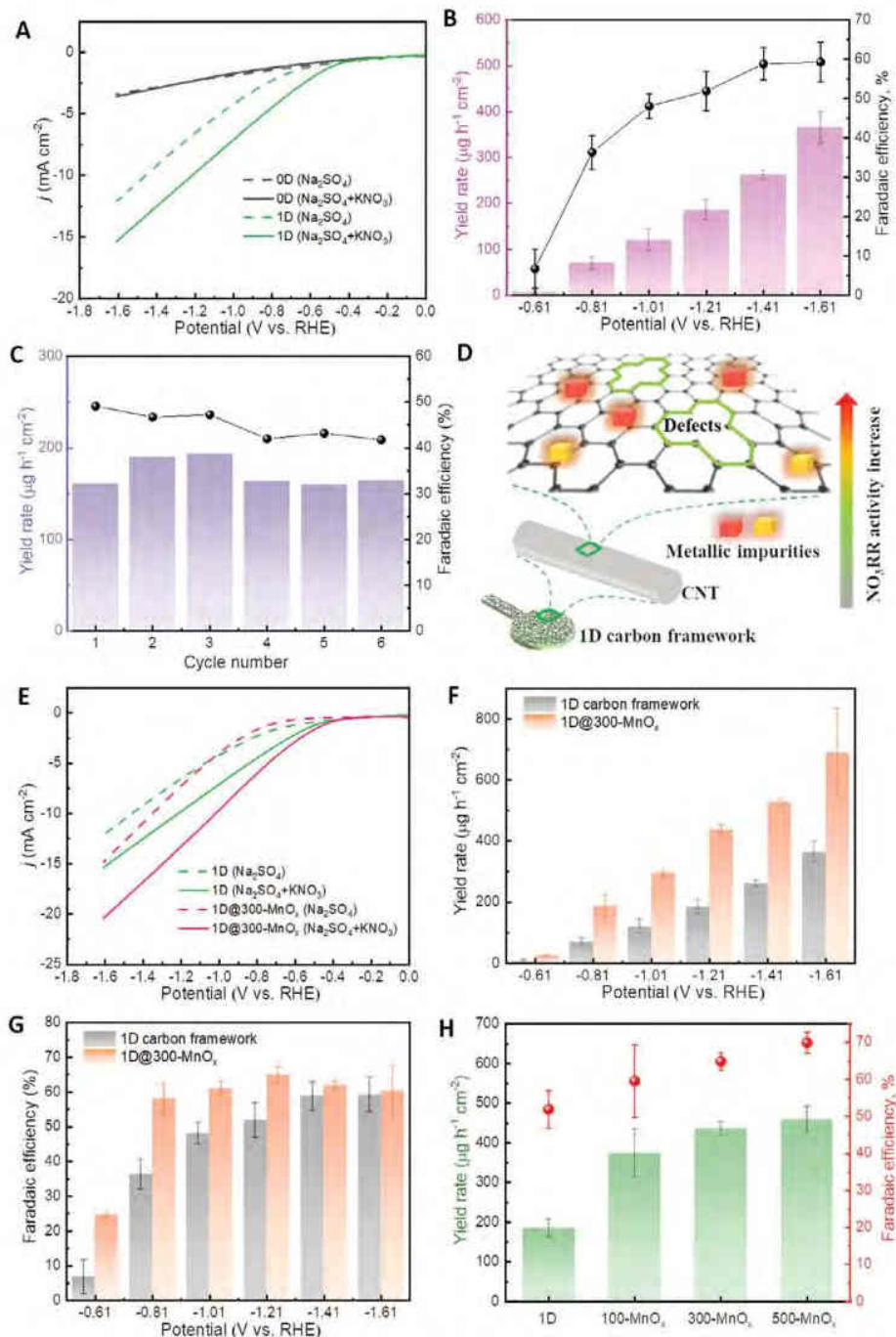
**Figure 6.** A) LSV profile of 0D and 1D 3D-printed carbon substrates in 0.5 M $Na_2SO_4$ electrolyte and 0.1 M $KNO_3$/0.5 M $Na_2SO_4$ mixed electrolyte. B) $NH_3$ yield rate and FE of 3D printed 1D carbon framework at multiple potentials. C) Durability assessments of tests of 3D printed 1D carbon framework at −1.21 V. D) Schematic representation of enhanced activity of 1D 3D-printed carbon framework. Electrochemical performance of 1D carbon framework and $MnO_x$ ALD-coated 1D carbon framework: E) LSV curve, F) yield rate, G) FE, and H) effect of varying ALD-coated MnOx thickness over 1D carbon framework for NRA activity. A–H) Reproduced with permission.[95] Copyright 2023, Elsevier.

**ADVANCED
SCIENCE NEWS**
www.advancedsciencenews.com

**ADVANCED
MATERIALS
TECHNOLOGIES**
www.advmattechnol.de

been studied as catalysts for energy conversion applications[37] substantiates the high possibilities of their use as electrocatalysts for ammonia production as well. Cu as a precursor material is also known to be cheap and nontoxic along with exhibiting good electrochemical activity toward reduction reactions, high sensitivity, and lower overpotential for reductive electron transfer.[38] In Cu/PLA metal filaments, Cu fillers provide good strength and high conductivity to the printed electrodes while PLA ensures structural integrity to filaments both before and after printing.

However, postprinting treatment of these 3D printed metal electrodes is conducted to improve the conductivity of electrodes for enhanced catalytic activity. For instance, sintering 3D printed Cu electrodes increases the contact between Cu metal particles to eventually realize a conductive Cu metal electrocatalyst.[38] This approach can also aid in controlling the morphology of the metal electrode substrate. For instance, in a recent study, 3D printed Cu electrodes were sintered at various temperatures, and their elemental states at different temperatures were examined using X-ray photoelectron spectroscopy (XPS).[38] From such observations, it is expected that researchers proceeding toward electrocatalyst fabrication would need to optimize the sintering conditions because variations in conditions such as temperature could modulate the composition of the Cu in printed electrodes. Indeed, such optimization can provide a viable strategy to fabricate and activate 3D printed metal electrodes that could be integrated into electrolyzers for enhanced NRA. Overall, research focusing on these metal 3D printed parts for ammonia production would be highly beneficial for the 3D metal printing industries and future electrochemical applications.

Ti/PLA: Transition metals such as Ti are interesting, owing to its cost-effectiveness, robustness, abundant availability, and being a poor HER catalyst. In addition, its electrochemical potential stability window is quite large, making Ti highly selective for nitrate anion reduction. In a study by Jaramillo and co-workers,[97] electrolyte engineering was carried out using Ti electrodes for the efficient NRA. The effect of various electrochemical conditions on selectivity and electrochemical activity at Ti cathode for ammonia production was examined using this study. The catalyst was successful in delivering 82% FE ($-1$ V vs RHE) and a partial current density to ammonia was also recorded at around $-22$ mA cm$^{-2}$ (nitrate concentration of 0.4 M; pH $\approx$ 0.77). Today, 3D printing technology allows the advanced facility of 3D printing Ti electrodes via FDM using Ti/PLA filaments. Commercial filaments for extrusion are available from sources like The Virtual Foundry. Employing postfabrication strategies such as sintering would result in the successful elimination of the possible nonconductive PLA from 3D printed Ti/PLA structures. This approach can result in constituting more than 90% Ti metal counterpart, making them suitable prototypes for catalysis such as NRA. Tuning the geometry, size, and porosity of 3D Ti printed structures can avail easy access to fabricate active Ti catalysts for NRA.

Fe/PLA: Fe-based catalytically active centers are long known to be capable of ammonia production, such as in the Haber–Bosch process.[98] In a very recent study by Wu et al.,[17] Fe single atom catalyst was used for NRA and showcased interesting results. In the context of 3D printing, we find that this technology gives the possibility of fabricating 3D printed Fe substrates via extrusion-based printing of Fe/PLA filaments[99] at around 185–195 °C and bed temperature of around 50 °C. The possibility for rapid proto-

typing of electrodes with varying geometry, porosity, and employing specific activation techniques to these printed platforms can make the 3D printed Fe substrates active for NRA applications.

### 4.1.3. Experimental Demonstration

To validate the possibility of ammonia production via 3D printed electrodes, an experimental demonstration is carried out by authors with their expertise in 3D printing devices/electrodes and ammonia electrocatalysis. A detailed study on 3D printed Cu electrodes for NRA is beyond the scope of this article, as the authors expect to show only a working model in this new domain, as no studies have been reported in this field, to date.

Original Prusa i3 MK3S+ 3D printer (**Figure 7**A), with a nozzle thickness of 0.6 mm (nozzle temperature [$T_{nozzle}$] = 230 °C, print bed temperature [$T_{bed}$] = 60 °C) was employed for 3D printing of Cu/PLA filaments. Commercial Cu/PLA filament (Figure 7B) was procured from the Virtual Foundry, USA, which was used for 3D printing Cu electrocatalyst substrates via FDM (Figure 7C). Sintering of the 3D printed Cu/PLA electrode substrate was further carried out at following temperature ramp: 0–300 °C at 5 °C min$^{-1}$; 300–1010 °C at 3 °C min$^{-1}$, 1010–1060 °C at 1 °C min$^{-1}$. Finally, the Cu electrodes were held at 1060 °C for 60 min and the oven was allowed to cool down to room temperature (Figure 7D). This protocol was carried out to reduce the nonconductive PLA counterpart in printed structures and eventually expose more conductive Cu active sites. Postactivation, the 3D printed electrodes were employed for NRA and quantification studies (Figure 7E).

Initially, the electrocatalytic activity of the 3D printed Cu electrodes toward NRA was evaluated using the LSV technique. The experiment was carried out in a three-electrode setup wherein, a 3D printed Cu electrode served as the working electrode, Ag/AgCl as the reference electrode, and platinum as the counter electrode. The LSV was performed in 1 M KOH electrolyte systems both with and without NO$_3^-$ at a scan rate of 20 mV s$^{-1}$. Analysis of the LSV curves revealed that the 3D printed Cu electrode was successful in reducing nitrate ions in the electrolyte at low onset potential.

Furthermore, the electrocatalysts displayed a very high current density in electrolyte systems containing NO$_3^-$ ($j_{max}$ = 56 mA cm$^{-2}$), while the catalyst delivered high onset potential and low current density in electrolyte solutions without NO$_3^-$ (**Figure 8**A). Hence, from the preliminary analysis, it becomes well evident that 3D printing Cu electrode substrate and subsequent activation treatment results in devising newer conductive active substrate for NRA applications. Further, NRA experimentation was performed on 3D printed electrocatalysts in an H-type cell at $-0.92$ V versus RHE. This is done to evaluate if the 3D printed electrocatalysts are ideal for delivering FE of a reasonable amount upon electrolysis. The electrolysis experiment was carried out for 1 h at room temperature with continuous magnetic stirring at 100 rpm.

Postelectrolysis, the analyte samples from the cathodic side were taken and quantified for ammonia as shown in Figure 8B, using the standard colorimetric method. Interestingly, the electrocatalysts delivered about more than 85% of FE and high yield rate. Thus, this experimental demonstration validates the

**ADVANCED
SCIENCE NEWS**

www.advancedsciencenews.com

**ADVANCED
MATERIALS
TECHNOLOGIES**

www.advmattechnol.de
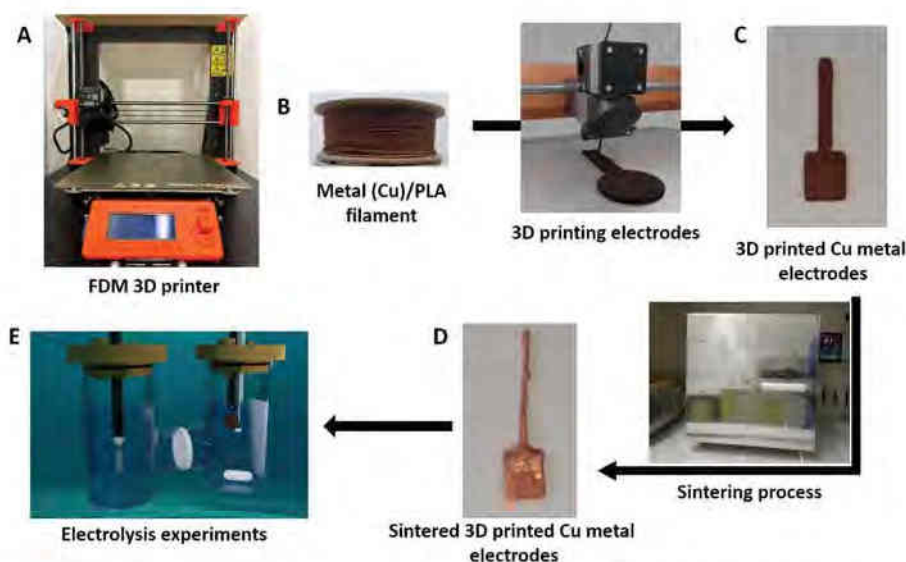
**Figure 7.** Schematic representation of designing and fabrication of 3D printed Cu electrocatalysts for ammonia production.
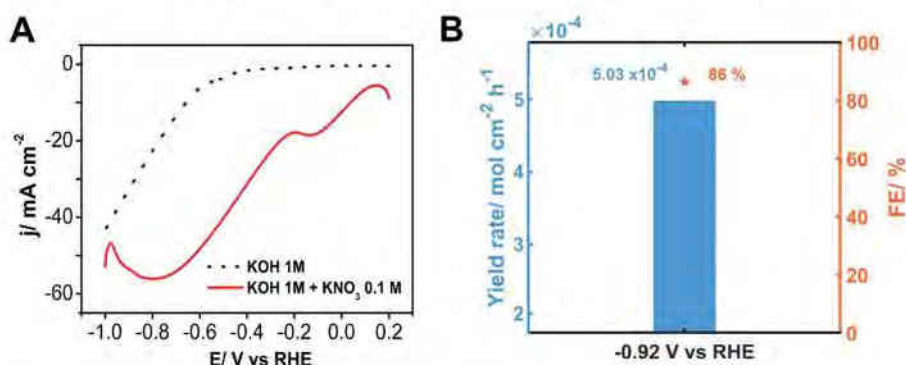


**Figure 8.** A) LSV profile of 3D printed Cu metal electrode. B) Calculated FE and yield rate.

potential of 3D printing technology toward ammonia production. Engineering of these catalysts and ideal optimization conditions can deliver FE and yield, beyond the one reported above. Furthermore, researchers and scientists are expected to explore the possibilities of this technology to fabricate multiple other electrocatalysts for ammonia production in the near future.

### 4.1.4. Customized Filament Fabrication

Besides commercially available carbon and metal-based filaments, the advanced research today provides the possibility of on-demand filament fabrication using various active materials, 2D materials, and nanomaterial composites, based on the user's choice.[19] For instance, in a recent work published by our group, filaments of 2D material were fabricated using a slurry containing $MoS_2$, graphite, activated charcoal, and multiwalled carbon nanotubes.[52] The slurry prepared from the above mixture was dried at room temperature and fed into a filament extruder (Felfil Evo, Italy, **Figure 9**A) to obtain $MoS_2$/C/PLA filament. The resultant filament was successfully FDM 3D printed to electrodes, ac-

tivated using optimized technique and further studied for electrochemical applications. Thus, advancements in 3D printing technology have given users the freedom to create their own 3D printable filaments of 2D transition metal dichalcogenides (TMDs).

TMDs such as $MoS_2$[100,101] with suitable modifications, are found to be ideal for ammonia conversion as well. Thus, the aforementioned observation gives a clear pathway to fabricate $MoS_2$/carbon filaments that are either modified or engineered, and later 3D printed and activated to fabricate a 3D printed $MoS_2$ electrocatalysts for NRA.

Literature also shows that TMDs other than $MoS_2$ are also being noticeably used as catalysts for ammonia production. Hence, appropriate optimizations and the adaptation of previous studies can result in designing and fabricating various 3D printed substrates/ catalysts other than $MoS_2$.[102] Since filament fabrication using graphene and TMDs is already shown to be successful, we expect that this approach can be expanded toward designing several similar electrocatalysts using other active materials such as MXenes[103] MAX phases,[104] MOFs,[105] COFs, other layered materials,[106] and so on. Such customized fabrication of

**ADVANCED**
**SCIENCE NEWS**
www.advancedsciencenews.com

**ADVANCED**
**MATERIALS**
TECHNOLOGIES
www.advmattechnol.de
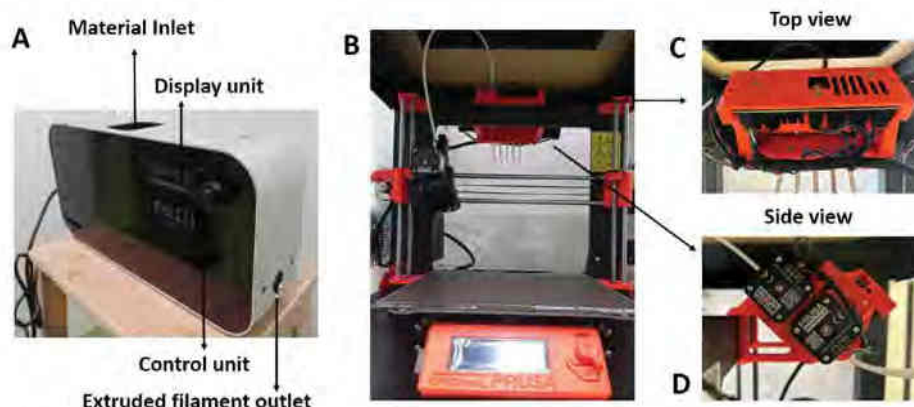
**Figure 9.** A) Filament fabricator offering customizable filaments. B) Multimaterial FDM 3D printer and components. (A) and (B) Adapted with permission under the term of CC-BY license.[19] Copyright 2023, The Authors, Advanced Materials Interfaces published by Wiley-VCH. C) and D) Printer components from different perspective.

filaments with the desired composition is expected to provide a huge advancement in the preparation of electrode materials for ammonia production. Also, it would truly be a landmark case if such customized filaments can be used for practical applications and provide users with extensive choices.

Furthermore, fabricating filaments using metal particles and polymers is highly beneficial in achieving active 3D printed substrates for various applications via FDM. For instance, in an article by Hwang et al., Cu and Fe particles were mixed with ABS thermoplastic to fabricate corresponding metal/polymer composite filaments.[107] Based on the loading of metal particles in the fabricated filaments (i.e., Cu/ABS and Fe/ABS), tensile strength and thermal conductivity were analyzed along with the optimization of parameters such as temperature and fill density. The investigation showcases the importance of both metals and polymers in filaments for enhancing conductivity and structural integrity, respectively. However, postfabrication approaches can resolve the conductivity issues without compromising the property of the active metal based material. Proper optimization of composition will lead to the fabrication of an ideal 3D printed metal substrate, which in turn can serve as an active electrocatalyst for NRA.

### 4.1.5. Multimaterial Printing and Catalytic Reactors

Multimaterial (MM) FDM 3D printing is another interesting printing technique that allows the users to sequentially extrude multiple filaments of entirely different compositions simultaneously (Figure 9B–D).[51,108,109] This can be considered a major revolution in the field of 3D printing, as earlier 3D printers were capable of extruding only one filament at a time. MM FDM 3D printing can be interesting for a wide range of applications, especially for catalysis, anticipating a synergistic effect of materials in these 3D printed hybrid electrode systems. Studies on Cu–Ni alloys for enhanced ammonia production are already reported.[16] Also, there are reports available on using metal polymer filaments of Ni for FDM printing.[110] Thus, in the context of 3D printing by taking advantage of the filaments of both ac-

tive materials, an alloy of 3D printed Cu–Ni hybrid catalyst can be fabricated using the MM FDM printing technique to procure 3D printed bifunctional catalysts. Furthermore, subjecting these 3D printed hybrid systems toward post-fabrication treatments is speculated to enhance the performance of the fabricated catalyst. Such 3D printed hybrid electrode systems can be highly innovative for catalytic applications such as NRA.

3D printing technology finds wide applications not only in the designing and fabrication of catalytic material for various energy applications[23,24,111] such as water splitting,[112] $CO_2$ reduction,[32,113] and artificial photosynthesis,[114] but also in the fabrication of electrolyzers[51] (electrolytic cells) that can be used for practical applications. Components of an electrolyzer device include electrodes and current collectors based on the intended application. Advancements in 3D printing technology have enhanced the prospects of this industry, especially with more precursor materials being added continuously to print hubs. Also, significant advancements are taking place in the integration of both insulating and conducting parts into the electrolyzers. In other words, the possibilities of manufacturing the casing and internal components of electrolyzers with complex shapes and architecture are infinite using 3D printing approach such as MM FDM.

As a general approach, the electrocatalysts developed are extensively tested in a standard three-electrode cell. However, the behavior of the electrocatalyst in terms of efficiency and stability is completely different when transferred to an electrolyzer (two-electrode cell) under real conditions. For this reason, the testing of developed electrocatalysts under actual working conditions is mandatory. In principle, MM FDM technology offers a promising breakthrough in cell design due to decentralized manufacturing, and customization possibilities for designing cost-effective and highly complex structures with minimal waste generation during the manufacturing process.

Thus, over time, this technology is expected to advance toward designing a complete electrolyzer cell that requires less labor, is cost-effective, efficient, and ideal for catalytic applications such as NRA. However, one of the drawbacks that need to be addressed is the integrity of the cell under operation. Owing to

131

**ADVANCED
SCIENCE NEWS**
www.advancedsciencenews.com

**ADVANCED
MATERIALS
TECHNOLOGIES**
www.advmattechnol.de

the layer-by-layer based printing technology, there is a possibility of liquid leakage with the consequent change in experimental conditions, making it difficult for direct application in the reactor design. However, these limitations are expected to be addressed by researchers over time. Nevertheless, at the onset, it appears to be a very beneficial technique due to its ease of usage and multiple possibilities in the designing and testing of new cell configurations in short time periods.

### 4.2. Direct Ink Writing

Designing 3D printed substrates using all types of precursor materials may not be feasible with the FDM-based technique; hence, there is a need for better and improved alternatives such as DIW. DIW is a well-known 3D printing technique that works on the principle of extruding a formulated ink dispersion of the active material out of the nozzle to obtain a final 3D printed structure.[22,40] This printing technique permits the user to 3D print any desirable material as long as the formulated precursor inks follow rheological behavior that is ideal for extrusion. Shear thinning and the viscoelastic properties of the ink also help retain the shape and continue to provide sufficient fluidity, and interlayer adhesion, resulting in an ideal 3D printed electrocatalyst. 2D materials, such as graphene,[115] TMDs,[101] and MXenes[116,117] with modifications and improvements, are known to serve as ideal catalysts/support material for ammonia production.

Like 2D materials, the scope of single-atom catalysts (SAC)[119] is also advancing in recent times, especially in the light of catalytic applications. SAC constitute isolated single metal atoms (active sites), anchored by support materials, with cost-effective, tunable catalytic sites, and high catalytic selectivity being added advantages. Complex wet chemistry synthesis approaches and costly precursors aggravate the overall cost of fabrication of SAC. Accounting for these critical material fabrication aspects, in a recent study, 3D printed SAC was proposed by Xie et al.,[118] to fabricate cost-effective target materials and mitigating the complexity associated with the wet chemistry process. Transition metal precursors along with natural polymers such as gelatin and gelatin methacryloyl (GelMA) was employed to formulate the extrudable ink for fabrication of 3D printed SAC catalysts. Postprinting, the sample was freeze-dried, followed by pyrolysis of dried samples to anchor active metal atoms onto the gelatin/GelMA-derived carbon. Employing the above synthesis approach, the researchers were successful to procure isolated Fe sites with $Fe(acac)_3$ (Tris(acetylacetonato)iron(III)) serving as Fe single atom precursor. The synthesis was also extended to other metal acetylacetonates, such as $Pt(acac)_2$, $Ni(acac)_2$, $Zn(acac)_2$, $Co(acac)_2$, $Cu(acac)_2$, and multiple others to procure PtSAC, NiSAC, ZnSAC, CoSAC, and CuSAC, respectively. In addition, the research provides an experimental demonstration of these 3D printed Fe SACs (Fe3DSAC) for NRA as an approach to exhibit the potential of this technology toward fabrication of active electrocatalysts. The electrochemical performance was evaluated in an Ar-saturated 0.10 M KOH aqueous solution with $10 \times 10^{-3}$ M $NO_3^-$. It was observed that Fe3DSAC showed a higher ammonia production over 3D carbon material. Also, the yield for Fe3DSAC at $-0.6$ V versus RHE was procured around $\approx 4.55\ \mu mol\ cm^{-2}\ h^{-1}$

which was about 7.5 times the value procured from 3D carbon. The SAC also displayed a high activity and stability during the NRA process. Furthermore, electrocatalytic performance of other metal sites was evaluated by changing the central elements and spatial geometries of 3D printed SACs. In principle, the technique has opened up enormous possibilities for fabricating large-scale commercial production of SACs for a sustainable production of fuels and chemicals and a broad spectrum of other applications.

3D printable inks of 2D materials for DIW[120,121] have gained attention for designing electrodes; however, using such electrodes for ammonia production remains unexplored. For instance, there are reports on DIW of 3D MXene substrates,[122] yet employing these 3D printed substrates as electrocatalysts for NRA has hitherto not been subject to experimentation. Technically, MXene dispersions are prepared in both aqueous and non-aqueous systems, provided that the rheological properties are optimized prior to 3D printing. Understanding the fluidic properties is an important task because the lack of proper optimizations can lead to deviation in the ink flow and result in bad printing.

In addition, there are a couple of studies on Cu-modified MXene that have emerged recently for NRA, wherein in one of the works by Li et al., Cu molecular catalyst (copper phthalocyanine, CuPc) was anchored to the $Ti_3C_2T_x$ MXene surface to obtain a CuPc@MXene catalyst. The catalyst delivered very high ammonia selectivity of 94.0% and a nitrate conversion rate of 90.5%.[123] The above works expand the possibilities of modification of MXene surfaces using various other transition metals for ammonia production. Using this approach, similar MXene slurries can be formulated for the DIW of 3D printed MXene electrocatalysts for NRA. Also, 3D printing of MOF-based catalysts was recently reported via DIW using aqueous Fe-based MOF/silicon carbide composite inks[124] enhancing its possibility as an electrocatalyst for NRA. In short, formulating slurries of 2D material composites or nanoparticles will be interesting for DIW as the extrusion of such composite materials may be more challenging via the FDM approach. However, fabricating multicomponent 3D printed substrates using 2D materials will be a good foundation for ambitious projects in the future, especially for NRA.

3D printed Cu substrate for NRA via FDM is already discussed in the previous section. Interestingly, metallic micro- or nanoparticles that are sintered at high temperatures are found to serve as dispersions for DIW. For example, in a study by Lim et al.,[125] Cu particles were mixed with Pluronic F127 to obtain a self-standing ink that was 3D printed successfully. This was followed by postprinting treatments to deliver efficient and conductive substrates. Taking advantage of the principle adopted in fabricating Cu electrodes via DIW, the possibility of 3D printing other metal nano/microparticles beyond Cu can be explored. Noticeably, the 3D printed electrode material prepared via DIW may also need to be treated using additional methods to activate and expose their catalytically active surfaces as in the case of FDM. Furthermore, gold- (Au)[126] and silver- (Ag)[127] based electrodes were also studied for NRA. Fabricating 3D printed structures using these active materials via DIW can enable robust and conductive platforms for catalytic applications as in a study reported by Zhu et al.[128] In short, the above work can be referred to and/or adapted for designing 3D printed substrates of Ag, Au, multiple alloy composites, and so on. Thus, designing

3D printed electrocatalysts using a wide variety of materials via DIW for ammonia production shall be a novel venture that guarantees wide-scale application in the future.

### 4.3. Other Printing Approaches

Metal 3D printing technology provides a rapid prototyping platform to fabricate robust and conductive 3D metal electrode substrates.[84,129,130] Integrating the design flexibility rendered by 3D printing technology with the mechanical properties of respective metals to fabricate electrocatalysts, substrates, and reactors are interesting material fabrication approaches. In previous sections, the ability of metal FDM 3D printing was discussed as a potential possibility of the recent advancements to design metal 3D printed catalysts. However, multiple other 3D printing technologies[19,54,131] are conventionally known for designing robust, conductive, and active metal 3D printed catalysts, and catalytic reactors. In principle, in this technology of 3D printing, high power laser sources are typically used for binding the powdered metal particles and then systematically printed to procure the final conductive 3D printed structures. Among these, SLS and SLM are the potential techniques that can be employed in designing 3D structures with the help of metal powders or metal-based precursor materials.

SLS-based metal 3D printing technology has been recently used by a group of researchers to fabricate self-catalytic reactors (SCR) for $CO_2RR$ applications using various active metal components of Fe, cobalt (Co), and Ni.[77] Hence, understanding the potential of 3D printing technology for the fabrication of metal 3D printed parts is regarded to be highly promising for devising active 3D printed substrates for NRA applications. SLM 3D printing techniques have also been employed to fabricate 3D printed conductive electrode substrates, where the precursor materials are either metal or metal alloys of Cu, Ti, Al, and so on.

3D printed metal electrodes can be printed efficiently using both SLM and direct metal laser sintering (DMLS) techniques, where metal powder particles are sintered using a laser source and fused in an inert gas-filled chamber.[132] During the process, metal powder is added over the sintered layer and the above procedure is repeated until the final component is printed based on the predesigned 3D modeled data file. While only a single metal powder is used with the SLM technique, multiple metal alloys with varying melting points are used to 3D print structures using DMLS. This approach can be used to 3D print metal substrates using single or multiple metallic components that would render the user the ability to design electrodes with different compositions and customize an electrocatalyst for ammonia production. The list of precursor materials available for metal 3D printing ranges from Cu, Ni, Ti, Al, etc., and their alloys, to precious metals such as Au, Ag, and metal powders. Based on discussions carried out in this paper, it can be observed that these metal precursors can be 3D printed as active materials toward NRA. However, we do not expect the alloy to be efficient by default for ammonia production but anticipate that metal printing via SLS, SLM, EBM, and DMLS will be advantageous in fabricating electrode materials with excellent mechanical and conductive properties, making it ideal for NRA. In short, improvements, modifications, and optimizations of these 3D printed alloy parts over time will

allow the user to devise an active electrocatalyst for large-scale applications.

## 5. Postfabrication Treatments and Modification

3D printed electrocatalysts/substrates can be considered a forerunner to next-generation energy applications in terms of devising electrode materials that are scalable and can be easily extended toward large-scale production. FDM 3D printing of graphene/PLA and metal/PLA filaments are well known for the fabrication of catalyst/substrate for a broad spectrum of applications. Although PLA in these substrates provides structural integrity to the printed structure, the conductivity of substrates is severely hampered by these nonconductive polymer counterparts. Thus, postfabrication approaches are introduced to limit the amount of polymers in the printed structures, with the objective of increasing the conductivity of the printed substrates, especially for catalysis applications.[20,47,94] Solvent,[31] thermal,[88] electrochemical,[46] enzyme activation,[133] among others, are some of the techniques employed to get rid of nonconductive PLA in carbon substrates or customized substrates.

In a broader context, especially for the FDM technique, solvent activation using DMF,[25,31] acetone,[94] $NaBH_4$,[49] and NaOH,[134] are commonly employed for activating carbon/polymer, graphene/polymer electrode substrates, with several other solvents being studied periodically. Electrochemical treatment is another possible strategy that has been suggested by researchers to improve the conductivity of 3D printed substrates. In a study by Browne et al.,[86] an interesting approach of material enhancement was proposed via sequential solvent activation of graphene/PLA electrodes in DMF, followed by electrochemical activation in phosphate-buffer solution, resulting in 3D printed electrodes with enhanced performance. These catalytic carbon surfaces can also be modified or surface-engineered with metal nanoparticles to fabricate electrocatalysts that are efficient for ammonia production.

Sintering is another strategy employed for metal/PLA electrodes,[37] such as Cu/PLA and Fe/PLA, wherein exposure of 3D printed substrates to high temperature can result in the removal of nonconductive PLA counterparts, delivering metal substrates with enhanced and exposed metal active sites.[37,38]

Modification of 3D printed substrates using appropriate strategies can render to electrocatalysts for various catalytic applications.[135] Electrodeposition,[25] ALD,[85] patterned coating techniques,[31,96] functionalization of active molecular materials, and so on, are a few among a host of other techniques known to fabricate active 3D printed structures for ammonia production.

Electrodeposition is a well-known and widely adopted technique employed to deposit a layer of active material from a corresponding precursor metal salt solution over the activated 3D printed substrates (**Figure 10**A). This approach can be used to electroplate 3D printed structures with a Cu and Ni layer,[25] or any similar salt of transition metal[81,136] provided they are active metal centers for ammonia production. Cu and Ni are well known as active electrocatalysts for ammonia production. Thus, techniques such as chronoamperometry can be employed using a Cu- and/or Ni-based salt solution at defined time intervals for the electrodeposition of Cu/Ni over carbon[25] or metal substrates.[83] TMDs like $MoS_2$ and $WS_2$ are promising materials

**ADVANCED
SCIENCE NEWS**
www.advancedsciencenews.com

**ADVANCED
MATERIALS
TECHNOLOGIES**
www.advmattechnol.de
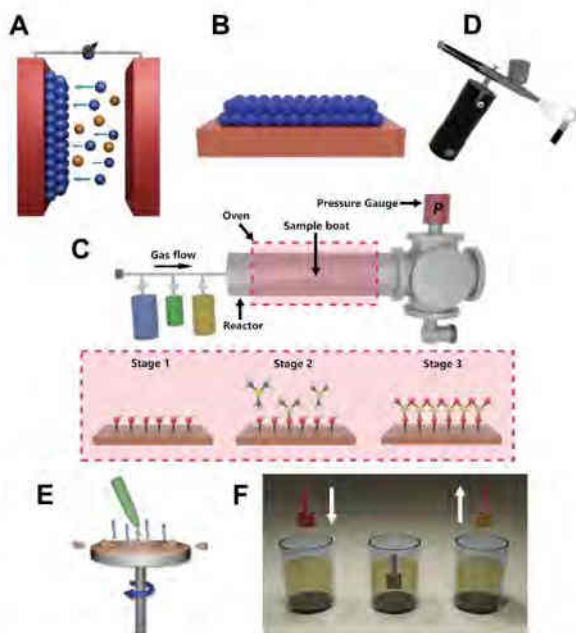


**Figure 10.** Modification of 3D printed electrocatalysts via A) electrodeposition, B,C) ALD, D) spray-coating, E) spin-coating, and F) dip-coating.

for ammonia production. Because electrodeposition of these materials is already reported,[137] we assume that these modified 3D printed electrocatalysts could be highly efficient for NRA as well.

Furthermore, techniques such as ALD deliver a feasible, homogeneous (Figure 10B), and conformal deposition of active layers, sequentially without compromising the 3D topography. A stepwise demonstration is given in Figure 10C. These are advanced deposition techniques with high reproducibility that are ideal for depositing material of tunable thickness over complex structures such as 3D printed electrodes.[138] For instance, in a study, 2D materials such as $MoS_2$ are shown to be coated efficiently over 3D printed titanium electrodes for catalytic applications.[50] This technique is ideal for depositing active material over carbon-based substrates as well.[138] Although limitations from electrodeposition can be mitigated by adopting better techniques such as ALD, they are expensive and require expert guidance, especially during coating over 3D printed electrodes. ALD also has a wide range of metal/metal oxide precursor materials that can be explored for obtaining a better electrode surface, ideal for NRA.

Patterned coatings of active material dispersions over 3D printed substrates are an interesting, rapid, and cost-effective electrode modification approach to devise electrocatalysts. This approach has attracted significant attention in recent years due to the low complexity of the instrumentation and minimal complications involved in ink formulation.[31,139] Techniques such as spray-coating (Figure 10D),[96] spin-coating (Figure 10E), and dip-coating[31] are commonly known approaches to fabricate substrates that are cheaper and less toxic, enabling successful coating over the desired 3D printed substrates. These techniques give users the freedom to develop a wide range of 3D printed material catalysts by patterning 2D materials, their composites,

nanoparticles, metal oxides, and so on, to be active for ammonia production. For instance, in a study, $MoS_2$ was spray-coated over 3D printed carbon-based (graphene/PLA) electrode surfaces, and evaluated for HER.[96] The approach aided in abundant and ideal coverage of electrode surfaces by $MoS_2$ sheets. Furthermore, in another interesting study from our groups, dip-coating (Figure 10F) of 2D materials such as MXenes and TMDs of $MoS_2$, $MoSe_2$, $WS_2$, and $WSe_2$ were coated over DMF-activated 3D printed graphene/ PLA electrode.[31] Postdrying, the electrode was evaluated for HER application in 0.5 M $H_2SO_4$ electrolyte solution, showcasing improved electrocatalytic activity of 3D electrode substrate. Thus, techniques such as dip-coating can be employed as a facile and cost-effective approach of electrode modification over conventional techniques.

Sputtering an active material can also be highly beneficial for designing 3D printed electrocatalysts. For instance, in a study, NRA was carried out over modified Au electrodes.[126] Modifications via sputtering of Au on 3D printed carbon electrodes and post-treatments also have been reported to improve the surface properties of electrode substrates. This can be extended to Ag or similar transition metals, which could be ideally sputtered over 3D printed electrode surfaces to fabricate newer electrodes for NRA. Thus, there is an immense possibility of improving the substrate surface for NRA in multiple ways. The major task lies in deciding the ideal modification approach for each catalytic material followed by its optimization. Hence, the 3D printing of active material substrates is expected to show high possibilities for the design of ideal electrocatalysts that are efficient, active, and highly selective for NRA.

## 6. 3D Printed Substrates for Nitrogen Reduction Reaction

Haber–Bosch process is the conventionally well-known industrial process for ammonia production. Owing to the limitations of this technique, as mentioned in the previous section, there have been constant efforts among researchers for finding alternatives. Among them, electrochemical NRR for ammonia production[59,140,141] has gained massive scientific interest in the recent past. NRR continues to be a well investigated domain, although recent studies consider NRA to be more efficient than NRR. Thus, a discussion on the possibilities of designing 3D printed electrocatalysts for NRR can be interesting to the researchers working in this area. NRR offers the possibility for large-scale applications owing to the abundant availability of nitrogen source in the atmosphere.[140,142,143] In addition, the clean and sustainable mode of $NH_3$ production with less energy-intensive working conditions and low or even zero $CO_2$ emissions makes this technique unique and preferable over the Haber–Bosch process.

Thus, the fundamental focus would be on developing ideal electrocatalysts with high activity and stability that can efficiently carry out ammonia synthesis under ambient conditions. Furthermore, it must also be capable of mitigating selectivity toward HER and favor ammonia production. 3D printed electrocatalysts for NRR are also relatively new and unexplored like NRA. The mechanism can be procured from the literature as detailing is beyond the scope of the article.[59,144,145] Although several catalysts for NRR, and the possibility of fabricating catalysts using these

**ADVANCED
SCIENCE NEWS**
www.advancedsciencenews.com

**ADVANCED
MATERIALS
TECHNOLOGIES**
www.advmattechnol.de

active materials via 3D printing are both well known, the interdisciplinary domains of 3D printing electrocatalysts for ammonia synthesis via NRR are still not explored well. In the following discussion, we focus on developing a bridge between existing reports on the possible active materials known for NRR and the feasibility of using these materials toward fabrication of 3D printed electrodes/devices via various techniques.

### 6.1. Carbon Substrates

Advantages of carbon substrates are very well discussed in Section 4.1.1 along with several reports on carbon/graphene substrates for NRR applications.[146,147] For instance, Zhang et al.[93] put forth a detailed discussion on multiple defect engineering strategies over carbon-based substrates for efficient ammonia production. Also, Majumder et al.[148] discuss the possibility of modifying graphene electrocatalysts for enhanced ammonia production from nitrogen. Therefore, adapting the possibilities of using carbon material from the above works into the realm of 3D printing technology can lead to the fabrication of 3D printed carbon substrates via FDM (black magic/protopasta/customized carbon-based filaments, etc.) for ammonia synthesis.

### 6.2. Metal Electrocatalysts

Cu,[149] Ti,[150] Ni,[151] Au,[152] and Ag[153] have been explored for NRR application as well. In the domain of 3D printing, employing the respective metal/PLA filaments of corresponding active material (Cu, Ti, Ni, etc.) and/or modification of 3D printed substrates via sputtering (Ag, Au), electrodeposition (Ag, Au, Ni, Cu, etc.), coatings of active material (Ni, Cu, etc.) over substrates, would help in designing ideal and efficient 3D printed electrocatalysts. In principle, this approach would help in designing 3D printed electrocatalysts for NRR applications at a large scale, in minimal time, and cost-effective manner. Advancements in 3D printing technology, such as customized filament fabrication (Section 4.1.4), MM 3D printing techniques (Section 4.1.5), and other known 3D printing techniques, would also help in designing ideal electrocatalysts for ammonia production via nitrogen reduction. The postfabrication techniques and electrode modifications discussed in Section 5 are also advantageous for the fabrication of conductive 3D printed electrodes with high selectivity and efficiency for NRR, as well as for high-yield ammonia production.

Furthermore, molybdenum (Mo) and Fe are considered to be theoretically feasible electrocatalysts for NRR. In a work by Zeng et al.,[154] nitrogen-doped $MoS_2$ nanoflowers were studied as electrocatalysts under ambient conditions. It was observed that the catalyst delivered high FE (9.14%) at −0.3 V versus RHE in 0.1 M $Na_2SO_4$ and provided $NH_3$ yield of 69.82 μg h$^{-1}$ mg$_{cat}^{-1}$. In our previous discussion about the FDM 3D printing technique, the work on $MoS_2$ 3D printed substrates conducted by our group was mentioned.[52] The possibility of modifying these electrode surfaces via nitrogen doping or similar method is also known to be technically feasible. Thus, we propose the possibility of designing nitrogen-doped 3D printed $MoS_2$ substrates via extrusion-based technique that are speculated to be ideal for NRR.

### 6.3. 2D Materials

Studies on combining 2D materials to fabricate electrocatalysts for ammonia production are known to be relatively new, one among them being the recent studies on loading 1T'-$MoS_2$ with $Ti_3C_2$ MXene.[155] The possibility of ideal ink formulation via DIW can also result in developing 3D printed $MoS_2$/MXene electrocatalysts for desired catalytic applications such as for NRR. These novel approaches of designing self-standing, robust, and active 3D printed electrocatalyst substrates can bring an impactful improvement in this field.

Though the major part of this article focuses on the possibility of utilizing 3D printed electrodes for NRA, we also claim that the technique of 3D printing electrocatalysts has not been hitherto introduced to NRR as well. Thus, a large possibility exists for designing electrocatalysts for NRR via several other techniques, given the fact that 3D printing shows enormous prospects of fabricating substrates similar to the ones that have been already reported for NRR. Also, the mechanism shared by these two reactions (NRA and NRR) to give the same product (ammonia) has a big difference, and their adaptability to serve as a catalyst via 3D printing technology is subject to repeated improvement, considering the geometry, porosity, and size with respect to the experimental conditions, systematic optimization, and tuning/optimizing the postfabrication approaches. However, considering the reports on the limitations of NRR over NRA, the major focus was shifted to 3D printing electrodes for NRA. Nevertheless, there is still scope for improvement in designing electrocatalysts of active material using FDM, DIW, SLA, or SLM among others for NRR.

## 7. Challenges and Solutions

The prospect of 3D printed substrates for NRA is relatively new and, thus, the expected uptake in this area can be a bit slow; however, once the abilities of this technology toward NRA are fully realized, it will represent a promising leap in the design of electrodes/devices. FDM-based electrode and device fabrication using graphene/PLA, carbon black/PLA, carbon black/ABS, customized 2D material/PLA, and so on, are well known. However, extruded 3D printed structures may not be ideal for direct catalysis applications owing to the presence of nonconductive constituents (PLA, ABS, etc.), requiring postfabrication treatments.[47,94] Although several techniques have been proposed,[19,20] very strict optimization measures are recommended because overexposure to postfabrication treatments such as solvents, and physical and/or chemical treatments can result in excess loss of polymer from printed parts. This eventually affects the strength of 3D printed structures, resulting in the weakening and breakage of the printed structures. Nevertheless, an initial exploration of this technique for the fabrication of 3D printed catalyst can be relatively time-consuming, where the user will initially need to fabricate multiple prototypes with varied compositions of active material, fillers, polymers, additives, and so on (e.g., customized filaments). Optimization also extends to the filament extrusion quality, extrusion temperature, and reproducibility. Postoptimization of the ideal filament composition can aid in employing these 3D printed structures as electrocatalysts for NRA applications.

Temperature is another vital factor for the extrusion of filaments, wherein the extrusion temperature will vary from filament to filament. Sometimes high temperatures can result in the oxidation of metal nanoparticles or filament composites, affecting the conductivity severely. A possible remedy would be to design a special chamber that would be capable of providing inert atmospheric conditions via constant purging of $Ar/N_2$ gas during printing.[19] In addition, sintering 3D printed metal electrodes such as Cu/PLA, Fe/PLA, and Ti/PLA, at elevated/unoptimized temperatures can result in the degradation or deformed shape of the printed electrodes. This could be mitigated by using covering materials and molds that help to preserve the shape of the electrode post thermal treatment. As a feasible strategy, experiments like thermogravimetric analysis could be initially employed to track the degradation of polymers from the printed structure. With such systematic understanding, the user can easily optimize the required temperature for activating the printed electrode substrate without losing the shape of the printed structures. DIW using certain active materials can result in clogging of the nozzle; however, the rheological properties of inks should be constantly assessed for better printability. Proper optimization of ink fluidity can also prevent bad printing or incomplete printed structures.

Electrode modification via various techniques was discussed in detail in the previous section. However, certain challenges are also associated with the modification of the electrocatalyst surface using conventional techniques, which has to be taken care of for efficient catalyst fabrication. For instance, although electrodeposition techniques are cheap, quick, and provide a wide range of choices for metal or metal oxides, the semiuniform deposition of material over the 3D printed structure can serve as a major limitation to this technique.[19] The techniques employed for electrodeposition are expected to be well optimized, prior to its coating over fabricated 3D electrode material.

Every technique has its pros and cons. Therefore, finding the ideal technique based on the experimental setup/targeted applications has to be carefully executed to fabricate ideal electrocatalysts/reactors/devices for applications such as ammonia production. Strategies to improve ammonia production have evolved over time and have come a long way from conventional techniques like Haber–Bosch and NRR to recent ones like NRA. Designing ideal electrocatalysts or catalytic reactors has been the primary goal of all these techniques, where the catalyst exhibits high activity, selectivity, efficiency, and stability during the reaction. 3D printing for ammonia production is a relatively new approach toward designing electrodes or electrolyzers; therefore, it is guaranteed to take a considerable amount of time and research to develop effective strategies for fabricating efficient catalysts for NRA.

## 8. Conclusion and Future Perspective

Catalysts can play a significant role in resolving several ongoing crises arising due to the declining availability of fossil fuels and the exhaustion of resources with the increasing population. The conversion of nitrate into ammonia has unfolded the scope of an alternative sustainable pathway for ammonia synthesis and, thus, the design of ideal electrocatalysts for this process has become a major task. This perspective article discusses how 3D printing

technology can be an asset in the fabrication and engineering of 3D printed electrodes that serve as active electrocatalysts for ammonia production. Several precursors materials have emerged in recent years that can be extruded/sintered/formulated successfully to procure 3D printed electrodes and devices. These precursors include carbon materials, 2D materials (graphene, MXene, TMDs, MOFs, etc.), metal/metal oxides, nano/microparticles, and many more. Interestingly, 3D printing techniques today provide the flexibility of printing self-supported catalyst substrates, SACs, for catalysis and possibly resolve several issues encountered by traditional printing techniques. We summarize that although several active materials are reportedly known to be ideal for ammonia production, 3D printing technology confers the freedom to 3D-print these active materials for catalytic applications like NRA. The technology of 3D printing was developed four decades ago; however, it has taken a considerable length of time to expand and flourish as a domain across multiple industries and sciences. This technique today has become exponentially cheaper as the cost of printers, precursor materials, and other accessories consistently declines. Although 3D printing electrodes for catalytic applications are primarily studied as a proof-of-concept, over time this technology is expected to potentially expand to large-scale manufacturing terrains, using structures that are less expensive and with large outputs. This process of escalating from small-scale laboratory operations to a large-scale industrial setup can be challenging and requires critical and creative resolutions in its design.

3D printing is known to have great potential in terms of designing reactors for catalytic systems as it holds a dual advantage of having a catalyst component as well as the ability to moderate the flow of reactants. This article, however, has focused on using 3D printing technology for the fabrication of functional catalysts, catalytic reactors, and similar systems for ammonia production. Significant advancements have been witnessed in recent years in fabricating 3D printed devices, with a major focus on catalysis applications. Thus, the fabrication of active electrocatalysts that could be integrated into the electrolytic system, along with the manufacturing of both framework and internal part of the electrolyzer, can be considered to be significant advancements in the field of NRA. This would also be an impactful technology in the future for diversifying ammonia production. In short, with ammonia production being a vital application, further advancements are expected in this direction and 3D printing would be a breakthrough in designing novel electrocatalyst structures that are more cost-effective, energy-efficient, and also mitigate the environmental concerns.

## Acknowledgements

## Conflict of Interest

The authors declare no conflict of interest.

[1] S. C. Peter, *ACS Energy Lett.* **2018**, *3*, 1557.
[2] L. Pokrajac, A. Abbas, W. Chrzanowski, G. M. Dias, B. J. Eggleton, S. Maguire, E. Maine, T. Malloy, J. Nathwani, L. Nazar, A. Sips, J. Sone, A. Van Den Berg, P. S. Weiss, S. Mitra, *ACS Nano* **2021**, *15*, 18608.
[3] A. Venkateshaiah, J. Y. Cheong, S. H. Shin, K. P. Akshaykumar, T. G. Yun, J. Bae, S. Wacławek, M. Černík, S. Agarwal, A. Greiner, V. V. T. Padil, I. D. Kim, R. S. Varma, *Green Chem.* **2020**, *22*, 1198.
[4] T. R. Karl, K. E. Trenberth, *Science* **2003**, *302*, 1719.
[5] D. R. MacFarlane, P. V. Cherepanov, J. Choi, B. H. R. Suryanto, R. Y. Hodgetts, J. M. Bakker, F. M. Ferrero Vallana, A. N. Simonov, *Joule* **2020**, *4*, 1186.
[6] A. Valera-Medina, F. Amer-Hatem, A. K. Azad, I. C. Dedoussi, M. De Joannon, R. X. Fernandes, P. Glarborg, H. Hashemi, X. He, S. Mashruk, J. McGowan, C. Mounaim-Rouselle, A. Ortiz-Prado, A. Ortiz-Valera, I. Rossetti, B. Shu, M. Yehia, H. Xiao, M. Costa, *Energy Fuels* **2021**, *35*, 6964.
[7] G. Jeerh, M. Zhang, S. Tao, *J. Mater. Chem. A* **2021**, *9*, 727.
[8] S. Ornes, *Proc. Natl. Acad. Sci. USA* **2021**, *118*, e2119584118.
[9] R. Schlögl, *Angew. Chem., Int. Ed.* **2003**, *42*, 2004.
[10] J. Guo, P. Chen, *Chem* **2017**, *3*, 709.
[11] L. Li, C. Tang, B. Xia, H. Jin, Y. Zheng, S. Z. Qiao, *ACS Catal.* **2019**, *9*, 2902.
[12] X. Lu, H. Song, J. Cai, S. Lu, *Electrochem. Commun.* **2021**, *129*, 107094.
[13] G. F. Chen, Y. Yuan, H. Jiang, S. Y. Ren, L. X. Ding, L. Ma, T. Wu, J. Lu, H. Wang, *Nat. Energy* **2020**, *5*, 605.
[14] J. Qin, K. Wu, L. Chen, X. Wang, Q. Zhao, B. Liu, Z. Ye, *J. Mater. Chem. A* **2022**, *10*, 3963.
[15] Z. Gao, Y. Lai, Y. Tao, L. Xiao, L. Zhang, F. Luo, *ACS Cent. Sci.* **2021**, *7*, 1066.
[16] Y. Wang, A. Xu, Z. Wang, L. Huang, J. Li, F. Li, J. Wicks, M. Luo, D. H. Nam, C. S. Tan, Y. Ding, J. Wu, Y. Lum, C. T. Dinh, D. Sinton, G. Zheng, E. H. Sargent, *J. Am. Chem. Soc.* **2020**, *142*, 5702.
[17] Z. Y. Wu, M. Karamad, X. Yong, Q. Huang, D. A. Cullen, P. Zhu, C. Xia, Q. Xiao, M. Shakouri, F. Y. Chen, J. Y. (Timothy) Kim, Y. Xia, K. Heck, Y. Hu, M. S. Wong, Q. Li, I. Gates, S. Siahrostami, H. Wang, *Nat. Commun.* **2021**, *12*, 2870.
[18] A. Ambrosi, R. R. S. Shi, R. D. Webster, *J. Mater. Chem. A* **2020**, *8*, 21902.
[19] A. K. K. Padinjareveetil, M. Pumera, *Adv. Mater. Interfaces* **2023**, *10*, 2201734.
[20] M. P. Browne, E. Redondo, M. Pumera, *Chem. Rev.* **2020**, *120*, 2783.
[21] M. R. Hartings, Z. Ahmed, *Nat. Rev. Chem.* **2019**, *3*, 305.
[22] K. P. A. Kumar, M. Pumera, *Adv. Funct. Mater.* **2021**, *31*, 2100450.
[23] A. Ambrosi, M. Pumera, *Chem. Soc. Rev.* **2016**, *45*, 2740.
[24] C. Y. Lee, A. C. Taylor, A. Nattestad, S. Beirne, G. G. Wallace, *Joule* **2019**, *3*, 1835.
[25] K. P. A. Kumar, K. Ghosh, O. Alduhaish, M. Pumera, *Electrochem. Commun.* **2020**, *120*, 106827.
[26] X. Tian, J. Jin, S. Yuan, C. K. Chua, S. B. Tor, K. Zhou, *Adv. Energy Mater.* **2017**, *7*, 1700127.
[27] J. Muñoz, M. Pumera, *TrAC, Trends Anal. Chem.* **2020**, *128*, 115933.

[28] C. Barnatt, 3D Printing: The Next Industrial Revolution, ExplainingTheFuture.com, **2013**.
[29] J. Sun, Z. Peng, W. Zhou, J. Y. H. Fuh, G. S. Hong, A. Chiu, *Proc. Manuf.* **2015**, *1*, 308.
[30] V. V. T. Padil, K. P. Akshay Kumar, S. Murugesan, R. Torres-Mendieta, S. Wacławek, J. Y. Cheong, M. Černík, R. S. Varma, *Green Chem.* **2022**, *24*, 3081.
[31] K. P. Akshay Kumar, K. Ghosh, O. Alduhaish, M. Pumera, *Electrochem. Commun.* **2021**, *122*, 106890.
[32] E. Vaněčková, M. Bouša, V. Shestivska, J. Kubišta, P. Moreno-García, P. Broekmann, M. Rahaman, M. Zlámal, J. Heyda, M. Bernauer, T. Sebechlebská, V. Kolivoška, *ChemElectroChem* **2021**, *8*, 2137.
[33] C. W. Foster, M. P. Down, Y. Zhang, X. Ji, S. J. Rowley-Neale, G. C. Smith, P. J. Kelly, C. E. Banks, *Sci. Rep.* **2017**, *7*, 42233.
[34] C. W. Pinger, M. K. Geiger, D. M. Spence, *J. Chem. Educ.* **2020**, *97*, 112.
[35] N. Shahrubudin, T. C. Lee, R. Ramlan, *Proc. Manuf.* **2019**, *35*, 1286.
[36] S. C. Ligon, R. Liska, J. Stampfl, M. Gurr, R. Mülhaupt, *Chem. Rev.* **2017**, *117*, 10212.
[37] C. Iffelsberger, D. Rojas, M. Pumera, *J. Phys. Chem. C* **2022**, *126*, 9016.
[38] E. Redondo, M. Pumera, *Appl. Mater. Today* **2021**, *25*, 101253.
[39] J. A. Lewis, *Adv. Funct. Mater.* **2006**, *16*, 2193.
[40] S. Tagliaferri, A. Panagiotopoulos, C. Mattevi, *Mater. Adv.* **2021**, *2*, 540.
[41] A. Shahzad, I. Lazoglu, *Composites, Part B* **2021**, *225*, 109249.
[42] C. Parra-Cabrera, C. Achille, S. Kuhn, R. Ameloot, *Chem. Soc. Rev.* **2018**, *47*, 209.
[43] formlabs, SLA vs. DLP: Guide to Resin 3D Printers, https://formlabs.com/eu/blog/resin-3d-printer-comparison-sla-vs-dlp/, (accessed: July 2022).
[44] E. O. Olakanmi, R. F. Cochrane, K. W. Dalgarno, *Prog. Mater. Sci.* **2015**, *74*, 401.
[45] Nick Loth, ALL3DP, Electron Beam Melting (EBM) – 3D Printing Simply Explained, https://all3dp.com/2/electron-beam-melting-ebm-3d-printing-simply-explained/. accessed October, 2022
[46] P. L. dos Santos, V. Katic, H. C. Loureiro, M. F. dos Santos, D. P. dos Santos, A. L. B. Formiga, J. A. Bonacin, *Sens. Actuators, B* **2019**, *281*, 837.
[47] D. P. Rocha, R. G. Rocha, S. V. F. Castro, M. A. G. Trindade, R. A. A. Munoz, E. M. Richter, L. Angnes, *Electrochem. Sci. Adv.* **2022**, *2*, e2100136.
[48] G. I. J. Salentijn, P. E. Oomen, M. Grajewski, E. Verpoorte, *Anal. Chem.* **2017**, *89*, 7053.
[49] E. Redondo, J. Muñoz, M. Pumera, *Carbon* **2021**, *175*, 413.
[50] V. Urbanová, J. Plutnar, M. Pumera, *Appl. Mater. Today* **2021**, *24*, 101131.
[51] A. Ambrosi, M. Pumera, *ACS Sustainable Chem. Eng.* **2018**, *6*, 16968.
[52] K. Ghosh, S. Ng, C. Iffelsberger, M. Pumera, *Appl. Mater. Today* **2022**, *26*, 101301.
[53] B. Y. Ahn, E. B. Duoss, M. J. Motala, X. Guo, S. Il Park, Y. Xiong, J. Yoon, R. G. Nuzzo, J. A. Rogers, J. A. Lewis, *Science* **2009**, *323*, 1590.
[54] J. Zhu, P. Wu, Y. Chao, J. Yu, W. Zhu, Z. Liu, C. Xu, *Chem. Eng. J.* **2022**, *433*, 134341.
[55] H. Liu, *Ammon. Synth. Catal.* **2013**, 1.
[56] J. Humphreys, R. Lan, S. Tao, *Adv. Energy Sustainability Res.* **2021**, *2*, 2000043.
[57] L. Zhang, X. Ji, X. Ren, Y. Ma, X. Shi, Z. Tian, A. M. Asiri, L. Chen, B. Tang, X. Sun, *Adv. Mater.* **2018**, *30*, 1800191.
[58] D. Liu, M. Chen, X. Du, H. Ai, K. H. Lo, S. Wang, S. Chen, G. Xing, X. Wang, H. Pan, *Adv. Funct. Mater.* **2021**, *31*, 2008983.

[59] S. L. Foster, S. I. P. Bakovic, R. D. Duda, S. Maheshwari, R. D. Milton, S. D. Minteer, M. J. Janik, J. N. Renner, L. F. Greenlee, *Nat. Catal.* **2018**, *1*, 490.

[60] J. Hou, M. Yang, J. Zhang, *Nanoscale* **2020**, *12*, 6900.

[61] Y. Wang, W. Zhou, R. Jia, Y. Yu, B. Zhang, *Angew. Chem., Int. Ed.* **2020**, *59*, 5350.

[62] J. Martínez, A. Ortiz, I. Ortiz, *Appl. Catal., B* **2017**, *207*, 42.

[63] W. Duan, G. Li, Z. Lei, T. Zhu, Y. Xue, C. Wei, C. Feng, *Water Res.* **2019**, *161*, 126.

[64] J. Wang, C. Cai, Y. Wang, X. Yang, D. Wu, Y. Zhu, M. Li, M. Gu, M. Shao, *ACS Catal.* **2021**, *11*, 15135.

[65] P. H. van Langevelde, I. Katsounaros, M. T. M. Koper, *Joule* **2021**, *5*, 290.

[66] M. Duca, M. T. M. Koper, *Energy Environ. Sci.* **2012**, *5*, 9726.

[67] A. Scheidleder, J. Grath, G. Winkler, U. Stark, C. Koreimann, C. Gmeiner, P. Gravesen, J. Leonard, M. Elvira, S. Nixon, J. Casillas, T. J. Lack, N. Thyssen, "Groundwater quality and quantity in Europe"@eng, Bernan Associates, U.S.A **1999**, 1.

[68] Y. Wang, C. Wang, M. Li, Y. Yu, B. Zhang, *Chem. Soc. Rev.* **2021**, *50*, 6720.

[69] A. C. A. De Vooys, R. A. Van Santen, J. A. R. Van Veen, *J. Mol. Catal. A: Chem.* **2000**, *154*, 203.

[70] A. R. Cook, N. Dimitrijevic, B. W. Dreyfus, D. Meisel, L. A. Curtiss, D. M. Camaioni, *J. Phys. Chem. A* **2001**, *105*, 3658.

[71] Y. Li, Y. K. Go, H. Ooka, D. He, F. Jin, S. H. Kim, R. Nakamura, *Angew. Chem., Int. Ed.* **2020**, *59*, 9744.

[72] R. Jia, Y. Wang, C. Wang, Y. Ling, Y. Yu, B. Zhang, *ACS Catal.* **2020**, *10*, 3533.

[73] A. C. A. de Vooys, M. T. M. Koper, R. A. Van Santen, J. A. R. Van Veen, *Electrochim. Acta* **2001**, *46*, 923.

[74] T. Yoshioka, K. Iwase, S. Nakanishi, K. Hashimoto, K. Kamiya, *J. Phys. Chem. C* **2016**, *120*, 15729.

[75] Y. Wang, Y. Yu, R. Jia, C. Zhang, B. Zhang, *Natl. Sci. Rev.* **2019**, *6*, 730.

[76] J. Crawford, H. Yin, A. Du, A. P. O'Mullane, *Angew. Chem. Int. Ed.* **2022**, *134*, e202201604.

[77] Q. Wei, H. Li, G. Liu, Y. He, Y. Wang, Y. E. Tan, D. Wang, X. Peng, G. Yang, N. Tsubaki, *Nat. Commun.* **2020**, *11*, 4098.

[78] X. Zhou, C. J. Liu, *Adv. Funct. Mater.* **2017**, *27*, 1701134.

[79] C. Iffelsberger, S. Ng, M. Pumera, *Appl. Mater. Today* **2020**, *20*, 100654.

[80] Y. Ying, M. P. Browne, M. Pumera, *Sustainable Energy Fuels* **2020**, *4*, 3732.

[81] P. L. dos Santos, S. J. Rowley-Neale, A. G. M. Ferrari, J. A. Bonacin, C. E. Banks, *ChemElectroChem* **2019**, *6*, 5633.

[82] M. P. Browne, A. Mills, *J. Mater. Chem. A* **2018**, *6*, 14162.

[83] A. Ambrosi, M. Pumera, *Adv. Funct. Mater.* **2018**, *28*, 1700655.

[84] A. Ambrosi, J. G. S. Moo, M. Pumera, *Adv. Funct. Mater.* **2016**, *26*, 698.

[85] M. P. Browne, J. Plutnar, A. M. Pourrahimi, Z. Sofer, M. Pumera, *Adv. Energy Mater.* **2019**, *9*, 1900994.

[86] M. P. Browne, F. Novotný, Z. Sofer, M. Pumera, *ACS Appl. Mater. Interfaces* **2018**, *10*, 40294.

[87] M. H. Omar, K. A. Razak, M. N. Ab Wahab, H. H. Hamzah, *RSC Adv.* **2021**, *11*, 16557.

[88] F. Novotný, V. Urbanová, J. Plutnar, M. Pumera, *ACS Appl. Mater. Interfaces* **2019**, *11*, 35371.

[89] Y. Zheng, Y. Jiao, S. Z. Qiao, *Adv. Mater.* **2015**, *27*, 5372.

[90] K. P. A. Kumar, O. Alduhaish, S. F. Adil, M. Pumera, *Adv. Mater. Interfaces* **2022**, *9*, 2102317.

[91] J. Zhu, S. Mu, *Adv. Funct. Mater.* **2020**, *30*, 2001097.

[92] Z. Chen, J. Chen, G. Barcaro, T. M. Budnyak, A. Rokicińska, R. Dronskowski, S. Budnyk, P. Kuśtrowski, S. Monti, A. Slabon, *Catal. Sci. Technol.* **2022**, *12*, 3582.

[93] L. H. Zhang, F. Yu, N. R. Shiju, *ACS Sustainable Chem. Eng.* **2021**, *9*, 7687.

[94] R. Gusmão, M. P. Browne, Z. Sofer, M. Pumera, *Electrochem. Commun.* **2019**, *102*, 83.

[95] W. Gao, J. V. Perales-Rondon, J. Michalička, M. Pumera, *Appl. Catal., B* **2023**, *330*, 122632.

[96] R. Gusmão, Z. Sofer, P. Marvan, M. Pumera, *Nanoscale* **2019**, *11*, 9888.

[97] J. M. McEnaney, S. J. Blair, A. C. Nielander, J. A. Schwalbe, D. M. Koshy, M. Cargnello, T. F. Jaramillo, *ACS Sustainable Chem. Eng.* **2020**, *8*, 2672.

[98] T. Kandemir, M. E. Schuster, A. Senyshyn, M. Behrens, R. Schlögl, *Angew. Chem., Int. Ed.* **2013**, *52*, 12723.

[99] Elegant3D, Iron PLA filament Proto-Pasta magnetic iron 1.75 mm 0.5 kg, https://www.elegant3d.cz/Iron-PLA-filament-Proto-Pasta-magneticke-zelezo-1-75-mm-0-5-kg-d213.htm. accessed July, 2022

[100] L. Yang, W. Zhu, *Appl. Surf. Sci.* **2022**, *596*, 153624.

[101] J. Li, Y. Zhang, C. Liu, L. Zheng, E. Petit, K. Qi, Y. Zhang, H. Wu, W. Wang, A. Tiberj, X. Wang, M. Chhowalla, L. Lajaunie, R. Yu, D. Voiry, *Adv. Funct. Mater.* **2022**, *32*, 2108316.

[102] J. P. Hughes, P. L. Dos Santos, M. P. Down, C. W. Foster, J. A. Bonacin, E. M. Keefe, S. J. Rowley-Neale, C. E. Banks, *Sustainable Energy Fuels* **2019**, *4*, 302.

[103] Y. Z. Zhang, Y. Wang, Q. Jiang, J. K. El-Demellawi, H. Kim, H. N. Alshareef, *Adv. Mater.* **2020**, *32*, 1908486.

[104] K. P. Akshay Kumar, O. Alduhaish, M. Pumera, *Electrochem. Commun.* **2021**, *125*, 106977.

[105] S. Mallakpour, E. Azadi, C. M. Hussain, *New J. Chem.* **2021**, *45*, 13247.

[106] S. Wert, C. Iffelsberger, A. K. K Padinjareveetil, M. Pumera, *ACS Appl. Electron. Mater.* **2023**, *5*, 928.

[107] S. Hwang, E. I. Reyes, K. sik Moon, R. C. Rumpf, N. S. Kim, *J. Electron. Mater.* **2015**, *44*, 771.

[108] R. Kelly, Multi-material 3D Printer: Types & Printing Guide, https://all3dp.com/2/multi-material-3d-printing-an-overview/, **2022**. accessed February, 2023

[109] A. Ambrosi, R. D. Webster, M. Pumera, *Appl. Mater. Today* **2020**, *18*, 100530.

[110] E. Mackiewicz, T. Wejrzanowski, B. Adamczyk-Cieślak, G. J. Oliver, *Materials* **2022**, *15*, 1360.

[111] S. Mooraj, Z. Qi, C. Zhu, J. Ren, S. Peng, L. Liu, S. Zhang, S. Feng, F. Kong, Y. Liu, E. B. Duoss, S. Baker, W. Chen, *Nano Res.* **2021**, *14*, 2105.

[112] S. Liu, R. Liu, D. Gao, I. Trentin, C. Streb, *Chem. Commun.* **2020**, *56*, 8476.

[113] D. Corral, J. T. Feaster, S. Sobhani, J. R. Deotte, D. U. Lee, A. A. Wong, J. Hamilton, V. A. Beck, A. Sarkar, C. Hahn, T. F. Jaramillo, S. E. Baker, E. B. Duoss, *Energy Environ. Sci.* **2021**, *14*, 3064.

[114] L. Chen, X. Tang, P. Xie, J. Xu, Z. Chen, Z. Cai, P. He, H. Zhou, D. Zhang, T. Fan, *Chem. Mater.* **2018**, *30*, 799.

[115] F. Lei, W. Xu, J. Yu, K. Li, J. Xie, P. Hao, G. Cui, B. Tang, *Chem. Eng. J.* **2021**, *426*, 131317.

[116] T. Hu, M. Wang, C. Guo, C. M. Li, *J. Mater. Chem. A* **2022**, *10*, 8923.

[117] J. Wang, T. Feng, J. Chen, J.-H. He, X. Fang, *Research* **2022**, *2022*, 9837012.

[118] F. Xie, F. Cui, X. Zhi, D. Yao, B. Johannessen, T. Lin, J. Tang, T. B. F. Woodfield, L. Gu, S.-Z. Qiao, *Nat. Synth.* **2023**, *2*, 129.

[119] X. Yang, A. Wang, B. Qiao, J. Li, J. Liu, T. Zhang, *Acc. Chem. Res.* **2013**, *46*, 1740.

[120] R. Yang, J. Zhou, C. Yang, L. Qiu, H. Cheng, *Adv. Mater. Technol.* **2020**, *5*, 1901066.

[121] K. Hassan, M. J. Nine, T. T. Tung, N. Stanley, P. L. Yap, H. Rastin, L. Yu, D. Losic, *Nanoscale* **2020**, *12*, 19007.

[122] C. Zhang, L. McKeon, M. P. Kremer, S.-H. Park, O. Ronan, A. Seral-Ascaso, S. Barwich, C. Ó. Coileáin, N. McEvoy, H. C. Nerl, B. Anasori, J. N. Coleman, Y. Gogotsi, V. Nicolosi, *Nat. Commun.* **2019**, *10*, 1795.

[123] L. X. Li, W. J. Sun, H. Y. Zhang, J. L. Wei, S. X. Wang, J. H. He, N. J. Li, Q. F. Xu, D. Y. Chen, H. Li, J. M. Lu, *J. Mater. Chem. A* **2021**, *9*, 21771.

[124] A. D. Salazar-Aguilar, A. Quintanilla, S. M. Vega-Díaz, J. A. Casas, P. Miranzo, M. I. Osendi, M. Belmonte, *Open Ceram.* **2021**, *5*, 100047.

[125] G. J. H. Lim, Z. Lyu, X. Zhang, J. J. Koh, Y. Zhang, C. He, S. Adams, J. Wang, J. Ding, *J. Mater. Chem. A* **2020**, *8*, 9058.

[126] M. S. El-Deab, *Electrochim. Acta* **2004**, *49*, 1639.

[127] Z. Liu, C. Wang, C. Chen, C. Li, C. Guo, *Electrochem. Commun.* **2021**, *131*, 107121.

[128] C. Zhu, Z. Qi, V. A. Beck, M. Luneau, J. Lattimer, W. Chen, M. A. Worsley, J. Ye, E. B. Duoss, C. M. Spadaccini, C. M. Friend, J. Biener, *Sci. Adv.* **2018**, *4*, eaas9459.

[129] T. Duda, L. V. Raghavan, *IFAC-PapersOnLine* **2016**, *49*, 103.

[130] T. S. Cheng, M. Z. M. Nasir, A. Ambrosi, M. Pumera, *Appl. Mater. Today* **2017**, *9*, 212.

[131] Formlabs, 3D Printing Technology Comparison: FDM vs. SLA vs. SLS, https://formlabs.com/blog/fdm-vs-sla-vs-sls-how-to-choose-the-right-3d-printing-technology/, accessed July, 2022.

[132] Sculpteo, 3D Printing with DMLS and SLM Technologies, https://www.sculpteo.com/en/materials/dmls-material/#:~:text=DMLS. accessed July, 2022.

[133] C. L. Manzanares-Palenzuela, S. Hermanova, Z. Sofer, M. Pumera, *Nanoscale* **2019**, *11*, 12124.

[134] D. M. Wirth, M. J. Sheaff, J. V. Waldman, M. P. Symcox, H. D. Whitehead, J. D. Sharp, J. R. Doerfler, A. A. Lamar, G. Leblanc, *Anal. Chem.* **2019**, *91*, 5553.

[135] J. Muñoz, M. Pumera, *ChemElectroChem* **2020**, *7*, 3404.

[136] X. Su, X. Li, C. Y. A. Ong, T. S. Herng, Y. Wang, E. Peng, J. Ding, *Adv. Sci.* **2019**, *6*, 1801670.

[137] C. Iffelsberger, M. Pumera, *J. Mater. Chem. A* **2021**, *9*, 22072.

[138] W. Gao, J. Michalička, M. Pumera, *Small* **2022**, *18*, 2105572.

[139] R. M. Pasquarelli, D. S. Ginley, R. O'hayre, *Chem. Soc. Rev.* **2011**, *40*, 5406.

[140] X. Guo, H. Du, F. Qu, J. Li, *J. Mater. Chem. A* **2019**, *7*, 3531.

[141] A. R. Singh, B. A. Rohr, J. A. Schwalbe, M. Cargnello, K. Chan, T. F. Jaramillo, I. Chorkendorff, J. K. Nørskov, *ACS Catal.* **2017**, *7*, 706.

[142] Y. Ren, C. Yu, X. Tan, H. Huang, Q. Wei, J. Qiu, *Energy Environ. Sci.* **2021**, *14*, 1176.

[143] X. W. Lv, C. C. Weng, Z. Y. Yuan, *ChemSusChem* **2020**, *13*, 3061.

[144] J. Wang, S. Chen, Z. Li, G. Li, X. Liu, *ChemElectroChem* **2020**, *7*, 1067.

[145] D. Wang, L. M. Azofra, M. Harb, L. Cavallo, X. Zhang, B. H. R. Suryanto, D. R. MacFarlane, *ChemSusChem* **2018**, *11*, 3416.

[146] Y. Liu, Y. Su, X. Quan, X. Fan, S. Chen, H. Yu, H. Zhao, Y. Zhang, J. Zhao, *ACS Catal.* **2018**, *8*, 1186.

[147] J. Deng, C. Liu, *Chem* **2018**, *4*, 1773.

[148] M. Majumder, H. Saini, I. Dědek, A. Schneemann, N. R. Chodankar, V. Ramarao, M. S. Santosh, A. K. Nanjundan, Š. Kment, D. Dubal, M. Otyepka, R. Zbořil, K. Jayaramulu, *ACS Nano* **2021**, *15*, 17275.

[149] Y. X. Lin, S. N. Zhang, Z. H. Xue, J. J. Zhang, H. Su, T. J. Zhao, G. Y. Zhai, X. H. Li, M. Antonietti, J. S. Chen, *Nat. Commun.* **2019**, *10*, 4380.

[150] H. Hirakawa, M. Hashimoto, Y. Shiraishi, T. Hirai, *J. Am. Chem. Soc.* **2017**, *139*, 10929.

[151] S. X. Wang, H. Maimaiti, B. Xu, Y. Guo, P. S. Zhai, H. Z. Zhang, *J. Phys. Chem. C* **2019**, *123*, 31119.

[152] H. Ma, Z. Chen, Z. Wang, *Nanoscale* **2021**, *13*, 1717.

[153] W. Li, K. Li, Y. Ye, S. Zhang, Y. Liu, G. Wang, C. Liang, H. Zhang, H. Zhao, *Commun. Chem.* **2021**, *4*, 10.

[154] L. Zeng, S. Chen, J. Van Der Zalm, X. Li, A. Chen, *Chem. Commun.* **2019**, *55*, 7386.

[155] X. Chen, S. Zhang, X. Qian, Z. Liang, Y. Xue, X. Zhang, J. Tian, Y. Han, M. Shao, *Appl. Catal., B* **2022**, *310*, 121277.

### 5.3.2 3D-printing technology towards $CO_2$ reduction and capture

**Motivation**

Massive use of fossil fuels has led to severe increase in atmospheric $CO_2$ resulting in an increase in global temperature, disturbing the innate carbon cycle of the Earth, and the present climatic conditions. Thus, a comprehensive perspective on this topic would be interesting for researchers in analyzing the field better and think for better possibilities of mitigating $CO_2$ via 3D-printing technology.

**Objective**

The perspective article outlines multiple strategies of fabricating 3D-printed catalysts, and customized devices for mitigating $CO_2$ and converting them to various products.

**Outcome**

Several recent studies of employing 3D-printing technology for $CO_2$ reduction and capture are discussed. Since studies reported in this area are minimal, the following report would be helpful for researchers as a motivation to broaden this field of 3D-printing for $CO_2$ mitigation.

**Contribution**

Writing (original draft, review and editing).

**Article**

The article was published and the details of the article are as follows:

Akshay Kumar K. Padinjareveetil, Martin Pumera*, *Advances in Designing 3D-Printed Systems for CO₂ Reduction,* **Adv. Mater. Interfaces**, 2023 ,10, 8, 2201734. https://doi.org/10.1002/admi.202201734, (IF=6.38).

# Advances in Designing 3D-Printed Systems for CO₂ Reduction

*Akshay Kumar K. Padinjareveetil and Martin Pumera\**

The increasing level of atmospheric carbon dioxide (CO₂), and the resultant global warming is a matter of growing concern among scientists, environmentalists, and climate experts across the globe over the past several decades. Numerous attempts are being undertaken today that seek solutions to mitigate this global crisis. This includes designing functional catalysts, devices and reactors to convert greenhouse gasses such as CO₂ into useful products like low-carbon fuels and chemicals, thereby reducing the amount of CO₂ considerably in the atmosphere. Advancements in emerging technologies like 3D-printing can effectively aid in the fabrication of electrodes and devices to tackle the rising CO₂ concerns. Low cost, rapid prototyping ability, and printing simple and complex structure are few of the significant merits of this technology. Thus, in this perspective article, discussions on fabricating 3D-printed (electro)catalysts, customized devices, reactors, etc., via multiple strategies are put forward with emphasis on the electrochemical reduction of CO₂. Also, a detailed discussion on the post-printing treatments, catalyst modifications, and other CO₂ mitigation strategies is provided as well. Although studies in this direction are scarcely reported, observations made hitherto show promising possibilities of broadening this field for large scale CO₂ reduction reaction applications, and similar catalytic applications in the near future.

## 1. Introduction

Global energy shortage and climate crisis have rattled the world over, with scientists, researchers, and policymakers trying to cope with these unprecedented atrocities at multiple levels.

A. K. K. Padinjareveetil, M. Pumera
Future Energy and Innovation Laboratory
Central European Institute of Technology
Brno University of Technology
Purkyňova 123, Brno 61200, Czech Republic
E-mail: martin.pumera@ceitec.vutbr.cz
M. Pumera
Energy Research Institute@NTU (ERI@N)
Research Techno Plaza
X-Frontier Block, Level 5, 50 Nanyang Drive, Singapore 637553, Singapore
M. Pumera
New Technologies - Research Centre
University of West Bohemia
Univerzitní 8, Plzeň 30100, Czech Republic

Human-centric activities, like the massive use of fossil fuels, chiefly contribute to the rise of atmospheric carbon dioxide (CO₂) and continue to have a devastating impact on the global temperature rise, the innate carbon cycle of the Earth, and the present climatic conditions.[1,2] Statistically, global CO₂ emissions are expected to rise at an alarming rate,[3] especially with the ongoing combustion rate of fossil fuels. Thus, stringent measures have been developed today to control and mitigate this menace by using alternatives such as renewable and nuclear energy sources, and employing strategies like decarbonization, carbon sequestration, carbon recycling, etc.[4,5] However, a complete shift has not been achieved and the search for replacements and improvements to minimize the CO₂ emission into the atmosphere continues.

Among various CO₂ reduction strategies, electrochemical reduction or electrolysis of CO₂ is an important approach that involves the conversion of CO₂ to several value-added chemicals, making them impactful as industrial feedstocks, yielding value-added low-carbon fuels and chemicals.[6–8] The sp hybridized CO₂ molecules with linear geometry are chemically inert, stable, and possess low electron affinity with a large band gap of 13.7 eV between its lowest unoccupied molecular orbital and highest occupied molecular orbital.[9,10] Further, CO₂ reduction reactions (CO₂RR) are thermodynamically uphill reactions that require significantly high energy to break the C=O bond (750 kJ mol⁻¹), when compared to the breaking of C−O (327 kJ mol⁻¹), C−C (336 kJ mol⁻¹), and C−H (441 kJ mol⁻¹) bonds. In short, the concern regarding the rising concentration of CO₂ in the atmosphere today has prompted the expansion of technologies associated with CO₂RR with immediate impact.

Electrocatalytic conversion of CO₂ involves various reaction pathways that proceed via multi-proton and multi-electron transfer, resulting in diverse reaction products[11–16] such as carbon monoxide (syngas production; CO+H₂), formic acid (HCOOH), alcohols (methanol, ethanol, etc.), hydrocarbons (e.g., methane, ethane, ethylene, etc.), aldehyde, ketone, etc., which in turn aids in a significant reduction in the CO₂ amount. This technique has made significant advances in recent years with advantages that include, scalability, compatibility, ease in adaptability for practical purposes, and possibility of employing other renewable energy sources to drive the reaction at milder conditions.[12,17] Literature reveals that the experimental conditions, pathways, and products are controllable and tunable with parameters such as catalyst, electrolytes, applied

**ADVANCED
SCIENCE NEWS**
www.advancedsciencenews.com

**ADVANCED
MATERIALS
INTERFACES**
Open Access
www.advmatinterfaces.de

potentials, temperature, etc.[9,18] Several homogeneous and heterogeneous based catalysts for $CO_2RR$ have been fabricated hitherto and continue to be devised for accelerating the kinetically slow reduction reaction, owing to the high chemical and/or electrochemical stability of $CO_2$.[19,20]

The field however requires better and newer solutions to make this process impactful, scalable, and cost-effective in terms of catalyst design, devices, electrodes, reactors, cell configurations, etc. Also, newer strategies are proposed to address the limitations of conventional techniques such as complex fabrication processes, heat and mass transfer limitations, stability, uneven flows, poor surface area, etc. Further, designing complex reactors or cell configurations via traditional approaches is expensive, requires massive resources, and is time-consuming at an industrial scale. Subjecting the catalytically active materials to high temperatures can also result in the deformation of catalysts with random size, shape, and porosity. These concerns increase the urgency for simple and flexible techniques that help in designing highly engineered functional structures for $CO_2RR$ that inevitably reduces $CO_2$ at a high rate.

Interestingly, emerging technologies like 3D-printing, also known as "additive manufacturing", are expected to offer a possible remedy for device fabrication towards $CO_2RR$, recognizing the difficulties and tedious efforts involved in the traditional methods.[21–23] This technology today provides significant opportunities towards rapid prototyping of electrodes and devices with better control of geometry and distribution, printing monolith structures, functional catalysts, integrated devices, and beyond. Though its initial applications were limited to creating prototypes, currently its possibilities have expanded to scientific and industry-level usages based across regions. Some of the notable features of this technique include its quick prototyping ability, scalability, replicability, flexibility in designing both simple and complex structures, and minimal waste generation.[24,25] The ability of 3D-printing technologies to fabricate conductive electrodes and/or substrates in minimal time with definite geometry and rigidity, cost-effectiveness, scalability, performance, and all-pervasive nature, has encouraged the research community to employ them for electrochemical energy conversion and storage applications.[21,26–28]

Recent studies on using 3D-printing technology for $CO_2RR$ are known to be, a highly promising approach for fabricating devices and active structures. The 3D-printed porous structures are expected to enhance the mass transport property and shorten the ion and electron pathway by retaining the large active area[29,30] overpowering the 2D nanostructures. They also provide a high degree of control over geometry, and material distribution and are also ideal for immobilization of the active material. This technology can also aid in the fabrication of highly efficient catalytic reactors, where it gives the freedom to directly load the catalyst over the 3D-printed reactor surface, eventually increasing the contact between the reactant and the catalyst. Also, the significance of metal electrodes for $CO_2RR$ has been well investigated since the mid-1980s,[31] which can be adapted today for the direct fabrication of 3D-printed metal substrates of choice via various 3D-printing techniques.[32,33] Advancements in the field of 3D-printing today equips the user with the possibility of direct 3D-printing of 2D materials as well.[34,35] Thus, the fundamental objective lies in selecting

appropriate precursor materials and printing techniques to fabricate the 3D-printed structures based on intended applications. Further, 3D-printing helps in rapid prototyping of complex geometric objects with great accuracy wherein such optimizations would be a foundation to develop catalysts delivering efficient performance. Interestingly, advancements in 3D-printing technology are also utilized to fabricate devices and electrode materials beyond electrochemical reduction of $CO_2$ for Fischer–Tropsch synthesis, $CO_2$ hydrogenation, $CO_2$ reforming of $CH_4$,[32] $CO_2$ capture,[36] separation, etc. Being an emerging field, discussions on the same are also carried out in subsequent sections.

In short, this perspective article discusses the large-scale possibilities of 3D-printing technology in fabricating devices and electrode materials for efficient $CO_2RR$, along with multiple strategies to decrease the $CO_2$ concentration, their technical difficulties, solution, and a future outlook. Systematic analysis can efficiently aid in understanding the potential of this field and is expected to contribute towards mitigating the ongoing challenges of climate change and the energy crisis faced by the global community to some extent.

## 2. Understanding $CO_2RR$ and Catalysts

Electrochemical reduction of $CO_2$ ($ERCO_2$) outweighs other technologies, owing to its mild operational conditions, in terms of temperature and pressure, and controllable reaction conditions. Further, this technique is economical and ecologically feasible together with renewable energy sources.[4,9,12,37] However, it still requires enhancement in terms of finding electrocatalysts that lower the overpotential for dissociation of the C=O bond and eventually accelerate reactions and enhance the product selectivity. The general expression for cathodic $ERCO_2$ is given by

$$xCO_2 + nH^+ + ne^- \rightarrow product + yH_2O \tag{1}$$
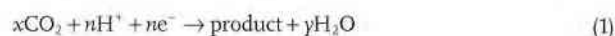
Studies on $ERCO_2$ are speculated to have evolved during the 1950s.[38] A significant leap in this direction, however, was made in 1985 by Yoshio Hori et al.,[31] who conducted a total analysis of gaseous and liquid products on cathodic $CO_2RR$ using various metal electrodes. Further, several other studies have been undertaken periodically on designing electrocatalysts for $CO_2RR$. This includes copper (Cu),[4,16,39] noble metal catalysts such as silver (Ag) and gold (Au),[40] transition metal-based catalysts,[41] carbon-supported catalysts,[42] hybrid catalysts,[43] metal-free catalysts,[44] etc., thus substantiating the vast possibilities of fabricating structures for this application. Also, the design of experimental cells or electrolyzers for $CO_2RR$ has undergone improvements from time to time. A schematic representation of various reactor designs for $CO_2RR$ is given in **Figure 1**, constituting H-cell (Figure 1A), proton exchange membranes (PEM) fuel cell (Figure 1B), gas diffusion electrode (GDE) flow cell (Figure 1C), and microfluidic flow cell (Figure 1D).[45]

Typically, at the laboratory scale, two-compartment cells called H-cell are employed with three electrode configurations constituting a working electrode, reference electrode, and

**ADVANCED
SCIENCE NEWS**
www.advancedsciencenews.com

**ADVANCED
MATERIALS
INTERFACES**
Open Access
www.advmatinterfaces.de
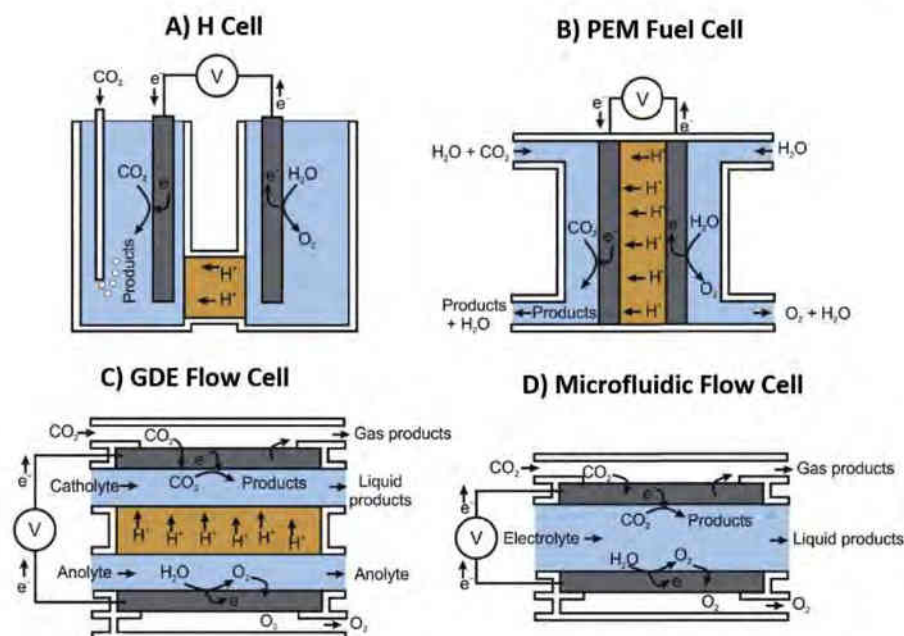
**Figure 1.** Schematic designs of reactors employed for $CO_2RR$. Adapted with permission.[45] Copyright 2020, Elsevier.

counter electrode.[9,46] The two compartments are separated either by a proton-conducting membrane such as Nafion 117 or by using an anion-exchange polymer membrane. The major advantage of this electrochemical setup is that they permit ionic conductivity and mitigate the movement of products from the cathodic to the anodic compartment. Further, the easiness of adapting to different electrode materials and operating conditions makes them promising.

However, due to the low solubility of $CO_2$ in the electrolyte, H cells encounter mass transportation limitations which call for newer designs, such as the continuous flow cells. For instance, microfluidic flow cells[9,47,48] are employed in $CO_2RR$ wherein the electrodes are separated by a flowing liquid electrolyte, and the electrodes are separated by a thin spacer. Further, the performance of the system can be analyzed using an external reference electrode. Catalyst immobilization has also gained attention towards $CO_2RR$ wherein the prepared catalysts are transferred to porous substrates, such as a gas diffusion layer (GDL) or a membrane to form membrane electrode assembly,[47] using techniques such as airbrush, painting, etc. Strategies such as catalyst immobilization over substrates are crucial for ideal measurements and product determinations since non-uniform coatings and distributions can lead to deviations and affect the stability and performance of the studied system. Fluoropolymers such as polytetrafluoroethylene (PTFE) coated carbon paper substrates with microporous layers, and fibrous expanded PTFE are commercially available GDL.[49,50] The hydrophobic nature of these polymers makes them ideal for the $CO_2RR$. Although conventional approaches are still in currency, researchers are working arduously towards finding the best experimental setup and conditions for $CO_2RR$. Quantification of products is carried out as part of the experimentation, using mass spectrometer, ion, or gas chromatography

technique, NMR, etc. Further, the performance of the catalytic reactions is evaluated using a set of parameters such as onset potential, faradaic efficiency (FE), catalytic current density, energetic efficiency (EE), voltage efficiency, overpotential, turnover frequency (TOF), Tafel plot, etc.[20,51] Theoretical studies such as density functional theory (DFT) also have been carried out to substantiate the experimental results. In principle, the results from both theoretical and experimental studies are evaluated systematically to track the reaction mechanism pathways, intermediates, and respective products.

$CO_2RR$ is a complicated process owing to the fact that the carbon atoms in $CO_2$ molecules are inert, thermodynamically stable, and in a high oxidation state. Thus, designing and fabricating devices and electrode materials that overcome the kinetically sluggish $CO_2RR$, is necessary prior to its commercialization for multiple applications as shown in **Figure 2**.

Further, studies towards employing electroactive materials to design newer catalysts, possessing high activity, selectivity, durability, and low overpotentials are being rapidly undertaken today to tackle the increasing $CO_2$ level in the atmosphere. $ERCO_2$ involves protons coupled with multi-electron transfer in an aqueous system with ideal electrocatalysts.[51,53] Based on the number of electrons involved, protons transferred, and pH, several products could be procured such as $HCOOH$, $CO$, $CH_3OH$, $CH_4$, $C_2H_4$, $C_2H_5OH$, $C_3H_7OH$, $C_3H_7O_2$, $C_4H_4O_3$, etc.

To substantiate this, the electrochemical half-reaction for $ERCO_2$ through different electron pathways has been given below, where the corresponding electrode potential versus standard hydrogen electrode (SHE) in aqueous electrolyte is shown in **Table 1**.[12]

In short, factors such as electrocatalysts (composition, morphology, structure), electrolyte (pH, concentration), electrode potential, temperature, pressure, cell design, etc. play a crucial

**ADVANCED
SCIENCE NEWS**
www.advancedsciencenews.com

**ADVANCED
MATERIALS
INTERFACES**
Open Access
www.advmatinterfaces.de
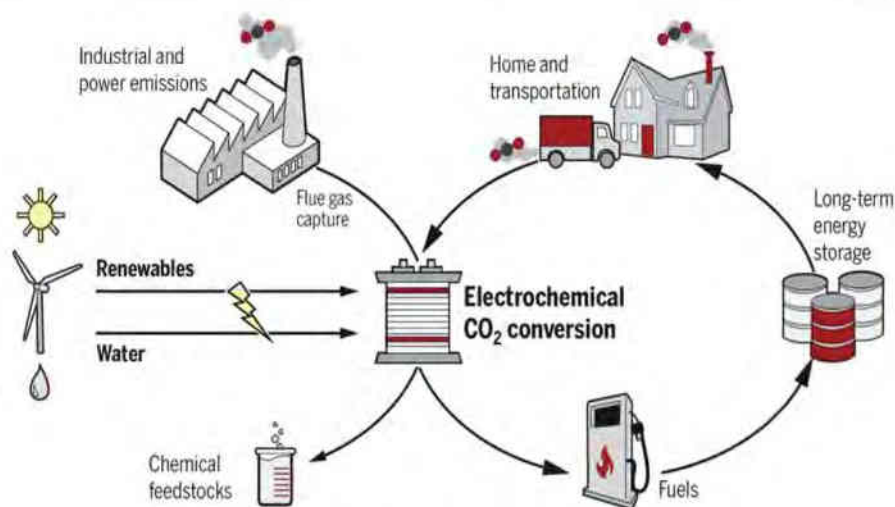
**Figure 2.** Schematic representation of ERCO$_2$ towards multiple applications. Reproduced with permission.[52] Copyright 2019, The American Association for the Advancement of Science.

role in ERCO$_2$. Discussions on detailed CO$_2$RR pathways for several systems are available in the literature,[54–56] however, they are beyond the scope of this perspective.

Realizing the importance of fabricating electrocatalysts with enhanced performance for CO$_2$RR experiments, several catalysts have been developed periodically and studied systematically. Some of these are discussed below. Multiple reports in the literature suggest using Cu catalysts for CO$_2$RR on account of its distinct characteristics, abundance, and cost-effectiveness.[4,7,57] Cu catalyst was also successful in exhibiting the two-electron reduction of CO$_2$ to CO along with its multi-electron reduction, delivering a variety of products (> 2e$^-$ products) that exhibited substantial FE and better performance, making this catalyst unique and high in demand. Further, in a study by M. J Sun et al.,[58] carbon-embedded diatomic nickel (Ni) electrocatalyst was used for the reduction of CO$_2$, and in another study brass and bronze were found to be effective as CO$_2$ reduction electrocatalysts.[59] A bimetallic electrocatalyst fabricated via chronoamperometric electrodeposition of cuprous oxide and Ni over carbon substrate was proposed by H Pan et al., wherein formate and CO were the major products of CO$_2$RR delivering FEs of 16.0% and 19.7%, respectively.[60] Interestingly, 2D materials, such as graphene-based structures,[61] MXenes,[62] transition metal chalcogenides (TMDs),[63] etc., have also gained significant importance for CO$_2$RR. With carbon in pristine graphene and graphene oxide being inactive for CO$_2$RR, modifications of graphene substrates using heteroatom doping, surface engineering, and/or by developing composites are known strategies employed for enhancing the efficiency of graphene-based catalysts for CO$_2$RR.[61] Further, CO$_2$RR experiments using Mo$_2$C catalyst showed an FE and overpotential around 90% and 250 mV, respectively, whereas for Ti$_3$C$_2$ MXenes they remained at 65% and 650 mV, respectively.[64] Studies on metal electrodes have also resulted in the classification of catalysts based on their ability to deliver respective products.[4,65–69] Carbon monoxide (CO) was produced using metal catalysts of Au, Ag, Zn, Pd, and Ga, and formate (HCOO$^-$)

was procured using Pb, Hg, Tl, In, Sn, Cd, and Bi. Surprisingly, Ni, Fe, Pt, and Ti contributed more toward reducing water to H$_2$ than reducing CO$_2$. Cu, on the other hand, gave multiple products such as hydrocarbons, aldehydes, and alcohols. The above reports can be adequately adapted to design 3D-printed substrates; however, this requires prior familiarization with 3D-printing techniques and strategies used to 3D-print devices and electrode substrates.

**Table 1.** Electrode potentials associated with electrochemical reduction of CO$_2$ and possible products. Adapted with permission.[12] Copyright 2017, The Authors, Published by WILEY-VCH Verlag GmbH & Co. KGaA, Weinheim.

| Electrochemical CO$_2$ reduction (possible half-reactions) | Electrode potentials (V vs SHE) at pH 7 |
|---|---|
| CO$_2$ (g) + e$^-$ → *COO$^-$ | −1.90 |
| CO$_2$ (g) + 2H$^+$ + 2e$^-$ → HCOOH (l) | −0.61 |
| CO$_2$ (g) + H$_2$O (l) + 2e$^-$ → HCOO$^-$ (aq) + OH$^-$ | −0.43 |
| CO$_2$ (g) + 2H$^+$ + 2e$^-$ → CO (g) + H$_2$O (l) | −0.53 |
| CO$_2$ (g) + H$_2$O (l) + 2e$^-$ → CO (g) + 2OH$^-$ | −0.52 |
| CO$_2$ (g) + 4H$^+$ + 2e$^-$ → HCHO (l) + H$_2$O (l) | −0.48 |
| CO$_2$ (g) + 3H$_2$O (l) + 4e$^-$ → HCHO (l) + 4OH$^-$ | −0.89 |
| CO$_2$ (g) + 6H$^+$ (l) + 6e$^-$ → CH$_3$OH (l) + H$_2$O (l) | −0.38 |
| CO$_2$ (g) + 5H$_2$O (l) + 6e$^-$ → CH$_3$OH (l) + 6OH$^-$ | −0.81 |
| CO$_2$ (g) + 8H$^+$ + 8e$^-$ → CH$_4$ (g) + 2H$_2$O (l) | −0.24 |
| CO$_2$ (g) + 6H$_2$O (l) + 8e$^-$ → CH$_4$ (g) + 8OH$^-$ | −0.25 |
| 2CO$_2$ (g) + 12H$^+$ + 12e$^-$ → C$_2$H$_4$ (g) + 4H$_2$O (l) | 0.06 |
| 2CO$_2$ (g) + 8H$_2$O (l) + 12e$^-$ → C$_2$H$_4$ (g) + 12OH$^-$ | −0.34 |
| 2CO$_2$ (g) + 12H$^+$ + 12e$^-$ → CH$_3$CH$_2$OH (l) + 3H$_2$O (l) | 0.08 |
| 2CO$_2$ (g) + 9H$_2$O (l) + 12e$^-$ → CH$_3$CH$_2$OH (l) + 12OH$^-$ (l) | −0.33 |

**ADVANCED
SCIENCE NEWS**
www.advancedsciencenews.com

**ADVANCED
MATERIALS
INTERFACES**
www.advmatinterfaces.de

## 3. 3D-Printing Overview

3D-printing is a bottom-up manufacturing approach that has created revolutionary changes in recent years with its multidimensional possibilities, ranging from scientific advancement to industrial and domestic applications.[21–23,70,71] Developed in the 1980s,[72] the technology has undergone periodic changes to incorporate unique features in designing and printing customized products. Further, the technology has undergone consistent advancement with respect to the principle involved in printing, precursor material, minimizing cost, time, complexity, and targeted applications based on the user's demand. Some commonly recognized and relevant printing techniques will be discussed in detail in the following section, as understanding the fundamental principle of this technology would be required in order to further exploit the possibilities of this domain towards $CO_2RR$.

### 3.1. Fused Deposition Modeling (FDM)

FDM, also known as "fused filament fabrication" (FFF), is an extrusion-based 3D-printing technique where a layer-by-layer deposition of material is carried out by melting the filaments at the hot zone of the nozzle, based on a predesigned model as dictated by the G code file (**Figure 3**a).[73] Some of the well-known precursor materials include graphene/ polylactic acid (PLA) filaments (black magic),[28] carbon black/PLA filaments

(protopasta),[74] metal/PLA filaments[75] (where metal = copper, titanium, stainless steel, brass, etc.), PLA, acrylonitrile butadiene styrene (ABS), polyurethane, polycarbonate (PC), polyamide, etc. Of these precursor materials available, extensive studies have been carried out on graphene/PLA and metal/PLA filaments to fabricate conductive electrode substrates for catalysis[26,28] and other applications.[76–79] Recently, metal-based FDM 3D-printing has become a promising platform that enables quick and easy fabrication of cheap, robust, and conductive metal substrates. Thus, the FDM printing technique has gained significant attention owing to its easiness, compatibility, cost-effectiveness, and varied choice of printable materials such as metal-based, carbon-based, customized 2D material filaments, etc.

### 3.2. Direct Ink Writing (DIW)

It is another well-known extrusion-based AM technique that enables the user to 3D-print any material of interest until the ink meets the required rheological properties for ideal extrusion (Figure 3b).[34,80,81] Here the active material in liquid-phase is typically referred to as "ink", which is dispensed out of the nozzle sequentially to procure a final solid conductive 3D-printed structure. Optimizing the printable inks is a major task prior to 3D-printing to prevent clogging or bad printing, wherein electrochemically active materials, along with additives, binders, solvents, etc. may be added additionally to improve the property of ink. Thus, this printing technology
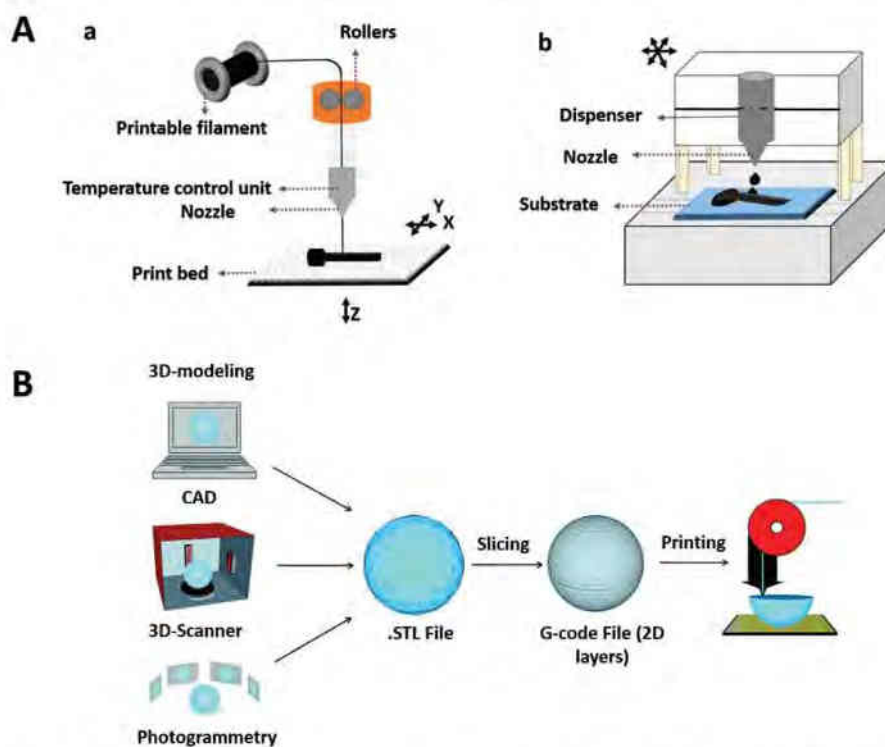


**Figure 3.** A) Schematic representation of 3D-printing techniques: a) Fused deposition modeling (FDM), b) direct ink writing (DIW). B) Procedure involved in the design and fabrication of a 3D-printed structure. Adapted with permission.[25] Copyright 2016, Royal Society of Chemistry.

**ADVANCED
SCIENCE NEWS**
www.advancedsciencenews.com

**ADVANCED
MATERIALS
INTERFACES**
Open Access
www.advmatinterfaces.de

has gained attention in the recent past owing to its ability to 3D-print a wide variety of materials that are not technically feasible using the FDM technique.

### 3.3. Stereolithography (SLA)

This 3D-printing technique is based on solidifying a liquid photopolymer (resin) using light sources such as UV light.[21,22,82] In this technique, exposure to resin with specific wavelengths of light can result in crosslinking of short molecular chains, and eventually polymerizing monomers and oligomers into robust and flexible structures. This technique enables advancement in speed, is versatile, and less expensive, along with providing flexibility with adequate precision of printed structures. Digital light processing (DLP)[22,83] is also a well-known technique similar to SLA, where photopolymer resin is solidified using a digital light source to obtain 3D-printed photopolymer parts and is relatively faster than the SLA technique.

### 3.4. Other 3D-Printing Techniques

Selective laser sintering (SLS) is an AM technology that employs a powder bed and a high-power laser source to sinter polymeric or metal powder into a 3D solid structure.[22,84,85] Fabricating complex geometries with high resolution and high productivity is an added advantage of this technique, although expensive equipment and high maintenance costs can be considered as a limitation. Also, the SLS printed parts have strong mechanical characteristics which are similar to the ones fabricated via the injection molding technique. On the contrary, selective laser melting (SLM)[82,85] is a 3D-printing technique where the laser is used to fuse the metal powders and fabricate objects in a layer-by-layer manner. The precursor metal powder is often heated during the process until the melting point is reached. The final 3D-printed parts are usually conductive metals and/or metal alloys, and the melting of powder beds is employed in this technique. Further, another rapid 3D printing called electron beam melting (EBM)[85] is found to be efficient for designing 3D-printed structures, wherein fully dense 3D structures are printed directly from the metal powder in a high vacuum using a computer-controlled electron gun. In techniques such as direct metal laser sintering (DMLS),[86] sintering of the metal powder particles is carried out using a laser source and then transported to an inert gas-filled chamber and fused together. The process of 3D-printing such structures makes use of several metal alloys of different melting points. Thus, several possibilities could be adopted to design and successfully fabricate 3D-printed structures for $CO_2RR$.

Achieving the final 3D-printed electrode substrate involves a series of steps, which is initiated by designing 3D structures using computer-aided design (CAD) software, 3D-scanner, or photogrammetry (Figure 3B).[22,25] Later, the design containing the STL file is sliced into a G code file using appropriate software that contains commands and geometrical information about the designed structure. Finally, the G code file is fed into the 3D-printer to procure the final 3D-printed structure.

Successful 3D-printed structures undergo certain post-printing treatments based on the 3D-printing technique employed, in order to make the final 3D-printed parts ideal for desired applications. A detailed discussion of these improvements on printed substrates has been carried out in Section 4.5.

3D-printing technology has shown exceptional advancement in several domains, with its major potential in recent years being the fabrication of electrochemical devices and cells for electrochemical applications. For instance, there are several existing reports available on using 3D-printed electrode substrates for catalysis applications through modifications, patterning, functionalization, or by integrating active materials for hydrogen evolution reaction (HER)[28,87–90] and oxygen evolution reactions (OER).[89–91] With the advancements in technology, rapid prototyping of 3D-printed substrates of specific geometry and composition can aid in successful 3D-printing of active structures beyond catalyst.

## 4. 3D-Printed Structures towards $CO_2RR$

3D-printed devices and electrodes for energy storage and conversion applications have received massive attention in the recent past owing to its ease in designing, printing, and testing compared to conventional techniques. Discussions on the potential strategies to mitigate the increasing level of $CO_2$ in the atmosphere, along with various 3D-printing strategies for device fabrication have been carried out in previous sections. In the following sections, we discuss certain studies that have already explored the potential of 3D-printed substrates for ERCO₂. Interestingly, there are still ample other unexplored electroactive materials that, if ideally researched, can build a good foundation for employing this technology for $CO_2RR$. With the advancement in 3D-printing technologies in recent times, we attempt to put forth our observation on bridging the two domains (**Scheme 1**) in the following sections, as an in-depth analysis of these disciplines could be impactful for designing newer materials that can resolve the ongoing energy crisis and control $CO_2$ emissions.

### 4.1. Geometry, Porosity, Size, and Electrolyte

3D-printed structures are generally in the order of μm resolution, wherein the thickness of the layer is in the order of 50–300 μm for FDM and DIW, while it is 1–50 μm for SLA and DLP, and 20–150 μm for SLS, SLM, and EBM techniques.[21,92] Interestingly, employing appropriate post-processing techniques can render these 3D-printed structures potentially active for desired catalytic applications such as $CO_2RR$. For instance, nanostructuring of these printed electrodes can enhance the porosity of the printed substrates delivering nm features, thus enhancing the catalytic activity predominantly. Surface patterning and activation techniques can be further employed towards enhancing the surface area. A detailed discussion is carried out in Section 4.5.

Further, the geometry of electrodes is a very crucial step from the catalysis point of view, as unoptimized electrode geometry can result in passivation of the electrode surface,
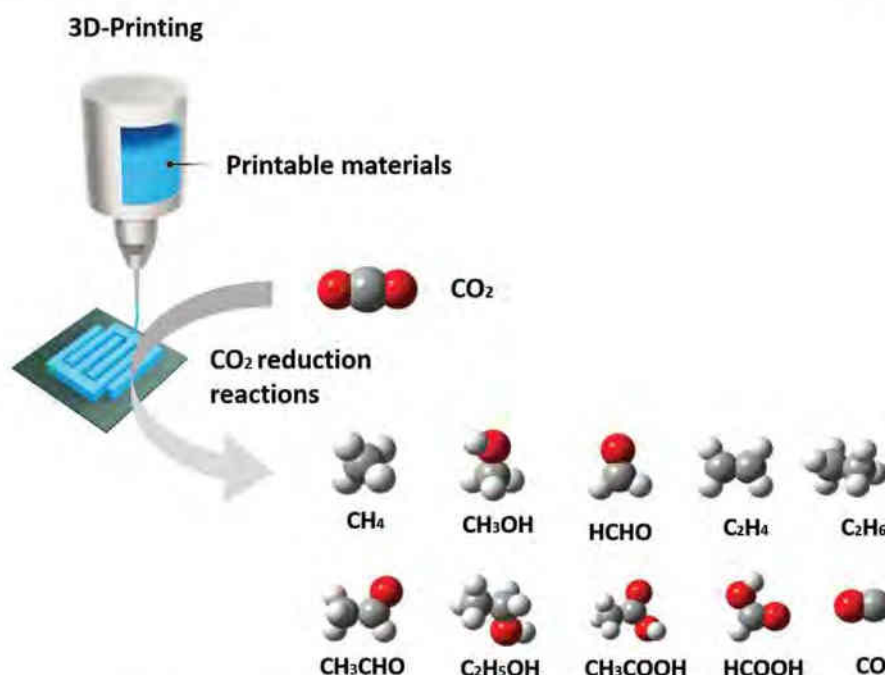
**3D-Printing**



**Scheme 1.** Schematic representation of $CO_2$ mitigation strategies via 3D-printing technology.

and may seemingly look inactive for catalytic applications.[21] Thus, one of the significant merits of 3D-printing technology is its ability to rapidly prototype electrode designs of diverse geometrical shapes such as honeycomb monoliths structure, porous lattice structures, fractal structures, etc., based on the experimental conditions that are often hard to be realized with traditional fabrication techniques. Further, the geometry of the printed structures can be controlled using parameters such as nozzle diameter, extrusion speed, viscosity of active material, etc. Engineering of catalyst structure via 3D-printing can enhance reaction conditions, deliver targeted products, provide long-term stability, and multiple other advantages. For instance, in a study by Yan et al., 3D hierarchically porous (hp) CuAg catalyst was fabricated via SLM 3D-printing technique, followed by an electrochemical dealloying approach (**Figure** 4A).[29] Importantly, catalysts of varying porosity and geometric configurations were fabricated, namely 3D hp CuAg (honeycomb) and 3D hp CuAg (rod). Figure 4B shows the 3D-printed bulk metallic glass honeycomb component. It was found that the 3D hp CuAg (honeycomb) gave a syngas production rate of 142 µmol cm$^{-2}$ h$^{-1}$ and stability of 136 h, while 3D hp CuAg (rod) gave around 85.78 µmol cm$^{-2}$ h$^{-1}$ and 40 h, respectively. Studies were also carried out on 2D nanoporous CuAg catalysts which exhibited low electrochemical stability of about 12 h. Thus the following studies clearly reveal the importance of catalyst structure and morphology in catalysis.

In another interesting study, 3D-printed electrodes from PLA-carbon nanotube (PLA-CNT) composite were electroplated with Cu and employed for ERCO$_2$.[93] Figure 4C shows scanning electron microscopy (SEM) image of the surface of 3D-printed PLA-CNT with randomly located Cu microparticles.

Upon evaluating hundreds of Cu microparticles, the average microparticle diameter was found to be in the range of 21 ± 5 µm. Further, detailed morphology and shape of microparticles were evaluated by transferring to an aluminum (Al) target, wherein the microparticle was found to have a hemispherical shape, and higher magnification showed that the crystals were in the order of 5–10 µm (Figure 4D). The electrodes were also further subjected to other characterization techniques and eventually evaluated for ERCO$_2$. Such electrode modification approaches are interesting for the fabrication of low-cost, facile 3D-printed substrates for CO$_2$RRs and beyond.

Advancements in printing technology have also aided the fabrication of porous electrodes and/or substrates that eventually help in improved mass transport properties. Gas diffusion electrodes (GDEs) are procured by employing active electrocatalysts on hydrophobic and porous substrates, and such strategies are crucial for the efficient transport of CO$_2$ to the local reaction environment. In a recent study by Wicks et al., 3D-printing was employed towards the fabrication of fluoropolymer GDL with tunable microporosity and structure and was further spray-coated with electrocatalytically active Cu nanoparticles (NP).[49] The influence of parameters such as porosity, micro/macro structures, and eventually their efficiency and selectivity for CO$_2$RR are investigated in the current study. Figure 4E represents the image of the 3D-printed GDL of homogeneous perfluoropolyether with a pyramid height of 1.6 mm tall represented as H-Δ-PFPE-1.6. The SEM image of the GDL and Cu catalyst layer interface of H-Δ-PFPE is shown in Figure 4F. Studies on varying heights and configurations of samples were evaluated, and a relative increase in C$_{2+}$ products was seen with increase in pyramid height. This accounts for the increasing

**ADVANCED
SCIENCE NEWS**
www.advancedsciencenews.com

**ADVANCED
MATERIALS
INTERFACES**
Open Access
www.advmatinterfaces.de
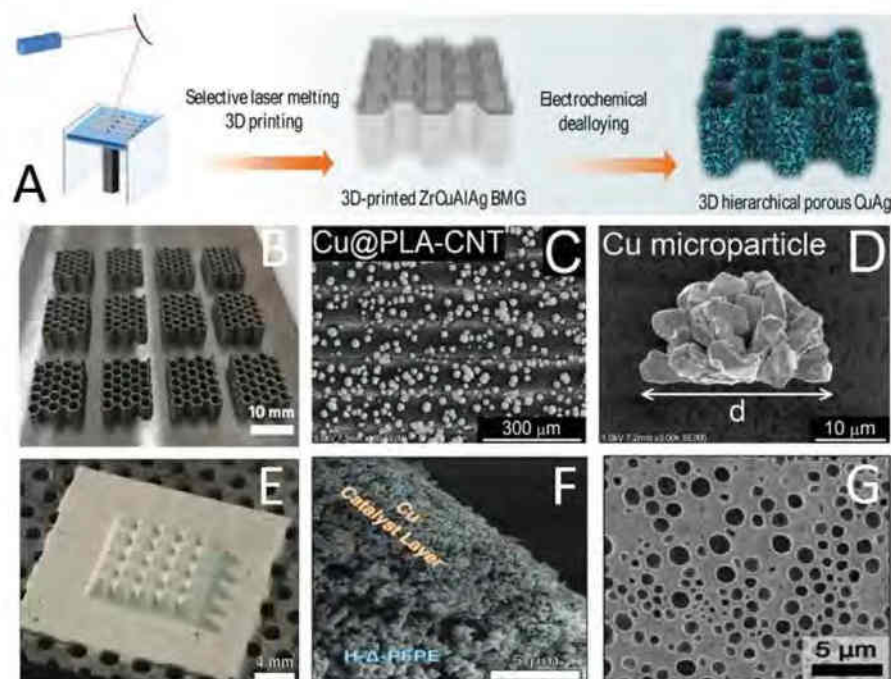
**Figure 4.** A) Schematic representation of 3D hp CuAg catalyst fabrication. B) 3D-printed bulk metallic glass honeycomb components. Figures (A,B) Adapted with permission.[29] Copyright 2021, American Chemical Society. C) Copper electroplated PLA-CNT electrode D) SEM image of Cu microparticle transferred to Al target. Figures (C,D) Adapted with permission.[93] Copyright 2021, Wiley-VCH GmbH. E) 3D-printed ternary GDL of H-Δ-PFPE-1.6. F) GDL:catalyst layer interface of H-Δ-PFPE macrostructure. G) Surface Morphology of LP-PFPE structure (Top view). Figures (E–G) Adapted with permission.[49] Copyright 2021, Wiley-VCH GmbH.

interfacial area between the GDL and Cu catalyst layers. Also, employing a higher intensity UV light, resulted in a large pore perfluoropolyether (LP-PFPE) possessing a different surface morphology and an SEM image is given in Figure 4G. Furthermore, variation in the surface morphologies of the catalyst along with increasing diffusive path length and residence time of the locally generated CO near the catalyst resulted in a shift in the product selectivity towards $C_{2+}$ products.

Thus, factors such as geometry, size, and porosity can influence catalytic reactions, making these parameters vital for fabrication and designing. In short, 3D-printing technology allows the fabrication of electrodes with definite geometry, which could otherwise be time-consuming using traditional techniques such as subtractive manufacturing, along with excessive resource wastage. Hence, 3D-printing shows enormous versatility in fabricating complex geometric structures, making it highly suitable over conventional methods.

Electrolytes also play a crucial role in $ERCO_2$, wherein they provide a medium to transfer coupled protons and electrons based on reaction parameters. $ERCO_2$ experiments are carried out in the electrolyte solutions of $KHCO_3$, KOH,[94] etc., based on the experimental conditions and anticipated products. Typically, the pH of electrolyte solutions is in the range of neutral (6.8) to basic. In the context of 3D-printing, the 3D-printed electrodes are ideal for their use in the following pH conditions as electrocatalytic experiments were reported in electrolytes of $KHCO_3$,[93] KOH,[89,91] etc.

## 4.2. Metal-based 3D-Printing

In an interesting study, SLM 3D-printing technique followed by an electrochemical dealloying approach was employed for the fabrication of 3D hp CuAg bimetallic catalyst for syngas production.[29] Catalyst morphology-based discussions were carried out in the previous section and a broader understanding of the electrochemical performance is carried out further. As part of the experimentation, the $CO_2RR$ of 3D hp CuAg rod and 3D hp Cu catalysts were carried out in an H cell containing $CO_2$-saturated 0.1 M $KHCO_3$ solution (pH = 6.8) and compared. Linear sweep voltammetric (LSV) measurements of 3D hp CuAg and 3D hp Cu catalysts were carried out as shown in **Figure 5**A. It was observed that 3D hp CuAg showed a higher current density when compared to 3D hp Cu, indicating a higher $CO_2RR$ activity of the former catalyst. Also, the onset potential for initial CO generation of the 3D hp CuAg catalyst was −0.495 V, which was about 158 mV lower than the 3D hp Cu catalyst.

Further, the FE of both the catalysts towards CO ($FE_{CO}$) and syngas ($FE_{syngas}$) was determined as shown in Figure 5B. It was found that 3D hp CuAg gave high $FE_{syngas}$ of above 92% (−0.8 to −1.0 V) and $FE_{CO}$ of 63.2% at −0.9 V, which are higher when compared to 3D hp Cu, clearly indicating the importance of Ag in enhancing $CO_2$ to CO conversion. Interestingly, the 3D hp CuAg catalyst showed a wide and tunable syngas ($H_2$/CO) ratio from 3:1 to 1:2 by varying applied potential. Also, Ag being the active site for CO generation, varying the Cu/Ag

**ADVANCED
SCIENCE NEWS**
www.advancedsciencenews.com

**ADVANCED
MATERIALS
INTERFACES**
www.advmatinterfaces.de

ratio in the resultant 3D hp CuAg catalysts can widen the range of syngas ratio. Further, total production rates of syngas linearly increase with the increasing applied potential for both 3D hp CuAg and 3D hp Cu, however, the former depicted a higher rate at each potential (Figure 5C). Interestingly, millimeter-level porosity was introduced into the 3D hp CuAg catalyst via SLM 3D-printing technique and evaluated for $CO_2RR$, wherein the catalyst showed milli-micro-nano porous configurations. Figure 5D shows the syngas production of the 3D hp CuAg (honeycomb) structure. It was observed that the overall production rate of syngas was around 5.7 mmol cm$^{-2}$ for the 3D hp CuAg (honeycomb) catalyst after 40 h continuous electrocatalysis, which is about 1.8 times higher than that of the 3D hp CuAg rod (Figure 5E). The syngas production rate and electrochemical stability of these catalysts were already discussed in the previous section. Thus, excellent electrochemical stability was shown by 3D hp CuAg honeycomb electrode structure, and morphological analysis using SEM and XRD confirmed that the nanoporous morphology and phases remain unaltered after employing them for about 140 h of continuous reaction. A comparison plot of $CO_2RR$ of noble, non-noble based catalyst along with 3D hp CuAg rod and 3D hp CuAg honeycomb is given in Figure 5F, wherein the 3D hp CuAg catalyst exhibited an excellent blend of long-term electrochemical stability and syngas gas production rate, making 3D-printed approach of catalyst fabrication highly promising. A schematic overview of the proposed mechanism of 3D np CuAg catalysts is given in Figure 5G, wherein phase-separated CuAg nanodomains deliver tunable syngas ratio and activity, while ultra-high electrochemical stability ascribes to its three-level milli/micro/nano hp structures.

### 4.3. Extrusion-based Printing

#### 4.3.1. Metal/Polymer

With recent progress in technology, FDM-based metal filaments for extrusion are available in the print hubs that help in the direct 3D-printing of metal electrode substrates.[33,76] This includes metal/PLA filaments of Cu, titanium (Ti), tungsten, brass, stainless steel (SS), and Al (Figure 6A). 3D-printing of metal/PLA filaments based on the predesigned geometry and size, followed by appropriate post-printing treatments can render them as active electrode substrate for $CO_2RR$. Thus, this approach can also serve as a possible alternative to the costly SLM technique, once the potential of FDM-based metal 3D-printing is realized. 3D-printed Cu/PLA electrodes fabricated via this approach were previously reported by our group for energy conversion[33] and sensing applications.[75]

Since extensive research is carried out on Cu-based materials for $CO_2RR$ in literature,[4,57] we emphasize on the potential of 3D-printing Cu filaments via FDM that can be employed for similar catalytic applications such as $CO_2RR$. At the laboratory scale, the Original Prusa i3 MK3S+ FDM 3D-printer (Figure 6B) can be employed for 3D-printing of Cu/PLA metal filament via extrusion technique as shown in Figure 6C. Sintering of 3D-printed Cu/PLA electrodes can increase the contact between metal NPs within the substrate and also remove

the non-conductive PLA polymer parts, resulting in a conductive metal substrate.[75,95]

Further, the Cu fillers in these 3D-printed substrates, upon sintering, can result in a highly conductive and robust 3D Cu metal substrate. Thus, FDM based technique of designing 3D-printed Cu and other metal electrode substrates can be considered as an interesting, feasible, yet unexplored approach to fabricate active electrode substrates for $CO_2RR$, in comparison to other conventional, tedious, and time-consuming techniques.

#### 4.3.2. Carbon/Polymer

Pristine carbon-based materials are generally found to be inert towards $CO_2RR$. However, studies have shown that approaches such as heteroatom doping, functionalization, and patterning of carbon substrates can facilitate them as active substrates for desired applications.[73,96] Also, there are reports on graphene-based materials for $CO_2RR$.[97,98] In a study by Ma et al.,[99] three different electrode structures were designed and sequentially studied for $CO_2RR$. Hence, the task relies on finding appropriate modification techniques for the fabrication of 3D-printed carbon-based substrates for desired applications.

Interestingly, the availability of graphene-printable filaments for 3D-printing expands its possibility of fabricating carbon-based substrates for multiple applications.[73,87] Introducing conductive nanoallotropes like graphene, along with thermoplastic polymers like PLA or ABS are known to be some of the efficient methods for the fabrication of carbon-based composite filaments. Graphene/PLA (black magic) filaments (Figure 6D), and carbon black/PLA are actively available commercial 3D-printable carbon-based filament materials that can be employed for designing 3D-printed carbon catalysts, or as substrates for multiple applications. Post-printing, the activation of these carbon electrode substrates is carried out via a variety of activation techniques in order to remove the non-conductive PLA parts and improve the conductivity.[100,101] Further, modifications of these 3D-printed activated carbon substrates using metal NPs,[73] inorganic NPs,[96] 2D materials,[28,102] etc. are also known, where such functionalization and surface engineering have easily resulted in the fabrication of the desired electrocatalysts. This opens up possibilities for designing newer 3D-printed functional carbon catalyst substrates for $CO_2RR$.

Although carbon-based filaments are well known for designing 3D-printed substrates for various electrochemical applications,[21,28,79] this field was surprisingly overlooked until recently for its possibilities for $ERCO_2$. A compelling approach was proposed by Dr. Eva et al.[93] towards designing metal microparticle-based 3D-printed PLA-CNT substrates for $CO_2RR$. Using this, electroplating of hemispherical Cu microparticles over 3D-printed PLA-CNT electrode substrates was carried out successfully and the catalyst delivered an appreciable amount of FE that was very close to the results reported in the literature. This study thus becomes elemental in propounding new possibilities of employing 3D-printed electrocatalysts for $CO_2RR$ application. Figure 6E–G shows the potential possibility of fabricating 3D-printed carbon electrodes of various geometries that could be employed as catalysts and as substrate based on the experimental conditions.

**ADVANCED
SCIENCE NEWS**
www.advancedsciencenews.com

**ADVANCED
MATERIALS
INTERFACES**
Open Access
www.advmatinterfaces.de
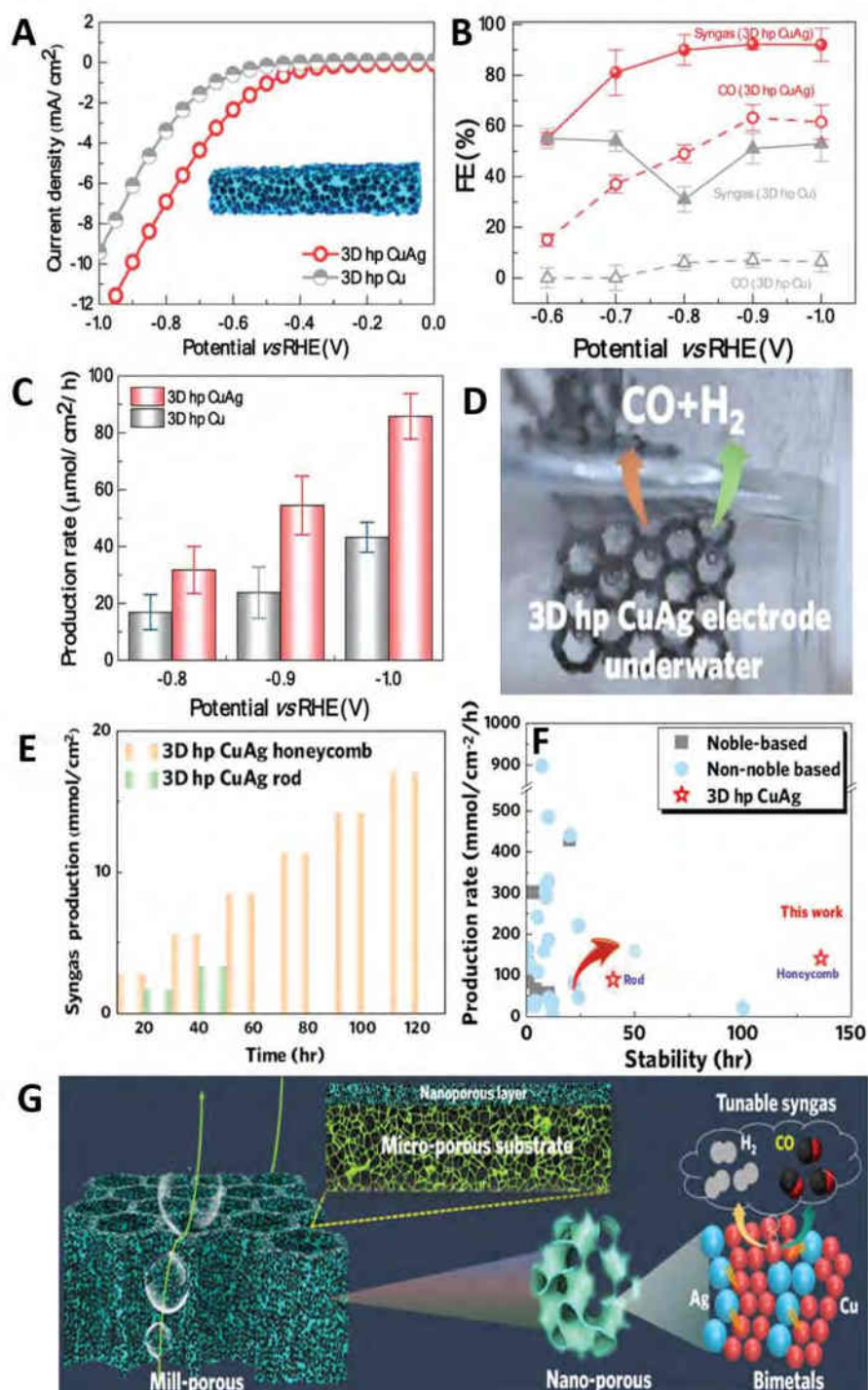
**Figure 5.** Electrochemical performance of catalysts for ERCO$_2$. A) LSV curves of 3D hp CuAg rod and 3D hp Cu catalysts. B) Faradic efficiency procured towards CO and syngas formation at various potentials. C) Syngas production rate of two studied catalysts. D) Syngas production using the 3D hp CuAg honeycomb electrode. E) Comparison of syngas production between catalysts. F) Performance comparison of different catalysts. G) Schematic representation of syngas production combining the 3D porous structure and electronic effect between Cu and Ag. Figures (A–G) Adapted with permission.[29] Copyright 2021, American Chemical Society.

**ADVANCED
SCIENCE NEWS**
www.advancedsciencenews.com

**ADVANCED
MATERIALS
INTERFACES**
Open Access
www.advmatinterfaces.de
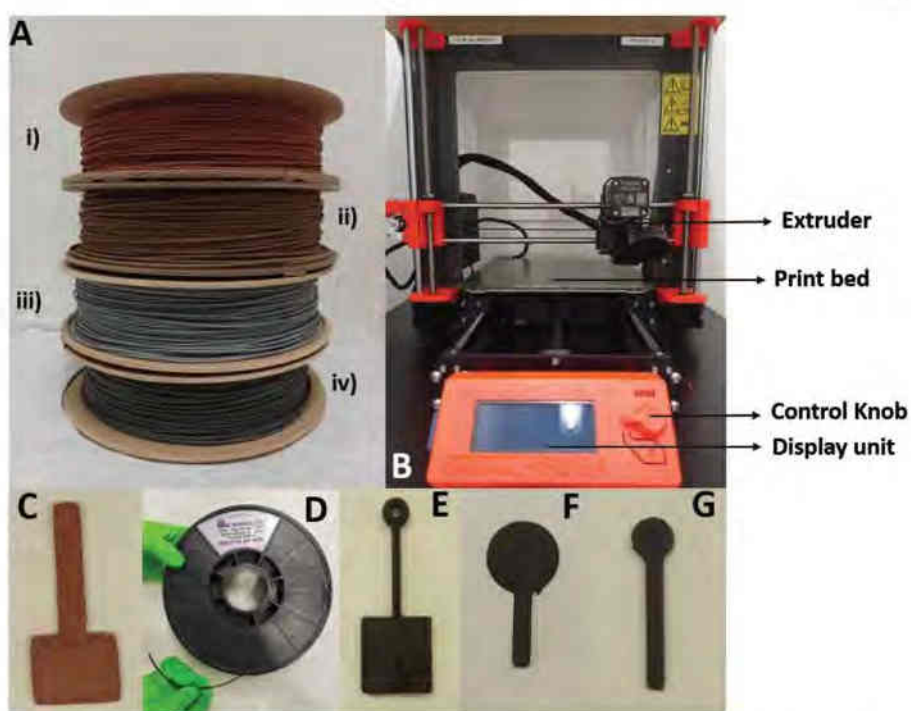
**Figure 6.** A) 3D-printable commercial filaments of i) Cu, ii) bronze, iii) Al, and iv) tungsten, B) FDM 3D-printer for printing commercial and customized filaments. C) 3D-printed Cu/PLA metal electrode. D) Spool of printable filament of graphene/ PLA. E–G) 3D-printed carbon electrode of various geometries.

Today, advancements in developing newer catalysts have also facilitated researchers to focus on metal-free catalysts.[44,103] Adapting such works, to modify or functionalize the 3D-printed carbon-based substrates is highly promising towards catalyst fabrication for $CO_2RR$. Although in its nascent stage, metal-free 3D-printed catalysts are expected to serve as an efficient catalyst for various catalysis applications. Such strategies aim to limit the cost of conventional catalysts owing to the high costs of noble metals and their oxides as active centers. Heteroatom-doped carbon materials were investigated for $CO_2RR$.[104,105] Hence, adopting ideal strategies of functionalizing nitrogen sources covalently or non-covalently[106] over 3D-printed carbon substrates can be carried out to design heteroatom-doped 3D carbon substrates for $CO_2RR$ that delivers higher selectivity, FE, stability, current density, etc.

### 4.3.3. Ink-based Extrusion

Incidentally, DIW is another efficient extrusion-based printing approach that can be used to fabricate 3D-printed active substrates via sequentially extruding ink of active materials out of the print nozzle.[80,81] The formulated inks are optimized, with the ink generally containing active 2D materials, transition metals, and/or NPs along with additives and binders. Post rheological optimization of ink, desired 3D-printed structures are fabricated via extrusion, giving the user the liberty to print any active materials of interest. This technique also provides the possibility of designing most of the known material or hybrid

composite mixtures that may not be feasible using FDM technique. Further, alloys of materials or molecular metal catalysts, or a combination of transition metal with 2D materials such as graphene-based materials, MXenes procured from various parent MAX phase material,[107] TMDs, etc., can also be successfully printed, making it an interesting and suitable approach towards designing 3D-printed active substrate for $CO_2RR$. However, some of the limitations of this technology with regard to ink formulation, ideal extrusion, and post-printing treatments can be resolved through periodic improvements and optimization. Perhaps, we propound that features like the ease in adaptability, user-friendly nature, and the ability to formulate and print complex structures of different catalytically active materials, make 3D-printing a highly promising technology in comparison to conventional printing techniques in both academia and industry.

### 4.4. Customized and Multi-Material 3D-Printing

The 3D-printing industry is rapidly advancing and has expanded to multiple domains in recent times. Although the major part of the discussions held above is on commercial filaments procured from 3D-printing hubs, today the technological progress in this field provides strategies for nanocomposite filament fabrication of various materials[108,109] based on the user's demand. For instance, 3D-printed $MoS_2$/carbon/PLA filaments were fabricated in our group and studied for energy conversion and storage applications.[110] In this study, a slurry of active

**ADVANCED
SCIENCE NEWS**
www.advancedsciencenews.com

**ADVANCED
MATERIALS
INTERFACES**
Open Access
www.advmatinterfaces.de

materials was optimized and fed into an extruder to fabricate a customized filament of active 2D material and later 3D-printed via FDM to procure electrode substrates for desired catalytic applications. In short, advancements in 3D-printing technology have also triggered the possibility of fabricating filaments of 2D materials via specific filament extruders (**Figure 7**A). With literature already explaining the role of TMDs for $CO_2RR$[111,112] and recent studies showing that TMDs such as $MoS_2$ can be 3D-printed to serve as a catalyst, the chances of linking 3D-printing and 2D materials (TMDs) for $CO_2RR$ application gets facilitated, and can be promising. Numerous works on other 2D materials have also been reported in the literature,[113] hence appropriate understanding of the material property, and experimental conditions employed would enable an adequate foundation towards designing active 3D-printed electrode substrates for $ERCO_2$.

Further, we assert that understanding the printable properties of 2D materials and analyzing their compatibility with other active materials such as metal NPs, would facilitate heterogeneous conductive, robust, and active electrocatalysts for $CO_2RR$ applications. Since this approach is relatively new and its benefits have only been recently recognized, establishing its wider possibilities requires further time and experimentation, especially for its application in large-scale industrial processes.

Multi-material (MM) FDM 3D-printing presents another interesting possibility of developing multi-component electrode/substrate systems by extruding multiple filaments of entirely different compositions, sequentially at the same time (Figure 7B–D).[114,115] This eventually opens up the prospects of designing 3D-printed hybrid electrodes, substrates, functional catalysts, and catalytic reactors. In the context of preparing hybrid electrodes, MM FDM 3D-printing can be an asset towards the fabrication of 3D-printed hybrid catalysts for $CO_2RR$, wherein a synergic effect of two or more active materials can lead to enhanced activity of 3D-printed electrode substrate. Commercially procured FDM-based metal 3D printing filaments such as Ti, brass, SS, and Al, customized filaments of 2D or other active nanomaterials, or integrated filaments of both 2D materials and metal NPs, etc. can leave the users with enormous choice of 3D-printing hybrid substrates/catalysts for desired catalytic applications.

The potential of SLS metal 3D-printing towards the fabrication of a self-catalytic reactor (SCR) is reported in the literature.[32] Interestingly, understanding the potential of MM FDM technology towards 3D-printing multiple components simultaneously, would be highly promising towards the fabrication of 3D-printed SCR systems with various active materials.

Such 3D-printed structures and strategies towards device fabrication are expected to be revolutionary owing to the feasibility of using 3D-printed machines for the customization of highly complex structures, its quick prototyping ability, scalability, and cost-effectiveness. Hence, we expect that technological advancements in the field of 3D-printing industry would open up further possibilities for designing a complete electrolyzer cell, SCRs, etc. for $CO_2RR$ with enhanced performance than the conventional systems used currently.

## 4.5. Post-Printing and Modification Approaches

### 4.5.1. Post-Printing Techniques

Successful 3D-printing of desired structures is generally followed by an additional step called post-printing treatments, which is employed to make these 3D-printed substrates desirable for specific applications. This step involves a set of techniques such as activation, surface finishing, curing, sintering, etc. that are often unique and vary from one printing technique to the other.[73,74,100,116] For instance, in FDM-based 3D-printed materials, these post-printing treatments can be conducted using various approaches such as solvent, electrochemical, enzymatic, biological treatments, sputtering, etc.[117] Commercial FDM-based filaments of carbon, metal-based materials often constitute non-conductive polymers, such as PLA, ABS, etc. along with it, wherein the polymer helps for structural integrity and ideal extrusion, but is non-conducting. Hence, the 3D-printed electrodes are subjected to post-printing treatment for removing non-conductive polymers from the printed structures to make them conductive, minimize their charge transfer resistance, and fabricate active surfaces.[21]

Optimizing the ideal activation technique, along with the activation time and temperature, are important aspects, as
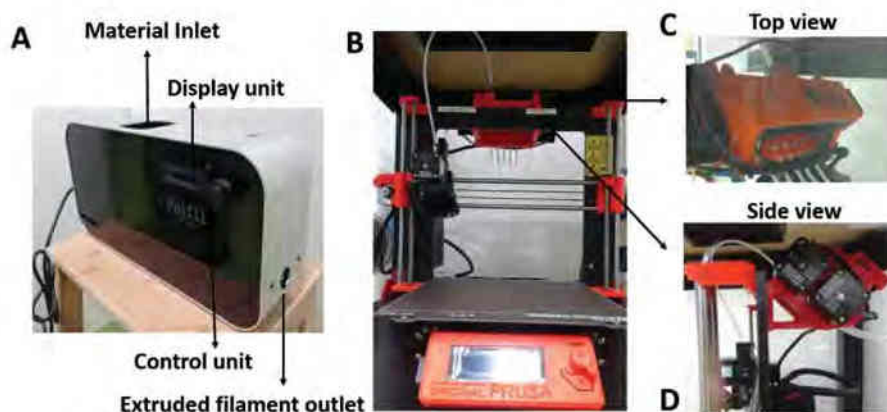


**Figure 7.** A,B) On-demand extruder for fabricating customized printable filaments. B–D) Multi-material FDM 3D printer setup.

**ADVANCED
SCIENCE NEWS**

www.advancedsciencenews.com

**ADVANCED
MATERIALS
INTERFACES**
Open Access

www.advmatinterfaces.de

unoptimized techniques can lead to excessive loss of polymer and distort the printed structure completely. For FDM-based carbon-graphene/ PLA filaments, solvent activation is commonly employed and well-reported using DMF, acetone, NaBH₄, NaOH, etc. to get rid of non-conductive polymer parts. Detailed discussion on other activation techniques can also be adapted from literature[21,28,118,119] and optimized accordingly. Ideal optimizations can aid in retaining the structural integrity of printed parts and also deliver active functional catalysts/ substrates for $CO_2RR$. Sintering of FDM 3D-printed metal/ PLA filaments is employed as post-printing approach to make them robust, conductive, and to get rid of non-conductive PLA counterparts for various applications.[33,70,76] Post-processing of 3D-printed structures procured by SLA involves washing with solvents such as isopropyl alcohol (IPA) or tripropylene glycol monomethyl ether (TPM), followed by exposure to light and heat sources to increase the mechanical strength of the printed parts.[120]

### 4.5.2. Electrode Modification

The patterning of 3D-printed electrode surfaces has also gained attention in recent years due to its facile, quick, and cost-effective approach to fabricating functional catalysts/ substrates for catalytic applications.[28,102] Electrodeposition of active material is one such adequately researched domain. Being a low-cost fabrication technique, it involves depositing a thin layer of active material using the desired precursor metal salt-containing solution. This provides a bifunctional advantage for catalysis applications from both the electrodeposited active layers and the substrates themselves. Electrodeposition of 2D materials,[121] Cu and Ni NPs[73] over 3D-printed carbon substrates have been reported along with recent findings on electrodeposition of Cu NPs over 3D-printed carbon substrates for $CO_2RR$.[93] Hence, electrodeposition over 3D-printed carbon substrates can be considered as a proven and feasible technique for designing functional catalysts for $CO_2RR$, while also extending its possibilities toward other salt solutions containing active metal centers such as nickel.[73]

Further, in studies related to heterogeneous catalysts, known metals such as Cu, Ni, Pd, Rh, etc., are hybridized with organic complexes such as porphyrin, and similar complexes for its application in $CO_2RR$.[122] Such active material and organic complexes can be adequately functionalized over 3D-printed carbon substrates in a variety of ways, paving way for designing newer electrocatalysts for $CO_2RR$. Other conventional techniques such as atomic layer deposition can also be employed towards designing 3D-printed electrocatalysts[123] using respective precursor solutions of active materials for catalysis, thus extending the possibilities towards $CO_2RR$ applications. Conventional patterning of 3D-printed substrates using active materials is another feasible and interesting approach to modifying 3D-printed structures, in order to develop a facile and cost-effective electrocatalyst for $CO_2RR$. This includes techniques such as spray coating,[102] dip coating,[28] spin coating, and Mayer rod coating of active materials. For instance, dip coating of MXene and TMDs, over 3D-printed carbon substrates were shown to be an efficient and successful approach toward catalyst fabrication

for catalytic applications.[28] Hence, adapting similar strategies to modify 3D-printed material surfaces using 2D materials, NPs, composites, etc. to fabricate quick, cheap, and efficient electrocatalysts for $CO_2RR$ are highly promising. Sputtering of noble metal NPs over 3D-printed graphene substrates, such as Au,[124] Ag can be highly beneficial to coat the electrode surfaces homogeneously, making them suitable for catalytic applications such as $CO_2RR$ as well.

## 5. Expanding Scope of 3D-Printing Technology in Mitigating $CO_2$

3D-printing technology has made remarkable advancements in recent times. This technology has also been crucial in devising newer strategies for electrode preparations, that are expected to slow down global warming by extracting $CO_2$ from multiple sources. Thus, we also put forth a discussion on these strategies, along with $ERCO_2$, to show the importance of 3D-printing technology in reducing $CO_2$ amount in the atmosphere. Such evaluations can aid in providing a better foundation and designing newer active substrates via these emerging technologies and eventually expand the scope of this field.

### 5.1. Catalytic Reactions

Metal 3D-printing[125,126] is a highly promising technology to fabricate robust and conductive 3D-printed metal structures and/or devices. This 3D-printing technology utilizes high-power laser sources to bind powdered metal particles, to eventually develop 3D-printed structures, which then undergo post-printing treatments to procure the final desired structures, based on the printing technique employed. In a conventional catalytic system, both catalysts and reactors are known to be significant components, where the former helps in enhancing the efficiency of the reaction, product selectivity, and altering reaction pathways, while the latter provides an ideal working environment for experimentation.[32,127] Integrating both the catalyst and the reactors is known to deliver systems with superior chemical synthesis, and/or can efficiently control the chemical reactions. Also, in the context of 3D-printing, both catalysts and reactors were fabricated and studied,[128–131] but the possibility of printing them together as a single system was surprisingly uninvestigated, until recently.

The potential of metal 3D-printing via SLS for designing simple and cost-effective SCR was realized in a study by Wei et al.,[32] (**Figure 8A**) where these printed parts can directly serve both as chemical reactors and catalysts. The advantages of metal 3D-printing reactor rely upon its ability to withstand extreme temperature and pressure conditions, and studies in this direction can result in devising SCRs that are efficient, cheap, and reaction systems of adequate dimensions. In the current study, three kinds of 3D-printed SCRs were fabricated, namely: Fe-SCR, Co-SCR, and Ni-SCR (Figure 8B) and their potential ability towards the direct conversion of C1 molecules (CO, $CO_2$, $CH_4$) into high value-added chemicals were evaluated systematically. It was observed that Fe-SCR and Co-SCR were ideal for the preparation of liquid fuel from Fischer–Tropsch synthesis

and $CO_2$ hydrogenation. Meanwhile, Ni-SCR efficiently produced syngas by $CO_2$ reforming of $CH_4$, and also exhibited the ability to function at very high-temperature conditions. The catalytic activity of Fe-SCR for $CO_2$ hydrogenation and Ni-SCR for dry reforming of methane is given in Figure 8C,D respectively. Further, geometric studies on multiple reactor designs were performed on Co-SCR catalysts by researchers which showed that enhanced catalytic performance could be achieved with differences in the geometric designs, eventually enhancing the scope of 3D-printing technology towards designing and fabrication of newer catalysts.

3D-fiber deposition (3D-FD) is also considered as an interesting approach toward the fabrication of catalytic structures via the extrusion of active materials.[135,136] The active materials include metallic, ceramic, and polymer materials, that are extruded through a nozzle to procure scaffolds and/or macrostructured catalytic supports of the desired shape, size, and geometry. In a study by S Danaci et al.,[132] 3D-FD based printing techniques were employed towards the fabrication of Cu support, followed by coating with active Ni/alumina suspension, and used for $CO_2$ methanation. SS supports were also fabricated, coated, and evaluated systematically in the study. 3D-printed Cu structures were procured upon extrusion of Cu paste through a nozzle of 400 um diameter as shown in Figure 8E. Post successful printing, support was dried and sintered. The optical microscopy image of the printed structure obtained after sintering at different magnifications is shown in Figure 8F,G. Catalyst-loaded 3D-printed Cu and SS supports are in the order of 1 and 1.2 g respectively. Further, it was observed that Cu and SS supported Ni/alumina catalysts showed slightly higher productivity over Ni/alumina powder catalysts for $CO_2$ methanation, with diluted reactant gas, and under atmospheric pressure. With the advancements in technology, 3D-printing of direct active material is also possible for fabricating catalysts. For instance, Ni/alumina-based 3D-printed catalysts were fabricated using 3D-FD technique and studied for $CO_2$ methanation.[137] Multiple studies on employing extrusion-based techniques for the fabrication of catalytic materials for $CO_2$ methanation have also been reported in the literature.[135,138,139] In short, exercising 3D-printing technology in the patterning of active devices and electrodes of appropriate geometry and size can aid in enhanced performance compared to conventional catalysts, broadening the scope of this field.

### 5.2. CO₂ Capture Technologies

Industries and fossil fuel power plants emit enormous amounts of $CO_2$ that can potentially alter global climatic conditions periodically. Carbon capture and storage (CCS) or carbon capture and sequestration involve strategies towards capturing $CO_2$ from emission sources before it enters the atmosphere, followed by transporting and storing them.[140–142] Commercial technologies are often expensive, and energy-intensive, which prompts research toward newer technologies and alternative ways of controlling $CO_2$ emissions. 3D-printing technologies have shown advancements in cutting down $CO_2$ emissions using multiple strategies. In a study by Du Nguyen et al., DIW was employed in 3D-printing structure using a polymer composite inks of solid sodium carbonate sorbent particles dispersed in an uncured silicone polymer (Figure 8H).[36] Figure 8I shows the SEM image of the composite filament, and Figure 8J showcase the 3D-printed gyroid structure. Post-printing, they are subjected to thermal treatment resulting in a solid structure. They are then exposed to water vapors resulting in aqueous sodium carbonate domains that are capable of capturing $CO_2$.

In another study by S Couck et al., 3D-FD printing technique was employed for the fabrication of ZSM-5 monoliths for gas separation (Figure 8K.)[133] Experimentation showed that among $CO_2$, $CH_4$ and $N_2$, $CO_2$ is the strongest adsorbing component followed by $CH_4$ and $N_2$, also the catalyst exhibited a good separation of $CO_2$ in both mixtures of $CO_2/N_2$ and $CO_2/CH_4$. Key merits of the 3D-printing technology towards the fabrication of structures owe to its improved heat transfer, better mass transfer, good separation performance, and the ability to complete regeneration of the active structure, upon being subjected to Helium flow. Interestingly, in another work, DIW technique was employed to procure honeycomb-like 3D-printed SAPO-34 zeolite-based structured adsorbents for gas separation (Figure 8L).[134] Two types of 3D-printed SAPO-34 monolith structures were fabricated, one containing polyacrylic acid and methylcellulose, and another one containing 5 wt.% graphite. Further, extrusion-based printing techniques were employed to procure polymer-zeolite (Torlon polymer and 13X and 5A zeolites) composite monoliths for $CO_2$ removal from flue gas.[143] Further studies on 3D printing structures employed for $CO_2$ capture technologies can be found in literature[144–149] as a detailed analysis is beyond the scope of this article.

## 6. Challenges and Solutions

Although the advancements in designing functional electrocatalysts, reactors, SCR, etc. for $CO_2$ mitigation using 3D-printing are reported by multiple groups,[29,32,93,132,137,150,151] yet the potential of it has not been fully realized. However, progress in this direction is expected to be achieved in a considerable amount of time. Strict optimization of the precursor materials is to be carried out for ideal fabrication of 3D-printed structures or reactors for $CO_2RR$. This includes a broader understanding of the filament (commercial/customized) compositions and extrusion temperature, ink compositions and rheological properties, metal, and metal-alloy composites employed. Importantly, designing and fabrication should be strictly related to the intended applications.

Excessive oxidation of active material during extrusion can lower the conductivity of printed structures and eventually affect the performance of the material. This could be solved by enclosing the 3D-printer with specially designed chambers around it, purged with continuous inert gas during the entire printing process. 3D-printed metal electrodes can deform its shape upon subjection to high sintering temperatures. This can be resolved by using ideal molds or protective layers capable of inhibiting the destruction of the posture of 3D-printed structures. Formulating ink that obeys ideal rheological properties for DIW techniques can be challenging at initial stages. The inks usually include active components such as 2D materials, NPs, and metal particles along with conductive fillers, binders,

**ADVANCED
SCIENCE NEWS**
www.advancedsciencenews.com

**ADVANCED
MATERIALS
INTERFACES**
Open Access
www.advmatinterfaces.de
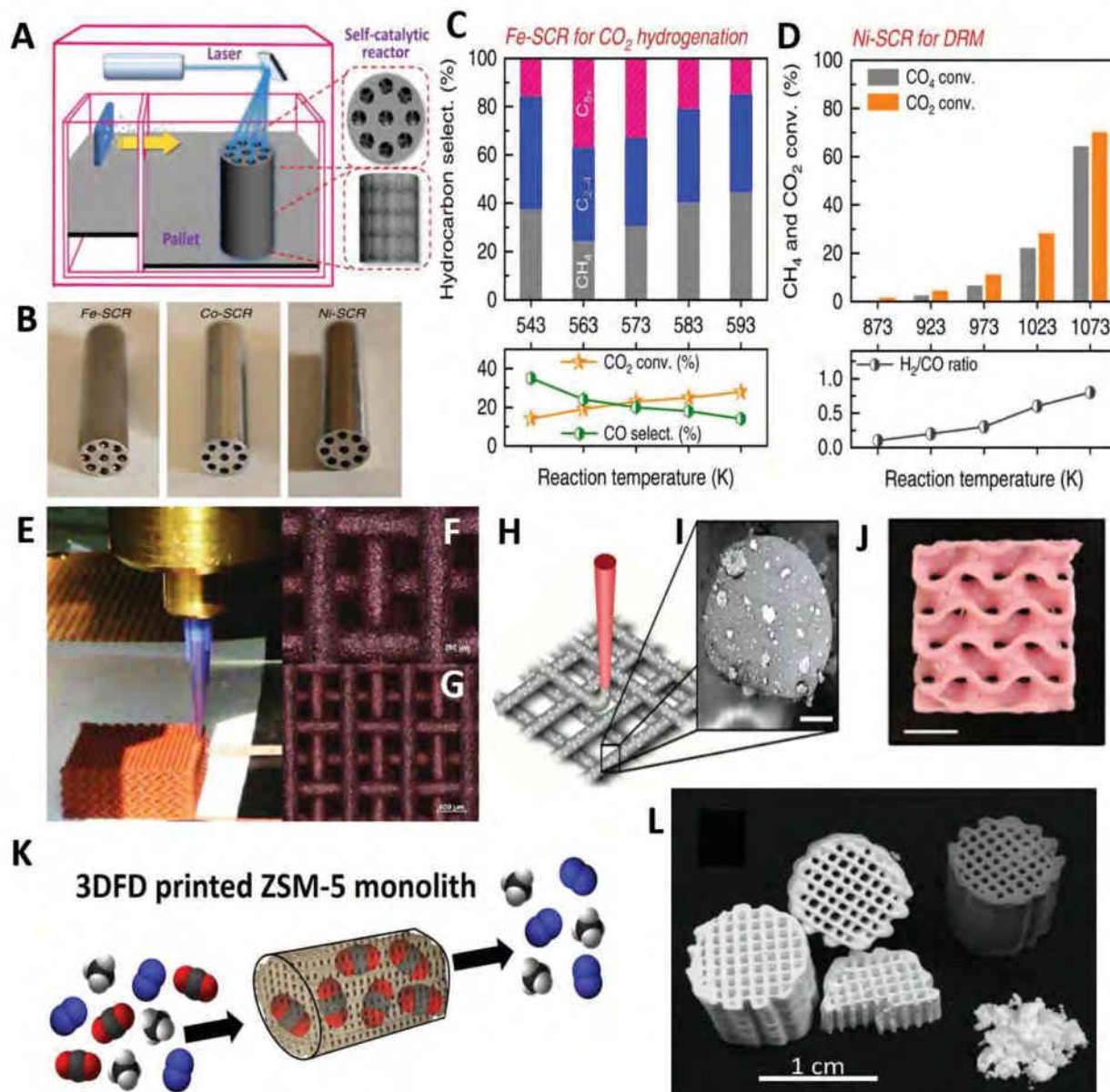


**Figure 8.** A) Schematic representation of 3D-printing SCR via SLS. B) 3D-printed SCR of Fe-SCR, Co-SCR, and Ni-SCR. C) Catalytic activity of the Fe-SCR for $CO_2$ hydrogenation. D) Catalytic activity of the Ni-SCR for the reforming of methane. Figures (A–D) Adapted with permission.[32] Copyright 2020, The Author(s), Published by Springer Nature. E) Copper supports for $CO_2$ methanation via 3D-FD technique. F,G) Optical microscope images post sintering (Scale bar is 200 and 500 μm respectively). Figures (E–G) Adapted with permission.[132] Copyright 2018, Published by Elsevier B.V. H) Schematic representation of a printing ink composite to simple cubic woodpile lattice to procure 3D printed $CO_2$ capture composite structures. I) SEM image of a printed composite filament (Scale bar is 50 μm). J) 3D-printed composite (Scale bar is 5 mm). Figures (H–J) Adapted with permission.[36] Copyright 2019, American Chemical Society. K) Schematic representation of ZSM-5 monoliths for gas separation. Adapted with permission.[133] Copyright 2016, Elsevier B.V. All rights reserved. L) SEM image of several SAPO-34 3D-printed monolith segments (white) and one SAPO-34/graphite 3D-printed monolith (grey). Adapted with permission.[134] Copyright 2017, Elsevier Inc. All rights reserved.

additives, etc. Improper optimization can result in the clogging of nozzles and incomplete printed parts. Employing a rheometer to study the fluidic properties would be an ideal choice prior to the extrusion-based DIW technique. Such approaches can aid in developing conductive, rigid, and ideal structures for $CO_2RR$ as well. Post-printing approaches such as curing, washing, activation techniques, and sintering conditions have to be carefully and closely optimized to make them desirable for various applications.[73,100,116,117] Unoptimized or excessive post-printing treatments can result in excessive loss of polymer,

making the 3D-printed structure fragile, and leading to the breakage of the printed parts.

Certain limitations associated with $CO_2RR$ in aqueous systems are the low dissolution of $CO_2$ at acidic or neutral pH conditions, competitive proton reduction, poor selectivity of carbonaceous products, etc. A few steps to overcome these limitations include the use of the non-aqueous solution for catalytic reactions, increasing $CO_2$ partial pressure, low-temperature experimental conditions, etc. Further, the stability of 3D-printed parts in solvents is also crucial for carrying out long-term experiments. Although there are reports on employing 3D-printed electrodes in basic solvents such as KOH and $KHCO_3$ for catalytic applications, there are certain limitations associated with the degradation of polymers in the course of the experiment. However, timely improvements with respect to the composition, customization, and design of carbon/polymer, metal/polymer, etc., may help to overcome this limitation.

Immobilization of active material over 3D-printed electrodes can also aid the fabrication of scalable, cost-effective substrates for $CO_2RR$. Designing such modified 3D-printed substrates call for various optimization approaches such as functionalization, surface engineering strategies, or patterning approaches, which though initially time-consuming, would be an ideal approach to modify 3D-printed substrates for catalytic applications. This can also limit the use of specialized and expensive equipment for fabricating electrocatalysts. Modifying 3D-printed substrates using techniques such as electroplating has been adopted by several groups for designing 3D-printed electrocatalysts.[73] Unoptimized techniques can result in non-conductive 3D-printed substrates, resulting in semi-uniform or no deposition of active material over the 3D-printed substrate. Hence optimization of electrode modification techniques, as well as associated parameters, are crucial for the successful electroplating of active layers over 3D-printed substrates.

Every technique has its own merits and demerits, and identifying an ideal and feasible approach for designing functional electrocatalysts, reactors, SCR, etc. based on the experimental conditions can enhance 3D-printing technology towards $CO_2RR$. Several challenges faced during the fabrication of 3D-printed structures have been addressed. This technique is also expected to make considerable progress with time by developing advanced technologies for $CO_2RR$. Thus, 3D-printing technology can be said to be highly promising in developing active components for catalytic applications. They can also eventually be capable of 3D-printing a complete electrolyzer cell with all components and also expand to large-scale industrial applications.

## 7. Conclusion and Future Outlook

The domain of 3D-printing technology has witnessed considerable developments over the last forty years, making it less expensive and more user-friendly. Added advantages of 3D-printing technology include rapid prototyping, scalability, facilitating improvements, quick modifications, etc. This technique finds application in diverse fields of manufacturing along with its fundamental usage as a proof-of-concept in academic circles. Since studies related to 3D-printed structures for $CO_2RR$

are scarcely reported, the anticipated outcome can take some time to become established among conventional catalysts. This perspective article has also discussed how 3D printing technology is gaining impetus towards the fabrication of 3D-printed structures for Fischer–Tropsch synthesis, $CO_2$ hydrogenation, $CO_2$ reforming of $CH_4$, $CO_2$ capture, separation, etc. This can, in turn, be ideal for mitigating the increasing $CO_2$ concentration in the atmosphere and also result in value-added products, fuels, and industrial feedstocks. Thus, once the potential of this field in designing 3D-printed electrocatalysts, substrates, reactors, integrated devices, SCR, etc. towards $CO_2RR$ is fully realized, it can be developed as a significant merit of this technology in the current scenario. Reportedly, several active materials, such as 2D materials, NPs, metal-based composites, integrated materials, etc. are known to be ideal for the present application. Interestingly, 3D-printing technology gives the liberty to fabricate 3D-printed active substrates of these materials and therefore revolutionizes the designing of active materials for catalytic applications like $CO_2RR$. In short, several further advancements are expected in the field of $CO_2RR$, considering its vital applicational benefits and ability to overcome the drawbacks of traditional manufacturing methods. Techniques like 3D-printing can be considered a breakthrough in designing novel electrocatalyst structures for $CO_2RR$ that are more economical, energy-efficient, and can significantly contribute towards mitigating environmental crises.

## Conflict of Interest

The authors declare no conflict of interest.

[1] J. D. Shakun, P. U. Clark, F. He, S. A. Marcott, A. C. Mix, Z. Liu, B. Otto-Bliesner, A. Schmittner, E. Bard, *Nature* **2012**, *484*, 49.

[2] W. Bach, *Environ. Int.* **1979**, *2*, 215.

[3] Z. Liu, Z. Deng, S. J. Davis, C. Giron, P. Ciais, *Nat. Rev. Earth Environ.* **2022**, *3*, 217.

[4] S. Nitopi, E. Bertheussen, S. B. Scott, X. Liu, A. K. Engstfeld, S. Horch, B. Seger, I. E. L. Stephens, K. Chan, C. Hahn, J. K. Nørskov, T. F. Jaramillo, I. Chorkendorff, *Chem. Rev.* **2019**, *119*, 7610.

[5] S. J. Davis, N. S. Lewis, M. Shaner, S. Aggarwal, D. Arent, I. L. Azevedo, S. M. Benson, T. Bradley, J. Brouwer, Y. M. Chiang, C. T. M. Clack, A. Cohen, S. Doig, J. Edmonds, P. Fennell, C. B. Field, B. Hannegan, B. M. Hodge, M. I. Hoffert, E. Ingersoll, P. Jaramillo, K. S. Lackner, K. J. Mach, M. Mastrandrea, J. Ogden, P. F. Peterson, D. L. Sanchez, D. Sperling, J. Stagner, J. E. Trancik, et al., *Science* **2018**, *360*, eaas9793.

[6] J. Resasco, A. T. Bell, *Trends Chem.* **2020**, *2*, 825.

[7] T. K. Todorova, M. W. Schreiber, M. Fontecave, *ACS Catal.* **2020**, *10*, 1754.

[8] K. Chan, *Nat. Commun.* **2020**, *11*, 5954.

[9] Z. Sun, T. Ma, H. Tao, Q. Fan, B. Han, *Chem* **2017**, *3*, 560.

[10] S. Samanta, R. Srivastava, *Mater. Adv.* **2020**, *1*, 1506.

[11] K. P. Kuhl, T. Hatsukade, E. R. Cave, D. N. Abram, J. Kibsgaard, T. F. Jaramillo, *J. Am. Chem. Soc.* **2014**, *136*, 14107.

[12] W. Zhang, Y. Hu, L. Ma, G. Zhu, Y. Wang, X. Xue, R. Chen, S. Yang, Z. Jin, *Adv. Sci.* **2018**, *5*, 1700275.

[13] S. Back, H. Kim, Y. Jung, *ACS Catal.* **2015**, *5*, 965.

[14] Y. Guan, M. Liu, X. Rao, Y. Liu, J. Zhang, *J. Mater. Chem. A* **2021**, *9*, 13770.

[15] Y. Quan, J. Zhu, G. Zheng, *Small Sci.* **2021**, 2100043.

[16] Z. Weng, J. Jiang, Y. Wu, Z. Wu, X. Guo, K. L. Materna, W. Liu, V. S. Batista, G. W. Brudvig, H. Wang, *J. Am. Chem. Soc.* **2016**, *138*, 8076.

[17] S. Garg, M. Li, A. Z. Weber, L. Ge, L. Li, V. Rudolph, G. Wang, T. E. Rufford, *J. Mater. Chem. A* **2020**, *8*, 1511.

[18] Y. Cheng, S. Yang, S. P. Jiang, S. Wang, *Small Methods* **2019**, *3*, 1800440.

[19] C. Costentin, M. Robert, J. M. Savéant, *Chem. Soc. Rev.* **2013**, *42*, 2423.

[20] B. Khezri, A. C. Fisher, M. Pumera, *J. Mater. Chem. A* **2017**, *5*, 8230.

[21] M. P. Browne, E. Redondo, M. Pumera, *Chem. Rev.* **2020**, *120*, 2783.

[22] K. P. A. Kumar, M. Pumera, *Adv. Funct. Mater.* **2021**, *31*, 2100450.

[23] T. D. Ngo, A. Kashani, G. Imbalzano, K. T. Q. Nguyen, D. Hui, *Compos. Part B Eng.* **2018**, *143*, 172.

[24] N. Shahrubudin, T. C. Lee, R. Ramlan, *Procedia Manuf.* **2019**, *35*, 1286.

[25] A. Ambrosi, M. Pumera, *Chem. Soc. Rev.* **2016**, *45*, 2740.

[26] A. Ambrosi, J. G. S. Moo, M. Pumera, *Adv. Funct. Mater.* **2016**, *26*, 698.

[27] S. Lawson, X. Li, H. Thakkar, A. A. Rownaghi, F. Rezaei, *Chem. Rev.* **2021**, *121*, 6246.

[28] K. P. Akshay Kumar, K. Ghosh, O. Alduhaish, M. Pumera, *Electrochem. Commun.* **2021**, *122*, 106890.

[29] W. Y. Yan, C. Zhang, L. Liu, *ACS Appl. Mater. Interfaces* **2021**, *13*, 45385.

[30] G. Hyun, J. T. Song, C. Ahn, Y. Ham, D. Cho, J. Oh, S. Jeon, *Proc. Natl. Acad. Sci. U. S. A.* **2020**, *117*, 5680.

[31] Y. Hori, K. Kikuchi, S. Suzuki, *Chem. Lett.* **1985**, *14*, 1695.

[32] Q. Wei, H. Li, G. Liu, Y. He, Y. Wang, Y. E. Tan, D. Wang, X. Peng, G. Yang, N. Tsubaki, *Nat. Commun.* **2020**, *11*, 4098.

[33] C. Iffelsberger, D. Rojas, M. Pumera, *J. Phys. Chem. C* **2022**, *126*, 9016.

[34] X. Tian, *2D Mater.* **2022**, *9*, 012001.

[35] K. Hassan, M. J. Nine, T. T. Tung, N. Stanley, P. L. Yap, H. Rastin, L. Yu, D. Losic, *Nanoscale* **2020**, *12*, 19007.

[36] D. Nguyen, M. Murialdo, K. Hornbostel, S. Pang, C. Ye, W. Smith, S. Baker, W. Bourcier, J. Knipe, R. Aines, J. Stolaroff, *Ind. Eng. Chem. Res.* **2019**, *58*, 22015.

[37] J. Qiao, Y. Liu, F. Hong, J. Zhang, *Chem. Soc. Rev.* **2014**, *43*, 631.

[38] T. E. Teeter, P. Van Rysselberghe, *J. Chem. Phys.* **1954**, *22*, 759.

[39] J. Zhao, S. Xue, J. Barber, Y. Zhou, J. Meng, X. Ke, *J. Mater. Chem. A* **2020**, *8*, 4700.

[40] S. Zhao, R. Jin, R. Jin, *ACS Energy Lett.* **2018**, *3*, 452.

[41] D. Johnson, Z. Qiao, A. Djire, *ACS Appl. Energy Mater.* **2021**, *4*, 8661.

[42] Y. Zhu, Y. Yang, C. Peng, C. Priest, Y. Mei, G. Wu, *Small* **2021**, *17*, 2005148.

[43] Y. Xu, Z. Zhou, M. Zou, Y. Liu, Y. Zheng, Y. Yang, S. Lan, J. Lan, C. W. Nan, Y. H. Lin, *Mater. Today* **2022**, *54*, 225.

[44] J. Wu, S. Ma, J. Sun, J. I. Gold, C. Tiwary, B. Kim, L. Zhu, N. Chopra, I. N. Odeh, R. Vajtai, A. Z. Yu, R. Luo, J. Lou, G. Ding, P. J. A. Kenis, P. M. Ajayan, *Nat. Commun.* **2016**, *7*, 13869.

[45] S. C. Perry, P. Leung, L. Wang, C. P. De León, *Curr. Opin. Electrochem.* **2020**, *20*, 88.

[46] X. Kang, Q. Zhu, X. Sun, J. Hu, J. Zhang, Z. Liu, B. Han, *Chem. Sci.* **2016**, *7*, 266.

[47] B. Endrődi, G. Bencsik, F. Darvas, R. Jones, K. Rajeshwar, C. Janáky, *Prog. Energy Combust. Sci.* **2017**, *62*, 133.

[48] D. Ma, T. Jin, K. Xie, H. Huang, *J. Mater. Chem. A* **2021**, *9*, 20897.

[49] J. Wicks, M. L. Jue, V. A. Beck, J. S. Oakdale, N. A. Dudukovic, A. L. Clemens, S. Liang, M. E. Ellis, G. Lee, S. E. Baker, E. B. Duoss, E. H. Sargent, *Adv. Mater.* **2021**, *33*, 2003855.

[50] Y. Wang, P. Han, X. Lv, L. Zhang, G. Zheng, *Joule* **2018**, *2*, 2551.

[51] D. D. Zhu, J. L. Liu, S. Z. Qiao, *Adv. Mater.* **2016**, *28*, 3423.

[52] P. De Luna, C. Hahn, D. Higgins, S. A. Jaffer, T. F. Jaramillo, E. H. Sargent, *Science* **2019**, *350*, 364.

[53] M. Gattrell, N. Gupta, A. Co, *J. Electroanal. Chem.* **2006**, *594*, 1.

[54] W. Ju, A. Bagger, X. Wang, Y. Tsai, F. Luo, T. Möller, H. Wang, J. Rossmeisl, A. S. Varela, P. Strasser, *ACS Energy Lett.* **2019**, *4*, 1663.

[55] R. Kortlever, J. Shen, K. J. P. Schouten, F. Calle-Vallejo, M. T. M. Koper, *J. Phys. Chem. Lett.* **2015**, *6*, 4073.

[56] S. Liang, L. Huang, L. Gao, Q. Wang, B. Liu, *Adv. Sci.* **2021**, *8*, 2102886.

[57] S. Popović, M. Smiljanić, P. Jovanovič, J. Vavra, R. Buonsanti, N. Hodnik, *Angew. Chem., Int. Ed.* **2020**, *59*, 14736.

[58] M. J. Sun, Z. W. Gong, J. D. Yi, T. Zhang, X. Chen, R. Cao, *Chem. Commun.* **2020**, *56*, 8798.

[59] J. He, K. E. Dettelbach, A. Huang, C. P. Berlinguette, *Angew. Chem., Int. Ed.* **2017**, *56*, 16579.

[60] H. Pan, C. J. Barile, *J. Mater. Chem. A* **2020**, *8*, 1741.

[61] A. Hasani, M. A. Teklagne, H. H. Do, S. H. Hong, Q. Van Le, S. H. Ahn, S. Y. Kim, *Carbon Energy* **2020**, *2*, 158.

[62] N. Li, X. Chen, W. J. Ong, D. R. Macfarlane, X. Zhao, A. K. Cheetham, C. Sun, *ACS Nano* **2017**, *11*, 10825.

[63] X. Mao, L. Wang, Y. Xu, Y. Li, *J. Phys. Chem. C* **2020**, *124*, 10523.

[64] N. H. Attanayake, H. R. Banjade, A. C. Thenuwara, B. Anasori, Q. Yan, D. R. Strongin, *Chem. Commun.* **2021**, *57*, 1675.

[65] Y. Hori, *Mod. Aspects Electrochem.* **2008**, *42*, 89.

[66] Y. Hori, A. Murata, R. Takahashi, *J. Chem. Soc., Faraday Trans. 1* **1989**, *85*, 2309.

[67] Y. Hori, H. Wakebe, T. Tsukamoto, O. Koga, *Electrochim. Acta* **1994**, *39*, 1833.

[68] Y. Hori, A. Murata, R. Takahashi, S. Suzuki, *J. Chem. Soc., Chem. Commun.* **1988**, 17.

[69] Y. Hori, K. Kikuchi, A. Murata, S. Suzuki, *Chem. Lett.* **1986**, *15*, 897.

[70] M. R. Hartings, Z. Ahmed, *Nat. Rev. Chem.* **2019**, *3*, 305.

[71] V. V. T. Padil, K. P. Akshay Kumar, S. Murugesan, R. Torres-Mendieta, S. Wacławek, J. Y. Cheong, M. Černík, R. S. Varma, *Green Chem.* **2022**, *24*, 3081.

[72] C. Barnatt, *3D Printing: The Next Industrial Revolution* **2013**, https://www.explainingthefuture.com/3dp_chapter1.pdf.

[73] K. P. A. Kumar, K. Ghosh, O. Alduhaish, M. Pumera, *Electrochem. Commun.* **2020**, *120*, 106827.

[74] D. P. Rocha, R. G. Rocha, S. V. F. Castro, M. A. G. Trindade, R. A. A. Munoz, E. M. Richter, L. Angnes, *Electrochem. Sci. Adv.* **2022**, *2*, e2100136.

**ADVANCED
SCIENCE NEWS**
www.advancedsciencenews.com

**ADVANCED
MATERIALS
INTERFACES**
Open Access
www.advmatinterfaces.de

[75] E. Redondo, M. Pumera, *Appl. Mater. Today* **2021**, *25*, 101253.

[76] J. Muñoz, E. Redondo, M. Pumera, *Appl. Mater. Today* **2022**, *28*, 101519.

[77] R. M. Cardoso, P. R. L. Silva, A. P. Lima, D. P. Rocha, T. C. Oliveira, T. M. do Prado, E. L. Fava, O. Fatibello-Filho, E. M. Richter, R. A. A. Muñoz, *Sens. Actuators, B* **2020**, *307*, 127621.

[78] M. Zafir Mohamad Nasir, F. Novotný, O. Alduhaish, M. Pumera, *Electrochem. Commun.* **2020**, *115*, 106735.

[79] W. Gao, M. Pumera, *Adv. Funct. Mater.* **2021**, *31*, 2007285.

[80] V. G. Rocha, E. Saiz, I. S. Tirichenko, E. García-Tuñón, *J. Mater. Chem. A* **2020**, *8*, 15646.

[81] M. A. S. R. Saadi, A. Maguire, N. T. Pottackal, M. S. H. Thakur, M. M. Ikram, A. J. Hart, P. M. Ajayan, M. M. Rahman, *Adv. Mater.* **2022**, *34*, 2108855.

[82] C. Parra-Cabrera, C. Achille, S. Kuhn, R. Ameloot, *Chem. Soc. Rev.* **2018**, *47*, 209.

[83] H. Quan, T. Zhang, H. Xu, S. Luo, J. Nie, X. Zhu, *Bioact. Mater.* **2020**, *5*, 110.

[84] S. Kumar, *JOM* **2003**, *55*, 43.

[85] S. C. Ligon, R. Liska, J. Stampfl, M. Gurr, R. Mülhaupt, *Chem. Rev.* **2017**, *117*, 10212.

[86] K. V. Venkatesh, V. V. Nandini, *J. Indian Prosthodont. Soc.* **2013**, *13*, 389.

[87] M. P. Browne, V. Urbanova, J. Plutnar, F. Novotný, M. Pumera, *J. Mater. Chem. A* **2020**, *8*, 1120.

[88] S. Chandrasekaran, J. Feaster, J. Ynzunza, F. Li, X. Wang, A. J. Nelson, M. A. Worsley, *ACS Mater. Au* **2022**, *2*, 596.

[89] R. A. Márquez, K. Kawashima, Y. J. Son, R. Rose, L. A. Smith, N. Miller, O. A. Carrasco Jaim, H. Celio, C. B. Mullins, *ACS Appl. Mater. Interfaces* **2022**, *14*, 42153.

[90] J. C. Bui, J. T. Davis, D. V. Esposito, *Sustainable Energy Fuels* **2019**, *4*, 213.

[91] J. Ahn, Y. S. Park, S. Lee, J. Yang, J. Pyo, J. Lee, G. H. Kim, S. M. Choi, S. K. Seol, *Sci. Rep.* **2022**, *12*, 346.

[92] J. Zhu, P. Wu, Y. Chao, J. Yu, W. Zhu, Z. Liu, C. Xu, *Chem. Eng. J.* **2022**, *433*, 134341.

[93] E. Vaněčková, M. Bouša, V. Shestivska, J. Kubišta, P. Moreno-García, P. Broekmann, M. Rahaman, M. Zlámal, J. Heyda, M. Bernauer, T. Sebechlebská, V. Kolivoška, *ChemElectroChem* **2021**, *8*, 2137.

[94] L. Li, A. Ozden, S. Guo, F. P. García de Arquer, C. Wang, M. Zhang, J. Zhang, H. Jiang, W. Wang, H. Dong, D. Sinton, E. H. Sargent, M. Zhong, *Nat. Commun.* **2021**, *12*, 5223.

[95] N. Dehdari Ebrahimi, Y. S. Ju, *Addit. Manuf.* **2018**, *24*, 479.

[96] J. Muñoz, E. Redondo, M. Pumera, *Small* **2021**, *17*, 2103189.

[97] Z. Sun, Y. H. Hu, *Acc. Mater. Res.* **2021**, *2*, 48.

[98] T. Ma, Q. Fan, X. Li, J. Qiu, T. Wu, Z. Sun, *J. CO2 Util.* **2019**, *30*, 168.

[99] S. Ma, R. Luo, J. I. Gold, A. Z. Yu, B. Kim, P. J. A. Kenis, *J. Mater. Chem. A* **2016**, *4*, 8573.

[100] M. P. Browne, F. Novotný, Z. Sofer, M. Pumera, *ACS Appl. Mater. Interfaces* **2018**, *10*, 40294.

[101] C. L. Manzanares Palenzuela, F. Novotný, P. Krupička, Z. Sofer, M. Pumera, *Anal. Chem.* **2018**, *90*, 5753.

[102] R. Gusmão, Z. Sofer, P. Marvan, M. Pumera, *Nanoscale* **2019**, *11*, 9888.

[103] W. Li, M. Seredych, E. Rodríguez-Castellón, T. J. Bandosz, *ChemSusChem* **2016**, *9*, 606.

[104] H. Cui, Y. Guo, L. Guo, L. Wang, Z. Zhou, Z. Peng, *J. Mater. Chem. A* **2018**, *6*, 18782.

[105] J. Wu, R. M. Yadav, M. Liu, P. P. Sharma, C. S. Tiwary, L. Ma, X. Zou, X. Zhou, B. I. Yakobson, J. Lou, P. M. Ajayan, *ACS Nano* **2015**, *9*, 5364.

[106] K. P. A. Kumar, O. Alduhaish, S. F. Adil, M. Pumera, *Adv. Mater. Interfaces* **2022**, *9*, 2102317.

[107] K. P. Akshay Kumar, O. Alduhaish, M. Pumera, *Electrochem. Commun.* **2021**, *125*, 106977.

[108] X. Wei, D. Li, W. Jiang, Z. Gu, X. Wang, Z. Zhang, Z. Sun, *Sci. Rep.* **2015**, *5*, 11181.

[109] S. Dul, L. Fambri, A. Pegoretti, *Compos. Part A Appl. Sci. Manuf.* **2016**, *85*, 181.

[110] K. Ghosh, S. Ng, C. Iffelsberger, M. Pumera, *Appl. Mater. Today* **2022**, *26*, 101301.

[111] M. Asadi, B. Kumar, A. Behranginia, B. A. Rosen, A. Baskin, N. Repnin, D. Pisasale, P. Phillips, W. Zhu, R. Haasch, R. F. Klie, P. Král, J. Abiade, A. Salehi-Khojin, *Nat. Commun.* **2014**, *5*, 4470.

[112] A. Datar, M. Bar-Sadan, A. Ramasubramaniam, *J. Phys. Chem. C* **2020**, *124*, 20116.

[113] M. A. Tekalgne, H. H. Do, A. Hasani, Q. Van Le, H. W. Jang, S. H. Ahn, S. Y. Kim, *Mater. Today Adv.* **2020**, *5*, 100038.

[114] R. F. Quero, B. M. de Castro Costa, J. A. F. da Silva, D. P. de Jesus, *Sens. Actuators, B* **2022**, *365*, 131959.

[115] A. Ambrosi, M. Pumera, *ACS Sustainable Chem. Eng.* **2018**, *6*, 16968.

[116] L. Greguric, *All3DP, 10 Methods for 3D Printing Post-Processing (PLA & More)*, **2022**, https://all3dp.com/2/fdm-3d-printing-post-processing-an-overview-for-beginners/ (accessed: November 2022).

[117] J. Muñoz, M. Pumera, *ChemElectroChem* **2020**, *7*, 3404.

[118] J. Muñoz, M. Pumera, *TrAC, Trends Anal. Chem.* **2020**, *128*, 115933.

[119] C. Kalinke, N. V. Neumsteir, G. D. O. Aparecido, T. V. D. B. Ferraz, P. L. Dos Santos, B. C. Janegitz, J. A. Bonacin, *Analyst* **2020**, *145*, 1207.

[120] Formlabs, *Guide to Post-Processing and Finishing SLA 3D Prints*, https://formlabs.com/eu/blog/post-processing-and-finishing-sla-prints/ (accessed: November 2022).

[121] C. Iffelsberger, S. Ng, M. Pumera, *Appl. Mater. Today* **2020**, *20*, 100654.

[122] C. Costentin, M. Robert, J. M. Savéant, *Curr. Opin. Electrochem.* **2017**, *2*, 26.

[123] V. Urbanová, J. Plutnar, M. Pumera, *Appl. Mater. Today* **2021**, *24*, 101131.

[124] C. Y. Foo, H. N. Lim, M. A. Mahdi, M. H. Wahid, N. M. Huang, *Sci. Rep.* **2018**, *8*, 7399.

[125] I. Kauppila, *All3DP, The Best Metal 3D Printers of 2022*, https://all3dp.com/1/3d-metal-3d-printer-metal-3d-printing (accessed: November 2022).

[126] A. Ambrosi, M. Pumera, *Adv. Funct. Mater.* **2018**, *28*, 1700655.

[127] D. Macquarrie, I. Chorkendorff, J. W. Niemantsverdriet, *Appl. Organomet. Chem.* **2005**, *19*, 696.

[128] X. Zhou, C. J. Liu, *Adv. Funct. Mater.* **2017**, *27*, 1701134.

[129] P. J. Kitson, S. Glatzel, W. Chen, C. G. Lin, Y. F. Song, L. Cronin, *Nat. Protoc.* **2016**, *11*, 920.

[130] P. J. Kitson, G. Marie, J. P. Francoia, S. S. Zalesskiy, R. C. Sigerson, J. S. Mathieson, L. Cronin, *Science* **2018**, *359*, 314.

[131] C. Zhu, Z. Qi, V. A. Beck, M. Luneau, J. Lattimer, W. Chen, M. A. Worsley, J. Ye, E. B. Duoss, C. M. Spadaccini, C. M. Friend, J. Biener, *Sci. Adv.* **2018**, *4*, eaas9459.

[132] S. Danaci, L. Protasova, F. Snijkers, W. Bouwen, A. Bengaouer, P. Marty, *Chem. Eng. Process.* **2018**, *127*, 168.

[133] S. Couck, J. Lefevere, S. Mullens, L. Protasova, V. Meynen, G. Desmet, G. V Baron, J. F. M. Denayer, *Chem. Eng. J.* **2017**, *308*, 719.

[134] S. Couck, J. Cousin-saint-remi, S. Van Der Perre, G. V Baron, C. Minas, P. Ruch, J. F. M. Denayer, *Microporous Mesoporous Mater.* **2018**, *255*, 185.

[135] H. L. Huynh, Z. Yu, *Energy Technol.* **2020**, *8*, 1901475.

[136] A. Gloria, T. Russo, R. De Santis, L. Ambrosio, *J. Appl. Biomater. Biomech.* **2009**, *7*, 141.

[137] V. Middelkoop, A. Vamvakeros, D. De Wit, S. D. M. Jacques, S. Danaci, C. Jacquot, Y. De Vos, D. Matras, S. W. T. Price, A. M. Beale, *J. CO2 Util.* **2019**, *33*, 478.

[138] S. Danaci, L. Protasova, J. Lefevere, L. Bedel, R. Guilet, P. Marty, *Catal. Today* **2016**, *273*, 234.

**ADVANCED
SCIENCE NEWS**

www.advancedsciencenews.com

**ADVANCED
MATERIALS
INTERFACES**

Open Access

www.advmatinterfaces.de

[139] S. Danaci, L. Protasova, V. Middelkoop, N. Ray, M. Jouve, A. Bengaouer, P. Marty, *React. Chem. Eng.* **2019**, *4*, 1318.

[140] P. Markewitz, W. Kuckshinrichs, W. Leitner, J. Linssen, P. Zapp, R. Bongartz, A. Schreiber, T. E. Müller, *Energy Environ. Sci.* **2012**, 7281.

[141] J. Gibbins, H. Chalmers, *Energy Policy* **2008**, *36*, 4317.

[142] N. Mac Dowell, P. S. Fennell, N. Shah, G. C. Maitland, *Nat. Clim. Change* **2017**, *7*, 243.

[143] H. Thakkar, S. Lawson, A. A. Rownaghi, F. Rezaei, *Chem. Eng. J.* **2018**, *348*, 109.

[144] J. E. Bara, C. I. Hawkins, D. T. Neuberger, S. W. Poppell, *Nanomater. Energy* **2013**, *2*, 235.

[145] S. N. Sluijter, J. Boon, J. James, S. Krishnamurthy, A. Lind, R. Blom, K. A. Andreassen, A. M. Cormos, V. C. Sandu, R. De Boer, *Int. J. Greenhouse Gas Control* **2021**, *112*, 103512.

[146] L. Zhao, G. Zeng, Y. Gu, Z. Tang, G. Wang, T. Tang, Y. Shan, Y. Sun, *Chem. Eng. Sci.* **2019**, *193*, 6.

[147] M. J. Regufe, A. F. P. Ferreira, J. M. Loureiro, A. Rodrigues, A. M. Ribeiro, *Microporous Mesoporous Mater.* **2019**, *278*, 403.

[148] H. Thakkar, S. Eastman, A. Al-mamoori, A. Hajari, A. A. Rownaghi, F. Rezaei, *ACS Appl. Mater. Interfaces* **2017**, *9*, 7489.

[149] B. Verougstraete, M. Schoukens, B. Sutens, N. Vanden Haute, Y. De Vos, M. Rombouts, J. F. M. Denayer, *Sep. Purif. Technol.* **2022**, *299*, 121660.

[150] T. Zheng, W. Zhou, D. Geng, Y. Li, Y. Liu, C. Zhang, *Int. J. Hydrogen Energy* **2020**, *45*, 14006.

[151] A. Soliman, N. Alamoodi, G. N. Karanikolos, C. C. Doumanidis, K. Polychronopoulou, *Nanomaterials* **2020**, *10*, 2198.

### 5.3.3 3D-printing technology towards emergency healthcare application

**Motivation**

3D-printing played a vital role during the COVID-19 pandemic by helping the health sector in printing face masks/shields, personal protection equipment, ventilators, nasal swab collectors, etc. As demand for the devices and equipment rose rapidly they were printed at several parts of the world in a short span of time. Such collaborative approach of 3D-printing industry along with the health community has enhanced the scope of this technology unfolding several other possibilities for the future.

**Objective**

This article outlines the contributions of 3D-printing technology from various sectors along with collaborative efforts from individuals and companies that resulted in forming an international grid to protect several lives during the COVID-19 pandemic health emergency.

**Outcome**

The article examines the key role played by 3D-printing technology during health emergencies, benefiting the medical community to fight the deadly pandemic situation. Articles reviewing such broader scope of the 3D-printing technology can aid in further realizing the potential of 3D-printing technique to fight emergency situations in the future as well.

**Contribution**

Writing (original draft, review and editing).

**Article**

The article was published and the details of the article are as follows:

Akshay Kumar K. Padinjareveetil, Martin Pumera*, *3D-Printing to Mitigate COVID-19 Pandemic*, **Adv. Funct. Mater**. 2021, 31, doi.org/10.1002/adfm.202100450, (IF=19.9).

# 3D-Printing to Mitigate COVID-19 Pandemic

*Kandambath Padinjareveetil Akshay Kumar and Martin Pumera**

3D-printing technology provided numerous contributions to the health sector during the recent Coronavirus disease 2019 (COVID-19) pandemic. Several of the 3D-printed medical devices like personal protection equipment (PPE), ventilators, specimen collectors, safety accessories, and isolation wards/chambers were printed in a short time as demands for these were rising significantly. The review discusses some of these contributions of 3D-printing that helped to protect several lives during this health emergency. By enlisting some of the significant benefits of using the 3D-printing technique during an emergency over other conventional methods, this review claims that the former opens enormous possibilities in times of serious shortage of supply and exceeding demands. This review acknowledges the collaborative approaches adopted by individuals, entrepreneurs, academicians, and companies that helped in forming a global network for delivering 3D-printed medical/non-medical components, when other supply chains were disrupted. The collaboration of the 3D-printing technology with the global health community unfolds new and significant opportunities in the future.

## 1. Introduction

3D-printing or additive manufacturing (AM) has gained phenomenal attention due to its scalable and rapid prototyping of 3D structures from various precursor materials.[1,2] Flexibility in structural design, waste minimization, mass customization, and complex architectural manufacturing are some of the notable features of this printing technique.[3,4] During the ongoing battle with the Coronavirus disease 2019 (COVID-19)

K. P. A. Kumar, Prof. M. Pumera
Future Energy and Innovation Laboratory
Central European Institute of Technology
Brno University of Technology
Purkyňova 123, Brno 61200, Czech Republic
E-mail: martin.pumera@ceitec.vutbr.cz
Prof. M. Pumera
Department of Chemistry and Biochemistry
3D Printing & Innovation Hub
Mendel University in Brno
Zemedelska 1, Brno 61300, Czech Republic
Prof. M. Pumera
Department of Chemical and Biomolecular Engineering
Yonsei University
50 Yonsei-ro, Seodaemun-gu, Seoul 03722, Korea
Prof. M. Pumera
Department of Medical Research
China Medical University Hospital
China Medical University
No. 91 Hsueh-Shih Road, Taichung 40402, Taiwan

The ORCID identification number(s) for the author(s) of this article can be found under https://doi.org/10.1002/adfm.202100450.

pandemic, this technology offered some of the best prototypes that has turned out to be exceedingly productive.[5,6]

COVID-19 is a severe acute respiratory syndrome (SARS) that was initially reported in Wuhan, China, and is rapidly spreading across the globe in no time.[7,8] The impact of which is so huge that the World Health Organization (WHO) has declared it as a pandemic on 12th March, 2020.[9] According to the WHO report, as of December 1, 2020, the number of cases reported globally is approximated to be 61.8 million. With a death rate of approximately 1.4 million, the situation remains acute even after a year, the case was first reported.[10] Leaving people clueless in the face of this invisible foe, this crisis is affecting both global health and economy in bizarre ways.[11] Surprisingly, people worldwide seem to have quickly adapted to the "new normal", stimulated by the pandemic, through regular sanitization, maintaining social distance, quarantining, and using personal protective equipment (PPE) as recommended by the WHO.[12,13]

The coronavirus initially affects the upper respiratory tracts leading to symptoms such as fever, dry cough, tiredness, shortness of breath, chest pain, muscle pain, hoarse voice, and diarrhea.[14] The extent of being infected by this virus is completely dependent on the immune system of individuals.[15] As per the available data, senior citizens, and people with multiple disease syndromes are more susceptible to COVID-19.[16] The mode of transmission can be either direct via aerosols, droplets of an infected individual, or indirect physical contact such as contaminated surfaces.[17,18] Airborne transmission of virus is found to be contagious like the droplet transmission, and the former has a longer lifespan in air.[17,19] COVID-19 is enlisted among the deadliest of diseases to have affected human life in the recent past,[20] along with others like smallpox, flu, plague, AIDS, H1N1, etc. The health emergency due to the non-availability of vaccines initially, in the case of the former had made the time more trying for the scientific community around the world.[21,22] Researches are focusing on the behavioral patterns of this virus with time as it shows continuous genetic mutation.[23–25] At present, scientists in top universities, institutes, and labs are working towards enhancing the mass distribution of clinically approved vaccines.[26,27] In the prevailing situation, lockdowns, self-isolation, and seeking the help of public health officials are the primary measures adopted to curb the spread of the virus, globally.[28,29] Those infected are being shifted to hospitals only if the situation worsens or due to the non-availability of isolation facilities.

Also, a sudden outbreak of the COVID-19 has led to an exponential increase in the number of people infected, leaving the global health care systems in deep stress.[30,31] Time constraints

**ADVANCED
SCIENCE NEWS**
www.advancedsciencenews.com

**ADVANCED
FUNCTIONAL
MATERIALS**
www.afm-journal.de

and unanticipated lockdowns has further resulted in the shortage of medical supplies and disruptions in the manufacturing and supply chain. The inadequacy of medical equipment such as PPE which includes masks, face shields, goggles, etc., and clinical care facilities such as ventilators and respirators has made the situation more challenging.[31–34] The increasing demand for medical staff and health workers is further magnifying the challenges, especially when, countries are still facing a severe shortage of medical equipment to support these health workers who have to attend to this situation $24 \times 7$.[35–37]

It is at this critical point, that the dependence on faster and efficient technologies, to meet the demands of the medical community, escalates. 3D-printing technology proved to be of enormous help by quickly responding to this unparalleled crisis by printing PPEs, medical devices, personal accessories, and also isolation wards.[6,38,39] Several research institutes, universities, companies, 3D-printing farms, and individuals working with 3D-printing technology came forward in fighting this pandemic by using their creative skills and also by collaborating with other sectors, to print medical equipment for hospitals and health workers.[40–44] The printable components were designed using software and printed directly from STL files which are easily accessible through websites or specific community sites. This method proved to be time-saving and at the same time ensures uniformity in the 3D-printed structures.[1,3,43,45]

In short, during the pandemic, 3D-printing has stood by the global community in overcoming the unexpected shortage of protective equipment. This review focuses on most of the contributions of the 3D-printing technology towards the health sector in the wake of this deadly pandemic. It includes discussions related to various 3D-printing techniques, prototypes for medical appliances, detailed analysis of printed parts, safety regulations, and certain shortcomings associated with this technique. We have incorporated the details on how 3D-printing techniques efficiently handled the pandemic over other conventional methods of printing. In short, the article examines how helpful 3D-printing technique can be in similar cases of emergency in the future as well.

## 2. 3D-Printing Overview

The idea of 3D-printing emerged in 1980's and thereafter, turned out to be revolutionary by printing objects and components that find applications in numerous fields.[4,46–48] This bottom-up approach offers a single step digitally controlled process of fabricating 3D structure in a layer-by-layer manner. The additive manufacturing (AM) technique is more user friendly due to its rapid production capacity, low waste generation, high accuracy, reproducibility, easy customization of shape and geometry, high durability, and usage of a wide range of printable materials, making this technique unique from others.[1–3]

Initially, a 3D structure is designed using a computer-aided design (CAD) software, or by 3D-scanner or by photogrammetry (a combination of images from different positions).[1,49] Successful designing is followed by conversion into a stereolithography file format (STL). The STL files undergo a slicing process and are converted to a G-code file that contains geometrical information about the structure as shown in **Figure 1**. In the final step, the printer starts printing 2D layers on top of each other to make a 3D structure as dictated by the G-code file.

3D-printing has been contributing phenomenally towards industry, academia, and is of relevance to various fields[47,50–54] and recently in handling pandemic.[5,6,39,55] Different types of printing techniques are available based on the printable material (metals, thermoplastics, carbon-based composites, ceramics), the complexity of printed structure, cost-effective approach, and targeted applications.[3]

### 2.1. Fused Deposition Modeling or Fused Filament Modeling

This approach, uses thermoplastic filaments that are melted/extruded, down the nozzle in a layer by layer stacked manner to form a final 3D-printed structure[53,56,57] as shown in **Figure 2**A. The functional active materials include thermoplastics such as polylactic acid (PLA), acrylonitrile butadiene styrene (ABS), polycarbonate (PC), polyamide, etc.
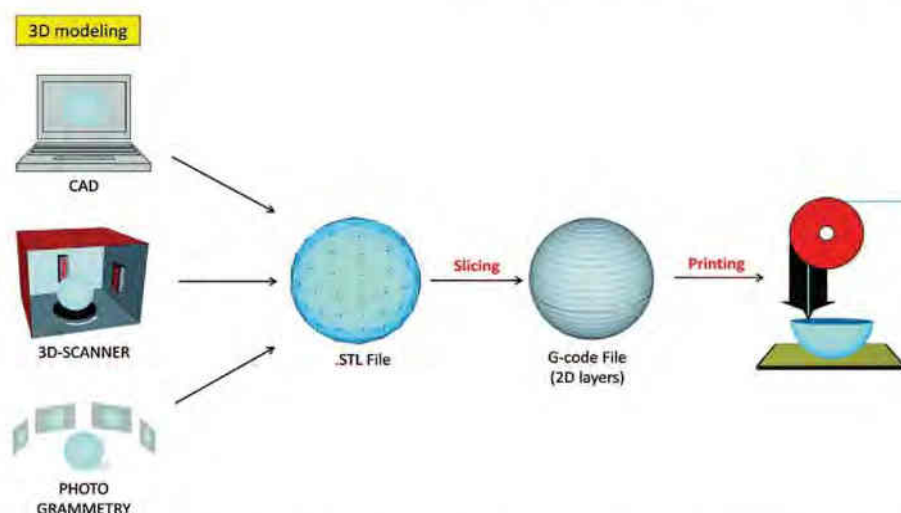


**Figure 1.** Steps involved in the 3D-printing of a desired object. Reproduced with permission.[1] Copyright 2016, Royal Society of Chemistry.
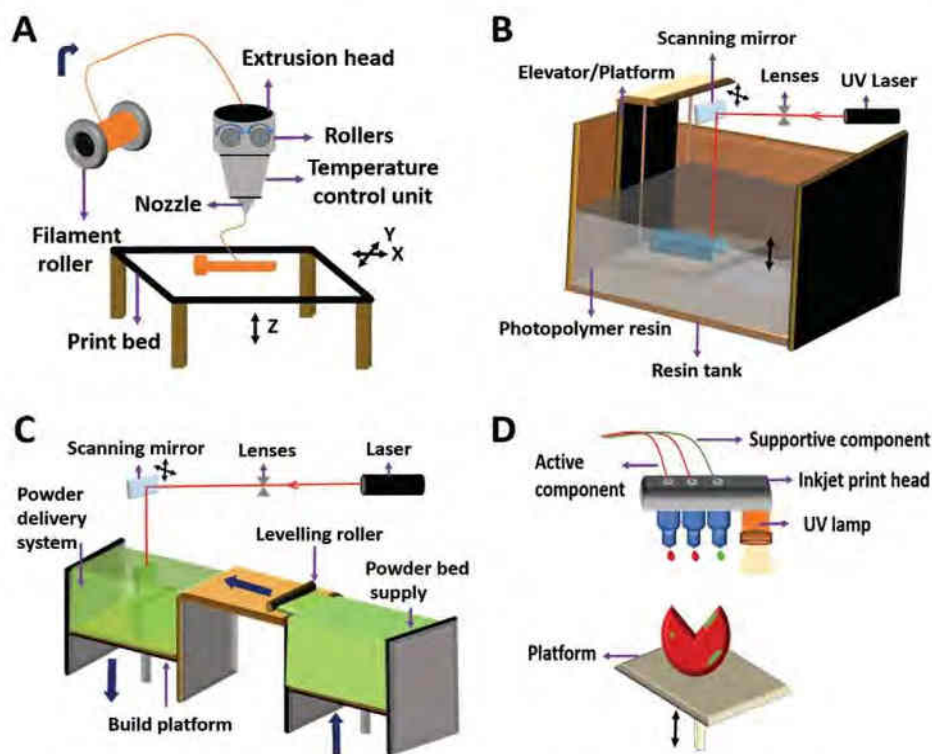
**Figure 2.** Schematic representation of various 3D-printing techniques. A) Fused deposition modeling (FDM). B) Stereolithography (SLA). C) Selective laser sintering (SLS). D) Polyjet technology. A–D) Adapted with permission.[47] Copyright 2020, Elsevier.

This technique is widely adopted due to its relative simplicity in printing and also because of the low cost of polymers. Copper-based filaments are also used for printing, which exhibits antiviral and antibacterial properties.[58,59] A discussion on these 3D-printed copper components and as coatings has been carried out in a few sections that follow (Sections 3.1, 3.5).

### 2.2. Vat Photopolymerisation

The rise of 3D-printing started with photopolymerization where it uses specific light sources to create 3D structures via selective curing of liquid photopolymer (resin). Stereolithography (SLA) uses UV light to focus on a thin film of photopolymer resin to solidify it to a 3D-printed structure[3,60] (Figure 2B). Digital light processing (DLP) also follows a similar pattern like SLA but uses a digital light source.[61]

### 2.3. Selective Laser Sintering

This method uses a powdery material (either nylon or polyamide) which is melted by thermal energy or laser heat source, into layers of a solid structure as shown in Figure 2C. The main advantage of selective laser sintering is that it doesn't require

any external support, hence it can easily produce designs, with complex geometries.[1,47]

### 2.4. Polyjet Technology

It is an alternative photocuring technique, where it uses inject methods to deposit photocurable multi-material structures as designed in layers and is followed by hardening these layer using UV light (Figure 2D). High-resolution flexible materials are printed mainly focused on fluidic devices.[1]

### 2.5. Multi Jet Fusion Technology

This is a printing technology that prints, by evenly heating a powder bed. Since this method does not use laser-based materials, it can print components with smooth surfaces, high density, and low porosity. This method produces functional parts which require limited finishing. The jetting of the fusing agent in portions where there has to be selectively molten particles, and jetting a detailing agent along the outline, improves the resolution of parts. When an energy source (a lamp in this case), is passed over the powder bed, the jetted materials capture the heat and distribute them within the system. This method has proved to have an upper hand over injection molding at multiple levels

ADVANCED
SCIENCE NEWS
www.advancedsciencenews.com

ADVANCED
FUNCTIONAL
MATERIALS
www.afm-journal.de

because of being cost-effective and producing prototypes with better mechanical properties.[62]

## 3. 3D-Printed Medical and Safety Devices

In the previous section, we have come across various 3D-printing techniques that are essential to device medical and hand free safety tools. In this section, we shall discuss how the digital printing world with the rapid prototyping ability of the tech community has been benefiting the health and scientific community in limiting the spread of the virus at a significant level. The 3D-printing of medical and safety devices extends from PPE to specimen collectors, isolation wards, and personal accessories printed by various enterprises.

### 3.1. Personal Protective Equipment

PPE helps to limit the spread of infection by protecting the user from airborne liquid contaminants/particles. It acts as a barrier between a healthy and an infected person. PPE includes face shields, facemasks, goggles, etc. The items are need-based and situational and therefore, find different purposes among individuals, health workers, and medical staff.

### 3.1.1. Face Shield (Class I)

The shortage of face shields was one of the critical challenges faced by medical staff especially during the interactions with patients. This protective equipment helps the user, by safeguarding their eyes and mouth from infectious airborne particles, droplets, splashes, and body fluids.[63,64] The face shields are printed using FDM, due to its simple geometry and improved choice of printable materials.[65] These 3D-printed frames contain a reusable headpiece and a plastic sheet attached to the frame that acts as a protective shield. Recently, Prusa, a well-known FDM manufacturer in the Czech Republic had 3D-printed nearly 200 000 face shields (**Figure 3**A) and donated them to medical practitioners and other professionals.[66] Also, during the pandemic, the engineering department of airline companies like Etihad collaborated with their own medical

wing to make 3D-printed face shields, using recyclable plastic, designed via SLS method, and supplied it to hospitals across UAE.[67] Celik et al.,[68] proposed designs of face shields that are lighter, simple to use, relatively more ergonomic, and avoids unnecessary components such as elastic bands, clips, etc. Each frame weighed < 10 g and was printed in a short time and showed remarkable productivity. A Canada based company called Next Generation Manufacturing Canada (NGen) invested more than $21 million in manufacturing companies to produce face shields, ventilators, and test kits in a limited time frame.[69]

### 3.1.2. Facemasks

Both N95 (class II by FDA) and surgical masks are used for protection against viruses and bacteria but differ in their filtration efficiency.[73–75] The efficiency of a 3D-printed mask is strictly correlated to its printing quality, facial anatomy, filters used, fitting, etc. 3D-printed N95 replacement masks with silicone cast masks that seal around the face of the user was proposed by Barrow neurological institute, (USA).[76] By making use of a 3M P100 filter, this model exhibits a high filtration rate and with an efficiency that can last up to three months. Replacing defective or broken bands by 3D-printed frames ensured a longer lifetime of masks in the case of both N95 and KN95 masks and also proved to be a better fit for the user.[77] CERN, the European Organization for Nuclear Research, followed all the regulatory and safety specifications similar to the surgical type I mask, to design 3D-printed flexible and washable masks with replaceable filters.[78] They also developed an alternative for 3D printers that lacks the capacity of printing flexible items, by separately printing a mould injected with silicon in a rigid plastic material. 3D-printed stopgap face masks are exclusively designed as a substitute to standard PPE, used only in cases of emergency or shortage.[79] These masks are 3D-printed using MJF, SLS using powder-bed nylon, or SLA using BioMed Clear.[80] Similar 3D-printing projects were also carried out to make 3D-printable masks, such as the Montana Mask and the Lowell makes mask. Montana mask is known for its high and effective filtration capacity and can also be easily printed on desktop machines.[81] They can also be sanitized after each use. Lowell makes mask,
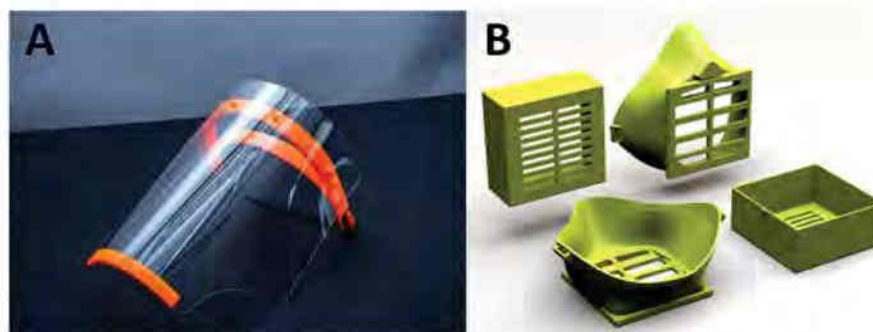


**Figure 3.** 3D-printed A) face shields from Prusa, Reproduced with permission.[66] Copyright 2021, Prusa Research a.s. B) Face masks from HEPA, Reproduced with permission.[70] Copyright 2020, Tovarna.Tech.

**ADVANCED
SCIENCE NEWS**
www.advancedsciencenews.com

**ADVANCED
FUNCTIONAL
MATERIALS**
www.afm-journal.de

being an alternative form of replaceable front filter designs, provides better and easy printing options with no support or adhesion.[82,83] Health workers are suggested to use full face snorkel masks connected using 3D-printed adaptor valves.[84,85] The use of a High-Efficiency Particulate Air (HEPA) filter makes this mask promising as well. However, conflicting results were obtained in the efficiency of snorkel masks in comparison to N95 respirators making their usage debatable and subjecting them to undergo further quality tests.[5] The use of PLA filaments as active materials to design HEPA masks (Figure 3B) was found to be interesting due to its replaceable filter port and better fitting, for both male and female users.[70] However, the fragile nature of PLA can harm the facial skin of the users in the case of an accident. Thingiverse user iczfirz, suggested a remedy by printing it on cloth, making it more flexible and comfortable.[86] Another notable method adopted for manufacturing 3D-printed masks was carried out using copper. Copper, known for its antimicrobial and antiviral properties in traditional as well as scientific societies has always found numerous applications in the field of biomedicine.[87,88] Studies suggest that copper, on reaction with oxygen, generates a reactive free radical that can effectively fight the virus.[89] Understanding the potentials of this metal, researchers and companies have made ample use of it in designing masks to fight the pandemic.[90] Copper 3D, a well-known US-based company has addressed the shortage of N95 masks using PLACTIVE and MDflex by FDM/FFF printing.[91] These printed masks known as NanoHack exhibited antiviral properties. Moreover, the same was modular, reusable, washable, recyclable, and cost-effective. To achieve the above mentioned target in minimum time, companies and other enterprises collaborated to manufacture 3D-printed copper masks.[92] An enterprise called Creality (China) also developed 3D-printed face masks, and 3D-printed face mask buckles which gives comfort and relief from pain in the ear of user.[71] They also donated a significant amount of their products to various hospitals.

### 3.1.3. Personalized 3D-Printed Masks

The severity of the pandemic has forced government agencies to ensure that their citizens wear masks. The uneasiness of adapting to this new accessory has caused several discomforts to the users and the gaps arising due to poor fitting of masks increases the chances of being infected. These discomforts also stem from the diversity of the facial anatomy of the users which differs from person to person. 3D-printed structures expect to bring a systematic resolution to these inadequacies with the use of 3D facial scanning software that can improve the fitting of the mask.[93] Personalized 3D printed face mask fitters were hence designed to improve the fit of the surgical masks, preventing fogging and better sealing. These mask fitters are customizable using a face app, developed by Bellus3D,[94] capable of capturing a 3D scan of the user's face to produce a 3D mask design file, which can subsequently be 3D printed. Imperial College London (UK) has also proposed ideas for creating customized face masks.[95]

### 3.1.4. Protective Eyewear

Safety goggles are used for sealing the eyes and giving them protection from the droplets of an infected individual. Boltian, a Spanish designer, designed protective goggles with 3D-printed frames.[96] The lens of this goggle was made using PVC or PC of 1 mm thickness. PVC can be cut easily, due to its flexible nature, either manually or by using a laser machine. Huaxiang, a Chinese company sketched a 3D design and printed it on the Farsoon 430P system. Sealing rings were made from LEHVOSS and transparent acrylic was used for lenses with an anti-fogging coating.[97] 3D-printed protective goggles were of huge help for hospitals in Wuhan, China, during massive shortage.[72]

### 3.2. 3D-Printed Medical Accessories

Mechanical ventilators are an essential secondary component that support patients experiencing difficulty in breathing. During the pandemic, even automobile companies such as Volkswagen manufactured 3D-printed ventilators which had benefited the concerned sectors.[98] Patients experiencing severe respiratory problems are incubated and treated in invasive mechanical ventilation (IMV) procedure.[99,100] Unfortunately, this procedure involves risking the patient's health (overdose of sedatives) and that of the health workers (risk of contamination) during intubation.[5,101,102] Hence, as per the recommendations of the WHO, patients are primarily subjected to a non-invasive ventilation (NIV) procedure such as continuous positive airways pressure (CPAP), which comparatively involves less risk.[103] HEPA filters, regarded as an improved safety measure, assist in the filtration of exhaled air after NIV. 3D-printed emergency valves such as ventilator valves are also among the key components that are being used during the pandemic to support a patient's breathing. Required concentrations of oxygen are given to patients via ventilator valves, connected to the patient's face masks.[83,104,105] At a time when the demand for 3D-printed valves for respirators was and is still on raise, in many parts of the world, a prompt action taken by an Italian engineering startup called Isinnova (Italy) proved to be life-saving. Isinnova 3D-printed what is called a venturi valve (**Figure 4A**), through reverse-engineering a design of the official part.[106,107] Though



**Figure 4.** A) 3D-printed venturi respirator valves by Italian company. Reproduced with permission[106] Copyright 2020, ISINNOVA S.R.L. B) Snorkeling EasyBreath masks connected to Charlotte Valves. Reproduced with permission.[107] Copyright 2020, ISINNOVA S.R.L.

**ADVANCED
SCIENCE NEWS**
www.advancedsciencenews.com

**ADVANCED
FUNCTIONAL
MATERIALS**
www.afm-journal.de

this method was of huge help to multiple hospitals in Italy, this prototype could not be widely distributed or used, due to quality concerns and copyright issues.

3D-printed connector valves named Charlotte Valves were designed by Isinnova, an Italian engineering company. Isinnova enhanced the Easybreath snorkeling mask from Decathlon using the Charlotte Valves, that when connected to an oxygen supply, performed like a functional ventilator (Figure 4B).[107] In case a reservoir is required, this model can also be equipped with a 3D-printed Dave valve. This approach was found to be a success, and attracted several companies, leading to a massive production via various printing techniques such as FFM, SLS, and SLA. Rosatom (Russia) also 3D-printed venturi valves which combined with aerosol masks, enabling the flow of oxygen at a low rate.[108]

### 3.2.1. Splitter

The sudden increase in the number of COVID patients during the pandemic caused a severe shortage of medical equipment such as ventilators as discussed in the above Section. 3D-printed splitters were of huge benefit in these circumstances since they could be used to supply oxygen to multiple patients at the same time using a single ventilator. Ayyıldız et al.,[109] 3D-printed two-port and four-port splitters using a 3D-printer with polyjet technology. Several experiments were carried out and it was concluded that two port splitters were more efficient for supplying airways using a single ventilator to more than one patient. In short, 3D-printed splitters were found to be an alternative to mechanical ventilators. While there are still concerns about the possible risks involved in using 3D splitters, several institutes, like Johns Hopkins University (USA),[110] Prisma Health[111] (a health organization in South Carolina, USA) and others have come up with innovative 3D-printed splitters that can be shared among multiple users. Some of which assure "free use", giving access to people across the world to print these designs and contribute to those concerned.

### 3.3. 3D-Printed Specimen Collectors

Test kits for COVID-19 is yet another significant medical apparatus that was widely used for confirmation of infection during the pandemic. The diagnosis is usually done using, either polymerize chain reaction (PCR) or antibody testing.[112,113] Nasal secretions from the nose and throat are collected by the nasopharyngeal (NP) swabs and oropharyngeal swabs. The former method was widely adopted and is a sensitive technique of virus detection in individuals.[114] During the initial days of the outbreak, there was a shortage of swabs, but in no time, this emergency was resolved using a novel 3D-printed swab. The University of South Florida's (USF), health collaborated (USA) with the Northwell Health to design 3D-printed alternative swabs via SLA as shown in **Figure 5**A,B.[115] These 3D-printed swabs are convenient tools that can strengthen the efficiency of sample collection, since they come up with complex tip structures, unlike swabs with flocks at the tips. They exhibit efficient flexibility, are sterilizable, durable, and are user friendly as they can be inserted



**Figure 5.** A) NP swabs designed using computer-assisted drawing (CAD) software. B) 3D-printed NP swabs produced in bulk, ready for post-processing. Reproduced with permission under the terms of the Creative Commons CC BY 4.0 license.[115] Copyright 2020, the Authors. Published by Springer Nature.

and removed easily by the medical professionals. EnvisionTEC engineers (Germany) designed a 3D printed collection tip for a flexible nasal swab which was 3D-printed in bulk, (hundreds of swabs in a single batch) and was rinsed in isopropanol, followed by dehydration for 30 min. The cooled swabs are irradiated with UV light and processed to check their quality to meet the required specifications. Finally, they are certified, sterilized, and dispatched to various health care units.[116–118]

FDM of polyethylene terephthalate glycol (PETG) filament using Prusa MK3s printer was carried out by Cox and Koepsell to fabricate 3D-printed swabs of 15 cm length and 600 mg weight.[119] They were clinically tested and were found to be similar to commercial swabs in performance. Another group, 3D-printed swabs with a domed tip possessing an open lattice design using direct light projection.[120] This showed that the 3D-printed swab with locally designed specifications was found to have a sensitivity and specificity of 89% and 92%, respectively. Also, 90% of the results obtained using 3D-printed swabs were found to be matching in comparison to the commercial one. Several companies came forward to 3D-print these swabs and extended their support to the medical community. Formlabs (USA),[121] 3D-printed swabs for PCR testing to support the medical crew in a US hospital and also shared their files with hospitals outside the USA. A well-known company Carbon (USA) quickly responded to the situation by designing and producing patient sampling swabs.[122] In short, 3D-printed nasopharyngeal swabs provide a cost-efficient and fast alternative to the standard NP swabs used for the COVID-19.

### 3.4. Isolation Chambers and Emergency Dwellings

Isolation of infected individuals and those under quarantine is a mandatory COVID protocol directed by the WHO.[123] However, the lack of facilities in the hospitals to isolate huge numbers of patients and individuals under observation increased the demand for an alternative solution. 3D printing of transitory dwellings to quarantine individuals was of huge advantage in these tough times. Since 3D-printed mobile wards require a shorter construction time, making this method more favorable for those in need.[5,6]
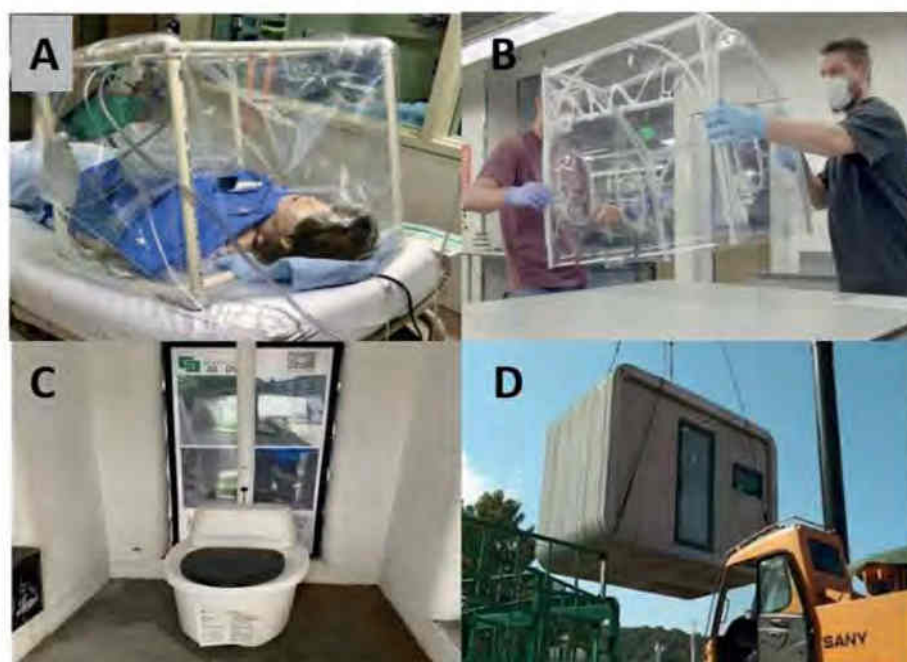
**Figure 6.** 3D-printed A) negative air flow isolation chamber. Reproduced with permission.[124] Copyright 2020, Elsevier. B) Isolation chamber from Texas A&M University (USA). Reproduced with permission.[125] Copyright 2021, Texas A&M University. C) Isolation wards with eco-friendly toilets. Reproduced with permission.[126] Copyright 2017, Yingchuang Building Technique (Shanghai) Co.Ltd. (WinSun). D) Mobile isolation wards. Reproduced with permission.[127] Copyright 2017, Yingchuang Building Technique (Shanghai) Co.Ltd. (WinSun).

Cubillos et al.[124] designed a cubical frame using PVC pipes and enveloped it with a plastic bag as shown in **Figure 6**A. Suction/vacuum mechanism was used inside the system to create a negative air flow isolation chamber, preventing the air outside the chamber from getting contaminated. Equipment was hanged inside the chamber on 3D-printed hooks and multiple ports were assigned for suction, oxygen delivery, and nebulization. A similar effort was done at the Texas A&M University (USA)[125] (Figure 6B), where 20 isolation chambers were designed to prevent the breath of incubated people from getting released to the surroundings. Since, virus transmission can also occur from the stool of infected individuals, 3D-printed isolation wards are also equipped with environmental friendly toilets (Figure 6C).[126] This method, therefore, ensures hygienic living during the isolation period. 3D-printed mobile homes, similar to isolation wards were printed in 2 hours (h) using concrete and recycled materials where each structure had an area of 10 m² and 2.8 m height. Reports also showed that the company printed nearly 200 wards (Figure. 6D) to house medical staff. Being mobile, these houses can be easily transported and electrified as per convenience.[127] WinSun/Yingchuan (China) transported nearly fifteen 3D-printed isolation wards to Pakistan to fight the pandemic.[128]

### 3.5. Hand Free Accessories and Antimicrobial Tools

The life-span of the COVID-19 virus differs significantly on various surfaces with an average stay of nearly 72 h.

They sustain for ≈3 h in the airborne droplets, 24 h on cardboard, and for a longer duration of up to 72 h over stainless steel and plastics.[129–132] High risk for contamination from the above situation through indirect contact at public places call for solutions that can reduce the risks. 3D-printed handfree tools work towards achieving this goal. To prevent direct contact with contaminated surfaces, Materialise (Belgium) 3D-printed door openers that can be opened using the elbow (**Figure 7**A) and button-pushers (Figure 7B).[133] François et al., have also developed hand-free door openers, door hooks, and button-pushers to prevent contamination.[134] Innovative inputs like, 3D-printed wrist band, to attach sanitizer was designed by an engineer from Saudi Arabia. The device, printed using the FDM approach, contains antiseptic gel attached to the wrist that can lather up the palms of the user without holding the bottle.[135]

Copper nanoparticles as coating over fabrics, cotton, polymers, etc. are commonly seen and are found to be effective in hindering the attacks of viruses like SARS CoV.[136] Copper is predominantly used as a coating material rather than being employed as a bulk material. This is due to the fact that the direct 3D-printing of copper is tedious due to the high conductivity of copper which results in thermal issues.[137] A similar approach was adopted where cold spraying technique was used to coat copper over steel parts to eradicate the virus from these surfaces.[138] The ability of copper in fighting viruses and bacteria are evident from the above examples and it is anticipated that their use shall lead to highly improved mechanisms that can limit contamination from viruses similar to COVID-19.

**ADVANCED
SCIENCE NEWS**
www.advancedsciencenews.com

**ADVANCED
FUNCTIONAL
MATERIALS**
www.afm-journal.de

**Figure 7.** 3D-printed A) door opener B) button pushers from Materialise to prevent contact from a contaminated surface. Reproduced with permission.[133] Copyright 2021, Materialise.

Doremalen, in his studies, showed that the stability of the virus over copper is limited to 4 h.[131] Therefore, the antimicrobial property of copper was used as a preventive measure against COVID-19 virus. A similar idea of using copper foils to coat doorknobs and the elevator buttons of buildings was carried out by the Ministry of Science and Technology of Taiwan.[139]

### 3.6. 3D-Printed Respiratory Swabs Simulators (Medical Manikin) and Visualization Aid

The pressing demand for trained staff to collect swabs during the pandemic was yet another critical situation that sought urgent attention. Since the number of individuals infected was huge, governments had to take the help of even non-professionals and train them to collect swabs, to increase the rate of testing. As can be understood, this requires a massive and effective task force, primarily for training individuals. 3D-printed respiratory swabs simulators or bio models

were of immediate help in these worrying times as shown in **Figure 8**A–D.[140]

To aid healthcare workers to perform swab testing, transparent 3D-printed respiratory swabs simulators that projected the internal structures were provided to the trainees for performing trials.[140,141] This ensured that these trained workers would work efficiently while collecting the samples without causing discomfort to those being tested. Visual and tactile education models were 3D-printed to educate visually challenged individuals for getting a better understanding of various structures.[142]

### 3.7. Data Sharing and Contributors

CAD, STL files related to 3D-printing medical accessories are readily shared with users in specific websites,[70,86,121] social media,[143,144] or at file repositories[45,145–147] saving a lot of time for the user in designing. Several institutes/community came
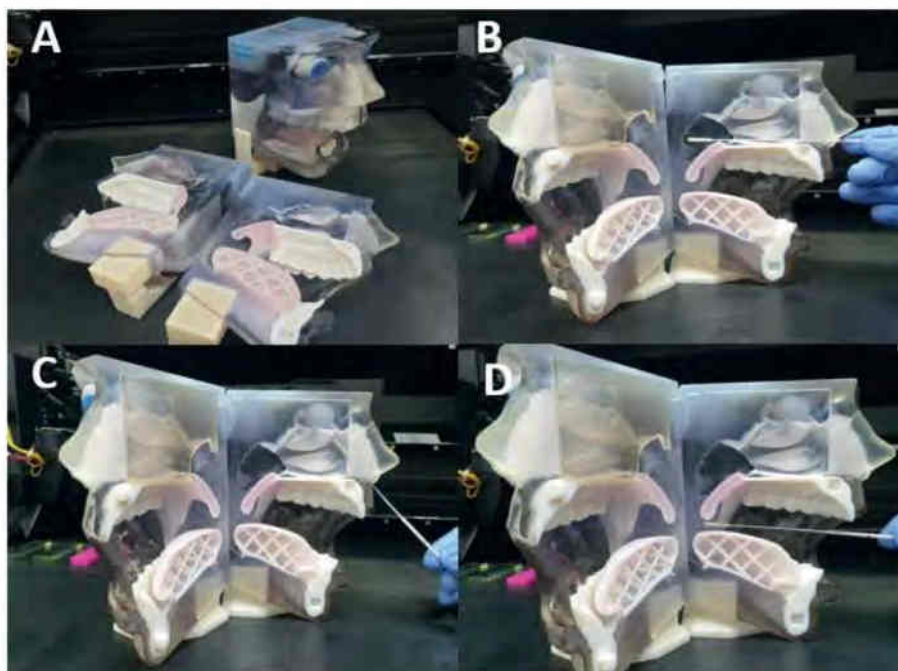


**Figure 8.** A–D) 3D-printed respiratory swabs simulators for swab collection from Creatz3D and Aumed (Singapore). Reproduced with permission.[140] Copyright 2021, AuMed.

**ADVANCED
SCIENCE NEWS**
www.advancedsciencenews.com

**ADVANCED
FUNCTIONAL
MATERIALS**
www.afm-journal.de

forward to print 3D-medical components to fight the pandemic of which few are listed as:

1) Print farms in USA, Europe, and China has contributed to printing during the pandemic to address the needs of the masses. Barcelona-based BCN3D (Spain) contributed their 63 in-house print farm to fight the pandemic.[148,149] Airwolf3D (USA) contributed towards pandemic by printing face shield, valves and other medical components.[150]

2) Universities such as the University of Washington (USA), Case Western Reserve University (USA), University of Tennessee (USA), Swansea University (UK), University of Hull (UK), Czech Technical University (Czech Republic), Brno University of Technology (Czech Republic), Michigan State University (USA), and Penn State University (USA) are a few to list[40,151,152]

3) Industries and Companies like Formlabs (USA, Spain),[121] Carbon (USA),[122] Desktop Metal (USA),[153] 3D Systems (Australia, Belgium, China, France, Italy, Netherlands, UK, USA),[154] Stratasys (US, Israel),[155] Johnson and Johnson (Ireland, Switzerland, UK, China & USA),[156] HP Inc. (Spain, US, Japan, and Europe),[157] Markforged (USA)[158] are leading the way with their machines and materials.[43]

Many notable designs were also found from repository files such as NIH 3D Print Exchange,[45] Grab CAD,[146] Thingiverse,[86] and projects from Creality,[159] Prusa,[66] Isinnova,[107] Materialise,[160] etc.

### 3.8. Regulatory Bodies

Though several countries have softened their safety and regulatory laws regarding medical devices due to the continuing medical emergency, the welfare and safety of individuals cannot be negotiated. Thus, designers and manufacturers of 3D-printing devices must maintain the safety regulations, dictated by various governmental bodies,[161–163] as they are still not waived off completely. Designers must use approved materials and ensure the basic quality of the materials used, based on the international risk classification system.[164] This includes documentation of pre and post-manufacturing processes,

running through ISO 13485-compliant quality-management system, and an internationally standardized biocompatibility check. Complying to these regulatory guidelines, guarantees trust among users of 3D-printed medical devices.[6] Other than these procedures of approval and certifications, concerned agencies must rectify issues of copyright violations. As confusions at these levels between various players of the market lead to slowing down of responses to the urgency and can risk lives. Therefore, manufacturers of 3D-printed medical devices must synchronize their production work with concerned sectors for accountability, quality, and safety assurance.

### 3.9. More 3D-Printed Devices

**Table 1** represents various 3D-printed components printed during the pandemic to support the global shortage of supply.[166–206]

### 3.10. 3D-Printing Versus Conventional Methods in COVID Times

The 3D-printing industry proved to be an efficient counterpart to the conventional methods of manufacturing during the COVID-19 pandemic. More than a question of contestation, 3D-printing sought only to enhance or parallelly co-exist with the existing printing techniques, in most cases during the emergency.[207] Both 3D-printing and traditional techniques were employed to tackle the pandemic. Having said that, this does not minimize the advantages that 3D-printing has over other conventional modes of printing, especially in cases of emergency. By producing health-care accessories in minimum time and reduced cost, this method proved to be beneficial at several levels. Traditional manufacturing (subtractive manufacturing) involves carving the desired structure out of a bulk material.[208,209] The end product obtained is cut down into several parts and are later put together. The excess waste generated during manufacturing, and the high complexity associated with the products, makes this technique highly expensive and limits its usage especially during times of emergency. Kunkel et al.,[210] put forth a comparative study between the two

**Table 1.** Table showing 3D-printed components printed using various techniques to fight the pandemic. (FDM-Fused deposition modeling, SLA-Stereolithography, SLS-Selective laser sintering, MJF-Multi Jet Fusion technology, Polyjet technology).

| 3D-Printed parts and their components | 3D-printing techniques | | | | |
|---|---|---|---|---|---|
| | FDM | SLA | SLS | MJF | Polyjet |
| Face shield | [66,165–168] | [154,168–171] | [154,172,173] | [157,174–176] | |
| Facemasks | [152,177–181] | | [80] | [80,174,182] | [183] |
| Facemask straps and fitter | [94,165,184–186] | [187] | | [174] | |
| Respirator (N-95 or similar) | [42,84,188,189] | | [190] | [191] | |
| Safety goggles | [97] | [97] | [97,192] | | |
| Valves / Ventilator | [193,194] | [194,195] | [154,196,197] | | [5] |
| Nasopharyngeal swabs | [119,198,199] | [199,200] | [201] | [202,203] | |
| Hand-free tools | [134,160,204,205] | | [160] | [160,174] | [134] |
| Camera mounts | [206] | | | | |

**ADVANCED
SCIENCE NEWS**
www.advancedsciencenews.com

**ADVANCED
FUNCTIONAL
MATERIALS**
www.afm-journal.de

techniques which suggests that while conventional methods of manufacturing, like injection molding, were able to produce a large number of products through a centralized mechanism, the initiation of process took more time and was expensive. Further, the products made could not be quickly accessed by hospitals due to the disruption in supply chain because of the pandemic. A major setback to the traditional manufacturing industry was felt due to the shutting down of factories and shortage of laborers during the pandemic and the lockdown that followed. 3D-printing, on the other hand, was quicker in manufacturing emergency medical equipment, such as the PPE, ventilators, test kits, emergency dwellings, medical accessories, etc. through rapid prototyping, from multiple locations, at a cheaper rate during COVID-19.[6,165,211] The time required for delivering these 3D-printed products was also lesser, since 3D-printing services functioned as a network where individuals, institutions, and companies usually collaborated in aiding the health sector and ensured faster delivery. A significant service was done using 3D-printed drones that helped in delivering medical equipment swiftly during the COVID-19 pandemic.[212] Another study also observed that a combination of both the methods (3D-printing and injection molding), especially reduces the cost and enhances the production speed of printing.[40,213,214]

Other findings also note that 3D-printing reduces the shipping and manufacturing costs and around 70% of prototyping costs involved in traditional manufacturing.[215] The digitally-enabled mechanisms of 3D printing techniques cut shorts a number of these processes, and thereby can be accessed at a cheap rate from any part of the world.[165,216] Generally, the cost involved in the updation of the product remains the same in case of 3D-printing at all stages, and also the product can be improved multiple times before its mass production at the initial cost itself. At a time of ample shortage and rising demands like the pandemic, conventional methods fail to deliver an immediate response, since, repeating the process of manufacturing takes more time via this method.[211] Also, a minor change in one of the parts can affect the whole design, in the case of conventional methods. The method, therefore, does not look ideal in case of an emergency. The cost of complexity is lesser in the case of 3D-printing since it creates a finished product in a single step, aborting the assembling process involved in conventional printing which reduces the labor cost and time as well. The speed of manufacturing the finished products is faster in comparison to the traditional manufacturing as well.[215] Hence, 3D-printing technology proves to be highly advantageous in order to handle exigencies like the current pandemic. Further advancements in this field can therefore, offer quality results in the future.

## 4. Limitations

Though 3D-printing of medical devices played a vital role in handling this health emergency, like any other technological innovation, this method also has certain flip sides that has to be addressed for future advancements. One of the drawbacks is the evasion of prime concerns like safety and legal precautions due to the rapid 3D-printing of medical devices to meet the urgent requirements during the pandemic. Since these devices are primarily used for medical purposes, safety of these printed equipment must be ensured.[161–163,217] Also, due to the same reason of being rapidly produced, manufacturers tend to show negligence towards biocompatibility and sterilizability of these printed medical devices. Since all this equipment is of long term use, it is important to have them clinically approved because even a small piece of defective equipment can harm the life of a medicated person.[115,218,219] As getting, sanitary and medical clearance from concerned authorities involves several formalities, hospitals are compelled to use unlicensed medical equipment from companies, due to the time constraints, during the emergency. At the same time, unlicensed products, randomly distributed at hospitals by the companies, can also get rejected due to lack of safety information about the printed medical equipment. This results in a wastage of time and resources, at the manufacturer's end. Hence, the concerned agencies must consider these things before the mass production of 3D-printed medical devices.[220]

Getting a legal sanction of printed materials, processing and clinical testing takes a lot of time and is expensive.[64] Since the demand for medical equipment during the COVID-19 pandemic was huge, the delay in approval from concerned authorities was another significant challenge that slowed down the procedures. Legal sanctions are also tied with ethical issues, especially while testing these 3D-printed devices for human compatibility which involves consent from concerned individuals. Using non-human entities for testing, in case of urgency also involves moral concerns.[6]

3D-printing of medical devices from the same STL file may aberrate from its standard configuration due to the variations in printable material, printer, and software used by different manufacturers. The failure in reproducing uniform structures can alter the physical properties of these printed materials, creating a confusion of choice among users. This dilemma about the approved configuration, may reduce printing efficiency, wastage of manpower, resources, and may come at varying costs.[165,221] Also, poor interface and unsealed protective covers may arise during printing, minimizing the quality of protection.[2] Regulation of customized 3D-printed face masks remains a significant limitation, though it ensures better fitting than the commercially available ones. Although primarily, this technology uses certain regulatory metrics such as fitness and filtering efficiency,[222] the lack of proper fit testing for individual masks, shall increase the chances of getting affected by the virus.[223] Hence, it reduces the overall filtering efficiency of these masks. Therefore, only a stringent evaluation of each of these individual masks would ensure improved safety which has to be monitored using both quantitative and qualitative fit tests, long-term stability tests, and checking its airborne particle protection levels.[224] Also, the medical community is unaware of the living conditions of people who are printing this medical equipment. If he/she happens to be an infected individual, then there are chances that the equipment printed by him/her may get contaminated and would risk the lives of others using it.

Choice of a functional material for printing includes thermoplastic filaments, powders, ceramics, metals, and many others. However, a study showed that 3D-printing respirators using FFF and powder bed fusion method showed low filtering

efficiency towards COVID-19 virus.[225] Studies that use ceramic and metal-based active materials as 3D-printing medical components have not been undertaken yet. This might be due to the high cost involved in the 3D-printing of metals.[5]

## 5. Conclusions and Future Prospective

This review is an account of the multiple ways in which 3D-printing benefited the medical community during a sudden disruption in supply. The various ways in which the COVID-19 pandemic affected the general nature of life on earth is immeasurable. Perhaps, only a "post COVID world" would tell us what has changed for the global community. One of the major impacts was felt on the global health care systems itself. The methods available to control the spread of the virus were too limited initially, due to obvious reasons of COVID-19 being a health emergency. The virus's unpredictable behavior, as it underwent repeated genetic mutation made the situation even harder for the global health communities. Since, the mass distribution of vaccines which has been recently developed, such as, Covishield (UK), Sputnik V (Russia), Moderna COVID-19 Vaccine (US), Covaxin (INDIA), CoronaVac (China), etc.,[226] is still underway, there has to be a feasible solution to reduce the death rate and methods to control the virus' spread. Hence, the significance of 3D-printed safety equipment remains, until the full-fledged distribution is achieved. 3D-printing technology offered enormous possibilities in these difficult times that proved to be life-saving. The shortage of medical devices and other components were resolved using a wide variety of 3D-printed structures. Equipment like face shields, facemasks, goggles, swabs, isolation wards, ventilators, splitters were 3D-printed in a limited time to meet the demands of hospitals and other concerned authorities. Rapid prototyping with customized fabrication and a low amount of waste makes 3D-printing an acceptable approach to meet various demands in a short period. Addressing a few challenges related to safety and approval of materials, quality concerns, legal and ethical issues, etc. shall certainly guarantee better advancements in this sector. Meanwhile, the timely involvement of universities, labs, companies, and entrepreneurs has improved the production of 3D printed equipment.

However, concerns on whether 3D-printing technology shall effectively replace the existing modes of conventional printing is still prevailing. Perhaps, we would suggest 3D-printing method to be a parallel technology of printing rather than a replacement of conventional mass production methods such as injection molding. 3D-printing proved to be efficient in situations of emergency like the current pandemic, when the supply-chain was interrupted, and conventional methods, found difficulty in transporting the products in a limited span of time. Due to its rapid prototyping ability, quick delivery through organized networks, ease in installation and accessing the designs from the internet from any part of the world, this technology came in handy during this unprecedented emergency. This method is cost-effective in terms of materials used and labor as well. However, for large scale production in a limited amount of time, the conventional methods still have an upper hand. Perhaps, the speed at which 3D-printing

is evolving, to go by the existing research, the conditions are promising. It is expected that this technology shall advance and will play a major role in industry, academics, and everyday life.

The use of bioactive material for 3D-printing is expected to open enormous possibilities in handling future pandemics as well. This is also true in the case of ceramic and metal-based active materials for 3D-printing. Studies on the use of bio-inks for bio-printing is at their initial stage now and if explored, would be a great contribution towards regenerative medicine. Thus, the COVID-19 pandemic facilitates itself to be a suitable case of recognizing collaborative approaches of 3D-printing technology for future prospects as well.

## Conflict of Interest

The authors declare no conflict of interest.

[1] A. Ambrosi, M. Pumera, *Chem. Soc. Rev.* **2016**, *45*, 2740.
[2] T. D. Ngo, A. Kashani, G. Imbalzano, K. T. Q. Nguyen, D. Hui, *Compos. Part B Eng.* **2018**, *143*, 172.
[3] M. P. Browne, E. Redondo, M. Pumera, *Chem. Rev.* **2020**, *120*, 2783.
[4] N. Shahrubudin, T. C. Lee, R. Ramlan, *Procedia Manuf.* **2019**, *35*, 1286.
[5] G. A. Longhitano, G. B. Nunes, G. Candido, J. V. L. da Silva, *Prog. Addit. Manuf.* **2020**, *6*, 19.
[6] Y. Y. C. Choong, H. W. Tan, D. C. Patel, W. T. N. Choong, C. H. Chen, H. Y. Low, M. J. Tan, C. D. Patel, C. K. Chua, *Nat. Rev. Mater.* **2020**, *5*, 637.
[7] B. Hu, H. Guo, P. Zhou, Z. L. Shi, *Nat. Rev. Microbiol.* **2021**, *19*, 141.
[8] T. Burki, *Lancet. Infect. Dis.* **2020**, *20*, 1018.
[9] World Health Organization, *WHO Director-General's opening remarks at the Mission briefing on COVID-19 –12 March 2020*, https://www.who.int/director-general/speeches/detail/who-director-general-s-opening-remarks-at-the-mission-briefing-on-covid-19---12-march-2020 (accessed: June 2020).
[10] World Health Organization, *Weekly epidemiological update –1 December 2020*, https://www.who.int/publications/m/item/weekly-epidemiological-update---1-december-2020 (accessed: December 2020).

**ADVANCED
SCIENCE NEWS**
www.advancedsciencenews.com

**ADVANCED
FUNCTIONAL
MATERIALS**
www.afm-journal.de

[11] World Health Organization, *Impact of COVID-19 on people's livelihoods, their health and our food systems*, https://www.who.int/news/item/13-10-2020-impact-of-covid-19-on-people's-livelihoods-their-health-and-our-food-systems (accessed: October 2020).

[12] World Health Organization, *COVID-19: "new normal"*, https://www.who.int/publications/m/item/weekly-epidemiological-update---1-december-2020 (accessed: August 2020).

[13] R. Mitchell, G. Nou, *Lancet Reg. Heal. – West. Pacific* **2020**, *1*, 100012.

[14] C. Menni, A. M. Valdes, M. B. Freidin, C. H. Sudre, L. H. Nguyen, D. A. Drew, S. Ganesh, T. Varsavsky, M. J. Cardoso, J. S. El-Sayed Moustafa, A. Visconti, P. Hysi, R. C. E. Bowyer, M. Mangino, M. Falchi, J. Wolf, S. Ourselin, A. T. Chan, C. J. Steves, T. D. Spector, *Nat. Med.* **2020**, *26*, 1037.

[15] M. A. Chowdhury, N. Hossain, M. A. Kashem, M. A. Shahid, A. Alam, *J. Infect. Public Health* **2020**, *13*, 1619.

[16] MAYO CLINIC, *COVID-19: Who's at higher risk of serious symptoms?*, https://www.mayoclinic.org/diseases-conditions/coronavirus/in-depth/coronavirus-who-is-at-risk/art-20483301 (accessed: November 2020).

[17] World Health Organization, *Modes of transmission of virus causing COVID-19: implications for IPC precaution recommendations*, https://www.who.int/news-room/commentaries/detail/modes-of-transmission-of-virus-causing-covid-19-implications-for-ipc-precaution-recommendations (accessed: August 2020).

[18] M. A. Shereen, S. Khan, A. Kazmi, N. Bashir, R. Siddique, *J. Adv. Res.* **2020**, *24*, 91.

[19] K. Nissen, J. Krambrich, D. Akaberi, T. Hoffman, J. Ling, Å. Lundkvist, L. Svensson, E. Salaneck, *Sci. Rep.* **2020**, *10*, 19589.

[20] V. Nueangnong, A. A. S. Hasan Subih, H. M. Al-Hattami, *Cogent Soc. Sci.* **2020**, *6*, 1818936.

[21] K. R. Myers, W. Y. Tham, Y. Yin, N. Cohodes, J. G. Thursby, M. C. Thursby, P. Schiffer, J. T. Walsh, K. R. Lakhani, D. Wang, *Nat. Hum. Behav.* **2020**, *4*, 880.

[22] S. H. Subramanya, B. Lama, K. P. Acharya, *Qatar Med. J.* **2020**, *2020*, https://doi.org/10.5339/qmj.2020.21.

[23] R. West, S. Michie, G. J. Rubin, R. Amlôt, *Nat. Hum. Behav.* **2020**, *4*, 451.

[24] D. S. Hui, E. I. Azhar, T. A. Madani, F. Ntoumi, R. Kock, O. Dar, G. Ippolito, T. D. Mchugh, Z. A. Memish, C. Drosten, A. Zumla, E. Petersen, *Int. J. Infect. Dis.* **2020**, *91*, 264.

[25] S. Reardon, *The U.K. Coronavirus Mutation Is Worrying but Not Terrifying*, https://www.scientificamerican.com/article/the-u-k-coronavirus-mutation-is-worrying-but-not-terrifying/ (accessed: December 2020).

[26] N. Nature, *COVID research updates: A coronavirus vaccine shows lasting benefit*, https://www.nature.com/articles/d41586-020-00502-w (accessed: December 2020).

[27] World Health Organization, *COVID-19 vaccines*, https://www.who.int/emergencies/diseases/novel-coronavirus-2019/covid-19-vaccines (accessed: December 2020).

[28] N. S. Diffenbaugh, C. B. Field, E. A. Appel, I. L. Azevedo, D. D. Baldocchi, M. Burke, J. A. Burney, P. Ciais, S. J. Davis, A. M. Fiore, S. M. Fletcher, T. W. Hertel, D. E. Horton, S. M. Hsiang, R. B. Jackson, X. Jin, M. Levi, D. B. Lobell, G. A. McKinley, F. C. Moore, A. Montgomery, K. C. Nadeau, D. E. Pataki, J. T. Randerson, M. Reichstein, J. L. Schnell, S. I. Seneviratne, D. Singh, A. L. Steiner, G. Wong-Parodi, *Nat. Rev. Earth Environ.* **2020**, *1*, 470.

[29] World Health Organization, *Coronavirus disease (COVID-19) advice for the public*, https://www.who.int/emergencies/diseases/novel-coronavirus-2019/advice-for-public (accessed: December 2020).

[30] D. Guan, D. Wang, S. Hallegatte, S. J. Davis, J. Huo, S. Li, Y. Bai, T. Lei, Q. Xue, D. M. Coffman, D. Cheng, P. Chen, X. Liang, B. Xu, X. Lu, S. Wang, K. Hubacek, P. Gong, *Nat. Hum. Behav.* **2020**, *4*, 577.

[31] K. R. Tuttle, *Nat. Rev. Nephrol.* **2020**, *16*, 562.

[32] M. L. Ranney, V. Griffeth, A. K. Jha, *N. Engl. J. Med.* **2020**, *382*, e41.

[33] N. Karim, S. Afroj, K. Lloyd, L. C. Oaten, D. V. Andreeva, C. Carr, A. D. Farmery, I. D. Kim, K. S. Novoselov, *ACS Nano* **2020**, *14*, 12313.

[34] *BDJ Pract* **2020**, *33*, 6, https://doi.org/10.1038/s41404-020-0410-z.

[35] O. Goldhill, *People are going to die': Hospitals in half the states are facing a massive staffing shortage as Covid-19 surges*, https://www.statnews.com/2020/11/19/covid19-hospitals-in-half-the-states-facing-massive-staffing-shortage/ (accessed: November 2020).

[36] A. Al Thobaity, F. Alshammari, *Dubai Med. J.* **2020**, *3*, 87.

[37] K. Houghton, *COVID-19 infections causing health care worker shortages*, https://apnews.com/article/pandemics-virus-outbreak-health-helena-montana-71b4a1f83cf6e2d6c97cba6613085d23 (accessed: November 2020).

[38] FDA, *3D Printing in FDA's Rapid Response to COVID-19*, https://www.fda.gov/emergency-preparedness-and-response/coronavirus-disease-2019-covid-19/3d-printing-fdas-rapid-response-covid-19 (accessed: November 2020).

[39] N. Bharti, S. Singh, *ACS Chem. Heal. Saf.* **2020**, *27*, 335.

[40] R. C. Advincula, J. R. C. Dizon, Q. Chen, I. Niu, J. Chung, L. Kilpatrick, R. Newman, *MRS Commun.* **2020**, *10*, 413.

[41] MUSC Medical University of South Carolina, *SAFE Cartridge Systems and Mask*, https://web.musc.edu/innovation/covid-19-innovation/safe-cartridge-system-and-masks (accessed: May 2020).

[42] Barrow Neurological Institute, *3D-printed N95 replacement mask*, https://www.barrowneuro.org/get-to-know-barrow/barrow-innovation-center-2/3d-printed-n95-mask/ (accessed: August 2020).

[43] World Economic Forum, *3D Printing COVID-19 Rapid Response Initiative*, https://www.weforum.org/platforms/covid-action-platform/projects/3d-printing-covid-19-rapid-response-initiative (accessed: September 2020).

[44] 3DGence, *How 3D printing can affect your broken supply chain during the crisis caused by the Covid-19 outbreak?*, https://3dgence.com/3dnews/how-3d-printing-can-affect-your-broken-supply-chain-coronavirus/ (accessed: August 2020).

[45] NIH 3D Print Exchange, *COVID-19 Supply Chain Response*, https://3dprint.nih.gov/collections/covid-19-response (accessed: September 2020).

[46] H. J. Steenhuis, X. Fang, T. Ulusemre, *Int. J. Innov. Technol. Manag.* **2020**, *17*, 2050005.

[47] J. Muñoz, M. Pumera, *TrAC – Trends Anal. Chem.* **2020**, *128*, 115933.

[48] C. Barnatt, *3D Printing: The Next Industrial Revolution*, ExplainingTheFuture.com **2013**.

[49] T. Mikolajczyk, T. Malinowski, L. Moldovan, H. Fuwen, T. Paczkowski, I. Ciobanu, *Procedia Manuf* **2019**, *32*, 22.

[50] K. P. A. Kumar, K. Ghosh, O. Alduhaish, M. Pumera, *Electrochem. Commun.* **2021**, *122*, 106890.

[51] F. Zhang, M. Wei, V. V. Viswanathan, B. Swart, Y. Shao, G. Wu, C. Zhou, *Nano Energy* **2017**, *40*, 418.

[52] J. C. Bui, J. T. Davis, D. V. Esposito, *Sustain. Energy Fuels* **2019**, *4*, 213.

[53] K. P. A. Kumar, K. Ghosh, O. Alduhaish, M. Pumera, *Electrochem. Commun.* **2020**, *120*, 106827.

[54] F. Novotný, V. Urbanová, J. Plutnar, M. Pumera, *ACS Appl. Mater. Interfaces* **2019**, *11*, 35371.

[55] J. Izhakoff, *3D Printing in a Pandemic*, https://healthadvancesblog.com/2020/04/16/3d-printing-in-a-pandemic/ (accessed: August 2020).

[56] M. Belka, S. Ulenberg, T. Bączek, *Anal. Chem.* **2017**, *89*, 4373.

[57] E. Mathew, J. Domínguez-Robles, S. A. Stewart, E. Mancuso, K. O'Donnell, E. Larrañeta, D. A. Lamprou, *ACS Biomater. Sci. Eng.* **2019**, *5*, 6300.

**ADVANCED
SCIENCE NEWS**
www.advancedsciencenews.com

**ADVANCED
FUNCTIONAL
MATERIALS**
www.afm-journal.de

[58] J. J. Coté, J. Haggstrom, R. Vivekanandan, K. A. Coté, D. L. Real, D. P. Weber, A. Cheng, N. G. Dubay, R. Farias-Eisner, *3D Print. Med.* **2020**, *6*, 20.

[59] D. Sher, *Copper3D organizing global campaign to 3D print antimicrobial masks on a global scale*, https://www.3dprintingmedia.network/copper3d-organizing-global-campaign-to-3d-print-antimicrobial-masks-on-a-global-scale (accessed: August 2020).

[60] X. Xu, P. Robles-Martinez, C. M. Madla, F. Joubert, A. Goyanes, A. W. Basit, S. Gaisford, *Addit. Manuf.* **2020**, *33*, 101071.

[61] H. Quan, T. Zhang, H. Xu, S. Luo, J. Nie, X. Zhu, *Bioact. Mater.* **2020**, *5*, 110.

[62] *Materialise, Powder based 3D printing, without the lasers*, https://www.materialise.com/en/manufacturing/3d-printing-technology/multi-jet-fusion (accessed: February 2021).

[63] R. J. Roberge, *J. Occup. Environ. Hyg.* **2016**, *13*, 235.

[64] J. I. Novak, J. Loy, *Emerald Open Res* **2020**, *2*, 24.

[65] D. Amin, N. Nguyen, S. M. Roser, S. Abramowicz, *J. Oral Maxillofac. Surg.* **2020**, *78*, 1275.

[66] Prusa3D, *3D printed face shields for medics and professionals*, https://www.prusa3d.com/covid19/ (accessed: August 2020).

[67] K. Clarke, *Coronavirus: Etihad engineer designs 3D-printed face shields*, https://www.thenationalnews.com/uae/health/coronavirus-etihad-engineer-designs-3d-printed-face-shields-1.1042959 (accessed: August 2020).

[68] H. K. Celik, O. Kose, M. E. Ulmeanu, A. E. W. Rennie, T. N. Abram, I. Akinci, *Int. J. Bioprinting* **2020**, *6*, 286.

[69] D. Horne, *NGen invests over $21M in COVID-19 manufacturing projects*, https://www.ippt.ca/ngen-invests-over-21m-in-covid-19-manufacturing-projects/ (accessed: November 2020).

[70] Kvatthro, *HEPA Covid Coronavirus Face Mask*, https://www.thingiverse.com/thing:4222563 (accessed: August 2020).

[71] Creality, *3D Printed Masks & Buckles Protecting You From Virus | Creality 3D*, https://www.creality.com/blog-detail/creality-3d-printed-masks-and-buckles (accessed: August 2020).

[72] Creality, *3D Printed Protective Goggles to Prevent Yourself from the Novel Coronavirus*, https://www.creality.com/blog-detail/3d-printed-protective-goggles (accessed: August 2020).

[73] S. Asadi, C. D. Cappa, S. Barreda, A. S. Wexler, N. M. Bouvier, W. D. Ristenpart, *Sci. Rep.* **2020**, *10*, 1.

[74] Mayo Clinic, *COVID-19: How much protection do face masks offer?*, https://www.mayoclinic.org/diseases-conditions/coronavirus/in-depth/coronavirus-mask/art-20485449 (accessed: December 2020).

[75] J. D. Smith, C. C. Macdougall, J. Johnstone, R. A. Copes, B. Schwartz, G. E. Garber, *Can. Med. Assoc. J.* **2016**, *188*, 567.

[76] Barrow Neurological Institute, *3D Printed N95 Replacement Mask*, https://www.barrowneuro.org/for-physicians-researchers/research/barrow-innovation-center-2/3d-printed-n95-mask/ (accessed: August 2020).

[77] M. McAvoy, A.-T. N. Bui, C. Hansen, D. Plana, J. T. Said, Z. Yu, H. Yang, J. Freake, C. Van, D. Krikorian, A. Cramer, L. Smith, L. Jiang, K. J. Lee, S. J. Li, B. Beller, M. Short, S. H. Yu, A. Mostaghimi, P. K. Sorger, N. R. LeBoeuf, *medRxiv Prepr. Serv. Heal. Sci.* **2020**, https://doi.org/10.1101/2020.07.20.20151019.

[78] CERN Against COVID-19, *CERN develops washable 3D-printed face mask*, https://againstcovid19.cern/articles/cern-develops-washable-3d-printed-face-mask (accessed: August 2020).

[79] Industry Week, *COVID-19 CRISIS: Stopgap Face Mask Addressing Need*, https://www.industryweek.com/covid19/article/21128377/stopgap-face-mask-addressing-need (accessed: August 2020).

[80] V. Ecosystem, *Stopgap Surgical Face Mask (SFM)*, https://3dprint.nih.gov/discover/3dpx-014168 (accessed: November 2020).

[81] THE MONTANA MASK™, https://www.makethemasks.com/ (accessed: August 2020).

[82] Lowell makes, *COVID-19 Response*, https://lowellmakes.com/covid-19-response/ (accessed: August **2020**).

[83] R. Tino, R. Moore, S. Antoline, P. Ravi, N. Wake, C. N. Ionita, J. M. Morris, S. J. Decker, A. Sheikh, F. J. Rybicki, L. L. Chepelev, *3D Print. Med.* **2020**, *6*, 11.

[84] P. R. Greig, C. Carvalho, K. El-Boghdadly, S. Ramessur, *Anaesthesia* **2020**, *75*, 970.

[85] L. Kroo, A. Kothari, M. Hannebelle, G. Herring, T. Pollina, R. Chang MD, S. Banavar, E. Flaum, H. Soto-Montoya, H. Li, K. Combes, E. Pan, K. Vu, K. Yen, J. Dale, P. Kolbay, S. Ellgas, R. Konte, R. Hajian, G. Zhong, N. Jacobs, A. Jain, F. Kober, G. Ayala, Q. Allinne, N. Cucinelli, D. Kasper, L. Borroni, P. Gerber, R. Venook, P. Baek MD, N. Arora M.D., P. Wagner MD, R. Miki MD, J. Kohn MD, D. Kohn Bitran MD, J. Pearson MD, C. M. Herrera MD, M. Prakash, *Preprint from medRxiv* **2020**, https://doi.org/10.1101/2020.04.24.20078907.

[86] Iczfirz, *Flexible Mask Valvy – Covid-19*, https://www.thingiverse.com/thing:4177128 (accessed: August **2020**).

[87] G. Borkow, S. S. Zhou, T. Page, J. Gabbay, *PLoS One* **2010**, *5*, e11295.

[88] Z. Al-Dulimi, M. Wallis, D. K. Tan, M. Maniruzzaman, A. Nokhodchi, *Drug Discov. Today* **2020**, https://doi.org/10.1016/j.drudis.2020.11.013.

[89] S. L. Warnes, Z. R. Little, C. W. Keevil, *MBio* **2015**, *6*, e01697-15.

[90] A. A. Cortes, J. M. Zuñiga, *Diagn. Microbiol. Infect. Dis.* **2020**, *98*, 115176.

[91] Copper 3D, *#HackThePandemic*, https://copper3d.com/hackthepandemic (accessed: October 2020).

[92] V. Carlota, *NanoHack, an open-source 3D printed mask against COVID-19*, https://www.3dnatives.com/en/mask-against-covid-19-180320205/#! (accessed: October 2020).

[93] K. Makowski, M. Okrasa, *Work* **2019**, *63*, 125.

[94] bellus3D, *How to Make Bellus3D's Face Mask Fitter*, https://bellus3d.com/solutions/facemask.html (accessed: August **2020**).

[95] BBC News, *Customised 3D printed masks: A more comfortable fit?*, https://www.bbc.com/news/av/technology-53432848 (accessed: August 2020).

[96] pinshape, *COVID-19 – Boltian Goggles*, https://pinshape.com/items/63340-3d-printed-covid-19-boltian-goggles (accessed: August 2020).

[97] V. Anusci, *Farsoon, Huaxiang & LEHVOSS Group additively manufacture safety goggles to fight COVID-19*, https://www.3dprintingmedia.network/safety-goggles-to-fight-covid-19/ (accessed: August 2020).

[98] DW AKADEMIE, *Volkswagen explores using 3D printers to produce ventilators*, https://www.dw.com/en/volkswagen-explores-using-3d-printers-to-produce-ventilators/a-52867155 (accessed: August 2020).

[99] S. Murthy, C. D. Gomersall, R. A. Fowler, *JAMA – J. Am. Med. Assoc.* **2020**, *323*, 1499.

[100] C. Carter, M. Osborn, G. Agagah, H. Aedy, J. Notter, *Clin. Integr. Care* **2020**, *1*, 100004.

[101] K. El-Boghdadly, D. J. N. Wong, R. Owen, M. D. Neuman, S. Pocock, J. B. Carlisle, C. Johnstone, P. Andruszkiewicz, P. A. Baker, B. M. Biccard, G. L. Bryson, M. T. V. Chan, M. H. Cheng, K. J. Chin, M. Coburn, M. Jonsson Fagerlund, S. N. Myatra, P. S. Myles, E. O'Sullivan, L. Pasin, F. Shamim, W. A. van Klei, I. Ahmad, *Anaesthesia* **2020**, *75*, 1437.

[102] J. F. Asenjo, *Can. J. Anesth.* **2020**, *67*, 1276.

[103] World Health Organization, *Interim Guid*, https://apps.who.int/iris/bitstream/handle/10665/331792/WHO-2019-nCoV-Clinical-Ventilator_Specs-2020.1-eng.pdf?sequence=1&isAllowed=y (accessed: December 2020).

[104] M. Naitove, *Coronavirus Emergency: Ventilator Valves 3D Printed at Hospital*, https://www.ptonline.com/blog/post/coronavirus-emergency-ventilator-valves-3d-printed-at-hospital (accessed: August 2020).

**ADVANCED
SCIENCE NEWS**

www.advancedsciencenews.com

**ADVANCED
FUNCTIONAL
MATERIALS**

www.afm-journal.de

[105] The Institute's Editorial Staff, *This 3D Printed Ventilator Could Support Up to 20 COVID-19 Patients at One Time*, https://spectrum.ieee.org/news-from-around-ieee/the-institute/ieee-member-news/this-3d-printed-ventilator-could-support-up-to-20-covid19-patients-at-one-time (accessed: November 2020).

[106] Z. Kleinman, *Coronavirus: 3D printers save hospital with valves*, https://www.bbc.com/news/technology-51911070 (accessed: August 2020).

[107] ISINNOVA, *Emergency mask for hospital ventilators*, https://www.isinnova.it/easy-covid19-eng/ (accessed: August 2020).

[108] ROSATOM, *Rosatom starts 3D printing Venturi valves for ventilators*, https://rosatom-centraleurope.com/press-centre/news/rosatom-starts-3d-printing-venturi-valves-for-ventilators/ (accessed: August 2020).

[109] S. Ayyıldız, A. M. Dursun, V. Ylldlrlm, M. E. Ince, M. A. Gülçelik, C. Erdöl, *3D Print. Addit. Manuf.* **2020**, 7, 181.

[110] C. Graham, *Johns Hopkins engineers develop 3D-printed ventilator splitters*, https://hub.jhu.edu/2020/04/02/3d-printed-ventilator-splitters-for-covid-19/ (accessed: August 2020).

[111] S. C. Greenville, *Innovative ventilator device developed by Prisma Health to quickly increase ventilator capacity for COVID-19 patients*, https://www.prnewswire.com/news-releases/innovative-ventilator-device-developed-by-prisma-health-to-quickly-increase-ventilator-capacity-for-covid-19-patients-301029995.html (accessed: August 2020).

[112] S. Bhadra, Y. S. Jiang, M. R. Kumar, R. F. Johnson, L. E. Hensley, A. D. Ellington, *PLoS One* **2015**, 10, e0123126.

[113] FDA, *Coronavirus Disease 2019 Testing Basics*, https://www.fda.gov/consumers/consumer-updates/coronavirus-disease-2019-testing-basics (accessed: August 2020).

[114] H. Wang, Q. Liu, J. Hu, M. Zhou, M. Q. Yu, K. Y. Li, D. Xu, Y. Xiao, J. Y. Yang, Y. J. Lu, F. Wang, P. Yin, S. Y. Xu, *Front. Med.* **2020**, 7, 334.

[115] J. Ford, T. Goldstein, S. Trahan, A. Neuwirth, K. Tatoris, S. Decker, *3D Print. Med.* **2020**, 6, 21.

[116] Envisiontec, *3D Printed NP Swabs*, https://envisiontec.com/wp-content/uploads/2020/04/EnvisionTEC-NP-Swabs.pdf (accessed: December 2020).

[117] EnvisionTEC, *3D Printed Test Swab Production*, https://www.youtube.com/watch?v=Z3v7o8LZvmY (accessed: August 2020).

[118] EnvisionTEC, *EnvisionTEC COVID-19 Efforts*, https://envisiontec.com/envisiontec-covid-19-efforts/ (accessed: August 2020).

[119] J. L. Cox, S. A. Koepsell, *Lab. Med.* **2020**, 51, e45.

[120] F. W. Arnold, G. Grant, P. F. Bressoud, S. Furmanek, N. Sbaih, D. Karmali, M. Cahill, G. Pantalos, *Univ. Louisv. J. Respir. Infect.* **2020**, 4, https://doi.org/10.18297/jri/vol4/iss1/41.

[121] Formlabs, *3D Printing to Support COVID-19 Response Efforts*, https://formlabs.com/eu/covid-19-response/ (accessed: August 2020).

[122] Carbon, *Carbon COVID-19 Response*, https://www.carbon3d.com/covid19/ (accessed: August **2020**).

[123] World Health Organization, *Considerations for quarantine of contacts of COVID-19 cases*, https://www.who.int/publications/i/item/considerations-for-quarantine-of-individuals-in-the-context-of-containment-for-coronavirus-disease-(covid-19) (accessed: November 2020).

[124] J. Cubillos, J. Querney, A. Rankin, J. Moore, K. Armstrong, *Br. J. Anaesth.* **2020**, 125, e179.

[125] Caitlin Clark, *How Texas A&M Is Using 3D Printing To Respond To Coronavirus*, https://today.tamu.edu/2020/05/26/how-texas-am-is-using-3d-printing-to-respond-to-coronavirus/ (accessed: August 2020).

[126] Winsun, *News-Yingchuang Building Technique (Shanghai)Co.Ltd.*, http://www.winsun3d.com/En/News/news_inner/id/543 (accessed: October 2020).

[127] T. Boissonneault, *WinSun deploys 3D printed isolation wards for coronavirus medical staff –3D Printing Media Network*, https://www.3dprintingmedia.network/winsun-3d-printed-isolation-wards-coronavirus-medical-workers/ (accessed: October 2020).

[128] D. Sher, *WinSun/Yingchuang ships 15 3D printed isolation wards to Pakistan to fight COVID-19*, https://www.3dprintingmedia.network/winsun-yingchuang-ships-15-3d-printed-isolation-wards-to-pakistan-to-fight-covid-19/ (accessed: November 2020).

[129] A. Woodward, S. Gal, *One chart shows how long the coronavirus lives on surfaces like cardboard, plastic, wood, and steel*, https://www.businessinsider.com/coronavirus-lifespan-on-surfaces-graphic-2020-3 (accessed: January 2021).

[130] CDC, *How It Spreads/CDC*, https://www.cdc.gov/coronavirus/2019-ncov/prevent-getting-sick/how-covid-spreads.html (accessed: November 2020).

[131] N. Van Doremalen, T. Bushmaker, D. H. Morris, M. G. Holbrook, A. Gamble, B. N. Williamson, A. Tamin, J. L. Harcourt, N. J. Thornburg, S. I. Gerber, J. O. Lloyd-Smith, E. de Wit, V. J. Munster, *N. Engl. J. Med.* **2020**, 382, 1564.

[132] B. Nazario, *How Long Does the Coronavirus Live on Surfaces?*, https://www.webmd.com/lung/how-long-covid-19-lives-on-surfaces (accessed: February 2021).

[133] Materialise, *Hands-Free 3D-Printed Door Openers to Help Against the Spread of Coronavirus*, https://www.materialise.com/en/hands-free-door-opener (accessed: November 2020).

[134] P. M. François, X. Bonnet, J. Kosior, J. Adam, R. H. Khonsari, *J. Stomatol. Oral Maxillofac. Surg.* **2020**, https://doi.org/10.1016/j.jormas.2020.06.010.

[135] M. Petch, *3D Printing Community Responds To COVID-19 and Coronavirus Resources*, https://3dprintingindustry.com/news/3d-printing-community-responds-to-covid-19-and-coronavirus-resources-169143/ (accessed: November 2020).

[136] E. V. R. Campos, A. E. S. Pereira, J. L. De Oliveira, L. B. Carvalho, M. Guilger-Casagrande, R. De Lima, L. F. Fraceto, *J. Nanobiotechnology* **2020**, 18, 125.

[137] T. Q. Tran, A. Chinnappan, J. K. Y. Lee, N. H. Loc, L. T. Tran, G. Wang, V. V. Kumar, W. A. D. M. Jayathilaka, D. Ji, M. Doddamani, S. Ramakrishna, *Metals* **2019**, 9, 756.

[138] N. Hutasoit, B. Kennedy, S. Hamilton, A. Luttick, R. A. Rahman Rashid, S. Palanisamy, *Manuf. Lett.* **2020**, 25, 93.

[139] H. Tzu-ti, *Taiwan government takes novel approach to fighting novel coronavirus*, https://www.taiwannews.com.tw/en/news/3904909 (accessed: November 2020).

[140] AuMed, *Accelerating COVID-19 Swab Collection Training with 3D Printed Medical Manikins*, https://au-med.com/casestudies/accelerating-covid-19-swab-collection-training-3d-printed-medical-manikin (accessed: November 2020).

[141] Creatz3D, *3D Printed Medical Manikins Become Effective Training Aids for Respiratory Swab Collection*, https://creatz3d.com.sg/3d-printed-medical-manikins-become-effective-training-aids-for-respiratory-swab-collection/ (accessed: August 2020).

[142] E. Buehler, S. K. Kane, A. Hurst, *ASSETS14 – Proc. 16th Int. ACM SIGACCESS Conf. Computers & Accessibility*, Association for Computing Machinery, New York **2014**, p. 107.

[143] N. Vordos, D. A. Gkika, G. Maliaris, K. E. Tilkeridis, A. Antoniou, D. V. Bandekas, A. C. Mitropoulos, *Saf. Sci.* **2020**, 130, 104870.

[144] L. Pecchia, D. Piaggio, A. Maccaro, C. Formisano, E. Iadanza, *Health Technol. (Berl).* **2020**, 10, 1375.

[145] Yeggi, *3D Printer Models Search Engine*, https://www.yeggi.com/ (accessed: August 2020).

[146] GrabCAD, *GrabCAD Community Library*, https://grabcad.com/library (accessed: August 2020).

[147] L. Fiorillo, T. Leanza, *Prosthesis* **2020**, 2, 87.

[148] BCN3D, *BCN3D*, https://www.bcn3d.com/ (accessed: August 2020).

[149] BCN3D, *3D printing at BCN3D to change the face of the global Covid-19 pandemic*, https://www.bcn3d.com/here-to-help-3d-printing-to-change-the-covid-19-pandemic/ (accessed: August 2020).

**ADVANCED
SCIENCE NEWS**
www.advancedsciencenews.com

**ADVANCED
FUNCTIONAL
MATERIALS**
www.afm-journal.de

[150] Airwolf3D, *The Latest 3D Printing News, Tips, and Tricks*, https://airwolf3d.com/?s=covid&post_type=product (accessed: August 2020).

[151] Universities UK, *How universities are helping fight Covid-19*, https://universitiesuk.ac.uk/covid19/supporting-national-effort/Documents/we-are-together-case-studies-covid-19.pdf (accessed: January 2021).

[152] B. U. of Technology, *COVID-19 Protection Halfmask BUT-H1*, https://www.vutbr.cz/en/but/f19528/d197642 (accessed: August 2020).

[153] Desktop Metal, *Metal 3D Printing Services for COVID-19 Supplies*, https://learn.desktopmetal.com/covid (accessed: August 2020).

[154] 3D Systems, *COVID-19 Call to Action*, https://www.3dsystems.com/covid-19-response (accessed: August 2020).

[155] Stratasys, *Stratasys Helps: Responding to the COVID-19 Crisis*, https://www.stratasys.com/covid-19 (accessed: August 2020).

[156] J. & Johnson, *Our COVID-19 Response Efforts*, https://www.jnj.com/coronavirus (accessed: August 2020).

[157] HP, *3D printing in support of COVID-19 containment efforts*, https://reinvent.hp.com/us-en-3dprint-COVID-19-containment-applications (accessed: August 2020).

[158] Markforged, *Markforged's Response to COVID-19*, https://markforged.com/resources/blog/markforged-covid-19-efforts (accessed: August 2020).

[159] Creality, *3D Printed Masks & Buckles Protecting You From Virus | Creality 3D*, https://www.creality.com/search/covid (accessed: August 2020).

[160] Materialise, *Materialise Acts: Our 3D Printing Response to COVID-19*, https://www.materialise.com/en/hands-free-door-opener (accessed: August 2020).

[161] E. Commission, *Conformity assessment procedures for 3D printing and 3D printed products to be used in a medical context for COVID-19*, https://ec.europa.eu/docsroom/documents/40562 (accessed: August 2020).

[162] Medicines and Healthcare products Regulatory Agency, *3D printing (additive manufacturing) of medical devices or component parts during the coronavirus (COVID-19) pandemic*, https://www.gov.uk/guidance/3d-printing-additive-manufacturing-of-medical-devices-or-component-parts-during-the-coronavirus-covid-19-pandemic (accessed: August 2020).

[163] FDA, *Coronavirus (COVID-19) and Medical Devices*, https://www.fda.gov/medical-devices/emergency-situations-medical-devices/coronavirus-covid-19-and-medical-devices (accessed: August 2020).

[164] FDA, *FDA's Role in 3D Printing*, https://www.fda.gov/medical-devices/3d-printing-medical-devices/fdas-role-3d-printing (accessed: October 2020).

[165] T. Mueller, A. Elkaseer, A. Charles, J. Fauth, D. Rabsch, A. Scholz, C. Marquardt, K. Nau, S. G. Scholz, *Appl. Sci.* **2020**, *10*, 4135.

[166] C. Wesemann, S. Pieralli, T. Fretwurst, J. Nold, K. Nelson, R. Schmelzeisen, E. Hellwig, B. C. Spies, *Materials (Basel)* **2020**, *13*, 1997.

[167] Kimberley Mok, *Open Source 3D-Printed Face Shields Protect Hospital Workers from COVID-19*, https://thenewstack.io/open-source-3d-printed-face-shields-protect-hospital-workers-from-covid-19/ (accessed: August 2020).

[168] E. Westphal, R. Mau, T. Dreier, H. Seitz, *Trans. AMMM* **2020**, *2*, https://doi.org/10.18416/AMMM.2020.2009008.

[169] L. Maracaja, D. Blitz, D. L. V. Maracaja, C. A. Walker, *J. Cardiothorac. Vasc. Anesth.* **2020**, *34*, 2847.

[170] Formlabs, Protective Face Shields Against COVID-19, https://formlabs.com/eu/covid-19-response/covid-face-shields (accessed: August 2020).

[171] G. Duquesnoy, *So-Boat is Committed TO THE COVID and Offers Protective Visors*, https://blog.so-boat.com/so-boat-sengage-contre-le-covid-et-offre-des-visieres-de-protection (accessed: August 2020).

[172] D. Belforte, *3DPRINTUK develops efficient 3D-printed face shield*, https://www.industrial-lasers.com/additive-manufacturing/article/14175776/3dprintuk-develops-efficient-3dprinted-face-shield (accessed: August 2020).

[173] 3DPRINTUK, The worlds most efficient 3D printable face shield, https://www.3dprint-uk.co.uk/worlds-most-efficient-sls-face-shield-covid19/ (accessed: August 2020).

[174] AVID PRODUCT DEVELOPMENT, *3D PRINTING PPE IN SUPPORT OF COVID-19 CONTAINMENT EFFORTS*, https://avidpd.com/knowledge-base/3d-printing-ppe-in-support-of-covid-19-containment-efforts/ (accessed: August 2020).

[175] T. Boissonneault, *HP and partners mobilize 3D printing resources for critical medical supplies*, https://www.3dprintingmedia.network/hp-mobilize-3d-printing-resources-critical-medical-supplies/ (accessed: August 2020).

[176] Siemens AG, *Siemens fast-tracks production of medical grade face shields for COVID-19 frontliners in Singapore*, https://press.siemens.com/sg/en/pressrelease/siemens-fast-tracks-production-medical-grade-face-shields-covid-19-frontliners (accessed: August 2020).

[177] Make The Masks, *The Montana Mask*, https://www.makethe-masks.com/ (accessed: August 2020).

[178] Copper 3D, *NANOHACK,THE OPEN SOURCE FACE MASK*, https://copper3d.com/hackthepandemic/ (accessed: August 2020).

[179] MUSC, *Rapid Assembly Filter Cartridge for 3D Printed Aerosol Masks*, https://web.musc.edu/innovation/covid-19-innovation/safe-cartridge-system-and-masks (accessed: August 2020).

[180] Rowan University, *Re-usable 3D-printed face mask*, https://engineering.rowan.edu/research-centers/mask/index.html (accessed: August 2020).

[181] F. Moretti, *Custom 3D printed Mask*, https://www.3dwasp.com/en/3d-printed-mask-from-3d-scanning/ (accessed: August 2020).

[182] CTU, *CIIRC CTU Develops Own Prototype of CIIRC RP95 Respirator /Half Mask*, https://www.ciirc.cvut.cz/covid-2/ (accessed: August 2020).

[183] Stratasys, *Startup launches ergonomic face mask with PolyJet 3D printing*, https://www.stratasys.com/explore/case-study/breathe99 (accessed: January 2021).

[184] Sean Daly, *Tampa engineer assembles 3D-printed strap to make surgical masks more comfortable*, https://www.abcactionnews.com/news/region-hillsborough/tampa-engineer-designs-3d-printed-strap-to-make-surgical-masks-more-comfortable (accessed: August 2020).

[185] SIEGE, *Surgical Mask Strap Tension Reliever*, https://www.siegeadvancedmanufacturing.com/covid-products/ (accessed: August 2020).

[186] Bdsearle, *Mask Comfort Strap*, https://3dprint.nih.gov/discover/3dpx-013440 (accessed: August 2020).

[187] Mark, *SLA Printable Face Mask Strap*, https://3dprint.nih.gov/discover/3dpx-013566 (accessed: November 2020).

[188] D. Provenzano, Y. J. Rao, K. Mitic, S. N. Obaid, D. Pierce, J. Huckenpahler, J. Berger, S. Goyal, M. H. Loew, *Preprints* **2020**, https://doi.org/10.20944/preprints202003.0444.v1.

[189] T. Papavasiliou, S. Chatzimichail, *J. Plast. Reconstr. Aesthetic Surg.* **2020**, https://doi.org/10.1016/j.bjps.2020.08.111.

[190] Intermountain3D, *Covid-respirators*, https://www.intermountain3d.com/covid-respirators.html (accessed: August 2020).

[191] Kerry Stevenson, *3D Printable Respirator Design Receives Certification*, https://www.fabbaloo.com/blog/2020/3/27/3d-printable-respirator-design-receives-certification (accessed: August 2020).

[192] S. Rendeki, B. Nagy, M. Bene, A. Pentek, L. Toth, Z. Szanto, R. Told, P. Maroti, *Polymers (Basel)* **2020**, *12*, 2703.

[193] Checkify, *Charlotte Valve 3D Printed Respirators*, https://checkify.com/blog/charlotte-valve-3d-printed-respirator/ (accessed: August 2020).

[194] GrabCAD, *Printable ventilator-free respiratory: Venturi Valve/3D CAD Model Library/GrabCAD*, https://grabcad.com/library/respirator-free-reanimation-venturi-s-valve-1 (accessed: August 2020).

[195] L. Cavallo, A. Marcianò, M. Cicciù, G. Oteri, *Prosthesis* **2020**, *2*, 46.

[196] A. Thomas, *Respiratory valves, other medical devices for coronavirus treatment could be 3D printed during shortage*, https://www.asianage.com/technology/in-other-news/250320/respiratory-valves-other-medical-devices-for-coronavirus-treatment-could-be-3d-printed-during-shortage.html (accessed: August 2020).

[197] M. Tarfaoui, M. Nachtane, I. Goda, Y. Qureshi, H. Benyahia, *Int. J. Adv. Manuf. Technol.* **2020**, *110*, 2913.

[198] M. Alghounaim, S. Almazeedi, S. Al Youha, J. Papenburg, O. Alowaish, G. AbdulHussain, R. Al-Shemali, A. Albuloushi, S. Alzabin, K. Al-Wogayan, Y. Al-Mutawa, S. Al-Sabah, *J. Clin. Microbiol.* **2020**, *58*, e01668.

[199] A. Manoj, M. Bhuyan, S. R. Banik, M. R. Sankar, *Mater. Today Proc.* **2020**, https://doi.org/10.1016/j.matpr.2020.11.505.

[200] E. D. Kouvelas, Formlabs First Response Medical Bundle, https://formlabs-media.formlabs.com/filer_public/7d/2e/7d2eb553-0a64-4299-b871-83ee7fcd68b6/200527-first-response-medical-bundle.pdf (accessed: December 2020).

[201] MarianneE, *3D-Printed Test Swabs*, https://3dprint.nih.gov/discover/3dpx-013730 (accessed: August 2020).

[202] Ariadna.conejos, *Nasopharyngeal swabs*, https://3dprint.nih.gov/discover/3dpx-014487 (accessed: August 2020).

[203] L. Russart, *Fast Spiral Nasopharyngeal Swab*, https://fathommfg.com/blog/npswab (accessed: August 2020).

[204] SimonSolar, *Ergonomic "Deri" Door Opener /grabber – Covid-19*, https://www.thingiverse.com/thing:4260659 (accessed: August 2020).

[205] bgiovanny, *GB 3D – Hands Free – Door Pull Opener – Button Press*, https://www.thingiverse.com/thing:4310110 (accessed: August 2020).

[206] E. J. Davis, K. Wheeler, *J. Chem. Educ.* **2020**, *97*, 2691.

[207] T. E. Team, *Injection Molding vs 3D Printing: Complementary, Not Competing Technologies*, https://www.essentium.com/injection-molding-vs-3d-printing/ (accessed: February 2021).

[208] B. P. Conner, G. P. Manogharan, A. N. Martof, L. M. Rodomsky, C. M. Rodomsky, D. C. Jordan, J. W. Limperos, *Addit. Manuf.* **2014**, *1*, 64.

[209] T. Pereira, J. V. Kennedy, J. Potgieter, *Procedia Manuf.* **2019**, *30*, 11.

[210] M. E. Kunkel, M. T. Vasques, J. A. J. Perfeito, N. R. M. Zambrana, T. S. Bina, L. H. M. Passoni, T. V. Ribeiro, S. M. S. Rodrigues, R. O. M. Castro, N. H. Ota, *Preprints, Reserach Square* **2020**, https://doi.org/10.21203/rs.3.rs-63872/v1.

[211] A. Nazir, A. Azhar, U. Nazir, Y. F. Liu, W. S. Qureshi, J. E. Chen, E. Alanazi, *J. Manuf. Syst.* **2020**, https://doi.org/10.1016/j.jmsy.2020.10.009.

[212] UNICEF, *How Drones Can Be Used to Combat COVID-19*, https://www.unicef.org/supply/media/5286/file/%20Rapid-guidance-how-can-drones-help-in-COVID-19-response.pdf.pdf (accessed: February 2021).

[213] J. R. C. Dizon, A. D. Valino, L. R. Souza, A. H. Espera, Q. Chen, R. C. Advincula, *MRS Commun.* **2019**, *9*, 1267.

[214] J. R. C. Dizon, A. D. Valino, L. R. Souza, A. H. Espera, Q. Chen, R. C. Advincula, *Mater. Sci. Forum* **2020**, *1005*, 150.

[215] C. Rathi, *Traditional Manufacturing Vs 3d Printing – A Cost Analysis*, https://precious3d.com/traditional-manufacturing-vs-3d-printing/ (accessed: February 2021).

[216] M. Salmi, J. S. Akmal, E. Pei, J. Wolff, A. Jaribion, S. H. Khajavi, *Appl. Sci.* **2020**, *10*, 4004.

[217] S. Hendrickson, V. Kailasanath, A. Habtemariam, E. Rothstein, D. Kracov, *3D Printing And The Shifting Legal Landscape For COVID-19*, https://www.law360.com/articles/1271240/3d-printing-and-the-shifting-legal-landscape-for-covid-19 (accessed: February 2021).

[218] G. Manchanda, *How biocompatible 3D printing is changing healthcare*, https://www.med-technews.com/medtech-insights/how-biocompatible-3d-printing-is-changing-healthcare/ (accessed: December 2020).

[219] K. Stevenson, *Some Advice To Makers Working On COVID-19 Projects*, https://www.fabbaloo.com/blog/2020/3/27/some-advice-to-makers-working-on-covid-19-projects (accessed: August 2020).

[220] FDA, *3D Printing of Medical Devices*, https://www.fda.gov/medical-devices/products-and-medical-procedures/3d-printing-medical-devices (accessed: August 2020).

[221] W. Clifton, A. Damon, A. K. Martin, *3D Print. Addit. Manuf.* **2020**, *7*, 97.

[222] G. R. J. Swennen, L. Pottel, P. E. Haers, *Int. J. Oral Maxillofac. Surg.* **2020**, *49*, 673.

[223] A. R. Scott, J. Hu, C. Gan, J. A. Morris, K. W. Meacham, D. H. Ballard, *Int. J. Oral Maxillofac. Surg.* **2020**, *49*, 1660.

[224] E. J. Sammut, Y. C. Yeap, J. Q.-H. Yeap, G. Mendonca, A. R. G. Cortes, *Nucl. Med. Med. Imaging* **2020**, https://doi.org/10.21203/rs.3.rs-24633/v1.

[225] L. B. Bezek, J. Pan, C, Harb, C. E. Zawaski, B. Molla, R. K. Joseph, C. M. Linsey, B. W. Christopher, *Preprints* **2020**, https://doi.org/10.1016/j.jmsy.2021.01.002.

[226] J. Craven, *COVID-19 vaccine tracker*, https://www.raps.org/news-and-articles/news-articles/2020/3/covid-19-vaccine-tracker (accessed: February 2021).

# CHAPTER 6

**Conclusions**

In this study multiple strategies that were employed towards fabrication of electrocatalysts are discussed along with the evaluation of their performance towards hydrogen evolution reaction. It is observed that in the covalent and the non-covalent synthesis strategy of electrocatalysts preparation via two different nitrogen dopant sources, covalently bonded electrocatalysts outperform the non-covalently bonded electrocatalysts. This is because the covalently bonded electrocatalysts aided towards anchoring of more palladium nanoparticles over it than the non-covalently bonded electrocatalysts. Such synthesis strategies or studies are ideal for designing application specific electrocatalysts. Among the set of MAX phase electrocatalysts, $Mo_2TiAlC_2$ exhibited superior HER activity. Further, improvements in material properties via improved synthesis strategy, functionalization can aid towards improving this family of MAX phase material towards catalysis application. 3D-printing technology was employed towards fabricating cost-effective, conductive electrodes, wherein appropriate modifications of these substrates via dip coating and metal plating has aided them towards fabrication of 3D-printed electrode substrates that are ideal for energy conversion and electrochemical sensing applications respectively. Further, newer possibilities of electrocatalysts for energy conversion applications such as ammonia production (3D-printed metal and carbon-based substrates, Fe-MOFs), and devising improved 3D-printed substrates for $CO_2$ reduction and capture are also elaborated. Also, employing 3D-printed substrates for electrochemical sugar sensing applications and their vital role during health emergencies shows the potential of 3D-printing technology for uses beyond electrochemical applications. In short, the thesis has outlined several material fabrication approaches for electrochemical sensing and energy applications such as HER, ammonia synthesis, $CO_2$ reduction etc.

# CHAPTER 7

## References

(1) Höök, M.; Tang, X. Depletion of Fossil Fuels and Anthropogenic Climate Change-A Review. *Energy Policy* **2013**, *52*, 797–809. https://doi.org/10.1016/j.enpol.2012.10.046.

(2) Shafiee, S.; Topal, E. When Will Fossil Fuel Reserves Be Diminished? *Energy Policy* **2009**, *37* (1), 181–189. https://doi.org/10.1016/j.enpol.2008.08.016.

(3) Kalair, A.; Abas, N.; Saleem, M. S.; Kalair, A. R.; Khan, N. Role of Energy Storage Systems in Energy Transition from Fossil Fuels to Renewables. *Energy Storage* **2021**, *3* (1), 1–27. https://doi.org/10.1002/est2.135.

(4) Peter, S. C. Reduction of $CO_2$ to Chemicals and Fuels: A Solution to Global Warming and Energy Crisis. *ACS Energy Lett.* **2018**, *3* (7), 1557–1561. https://doi.org/10.1021/acsenergylett.8b00878.

(5) Shakun, J. D.; Clark, P. U.; He, F.; Marcott, S. A.; Mix, A. C.; Liu, Z.; Otto-Bliesner, B.; Schmittner, A.; Bard, E. Global Warming Preceded by Increasing Carbon Dioxide Concentrations during the Last Deglaciation. *Nature* **2012**, *484*, 49–54. https://doi.org/10.1038/nature10915.

(6) Khezri, B.; Fisher, A. C.; Pumera, M. $CO_2$ Reduction: The Quest for Electrocatalytic Materials. *J. Mater. Chem. A* **2017**, *5* (18), 8230–8246. https://doi.org/10.1039/c6ta09875d.

(7) Padinjareveetil, A. K. K.; Pumera, M. Advances in Designing 3D-Printed Systems for CO2 Reduction. *Adv. Mater. Interfaces* **2023**, 10 (8), 2201734. https://doi.org/10.1002/admi.202201734.

(8)     Wuebbles, D. J.; Hayhoe, K. Atmospheric Methane and Global Change. *Earth-Science Rev.* **2002**, *57* (3–4), 177–210. https://doi.org/10.1016/S0012-8252(01)00062-9.

(9)     Anya    Biferno.    Understanding    our    planet    to    benefit    humankind https://climate.nasa.gov/ (accessed Sep 27, 2023).

(10)    Pokrajac, L.; Abbas, A.; Chrzanowski, W.; Dias, G. M.; Eggleton, B. J.; Maguire, S.; Maine, E.; Malloy, T.; Nathwani, J.; Nazar, L.; et al. Nanotechnology for a Sustainable Future: Addressing Global Challenges with the International Network4Sustainable Nanotechnology. *ACS Nano* **2021**, *15* (12), 18608–18623. https://doi.org/10.1021/acsnano.1c10919.

(11)    Padinjareveetil, A. K. K.; Perales-Rondon, J. V.; Pumera, M. Engineering 3D Printed Structures Towards Electrochemically Driven Green Ammonia Synthesis: A Perspective.    *Adv.    Mater.    Technol.*    **2023**,    8    (13),    202202080. https://doi.org/10.1002/admt.202202080.

(12)    Carpenter, N. E. Chemistry of Sustainable Energy. *Chem. Sustain. Energy* **2014**, 1–401. https://doi.org/10.1201/b16687.

(13)    Zhang, Q.; Suresh, L.; Liang, Q.; Zhang, Y.; Yang, L.; Paul, N.; Tan, S. C. Emerging Technologies for Green Energy Conversion and Storage. *Adv. Sustain. Syst.* **2021**, *5* (3), 1–19. https://doi.org/10.1002/adsu.202000152.

(14)    Yang, J.; Li, W.; Wang, D.; Li, Y. Electronic Metal–Support Interaction of Single-Atom Catalysts and Applications in Electrocatalysis. *Adv. Mater.* **2020**, *32* (49), 1–29. https://doi.org/10.1002/adma.202003300.

(15)    Jin, H.; Guo, C.; Liu, X.; Liu, J.; Vasileff, A.; Jiao, Y.; Zheng, Y.; Qiao, S. Z.

Emerging Two-Dimensional Nanomaterials for Electrocatalysis. *Chem. Rev.* **2018**, *118* (13), 6337–6408. https://doi.org/10.1021/acs.chemrev.7b00689.

(16)  Voiry, D.; Yamaguchi, H.; Li, J.; Silva, R.; Alves, D. C. B.; Fujita, T.; Chen, M.; Asefa, T.; Shenoy, V. B.; Eda, G.; et al. Enhanced Catalytic Activity in Strained Chemically Exfoliated $WS_2$ Nanosheets for Hydrogen Evolution. *Nat. Mater.* **2013**, *12* (9), 850–855. https://doi.org/10.1038/nmat3700.

(17)  Lee, C. Y.; Taylor, A. C.; Nattestad, A.; Beirne, S.; Wallace, G. G. 3D Printing for Electrocatalytic Applications. *Joule* **2019**, *3* (8), 1835–1849. https://doi.org/10.1016/j.joule.2019.06.010.

(18)  Akshay Kumar, K. P.; Alduhaish, O.; Pumera, M. Electrocatalytic Activity of Layered MAX Phases for the Hydrogen Evolution Reaction. *Electrochem. Commun.* **2021**, *125* (March), 106977. https://doi.org/10.1016/j.elecom.2021.106977.

(19)  Stark, M. S.; Kuntz, K. L.; Martens, S. J.; Warren, S. C. Intercalation of Layered Materials from Bulk to 2D. *Adv. Mater.* **2019**, 31 (27), *1808213*. https://doi.org/10.1002/adma.201808213.

(20)  Gusmão, R.; Sofer, Z.; Pumera, M. Exfoliated Layered Manganese Trichalcogenide Phosphite (MnPX3, X = S, Se) as Electrocatalytic van Der Waals Materials for Hydrogen Evolution. *Adv. Funct. Mater.* **2019**, *29* (2), 1805975. https://doi.org/10.1002/adfm.201805975.

(21)  Browne, M. P.; Novotný, F.; Sofer, Z.; Pumera, M. 3D Printed Graphene Electrodes' Electrochemical Activation. *ACS Appl. Mater. Interfaces* **2018**, *10* (46), 40294–40301. https://doi.org/10.1021/acsami.8b14701.

(22)  Novotný, F.; Urbanová, V.; Plutnar, J.; Pumera, M. Preserving Fine Structure Details

and Dramatically Enhancing Electron Transfer Rates in Graphene 3D-Printed Electrodes via Thermal Annealing: Toward Nitroaromatic Explosives Sensing. *ACS Appl. Mater. Interfaces* **2019**, *11* (38), 35371–35375. https://doi.org/10.1021/acsami.9b06683.

(23) Wang, L.; Sofer, Z.; Pumera, M. Will Any Crap We Put into Graphene Increase Its Electrocatalytic Effect? *ACS Nano* **2020**, *14* (1), 21–25. https://doi.org/10.1021/acsnano.9b00184.

(24) Liu, H.; Liu, Y.; Zhu, D. Chemical Doping of Graphene. *J. Mater. Chem.* **2011**, *21* (10), 3335–3345. https://doi.org/10.1039/c0jm02922j.

(25) Kumar, K. P. A.; Alduhaish, O.; Adil, S. F.; Pumera, M. Grafting of Pd on Covalently and Noncovalently Modified N-Doped Graphene for Electrocatalysis. *Adv. Mater. Interfaces* **2022**, *9* (27), 2102317. https://doi.org/10.1002/admi.202102317.

(26) Teo, E. Y. L.; Lim, H. N.; Jose, R.; Chong, K. F. Aminopyrene Functionalized Reduced Graphene Oxide as a Supercapacitor Electrode. *RSC Adv.* **2015**, *5* (48), 38111–38116. https://doi.org/10.1039/c5ra02578h.

(27) Bakandritsos, A.; Pykal, M.; Boński, P.; Jakubec, P.; Chronopoulos, D. D.; Poláková, K.; Georgakilas, V.; Čépe, K.; Tomanec, O.; Ranc, V.; et al. Cyanographene and Graphene Acid: Emerging Derivatives Enabling High-Yield and Selective Functionalization of Graphene. *ACS Nano* **2017**, *11* (3), 2982–2991. https://doi.org/10.1021/acsnano.6b08449.

(28) Zhang, Y. Z.; Wang, Y.; Jiang, Q.; El-Demellawi, J. K.; Kim, H.; Alshareef, H. N. MXene Printing and Patterned Coating for Device Applications. *Adv. Mater.* **2020**, *32* (21), 1908486. https://doi.org/10.1002/adma.201908486.

(29) Seh, Z. W.; Fredrickson, K. D.; Anasori, B.; Kibsgaard, J.; Strickler, A. L.; Lukatskaya, M. R.; Gogotsi, Y.; Jaramillo, T. F.; Vojvodic, A. Two-Dimensional Molybdenum Carbide (MXene) as an Efficient Electrocatalyst for Hydrogen Evolution. *ACS Energy Lett.* **2016**, *1* (3), 589–594. https://doi.org/10.1021/acsenergylett.6b00247.

(30) Guo, J.; Chen, P. Catalyst: $NH_3$ as an Energy Carrier. *Chem* **2017**, *3* (5), 709–712. https://doi.org/10.1016/j.chempr.2017.10.004.

(31) Ross, S. A.; Gulve, E. A.; Wang, M. Chemistry and Biochemistry of Type 2 Diabetes. *Chem. Rev.* **2004**, *104* (3), 1255–1282. https://doi.org/10.1021/cr0204653.

(32) Cho, N. H.; Shaw, J. E.; Karuranga, S.; Huang, Y.; da Rocha Fernandes, J. D.; Ohlrogge, A. W.; Malanda, B. IDF Diabetes Atlas: Global Estimates of Diabetes Prevalence for 2017 and Projections for 2045. *Diabetes Res. Clin. Pract.* **2018**, *138*, 271–281. https://doi.org/10.1016/j.diabres.2018.02.023.

(33) Kumar, K. P. A.; Ghosh, K.; Alduhaish, O.; Pumera, M. Metal-Plated 3D-Printed Electrode for Electrochemical Detection of Carbohydrates. *Electrochem. Commun.* **2020**, *120* , 106827. https://doi.org/10.1016/j.elecom.2020.106827.

(34) Teymourian, H.; Barfidokht, A.; Wang, J. Electrochemical Glucose Sensors in Diabetes Management: An Updated Review (2010-2020). *Chem. Soc. Rev.* **2020**, *49* (21), 7671–7709. https://doi.org/10.1039/d0cs00304b.

(35) Lipińska, W.; Siuzdak, K.; Karczewski, J.; Dołęga, A.; Grochowska, K. Electrochemical Glucose Sensor Based on the Glucose Oxidase Entrapped in Chitosan Immobilized onto Laser-Processed Au-Ti Electrode. *Sensors Actuators, B Chem.* **2021**, *330* (December 2020). https://doi.org/10.1016/j.snb.2020.129409.

(36)     Onay, A.; Dogan, Ü.; Ciftci, H.; Cetin, D.; Suludere, Z.; Tamer, U. Amperometric Glucose Sensor Based on the Glucose Oxidase Enzyme Immobilized on Graphite Rod Electrode Modified with $Fe_3O_4$-CS-Au Magnetic Nanoparticles. *Ionics.*. **2018**, *24*, 4015–4022. https://doi.org/10.1007/s11581-018-2559-6.

(37)     Haghparas, Z.; Kordrostami, Z.; Sorouri, M.; Rajabzadeh, M.; Khalifeh, R. Highly Sensitive Non-Enzymatic Electrochemical Glucose Sensor Based on Dumbbell-Shaped Double-Shelled Hollow Nanoporous CuO/ZnO Microstructures. *Sci. Rep.* **2021**, *11*, 344, 1–12. https://doi.org/10.1038/s41598-020-79460-2.

(38)     Luo, J.; Jiang, S.; Zhang, H.; Jiang, J.; Liu, X. A Novel Non-Enzymatic Glucose Sensor Based on Cu Nanoparticle Modified Graphene Sheets Electrode. *Anal. Chim. Acta* **2012**, *709*, 47–53. https://doi.org/10.1016/j.aca.2011.10.025.

(39)     Crabtree, G. W.; Dresselhaus, M. S.; Buchanan, M. V. The Hydrogen Economy. *Phys. Today* **2004**, *57* (12), 39–44. https://doi.org/10.1063/1.1878333.

(40)     Kong, D.; Cha, J. J.; Wang, H.; Lee, H. R.; Cui, Y. First-Row Transition Metal Dichalcogenide Catalysts for Hydrogen Evolution Reaction. *Energy Environ. Sci.* **2013**, *6* (12), 3553–3558. https://doi.org/10.1039/c3ee42413h.

(41)     Zheng, Y.; Jiao, Y.; Jaroniec, M.; Qiao, S. Z. Advancing the Electrochemistry of the Hydrogen- Evolution Reaction through Combining Experiment. *Angew. Chemie - Int. Ed.* **2015**, *54* (1), 52–65. https://doi.org/10.1002/anie.201407031.

(42)     Mayorga-Martinez, C. C.; Mohamad Latiff, N.; Eng, A. Y. S.; Sofer, Z.; Pumera, M. Black Phosphorus Nanoparticle Labels for Immunoassays via Hydrogen Evolution Reaction Mediation. *Anal. Chem.* **2016**, *88* (20), 10074–10079. https://doi.org/10.1021/acs.analchem.6b02422.

(43) Márquez, R. A.; Kawashima, K.; Son, Y. J.; Rose, R.; Smith, L. A.; Miller, N.; Carrasco Jaim, O. A.; Celio, H.; Mullins, C. B. Tailoring 3D-Printed Electrodes for Enhanced Water Splitting. *ACS Appl. Mater. Interfaces* **2022**, *14* (37), 42153–42170. https://doi.org/10.1021/acsami.2c12579.

(44) Ambrosi, A.; Pumera, M. Self-Contained Polymer/Metal 3D Printed Electrochemical Platform for Tailored Water Splitting. *Adv. Funct. Mater.* **2018**, *28* (27), 1700655. https://doi.org/10.1002/adfm.201700655.

(45) Iffelsberger, C.; Ng, S.; Pumera, M. Catalyst Coating of 3D Printed Structures via Electrochemical Deposition: Case of the Transition Metal Chalcogenide MoSx for Hydrogen Evolution Reaction. *Appl. Mater. Today* **2020**, *20*, 100654. https://doi.org/10.1016/j.apmt.2020.100654.

(46) Antolini, E.; Zignani, S. C.; Santos, S. F.; Gonzalez, E. R. Palladium-Based Electrodes: A Way to Reduce Platinum Content in Polymer Electrolyte Membrane Fuel Cells. *Electrochim. Acta* **2011**, *56* (5), 2299–2305. https://doi.org/10.1016/j.electacta.2010.11.101.

(47) Liu, M.; Wang, X.; Liu, J.; Wang, K.; Jin, S.; Tan, B. Palladium as a Superior Cocatalyst to Platinum for Hydrogen Evolution Using Covalent Triazine Frameworks as a Support. *ACS Appl. Mater. Interfaces* **2020**, *12* (11), 12774–12782. https://doi.org/10.1021/acsami.9b21903.

(48) Chia, X.; Adriano, A.; Lazar, P.; Sofer, Z.; Luxa, J.; Pumera, M. Layered Platinum Dichalcogenides ($PtS_2$, $PtSe_2$, and $PtTe_2$) Electrocatalysis: Monotonic Dependence on the Chalcogen Size. *Adv. Funct. Mater.* **2016**, *26* (24), 4306–4318. https://doi.org/10.1002/adfm.201505402.

(49) Akshay Kumar, K. P.; Ghosh, K.; Alduhaish, O.; Pumera, M. Dip-Coating of MXene

and Transition Metal Dichalcogenides on 3D-Printed Nanocarbon Electrodes for the Hydrogen Evolution Reaction. *Electrochem. Commun.* **2021**, *122*, 106890. https://doi.org/10.1016/j.elecom.2020.106890.

(50)  Prats, H.; Chan, K. The Determination of the HOR/HER Reaction Mechanism from Experimental Kinetic Data. *Phys. Chem. Chem. Phys.* **2021**, *23* (48), 27150–27158. https://doi.org/10.1039/d1cp04134g.

(51)  Banoth, P.; Kandula, C.; Kollu, P. Introduction to Electrocatalysts. *ACS Symp. Ser.* **2022**, *1432*, 1–37. https://doi.org/10.1021/bk-2022-1432.ch001.

(52)  McCrory, C. C. L.; Jung, S.; Ferrer, I. M.; Chatman, S. M.; Peters, J. C.; Jaramillo, T. F. Benchmarking Hydrogen Evolving Reaction and Oxygen Evolving Reaction Electrocatalysts for Solar Water Splitting Devices. *J. Am. Chem. Soc.* **2015**, *137* (13), 4347–4357. https://doi.org/10.1021/ja510442p.

(53)  MacFarlane, D. R.; Cherepanov, P. V.; Choi, J.; Suryanto, B. H. R.; Hodgetts, R. Y.; Bakker, J. M.; Ferrero Vallana, F. M.; Simonov, A. N. A Roadmap to the Ammonia Economy. *Joule* **2020**, *4* (6), 1186–1205. https://doi.org/10.1016/j.joule.2020.04.004.

(54)  Lu, X.; Song, H.; Cai, J.; Lu, S. Recent Development of Electrochemical Nitrate Reduction to Ammonia: A Mini Review. *Electrochem. commun.* **2021**, *129*, 107094. https://doi.org/10.1016/j.elecom.2021.107094.

(55)  Kandemir, T.; Schuster, M. E.; Senyshyn, A.; Behrens, M.; Schlögl, R. The Haber-Bosch Process Revisited: On the Real Structure and Stability of "Ammonia Iron" under Working Conditions. *Angew. Chemie - Int. Ed.* **2013**, *52* (48), 12723–12726. https://doi.org/10.1002/anie.201305812.

(56)   Foster, S. L.; Bakovic, S. I. P.; Duda, R. D.; Maheshwari, S.; Milton, R. D.; Minteer, S. D.; Janik, M. J.; Renner, J. N.; Greenlee, L. F. Catalysts for Nitrogen Reduction to Ammonia. *Nat. Catal.* **2018**, *1* (7), 490–500. https://doi.org/10.1038/s41929-018-0092-7.

(57)   Padinjareveetil, A. K. K.; Perales-rondon, J. V; Zaoralov, D.; Otyepka, M.; Alduhaish, O.; Pumera, M. Fe-MOF Catalytic Nanoarchitectonic toward Electrochemical Ammonia Production. *ACS Appl. Mater. Interfaces* **2023**, *15*, 47294–47306. https://doi.org/10.1021/acsami.3c12822.

(58)   Wang, Y.; Yu, Y.; Jia, R.; Zhang, C.; Zhang, B. Electrochemical Synthesis of Nitric Acid from Air and Ammonia through Waste Utilization. *Natl. Sci. Rev.* **2019**, *6* (4), 730–738. https://doi.org/10.1093/nsr/nwz019.

(59)   Ju, W.; Bagger, A.; Wang, X.; Tsai, Y.; Luo, F.; Möller, T.; Wang, H.; Rossmeisl, J.; Varela, A. S.; Strasser, P. Unraveling Mechanistic Reaction Pathways of the Electrochemical $CO_2$ Reduction on Fe-N-C Single-Site Catalysts. *ACS Energy Lett.* **2019**, *4* (7), 1663–1671. https://doi.org/10.1021/acsenergylett.9b01049.

(60)   Kortlever, R.; Peters, I.; Koper, S.; Koper, M. T. M. Electrochemical $CO_2$ Reduction to Formic Acid at Low Overpotential and with High Faradaic Efficiency on Carbon-Supported Bimetallic Pd-Pt Nanoparticles. *ACS Catal.* **2015**, *5* (7), 3916–3923. https://doi.org/10.1021/acscatal.5b00602.

(61)   Asmare, M.; Do, H. H.; Hasani, A.; Le, Q. Van; Jang, H. W.; Ahn, S. H.; Kim, S. Y. Two-Dimensional Materials and Metal-Organic Frameworks for the $CO_2$ Reduction Reaction. *Mater. Today Adv.* **2020**, *5*, 100038. https://doi.org/10.1016/j.mtadv.2019.100038.

(62)   Resasco, J.; Bell, A. T. Electrocatalytic $CO_2$ Reduction to Fuels: Progress and

Opportunities. *Trends Chem.* **2020**, *2* (9), 825–836. https://doi.org/10.1016/j.trechm.2020.06.007.

(63)  Boutin, E.; Merakeb, L.; Ma, B.; Boudy, B.; Wang, M.; Bonin, J.; Anxolabéhère-Mallart, E.; Robert, M. Molecular Catalysis of $CO_2$ reduction: Recent Advances and Perspectives in Electrochemical and Light-Driven Processes with Selected Fe, Ni and Co Aza Macrocyclic and Polypyridine Complexes. *Chem. Soc. Rev.* **2020**, *49* (16), 5772–5809. https://doi.org/10.1039/d0cs00218f.

(64)  Zhang, W.; Hu, Y.; Ma, L.; Zhu, G.; Wang, Y.; Xue, X.; Chen, R.; Yang, S.; Jin, Z. Progress and Perspective of Electrocatalytic $CO_2$ Reduction for Renewable Carbonaceous Fuels and Chemicals. *Adv. Sci.* **2018**, *5* (1), 1700275. https://doi.org/10.1002/advs.201700275.

(65)  Areir, M.; Xu, Y.; Harrison, D.; Fyson, J. 3D Printing of Highly Flexible Supercapacitor Designed for Wearable Energy Storage. *Mater. Sci. Eng. B,* **2017**, *226*, 29–38. https://doi.org/10.1016/j.mseb.2017.09.004.

(66)  Shen, K.; Li, B.; Yang, S. 3D Printing Dendrite-Free Lithium Anodes Based on the Nucleated MXene Arrays. *Energy Storage Mater.* **2020**, *24*, 670–675. https://doi.org/10.1016/j.ensm.2019.08.015.

(67)  Zhu, J.; Wu, P.; Chao, Y.; Yu, J.; Zhu, W.; Liu, Z, Xu, C. Recent Advances in 3D Printing for Catalytic Applications. *Chem. Eng. J.* **2022**, *433* (P1), 134341. https://doi.org/10.1016/j.cej.2021.134341.

(68)  Foster, C. W.; Down, M. P.; Zhang, Y.; Ji, X.; Rowley-Neale, S. J.; Smith, G. C.; Kelly, P. J.; Banks, C. E. 3D Printed Graphene Based Energy Storage Devices. *Sci. Rep.* **2017**, *7*, 42233. https://doi.org/10.1038/srep42233.

(69) Ambrosi, A.; Pumera, M. 3D-Printing Technologies for Electrochemical Applications. *Chem. Soc. Rev.* **2016**, *45* (10), 2740–2755. https://doi.org/10.1039/c5cs00714c.

(70) Quero, R. F.; Costa, B. M. de C.; da Silva, J. A. F.; de Jesus, D. P. Using Multi-Material Fused Deposition Modeling (FDM) for One-Step 3D Printing of Microfluidic Capillary Electrophoresis with Integrated Electrodes for Capacitively Coupled Contactless Conductivity Detection. *Sensors Actuators B Chem.* **2022**, *365* 131959. https://doi.org/10.1016/j.snb.2022.131959.

(71) Hartings, M. R.; Ahmed, Z. Chemistry from 3D Printed Objects. *Nat. Rev. Chem.* **2019**, *3* (5), 305–314. https://doi.org/10.1038/s41570-019-0097-z.

(72) Browne, M. P.; Redondo, E.; Pumera, M. 3D Printing for Electrochemical Energy Applications. *Chem. Rev.* **2020**, *120* (5), 2783–2810. https://doi.org/10.1021/acs.chemrev.9b00783.

(73) Redondo, E.; Muñoz, J.; Pumera, M. Green Activation Using Reducing Agents of Carbon-Based 3D Printed Electrodes: Turning Good Electrodes to Great. *Carbon.* **2021**, *175*, 413–419. https://doi.org/10.1016/j.carbon.2021.01.107.

(74) Shahrubudin, N.; Lee, T. C.; Ramlan, R. An Overview on 3D Printing Technology: Technological, Materials, and Applications. *Procedia Manuf.* **2019**, *35*, 1286–1296. https://doi.org/10.1016/j.promfg.2019.06.089.

(75) Fu, K.; Yao, Y.; Dai, J.; Hu, L. Progress in 3D Printing of Carbon Materials for Energy-Related Applications. *Adv. Mater.* **2017**, *29* (9), 1603486. https://doi.org/10.1002/adma.201603486.

(76) dos Santos, P. L.; Rowley-Neale, S. J.; Ferrari, A. G. M.; Bonacin, J. A.; Banks, C.

E. Ni−Fe (Oxy)Hydroxide Modified Graphene Additive Manufactured (3D-Printed) Electrochemical Platforms as an Efficient Electrocatalyst for the Oxygen Evolution Reaction. *ChemElectroChem* **2019**, *6* (22), 5633–5641. https://doi.org/10.1002/celc.201901541.

(77) Iffelsberger, C.; Rojas, D.; Pumera, M. Photo-Responsive Doped 3D-Printed Copper Electrodes for Water Splitting: Refractory One-Pot Doping Dramatically Enhances the Performance. *J. Phys. Chem. C* **2022**, *126* (21), 9016–9026. https://doi.org/10.1021/acs.jpcc.1c10686.

(78) Gusmão, R.; Sofer, Z.; Marvan, P.; Pumera, M. MoS2 Versatile Spray-Coating of 3D Electrodes for the Hydrogen Evolution Reaction. *Nanoscale* **2019**, *11* (20), 9888–9895. https://doi.org/10.1039/c9nr01876j.

(79) Ghosh, K.; Ng, S.; Iffelsberger, C.; Pumera, M. 2D MoS2/Carbon/Polylactic Acid Filament for 3D Printing: Photo and Electrochemical Energy Conversion and Storage. *Appl. Mater. Today* **2022**, *26*. https://doi.org/10.1016/j.apmt.2021.101301.

(80) Vaněčková, E.; Bouša, M.; Shestivska, V.; Kubišta, J.; Moreno-García, P.; Broekmann, P.; Rahaman, M.; Zlámal, M.; Heyda, J.; Bernauer, M.; et al. Electrochemical Reduction of Carbon Dioxide on 3D Printed Electrodes. *ChemElectroChem* **2021**, *8* (11), 2137–2149. https://doi.org/10.1002/celc.202100261.

(81) Wicks, J.; Jue, M. L.; Beck, V. A.; Oakdale, J. S.; Dudukovic, N. A.; Clemens, A. L.; Liang, S.; Ellis, M. E.; Lee, G.; Baker, S. E.; et al. 3D-Printable Fluoropolymer Gas Diffusion Layers for $CO_2$ Electroreduction. *Adv. Mater.* **2021**, *33* (7), 1–8, 2003855. https://doi.org/10.1002/adma.202003855.

(82) Perales-Rondon, J. V.; Rojas, D.; Gao, W.; Pumera, M. Copper 3D-Printed

Electrodes for Ammonia Electrosynthesis via Nitrate Reduction. *ACS Sustain. Chem. Eng.* **2023**, *11* (18), 6923–6931. https://doi.org/10.1021/acssuschemeng.2c06851.

(83)   Strmcnik, D.; Lopes, P. P.; Genorio, B.; Stamenkovic, V. R.; Markovic, N. M. Design Principles for Hydrogen Evolution Reaction Catalyst Materials. *Nano Energy* **2016**, *29*, 29–36. https://doi.org/10.1016/j.nanoen.2016.04.017.

(84)   Ge, Z.; Fu, B.; Zhao, J.; Li, X.; Ma, B.; Chen, Y. A Review of the Electrocatalysts on Hydrogen Evolution Reaction with an Emphasis on Fe, Co and Ni-Based Phosphides. *J. Mater. Sci.* **2020**, *55* (29), 14081–14104. https://doi.org/10.1007/s10853-020-05010-w.

(85)   Ji, J.; Zhang, Y.; Tang, L.; Liu, C.; Gao, X.; Sun, M.; Zheng, J.; Ling, M.; Liang, C.; Lin, Z. Platinum Single-Atom and Cluster Anchored on Functionalized MWCNTs with Ultrahigh Mass Efficiency for Electrocatalytic Hydrogen Evolution. *Nano Energy* **2019**, *63*, 103849. https://doi.org/10.1016/j.nanoen.2019.06.045.

(86)   Zhang, J.; Zhao, Y.; Guo, X.; Chen, C.; Dong, C. L.; Liu, R. S.; Han, C. P.; Li, Y.; Gogotsi, Y.; Wang, G. Single Platinum Atoms Immobilized on an MXene as an Efficient Catalyst for the Hydrogen Evolution Reaction. *Nat. Catal.* **2018**, *1*, 985–992. https://doi.org/10.1038/s41929-018-0195-1.

(87)   Huang, B.; Zhao, Y. Iridium-based Electrocatalysts toward Sustainable Energy Conversion. *EcoMat* **2022**, *4* (2), e12176. https://doi.org/10.1002/eom2.12176.

(88)   Chen, Z.; Duan, X.; Wei, W.; Wang, S.; Ni, B. J. Iridium-Based Nanomaterials for Electrochemical Water Splitting. *Nano Energy* **2020**, *78* (August), 105270. https://doi.org/10.1016/j.nanoen.2020.105270.

(89)   Yu, J.; He, Q.; Yang, G.; Zhou, W.; Shao, Z.; Ni, M. Recent Advances and

Prospective in Ruthenium-Based Materials for Electrochemical Water Splitting. *ACS Catal.* **2019**, *9* (11), 9973–10011. https://doi.org/10.1021/acscatal.9b02457.

(90) Bae, S. Y.; Mahmood, J.; Jeon, I. Y.; Baek, J. B. Recent Advances in Ruthenium-Based Electrocatalysts for the Hydrogen Evolution Reaction. *Nanoscale Horizons* **2020**, *5*, 43–56. https://doi.org/10.1039/c9nh00485h.

(91) Hu, K.; Ohto, T.; Nagata, Y.; Wakisaka, M.; Aoki, Y.; Fujita, J. ichi; Ito, Y. Catalytic Activity of Graphene-Covered Non-Noble Metals Governed by Proton Penetration in Electrochemical Hydrogen Evolution Reaction. *Nat. Commun.* **2021**, *12*, 203, 1–3. https://doi.org/10.1038/s41467-020-20503-7.

(92) Wu, T.; Sun, M.; Wong, H. H.; Chan, C. H.; Lu, L.; Lu, Q.; Chen, B.; Huang, B. Recent Advances and Strategies of Electrocatalysts for Large Current Density Industrial Hydrogen Evolution Reaction. *Inorg. Chem. Front.* **2023**, *10* (16), 4632–4649. https://doi.org/10.1039/d3qi00799e.

(93) Liu, T.; Li, P.; Yao, N.; Cheng, G.; Chen, S.; Luo, W.; Yin, Y. CoP-Doped MOF-Based Electrocatalyst for pH-Universal Hydrogen Evolution Reaction. *Angew. Chemie - Int. Ed.* **2019**, *58* (14), 4679–4684. https://doi.org/10.1002/anie.201901409.

(94) Browne, M. P.; Novotný, F.; Manzanares Palenzuela, C. L.; Šturala, J.; Sofer, Z.; Pumera, M. 2H and 2H/1T-Transition Metal Dichalcogenide Films Prepared via Powderless Gas Deposition for the Hydrogen Evolution Reaction. *ACS Sustain. Chem. Eng.* **2019**, *7* (19), 16440–16449. https://doi.org/10.1021/acssuschemeng.9b03637.

(95) Wang, P.; Wang, B. Designing Self-Supported Electrocatalysts for Electrochemical Water Splitting: Surface/Interface Engineering toward Enhanced Electrocatalytic Performance. *ACS Appl. Mater. Interfaces* **2021**, *13* (50), 59593–59617.

https://doi.org/10.1021/acsami.1c17448.

(96) Yang, H.; Driess, M.; Menezes, P. W. Self-Supported Electrocatalysts for Practical Water Electrolysis. *Adv. Energy Mater.* **2021**, *11* (39). https://doi.org/10.1002/aenm.202102074.

(97) Sun, C.; Zhang, J.; Ma, J.; Liu, P.; Gao, D.; Tao, K.; Xue, D. N-Doped $WS_2$ Nanosheets: A High-Performance Electrocatalyst for the Hydrogen Evolution Reaction. *J. Mater. Chem. A* **2016**, *4* (29), 11234–11238. https://doi.org/10.1039/c6ta04082a.

(98) Xiong, L.; Wang, B.; Cai, H.; Hao, H.; Li, J.; Yang, T.; Yang, S. Understanding the Doping Effect on Hydrogen Evolution Activity of Transition-Metal Phosphides: Modeled with Ni2P. *Appl. Catal. B Environ.* **2021**, *295* (28), 120283. https://doi.org/10.1016/j.apcatb.2021.120283.

(99) Ma, Z.; Niu, L.; Jiang, W.; Dong, C.; Liu, G.; Qu, D.; An, L.; Sun, Z. Recent Advances of Single-Atom Electrocatalysts for Hydrogen Evolution Reaction. *JPhys Mater.* **2021**, *4* (4). https://doi.org/10.1088/2515-7639/ac01ac.

(100) Gao, X.; Dai, Q.; Lu, X.; Kawi, S. Carbon-Supported Non-Noble Metal Single-Atom Catalysts for Electro-Catalytic Hydrogen Evolution Reaction. *Int. J. Hydrogen Energy* **2023**, *48* (45), 17106–17136. https://doi.org/10.1016/j.ijhydene.2023.01.213.

(101) Wang, Z.; Tang, M. T.; Cao, A.; Chan, K.; Norskov, J. K. Insights into the Hydrogen Evolution Reaction on 2D Transition-Metal Dichalcogenides. *J. Phys. Chem. C* **2022**, *126* (11), 5151–5158. https://doi.org/10.1021/acs.jpcc.1c10436.

(102) Najafi, L.; Bellani, S.; Oropesa-Nuñez, R.; Martín-García, B.; Prato, M.; Bonaccorso, F. Single-/Few-Layer Graphene as Long-Lasting Electrocatalyst for Hydrogen

Evolution Reaction. *ACS Appl. Energy Mater.* **2019**, *2* (8), 5373–5379. https://doi.org/10.1021/acsaem.9b00949.

(103) van Langevelde, P. H.; Katsounaros, I.; Koper, M. T. M. Electrocatalytic Nitrate Reduction for Sustainable Ammonia Production. *Joule* **2021**, *5* (2), 290–294. https://doi.org/10.1016/j.joule.2020.12.025.

(104) Crawford, J.; Yin, H.; Du, A.; O'Mullane, A. P. Nitrate-to-Ammonia Conversion at an InSn-Enriched Liquid-Metal Electrode. *Angew. Chemie - Int. Ed.* **2022**, 61 (23), e202201604. https://doi.org/10.1002/anie.202201604.

(105) Li, L. X.; Sun, W. J.; Zhang, H. Y.; Wei, J. L.; Wang, S. X.; He, J. H.; Li, N. J.; Xu, Q. F.; Chen, D. Y.; Li, H.; Lu, J. . Highly Efficient and Selective Nitrate Electroreduction to Ammonia Catalyzed by Molecular Copper Catalyst@Ti3C2Tx MXene. *J. Mater. Chem. A* **2021**, 9 (38), 21771–21778. https://doi.org/https://doi.org/10.1039/d1ta06664a.

(106) Chen, G. F.; Yuan, Y.; Jiang, H.; Ren, S. Y.; Ding, L. X.; Ma, L.; Wu, T.; Lu, J.; Wang, H. Electrochemical Reduction of Nitrate to Ammonia via Direct Eight-Electron Transfer Using a Copper–Molecular Solid Catalyst. *Nat. Energy* **2020**, *5* (8), 605–613. https://doi.org/10.1038/s41560-020-0654-1.

(107) Wang, Y.; Xu, A.; Wang, Z.; Huang, L.; Li, J.; Li, F.; Wicks, J.; Luo, M.; Nam, D. H.; Tan, C. S.; et al. Enhanced Nitrate-to-Ammonia Activity on Copper-Nickel Alloys via Tuning of Intermediate Adsorption. *J. Am. Chem. Soc.* **2020**, *142* (12), 5702–5708. https://doi.org/10.1021/jacs.9b13347.

(108) Wang, C.; Ye, F.; Shen, J.; Xue, K. H.; Zhu, Y.; Li, C. In Situ Loading of $Cu_2O$ Active Sites on Island-like Copper for Efficient Electrochemical Reduction of Nitrate to Ammonia. *ACS Appl. Mater. Interfaces* **2022**, *14* (5), 6680–6688.

https://doi.org/10.1021/acsami.1c21691.

(109) Wang, Y.; Zhou, W.; Jia, R.; Yu, Y.; Zhang, B. Unveiling the Activity Origin of a Copper-Based Electrocatalyst for Selective Nitrate Reduction to Ammonia. *Angew. Chemie - Int. Ed.* **2020**, *59* (13), 5350–5354. https://doi.org/10.1002/anie.201915992.

(110) McEnaney, J. M.; Blair, S. J.; Nielander, A. C.; Schwalbe, J. A.; Koshy, D. M.; Cargnello, M.; Jaramillo, T. F. Electrolyte Engineering for Efficient Electrochemical Nitrate Reduction to Ammonia on a Titanium Electrode. *ACS Sustain. Chem. Eng.* **2020**, *8* (7), 2672–2681. https://doi.org/10.1021/acssuschemeng.9b05983.

(111) Wu, Z. Y.; Karamad, M.; Yong, X.; Huang, Q.; Cullen, D. A.; Zhu, P.; Xia, C.; Xiao, Q.; Shakouri, M.; Chen, F. Y.; et al. Electrochemical Ammonia Synthesis via Nitrate Reduction on Fe Single Atom Catalyst. *Nat. Commun.* **2021**, *12* (1), 2870. https://doi.org/10.1038/s41467-021-23115-x.

(112) Hu, T.; Wang, M.; Guo, C.; Li, C. M. Functionalized MXenes for Efficient Electrocatalytic Nitrate Reduction to Ammonia. *J. Mater. Chem. A* **2022**, 10 (16), 8923–8931. https://doi.org/10.1039/d2ta00470d.

(113) Huang, L.; Cheng, L.; Ma, T.; Zhang, J. J.; Wu, H.; Su, J.; Song, Y.; Zhu, H.; Liu, Q.; Zhu, M.; et al. Direct Synthesis of Ammonia from Nitrate on Amorphous Graphene with Near 100% Efficiency. *Adv. Mater.* **2023**, *35* (24), 1–11. https://doi.org/10.1002/adma.202211856.

(114) Zhang, S.; Li, M.; Li, J.; Song, Q.; Liu, X. High-Ammonia Selective Metal-Organic Framework-Derived Co-Doped $Fe/Fe_2O_3$ Catalysts for Electrochemical Nitrate Reduction. *Proc. Natl. Acad. Sci. U. S. A.* **2022**, *119* (6), e2115504119. https://doi.org/10.1073/pnas.2115504119.

(115) Qin, J.; Wu, K.; Chen, L.; Wang, X.; Zhao, Q.; Liu, B.; Ye, Z. Achieving High Selectivity for Nitrate Electrochemical Reduction to Ammonia over MOF-Supported RuxOy clusters. *J. Mater. Chem. A* **2022**, *10* (8), 3963–3969. https://doi.org/10.1039/d1ta09441f.

(116) Gao, Z.; Lai, Y.; Tao, Y.; Xiao, L.; Zhang, L.; Luo, F. Constructing Well-Defined and Robust Th-MOF-Supported Single-Site Copper for Production and Storage of Ammonia from Electroreduction of Nitrate. *ACS Cent. Sci.* **2021**, *7* (6), 1066–1072. https://doi.org/10.1021/acscentsci.1c00370.

(117) Gao, W; Perales-Rondon, J. V, Michalička, J; Pumera M. Ultrathin Manganese Oxides Enhance the Electrocatalytic Properties of 3D Printed Carbon Catalysts for Electrochemical Nitrate Reduction to Ammonia. *Appl. Catal. B Environ.* **2023**, 330, 122632. https://doi.org/10.1016/j.apcatb.2023.122632.

(118) Zhao, S.; Jin, R.; Jin, R. Opportunities and Challenges in $CO_2$ Reduction by Gold- and Silver-Based Electrocatalysts: From Bulk Metals to Nanoparticles and Atomically Precise Nanoclusters. *ACS Energy Lett.* **2018**, *3* (2), 452–462. https://doi.org/10.1021/acsenergylett.7b01104.

(119) Bach, W. Impact of Increasing Atmospheric $CO_2$ Concentrations on Global Climate: Potential Consequences and Corrective Measures. *Environ. Int.* **1979**, *2* (4–6), 215–228. https://doi.org/10.1016/0160-4120(79)90004-7.

(120) Nitopi, S.; Bertheussen, E.; Scott, S. B.; Liu, X.; Engstfeld, A. K.; Horch, S.; Seger, B.; Stephens, I. E. L.; Chan, K.; Hahn, C.; et al. Progress and Perspectives of Electrochemical $CO_2$ Reduction on Copper in Aqueous Electrolyte. *Chem. Rev.* **2019**, *119* (12), 7610–7672. https://doi.org/10.1021/acs.chemrev.8b00705.

(121) Pan, F., Yang, X., O'Carroll, T., Li, H., Chen, K.-J., Wu, G. Carbon Catalysts for

Electrochemical CO2 Reduction toward Multicarbon Products. *Adv. Energy Mater.* **2022**, 12, 2200586. https://doi.org/10.1002/aenm.202200586

(122) Pan, H.; Barile, C. J. Bifunctional Nickel and Copper Electrocatalysts for $CO_2$ Reduction and the Oxygen Evolution Reaction. *J. Mater. Chem. A* **2020**, *8* (4), 1741– 1748. https://doi.org/10.1039/c9ta12055f.

(123) Yan, W. Y.; Zhang, C.; Liu, L. Hierarchically Porous CuAg via 3D Printing/Dealloying for Tunable $CO_2$ Reduction to Syngas. *ACS Appl. Mater. Interfaces* **2021**, *13* (38), 45385–45393. https://doi.org/10.1021/acsami.1c10564.

(124) Browne, M. P.; Plutnar, J.; Pourrahimi, A. M.; Sofer, Z.; Pumera, M. Atomic Layer Deposition as a General Method Turns Any 3D-Printed Electrode into a Desired Catalyst: Case Study in Photoelectrochemisty. *Adv. Energy Mater.* **2019**, *9* (26), 1900994. https://doi.org/10.1002/aenm.201900994.

(125) Madhu, R.; Veeramani, V.; Chen, S. M.; Manikandan, A.; Lo, A. Y.; Chueh, Y. L. Honeycomb-like Porous Carbon-Cobalt Oxide Nanocomposite for High-Performance Enzymeless Glucose Sensor and Supercapacitor Applications. *ACS Appl. Mater. Interfaces* **2015**, *7* (29), 15812–15820. https://doi.org/10.1021/acsami.5b04132.

(126) Zhu, H.; Li, L.; Zhou, W.; Shao, Z.; Chen, X. Advances in Non-Enzymatic Glucose Sensors Based on Metal Oxides. *J. Mater. Chem. B* **2016**, *4* (46), 7333–7349. https://doi.org/10.1039/C6TB02037B.

(127) Liao, L.; Peng, H.; Liu, Z. Chemistry Makes Graphene beyond Graphene. *J. Am. Chem. Soc.* **2014**, *136* (35), 12194–12200. https://doi.org/10.1021/ja5048297.

(128) Eigler, S.; Hirsch, A. Chemistry with Graphene and Graphene Oxide - Challenges

for Synthetic Chemists. *Angew. Chemie - Int. Ed.* **2014**, *53* (30), 7720–7738. https://doi.org/10.1002/anie.201402780.

(129) Zhang, L. L.; Zhou, R.; Zhao, X. S. Graphene-Based Materials as Supercapacitor Electrodes. *J. Mater. Chem.* **2010**, *20* (29), 5983–5992. https://doi.org/10.1039/c000417k.

(130) Goubaa, H.; Escobar-Teran, F.; Ressam, I.; Gao, W.; El Kadib, A.; Lucas, I. T.; Raihane, M.; Lahcini, M.; Perrot, H.; Sel, O. Dynamic Resolution of Ion Transfer in Electrochemically Reduced Graphene Oxides Revealed by Electrogravimetric Impedance. *J. Phys. Chem. C* **2017**, *121* (17), 9370–9380. https://doi.org/10.1021/acs.jpcc.7b01421.

(131) Choi, S.; Kim, C.; Suh, J. M.; Jang, H. W. Reduced Graphene Oxide-based Materials for Electrochemical Energy Conversion Reactions. *Carbon Energy* **2019**, *1* (1), 85–108. https://doi.org/10.1002/cey2.13.

(132) Ayala, P.; Arenal, R.; Rümmeli, M.; Rubio, A.; Pichler, T. The Doping of Carbon Nanotubes with Nitrogen and Their Potential Applications. *Carbon* **2010**, *48* (3), 575–586. https://doi.org/10.1016/j.carbon.2009.10.009.

(133) Zhao, Y.; Yang, L.; Chen, S.; Wang, X.; Ma, Y.; Wu, Q.; Jiang, Y.; Qian, W.; Hu, Z. Can Boron and Nitrogen Co-Doping Improve Oxygen Reduction Reaction Activity of Carbon Nanotubes? *J. Am. Chem. Soc.* **2013**, *135* (4), 1201–1204. https://doi.org/10.1021/ja310566z.

(134) Lazar, P.; Mach, R.; Otyepka, M. Spectroscopic Fingerprints of Graphitic, Pyrrolic, Pyridinic, and Chemisorbed Nitrogen in N-Doped Graphene. *J. Phys. Chem. C* **2019**, *123* (16), 10695–10702. https://doi.org/10.1021/acs.jpcc.9b02163.

(135)  Li, C.; Hu, Y.; Yu, M.; Wang, Z.; Zhao, W.; Liu, P.; Tong, Y.; Lu, X. Nitrogen Doped Graphene Paper as a Highly Conductive, and Light-Weight Substrate for Flexible Supercapacitors. *RSC Adv.* **2014**, *4* (94), 51878–51883. https://doi.org/10.1039/c4ra11024b.

(136)  Sokol, M.; Natu, V.; Kota, S.; Barsoum, M. W. On the Chemical Diversity of the MAX Phases. *Trends Chem.* **2019**, *1* (2), 210–223. https://doi.org/10.1016/j.trechm.2019.02.016.

(137)  Radovic, M.; Barsoum, M. W. MAX Phases: Bridging the Gap between Metals and Ceramics. *Am. Ceram. Soc. Bull.* **2013**, *92* (3), 20–27. https://ceramics.org/wp-content/uploads/2013/03/bulletin042013_maxphases.pdf.

(138)  Rosli, N. F.; Nasir, M. Z. M.; Antonatos, N.; Sofer, Z.; Dash, A.; Gonzalez-Julian, J.; Fisher, A. C.; Webster, R. D.; Pumera, M. MAX and MAB Phases: Two-Dimensional Layered Carbide and Boride Nanomaterials for Electrochemical Applications. *ACS Appl. Nano Mater.* **2019**, 2 (9), 6010–6021. https://doi.org/10.1021/acsanm.9b01526.

(139)  Zhang, C. J.; Ma, Y.; Zhang, X.; Abdolhosseinzadeh, S.; Sheng, H.; Lan, W.; Pakdel, A.; Heier, J.; Nüesch, F. Two-Dimensional Transition Metal Carbides and Nitrides ( MXenes ): Synthesis , Properties , and Electrochemical Energy Storage Applications. **2020**, 3 (1),  29-55. https://doi.org/10.1002/eem2.12058.

(140)  Abdolhosseinzadeh, S.; Jiang, X.; Zhang, H.; Qiu, J.; Zhang, C. J. Perspectives on Solution Processing of Two-Dimensional MXenes. *Mater. Today* **2021**, *48*, 214–240. https://doi.org/10.1016/j.mattod.2021.02.010.

(141)  Iffelsber, C.; Ng, S.; Pumera, M. Catalyst Coating of 3D Printed Structures via Electrochemical Deposition : Case of the Transition Metal Chalcogenide MoS x for

Hydrogen Evolution Reaction. *Appl. Mater. Today* **2020**, *20*, 100654. https://doi.org/10.1016/j.apmt.2020.100654.

(142) Manzeli, S.; Ovchinnikov, D.; Pasquier, D.; Yazyev, O. V.; Kis, A. 2D Transition Metal Dichalcogenides. *Nat. Rev. Mater.* **2017**, *2, 17033*. https://doi.org/10.1038/natrevmats.2017.33.

(143) Yuan, S.; Sun, X.; Pang, J.; Lollar, C.; Qin, J. S.; Perry, Z.; Joseph, E.; Wang, X.; Fang, Y.; Bosch, M.; et al. PCN-250 under Pressure: Sequential Phase Transformation and the Implications for MOF Densification. *Joule* **2017**, *1* (4), 806–815. https://doi.org/10.1016/j.joule.2017.09.001.

(144) Strem Chemicals. Metal Organic Frameworks and Ligands for MOF Synthesis. *Strem Chem. Inc.* **2018**.

(145) Wang, Q.; Astruc, D. State of the Art and Prospects in Metal-Organic Framework (MOF)-Based and MOF-Derived Nanocatalysis. *Chem. Rev.* **2020**, *120* (2), 1438–1511. https://doi.org/10.1021/acs.chemrev.9b00223.

(146) An, J. R.; Wang, Y.; Dong, W. W.; Gao, X. J.; Yang, O. Y.; Liu, Y. L.; Zhao, J.; Li, D. S. Efficient Visible-Light Photoreduction of $CO_2$ to $CH_4$ over an Fe-Based Metal-Organic Framework (PCN-250-Fe3) in a Solid-Gas Mode. *ACS Appl. Energy Mater.* **2022**, *5* (2), 2384–2390. https://doi.org/10.1021/acsaem.1c03868.

(147) Feng, D.; Wang, K.; Wei, Z.; Chen, Y. P.; Simon, C. M.; Arvapally, R. K.; Martin, R. L.; Bosch, M.; Liu, T. F.; Fordham, S.; et al. Kinetically Tuned Dimensional Augmentation as a Versatile Synthetic Route towards Robust Metal-Organic Frameworks. *Nat. Commun.* **2014**, *5, 5723*. https://doi.org/10.1038/ncomms6723.

(148) Wert, S.; Iffelsberger, C.; K Padinjareveetil, A. K.; Pumera, M. Edges of Layered

FePSe3 Exhibit Increased Electrochemical and Electrocatalytic Activity Compared to Basal Planes. *ACS Appl. Electron. Mater.* **2023**, 5 (2), 928−934. https://doi.org/10.1021/acsaelm.2c01493.

# CHAPTER 8

## Chapter 8:  Conferences, presentations and achievements

### 8.1 Oral and poster presentations at international conferences

1. 07/2022- MXenes: Addressing Global Challenges with Innovation, The 2$^{nd}$ International Conference at Drexel University, Philadelphia, USA; Poster Presentation; Title: Patterning and printing of MXene 3D-printed electrode for energy conversion applications.

2. 10/2021-NANOCON, 13$^{th}$ International Conference on Nanomaterials - Research & Application, Brno, Czech Republic; Oral Presentation. Title: Expanding Horizons of 3D-Printing Industry Towards Multidimensional Applications

### 8.2 Online conferences/workshops

1. 2021- Emerging Frontiers in Chemical Sciences (EFCS), International conference conducted by Research Department of Chemistry, Farook college, INDIA, Online.

2. 2021- 3$^{rd}$ Cross-Border Seminar on Electroanalytical Chemistry, University of Regensburg, Oral Presentation.

3.    2021-MXene workshop lead by Prof. Yury Gogotsi and team. Topic: Synthesis, Characterization and electrochemical measurements of MXenes (5 days), Drexel University USA, Online.

## 8.3 Achievements

1.    Specific Research Grant 2020-2021, Principal investigator, (CEITEC VUT-J-20-6527)

2.    Specific Research Grant 2021-2022, Principal investigator, (CEITEC BUT-J-21-7560)

3.    European Union - Internal grant competition 2021 – 2023, Principal investigator, grant CEITEC-K-21-7059, realized within the project Quality Internal Grants of BUT (KInG BUT), Reg. No. CZ.02.2.69/0.0/0.0/19_073/0016948 and financed from the OP RDE.

4.    ERASMUS International Mobility grant, May-July 2023.

5.    2021- Most downloaded article in EC web (#9)-MXene and Transition Metal Dichalcogenides Dip-Coating on 3D-printed Nanocarbon Electrode for Hydrogen Evolution Reaction.

6.    2020-Most downloaded article in EC web (#2)-Metal plated 3D-printed electrode for electrochemical detection of carbohydrates.

# CHAPTER 9

## Appendix A

## Edge vs. Basal plane activity of layered FePSe$_3$ crystal for HER

**Motivation**

The origin of electrocatalytic activity is always curious driven, as understanding of these active hotspots can yield catalysts for specific applications. With the increasing interest in understanding the origin of activity (edge vs basal planes) of layered materials, advanced technologies such as scanning electrochemical microscopy (SECM) can play key role in providing vital information about active sites.

**Objective**

Edges or basal planes of FePSe$_3$ crystal will be evaluated for local electrochemical and electrocatalytic activity. Morphological characterization will be carried out and SECM will be employed to track active sites of the layered crystal, along with evaluation of the HER activity of FePSe$_3$ catalyst.

**Outcome**

Electrochemical processes and H$_2$ generation were found to be driven by edge-like defects of FePSe$_3$ crystals, over basal planes. In short, advanced technologies like SECM can be employed to identify the active sites in layered materials for applications such as H$_2$

production. Also, such studies can be vital for application of layered materials for electrochemistry related applications.

**Contribution**

XRD measurements, writing (review and editing).

**Article**

The article was published and the details of the article are as follows:

Stefan Wert, Christian Iffelsberger, Akshay Kumar K. Padinjareveetil, and Martin Pumera*, *Edges of Layered FePSe3 Exhibit Increased Electrochemical and Electrocatalytic Activity Compared to Basal Planes*, **ACS Appl. Electron. Mater.** 2023, 5, 2, 928–934 https://doi.org/10.1021/acsaelm.2c01493, (IF=4.49).

# Edges of Layered FePSe₃ Exhibit Increased Electrochemical and Electrocatalytic Activity Compared to Basal Planes

Stefan Wert, Christian Iffelsberger, Akshay Kumar K. Padinjareveetil, and Martin Pumera*

ACCESS | 　Metrics & More | 　Article Recommendations

**ABSTRACT:** Transition metal trichalcogenphosphites (MPX₃), belonging to the class of 2D materials, are potentially viable electrocatalysts for the hydrogen evolution reaction (HER). Many 2D and layered materials exhibit different magnitudes of electrochemical and electrocatalytic activity at their edge and basal sites. To find out whether edges or basal planes are the primary sites for catalytic processes at these compounds, we studied the local electrochemical and electrocatalytic activity of FePSe₃, an MPX₃ representative that was previously found to be catalytically active. Using scanning electrochemical microscopy, we discovered that electrochemical processes and the HER are occurring at an increased rate at edge-like defects of FePSe₃ crystals. We correlate our observations using optical microscopy, confocal laser scanning microscopy, scanning electron microscopy, and electron-dispersive X-ray spectroscopy. These findings have profound implications for the application of these materials for electrochemistry as well as for understanding general rules governing the electrochemical performance of layered compounds.

**KEYWORDS:** *scanning electrochemical microscopy, 2D materials, transition metal trichalcogenphosphites, iron phosphotriselenide, hydrogen evolution reaction, electrocatalysis, electrochemistry*
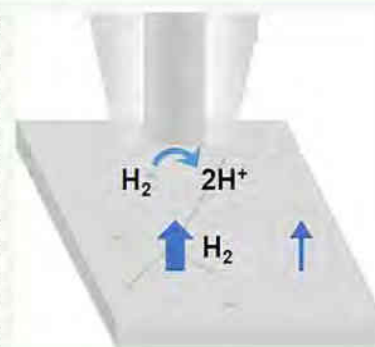
## INTRODUCTION

Hydrogen has been identified as a promising medium to store energy and as a green fuel for the transport sector. However, obtaining green hydrogen in an economically feasible manner remains a big challenge. The main green route for producing hydrogen is electrochemical water splitting.[1] The energy consumption of this process can be decreased using suitable electrocatalysts such as platinum, but its rarity and high cost are the main reasons why electrochemical water splitting cannot be performed on an industrial scale yet.[2]

Consequently, research for alternative catalyst materials has sparked in recent years.[2] A large group of promising candidates can be found among the so-called 2D materials, which consist of layers of atomic thickness held together by van der Waals forces.[3] Starting from graphene,[4] multiple classes of 2D materials have been identified, including, but not limited to, layered pnictogens,[5−8] transition metal dichalcogenides,[9−13] transition metal oxides,[14] metal−organic frameworks,[15,16] and MXenes.[17−19] They cover a wide array of remarkable properties such as high electrical conductivity, charge capacity,[20,21] or electrocatalytic activity[10−13,19,22,23] depending on the individual material. Another group of 2D materials that has emerged recently is the group of transition metal trichalcogenphosphites (MPX₃; M: transition metal, P: phosphor, and X: chalcogenide).[24] They were initially studied mainly for their magnetic properties.[25] Recent studies however

have shown their remarkable electrocatalytic and photocatalytic properties.[26−30]

For the optimization of catalyst materials, it is important to know where the catalytic hotspots are located. It was found that graphite,[31] graphene,[32−34] transition metal dichalcogenides,[35−40] and layered pnictogens[41,42] show increased electrochemical and electrocatalytic activity at the edges of individual layers compared to their basal planes. In the case of MXenes, the opposite was observed in a study by Djire et al.,[43] suggesting that the basal planes are more electrocatalytically active. For MPX₃ compounds, a theoretical study of catalytic hotspots for the cases of FePSe₃ and MnPSe₃ was performed.[44] Based on density functional theory, the authors conclude that edges are more active for the hydrogen evolution reaction (HER) than basal planes. However, these results need to be confirmed by electrochemical experiments. A useful technique to investigate the local electrochemistry of catalysts is scanning electrochemical microscopy (SECM).[45] It was recently applied for the investigation of the local electrochemical[40] and
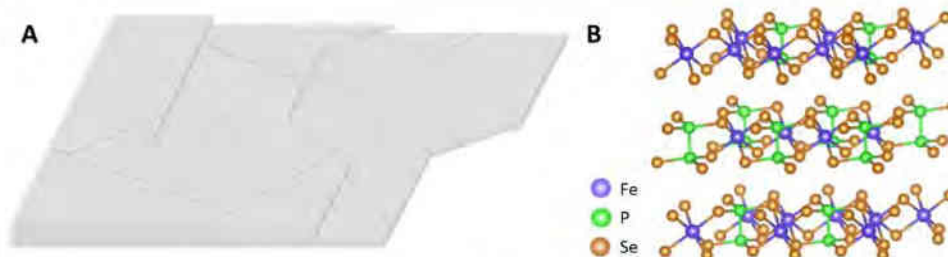
**Figure 1.** (A) Schematic representation of the surface morphology of a FePSe$_3$ crystal. (B) Atomic structure of the FePSe$_3$ crystal layers.
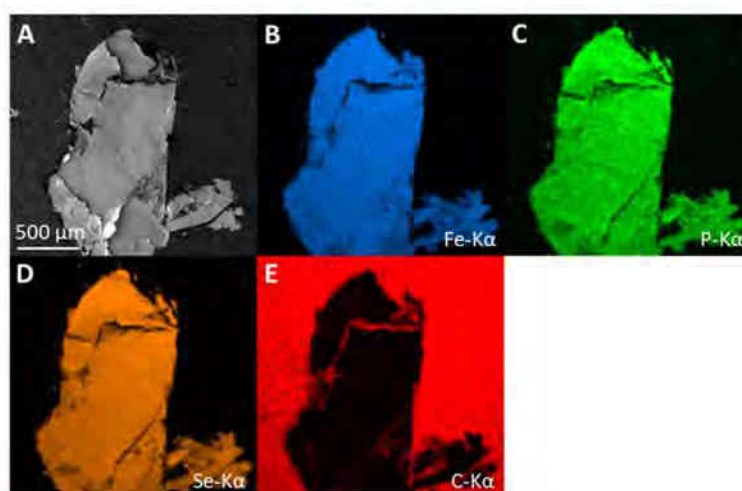


**Figure 2.** SEM image of the FePSe$_3$ sample (A) with EDS elemental maps of Fe (B), P (C), Se (D), and C (E).

electrocatalytic[37,39] activity of transition metal dichalcogenides. Consequently, the aim of our work was to localize the electrochemical and electrocatalytic hotspots of FePSe$_3$ using SECM. We correlated our observations using scanning electron microscopy (SEM) combined with electron-dispersive X-ray spectroscopy (EDS). In addition, X-ray diffraction (XRD) was employed to confirm the composition of the FePSe$_3$ sample. For correlating SECM measurements to the sample topography, optical microscopy (OM) and confocal laser scanning microscopy (CLSM) were employed.

## ■ EXPERIMENTAL SECTION

**Materials and Chemicals.** Crystalline FePSe$_3$ was bought from XFNANO, China. A scheme of the surface morphology of the bulk crystal in given in Figure 1A, with the atomic structure given in Figure 1B. The crystal was prepared according to a previous study[40] to obtain a flat FePSe$_3$ electrode using the following materials. The crystal was embedded in a matrix consisting of a 1:1 (m/m) mixture of two-component epoxy resin (Struers Aps, Denmark) and graphite powder (<20 μm, synthetic, Sigma-Aldrich). Carbon SEM stubs obtained from Micro to Nano, Netherlands, were used as conductive support for the sample. Polydimethylsiloxane (SYLGARD 184) used during the electrode fabrication process was bought from Dow Inc., Michigan, USA. Conductive copper tape was used to establish electrical contact with the sample. All measurements in this work were executed with this sample. Feedback mode and substrate generation/tip collection (SG/TC) mode SECM images were recorded in a solution containing 1.5 mM ferrocene methanol (FcMeOH, 99%, ABCR GmbH, Germany) and 0.2 M potassium nitrate (KNO$_3$, analytical grade, Merck KGaA, Germany). For studying the local differences in HER, 0.5 M sulfuric acid (H$_2$SO$_4$, 96%, analytical grade,

Penta, Czech Republic) was used. Deionized water with a resistivity >18.2 MΩ cm (Milli-Q Advantage A10 system, Merck Millipore, Germany) was used to prepare solutions.

**Instrumentation.** Localized electrochemical and electrocatalytic activity studies were carried out using a commercially available scanning electrochemical microscope (SECM, Sensolytics, Germany) with a bipotentiostat (PGSTAT302N, Autolab, Netherlands). A 25 μm diameter Pt disk ultramicroelectrode (UME, RG = 11, Sensolytics, Germany) was used for SECM experiments. As counter and reference electrodes for electrochemical measurements, a graphite rod and a Ag/AgCl (3 M KCl) reference electrode were employed. The potentials stated herein refer to this reference system.

Scanning electron micrographs were recorded using a MIRA 3 SEM (Tescan, Czech Republic). For EDS maps, this setup was expanded with a Bruker XFlash 5010 EDS. Accelerating voltages of 5 or 20 kV for SEM and EDS, respectively. Gwyddion 2.55 and Origin 2020 software were used for analyzing and visualizing SECM experiments.

Before recording SECM images, the SECM probe was positioned close to the sample by performing a probe approach curve (PAC) toward the sample surface. The PAC was executed with a probe velocity of 1 μm s$^{-1}$ and a probe potential of $E_{probe}$ = 0.5 V. The PAC was stopped when the probe current reached 50% of the current measured in bulk solution. At that distance, SECM images were recorded with a pixel size of 10 μm, a scan rate of 100 μm s$^{-1}$, and a waiting time of 10 ms. Feedback and SG/TC mode images were recorded in a solution of 1.5 mM FcMeOH and 0.2 M KNO$_3$. Feedback mode images were obtained with $E_{probe}$ = 0.5 V and the substrate at open circuit potential. The SG/TC mode images in FcMeOH were recorded with $E_{probe}$ = −0.2 and $E_{substrate}$ = 0.5 V, respectively. HER experiments were performed in a solution of 0.5 M H$_2$SO$_4$. Among these experiments, a linear scan voltammogram was
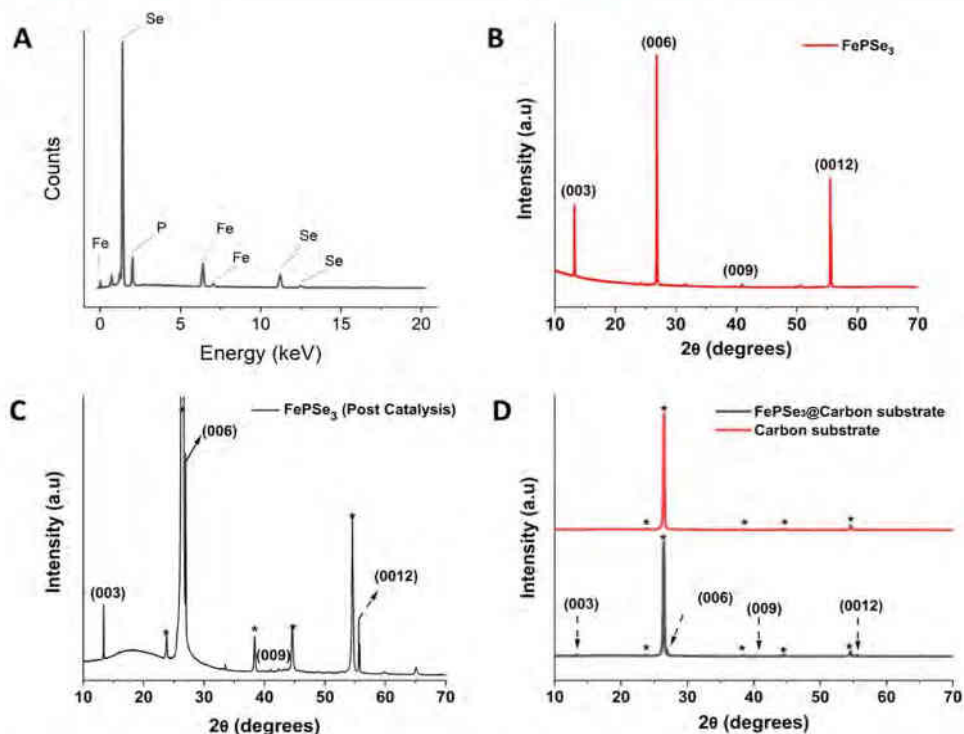
**Figure 3.** EDS (A) and XRD spectra of FePSe$_3$. (B) XRD of the FePSe$_3$ crystal prior to sample preparation and HER. (C) XRD spectrum of the crystal embedded in the carbon matrix after HER. (D): Top: XRD of the conductive carbon matrix the FePSe$_3$ crystal was embedded into. Bottom: FePSe$_3$ sample after HER, embedded in the carbon matrix (same spectrum as in C).
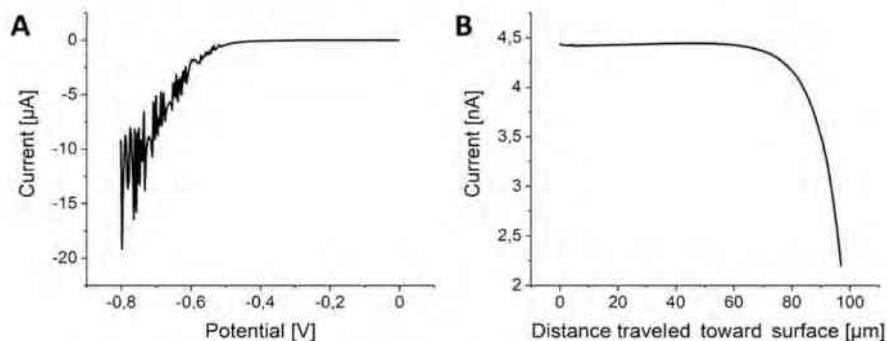


**Figure 4.** (A) Linear scan voltammogram recorded with the FePSe$_3$ sample in 0.5 M H$_2$SO$_4$ at a scan rate of 5 mV s$^{-1}$. (B) PAC toward the graphite/epoxy region of the FePSe$_3$ crystal sample. Parameters: max speed: 1.0 $\mu$m s$^{-1}$, step width: 1.0 $\mu$m, $E_{probe}$ = 0.5 V.

recorded at the FePSe$_3$ sample, decreasing the potential from 0.0 to −0.8 V at a scan rate of 5 mV s$^{-1}$. To obtain images of the local catalytic activity of the sample toward the HER, SECM images of the local hydrogen evolution were obtained using potentials of $E_{probe}$ = 0.2 V and $E_{substrate}$ = −0.5 V. XRD using a diffractometer (SmartLab 3 kW, Rigaku) with a Bragg−Brentano geometry was employed for the structural analysis of the sample. The optical images and height profile measurements of the sample surface were carried out using CLSM (Olympus LEXT OLS4100) with a laser light source ($\lambda$ = 405 nm).

## ■ RESULTS AND DISCUSSION

Before electrochemical investigation, an SEM image and EDS elemental maps of the sample were recorded to evaluate the purity and location of the crystal (Figure 2). The SEM image in Figure 2A shows a black area corresponding to the carbon/

epoxy matrix surrounding the crystal, which is visible as a gray structure. The EDS elemental maps of Fe, P, and Se (Figure 2B−D, respectively) show a mostly homogeneous distribution within the crystal, with lower amounts detected at large cracks in the sample. Furthermore, local carbon impurities are visible in the crystal (Figure 2E). Nevertheless, most of the crystal surface appears clean. From the EDS spectrum in Figure 3A, atomic percentages for Fe, P, and Se of 21.0%, 19.7%, and 59.3% were derived, indicating high purity of the crystal. The purity of the sample was confirmed by XRD (Figure 3B). The sample gave characteristic crystalline peaks at their respective 2$\theta$ value. The values were found to be similar to the ones in the spectrum provided by the crystal manufacturer.[46] The application of hydrogen evolution to the sample resulted in changes in the relative peak intensity in the FePSe$_3$ sample.
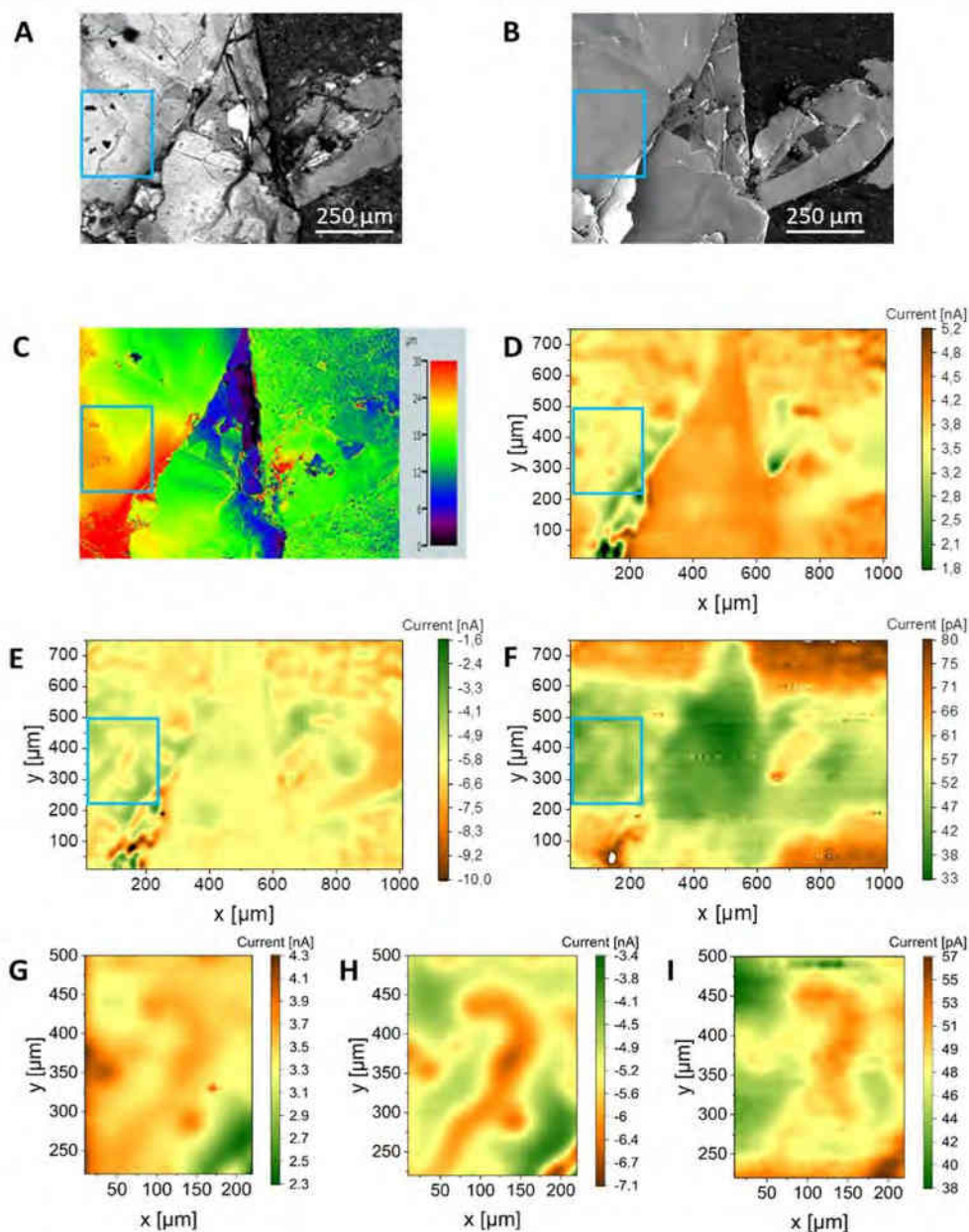
**Figure 5.** OM (A), SEM (B), CLSM (C), and SECM images of the FePSe$_3$ sample (D−F). (D) Feedback SECM image recorded in 1.5 mM FcMeOH. $E_{probe}$ = 0.5 V. (E) SG/TC SECM image recorded in 1.5 mM FcMeOH. $E_{probe}$ = −0.2 V, $E_{substrate}$ = 0.5 V. (F) SG/TC SECM image recorded in 0.5 M H$_2$SO$_4$. $E_{probe}$ = 0.2 V, $E_{substrate}$ = −0.5 V. Images (G−I) are extracted from the SECM images (D−F), highlighting the area included by the blue boxes. (G) Feedback SECM image. (H) SG/TC SECM image recorded in FcMeOH. (I) SG/TC SECM image recorded in H$_2$SO$_4$.

Figure 3C shows the XRD spectrum of the FePSe$_3$ sample after HER. Because the crystal was embedded into a conductive carbon epoxy matrix, the peaks stemming from this matrix are visible as well. They are marked by a *-symbol. XRD spectra of the carbon epoxy matrix and the crystal embedded in said matrix after HER application are given in Figure 3D. Comparing Figure 3B,C, it can be seen that all XRD peaks of the pristine FePSe$_3$ crystal are present post-HER as well, and no additional peaks aside the matrix peaks appeared. Thus, it

can be assumed that the crystal edges did not undergo reorganization during the HER.

Prior to spatially resolved electrochemical analysis of the FePSe$_3$ crystal, an LSV in 0.5 M H$_2$SO$_4$ was recorded (Figure 4A). Upon scanning toward more negative potentials, the measured current starts decreasing at a potential of −0.5 V due to the beginning of the HER. Decreasing the potential further led to a lower and noisier cathodic current resulting from H$_2$ bubble formation at the sample surface. Because a continuous and steady hydrogen evolution is required for SECM imaging,

a potential of −0.5 V was applied to the crystal sample during the SECM experiments for imaging the HER.

Before SECM imaging, the probe was brought close to the sample by performing a PAC toward the carbon matrix around the crystal (Figure 4B). As the probe approached the surface, the measured current started to decrease significantly after the probe traveled 60 $\mu$m. The approach was stopped when the current decreased by 50% with respect to the initially measured value.

For correlating the local activity of the $FePSe_3$ crystal, an OM image and an SEM image were recorded (Figure 5A+B). Because the topography of samples can impact the current measured in SECM, a CLSM image of the sample was recorded as well. The CLSM image in Figure 5C shows the height profile of the investigated area. The feedback mode image (Figure 5D), indicating the local conductivity of the sample, shows that the electron transport at the crystal surface is nonuniform. While the central piece of the crystal appears uniformly conductive, the left part shows local differences in conductivity (highlighted by a blue box, see Figure 5G for better visibility). In that region, the areas where higher currents were recorded are located where cracks (and thus crystal edges) are visible in the image in Figure 5A. Moreover, in the bottom left of the optical image, both low and high currents were measured by SECM. This high contrast in the SECM image indicates a low substrate-to-tip distance and that this piece of crystal protrudes from the sample surface. The CLSM image in Figure 5C proves that the crystal is protruding from the surface compared to the rest of the imaged area. The SG/TC SECM image in Figure 5E gives an insight into the local electrochemical activity of the $FePSe_3$ crystal surface. The image shows well-pronounced local differences over the entirety of the investigated area. Especially in the left highlighted area (extracted in Figure 5H), the regions where a high current was recorded correlate to cracks visible in the optical image in Figure 5A. Because high currents in the SG/TC mode image indicate a high electrochemical activity, we can conclude that the edges of the crystal tend to be more electrochemically active than the basal planes. To investigate whether the electrocatalytic activity for the HER follows the same trend, another SG/TC mode image in 0.5 M $H_2SO_4$ was recorded. This resulted in an image showing local differences in the HER (Figure 5F). Relatively large current differences were located at the top and bottom borders of the image. Consequently, clearly distinguishing edge versus basal plane activity in these regions is not possible. In the left highlighted part (see Figure 5I for an extract of that area), however, more clear local differences in current were measured. Here, lines of high current, and thus high electrocatalytic activity, can be localized. They correspond to both electrochemically active regions (Figure 5D) and cracks within the sample (Figure 5A). Furthermore, the current pattern recorded in SECM images does not match the topography of the sample shown in Figure 5C, and consequently, these patterns of high currents are not caused by topographic effects. Thus, these results show that edges of $FePSe_3$ are both more electrochemically and electrocatalytically active than the basal planes.

## CONCLUSIONS

In this work, we investigated whether the theoretical prediction that edges of $MPX_3$ materials are more electroactive than their basal planes is valid. The local electrochemical investigation of an $MPX_3$ representative, namely, $FePSe_3$, via SECM has shown

that edges exhibit both increased electrochemical and electrocatalytic activity toward the HER. Thus, our measurements indicate that the ideal $MPX_3$-based electrocatalyst is rich in edge planes. This knowledge is very important for future catalyst design. It also adds $MPX_3$ compounds to the family of materials where edges and defects are more active than the basal planes of 2D materials. Our work took a qualitative approach for basal plane and edge activity characterization. Thus, this study opens the door toward quantitative analysis of the activity of the basal planes and edges of $MPX_3$ compounds. Another important question is whether the edges and basal planes of single layers of $FePSe_3$ show similar characteristics as the bulk material analyzed in this study.

## AUTHOR INFORMATION

### Corresponding Author

**Martin Pumera** − *Future Energy and Innovation Laboratory, Central European Institute of Technology, Brno University of Technology, Brno 61200, Czech Republic; Energy Research Institute@NTU (ERI@N), Singapore 637553, Singapore; New Technologies—Research Centre, University of West Bohemia, Plzeň 30100, Czech Republic; Department of Medical Research, China Medical University Hospital, China Medical University, Taichung 40402, Taiwan;* orcid.org/0000-0001-5846-2951; Email: pumera.research@gmail.com

### Authors

**Stefan Wert** − *Future Energy and Innovation Laboratory, Central European Institute of Technology, Brno University of Technology, Brno 61200, Czech Republic*

**Christian Iffelsberger** − *Future Energy and Innovation Laboratory, Central European Institute of Technology, Brno University of Technology, Brno 61200, Czech Republic*

**Akshay Kumar K. Padinjareveetil** − *Future Energy and Innovation Laboratory, Central European Institute of Technology, Brno University of Technology, Brno 61200, Czech Republic*

Complete contact information is available at:
https://pubs.acs.org/10.1021/acsaelm.2c01493

### Author Contributions

S.W. performed SECM, OM, and EDS measurements and wrote the paper. C.I. was involved in the conceptualization and discussion. A.K.K.P. performed the XRD and CLSM measurements. M.P. supervised and conceptualized this work. All authors have given approval to the final version of the paper.

### Notes

The authors declare no competing financial interest.

Nano Research Infrastructure. The authors thank Dr. Kalyan Ghosh for his assistance in CLSM measurements.

## ABBREVIATIONS

EDS    energy-dispersive X-ray spectroscopy
HER    hydrogen evolution reaction
LSV    linear scan voltammogram
OM    optical microscopy
PAC    probe approach curve
PDMS    polydimethylsiloxane
SECM    scanning electrochemical microscopy
SEM    scanning electron microscopy
SG/TC    substrate generation/tip collection

## REFERENCES

(1) Wang, M.; Zhang, L.; He, Y.; Zhu, H. Recent advances in transition-metal-sulfide-based bifunctional electrocatalysts for overall water splitting. *J. Mater. Chem. A* **2021**, *9*, 5320−5363.

(2) Anasori, B.; Lukatskaya, M. R.; Gogotsi, Y. 2D metal carbides and nitrides (MXenes) for energy storage. *Nat. Rev. Mater.* **2017**, *2*, 16098.

(3) Khan, K.; Tareen, A. K.; Aslam, M.; Wang, R.; Zhang, Y.; Mahmood, A.; Ouyang, Z.; Zhang, H.; Guo, Z. Recent developments in emerging two-dimensional materials and their applications. *J. Mater. Chem. C* **2020**, *8*, 387−440.

(4) Novoselov, K. S.; Geim, A. K.; Morozov, S. V.; Jiang, D.; Zhang, Y.; Dubonos, S. V.; Grigorieva, I. V.; Firsov, A. A. Electric field effect in atomically thin carbon films. *Science* **2004**, *306*, 666−669.

(5) Gusmão, R.; Sofer, Z.; Bouša, D.; Pumera, M. Pnictogen (As, Sb, Bi) Nanosheets for Electrochemical Applications Are Produced by Shear Exfoliation Using Kitchen Blenders. *Angew. Chem., Int. Ed.* **2017**, *56*, 14417−14422.

(6) Pumera, M.; Sofer, Z. 2D Monoelemental Arsenene, Antimonene, and Bismuthene: Beyond Black Phosphorus. *Adv. Mater.* **2017**, *29*, 1605299.

(7) Sturala, J.; Sofer, Z.; Pumera, M. Chemistry of Layered Pnictogens: Phosphorus, Arsenic, Antimony, and Bismuth. *Angew. Chem., Int. Ed.* **2019**, *58*, 7551−7557.

(8) Beladi-Mousavi, S. M.; Pumera, M. 2D-Pnictogens: alloy-based anode battery materials with ultrahigh cycling stability. *Chem. Soc. Rev.* **2018**, *47*, 6964−6989.

(9) Chia, X.; Eng, A. Y. S.; Ambrosi, A.; Tan, S. M.; Pumera, M. Electrochemistry of Nanostructured Layered Transition-Metal Dichalcogenides. *Chem. Rev.* **2015**, *115*, 11941−11966.

(10) Chia, X.; Pumera, M. Characteristics and performance of two-dimensional materials for electrocatalysis. *Nat. Catal.* **2018**, *1*, 909−921.

(11) Eng, A. Y. S.; Ambrosi, A.; Sofer, Z.; Šimek, P.; Pumera, M. Electrochemistry of transition metal dichalcogenides: strong dependence on the metal-to-chalcogen composition and exfoliation method. *ACS Nano* **2014**, *8*, 12185−12198.

(12) Toh, R. J.; Sofer, Z.; Pumera, M. Catalytic properties of group 4 transition metal dichalcogenides (MX2; M = Ti, Zr, Hf; X = S, Se, Te). *J. Mater. Chem. A* **2016**, *4*, 18322−18334.

(13) Wang, Z.; Wu, H.-H.; Li, Q.; Besenbacher, F.; Li, Y.; Zeng, X. C.; Dong, M. Reversing Interfacial Catalysis of Ambipolar WSe 2 Single Crystal. *Adv. Sci.* **2020**, *7*, 1901382.

(14) Hu, F.; Yu, D.; Ye, M.; Wang, H.; Hao, Y.; Wang, L.; Li, L.; Han, X.; Peng, S. Lattice-Matching Formed Mesoporous Transition Metal Oxide Heterostructures Advance Water Splitting by Active Fe-O-Cu Bridges. *Adv. Energy Mater.* **2022**, *12*, 2200067.

(15) Huang, H.; Yu, D.; Hu, F.; Huang, S.-C.; Song, J.; Chen, H.-Y.; Li, L. L.; Peng, S. Clusters Induced Electron Redistribution to Tune Oxygen Reduction Activity of Transition Metal Single-Atom for Metal-Air Batteries. *Angew. Chem., Int. Ed.* **2022**, *61*, No. e202116068.

(16) Deng, L.; Hu, F.; Ma, M.; Huang, S.-C.; Xiong, Y.; Chen, H.-Y.; Li, L.; Peng, S. Electronic Modulation Caused by Interfacial Ni-O-M

(M=Ru, Ir, Pd) Bonding for Accelerating Hydrogen Evolution Kinetics. *Angew. Chem., Int. Ed.* **2021**, *60*, 22276−22282.

(17) Kang, Z.; Khan, M. A.; Gong, Y.; Javed, R.; Xu, Y.; Ye, D.; Zhao, H.; Zhang, J. Recent progress of MXenes and MXene-based nanomaterials for the electrocatalytic hydrogen evolution reaction. *J. Mater. Chem. A* **2021**, *9*, 6089−6108.

(18) Seh, Z. W.; Fredrickson, K. D.; Anasori, B.; Kibsgaard, J.; Strickler, A. L.; Lukatskaya, M. R.; Gogotsi, Y.; Jaramillo, T. F.; Vojvodic, A. Two-Dimensional Molybdenum Carbide (MXene) as an Efficient Electrocatalyst for Hydrogen Evolution. *ACS Energy Lett.* **2016**, *1*, 589−594.

(19) Qin, T.; Wang, Z.; Wang, Y.; Besenbacher, F.; Otyepka, M.; Dong, M. Recent Progress in Emerging Two-Dimensional Transition Metal Carbides. *Nano-Micro Lett.* **2021**, *13*, 183.

(20) Muller, G. A.; Cook, J. B.; Kim, H.-S.; Tolbert, S. H.; Dunn, B. High performance pseudocapacitor based on 2D layered metal chalcogenide nanocrystals. *Nano Lett.* **2015**, *15*, 1911−1917.

(21) Ghosh, K.; Pumera, M. Free-standing electrochemically coated MoSx based 3D-printed nanocarbon electrode for solid-state supercapacitor application. *Nanoscale* **2021**, *13*, 5744−5756.

(22) Liu, Y.; Wu, J.; Hackenberg, K. P.; Zhang, J.; Wang, Y. M.; Yang, Y.; Keyshar, K.; Gu, J.; Ogitsu, T.; Vajtai, R.; Lou, J.; Ajayan, P. M.; Wood, B. C.; Yakobson, B. I. Self-optimizing, highly surface-active layered metal dichalcogenide catalysts for hydrogen evolution. *Nat. Energy* **2017**, *2*, 17127.

(23) Li, L.; Yu, D.; Li, P.; Huang, H.; Xie, D.; Lin, C.-C.; Hu, F.; Chen, H.-Y.; Peng, S. Interfacial electronic coupling of ultrathin transition-metal hydroxide nanosheets with layered MXenes as a new prototype for platinum-like hydrogen evolution. *Energy Environ. Sci.* **2021**, *14*, 6419−6427.

(24) Samal, R.; Sanyal, G.; Chakraborty, B.; Rout, C. S. Two-dimensional transition metal phosphorous trichalcogenides (MPX3): a review on emerging trends, current state and future perspectives. *J. Mater. Chem. A* **2021**, *9*, 2560−2591.

(25) Mayorga-Martinez, C. C.; Sofer, Z.; Sedmidubský, D.; Huber, Š.; Eng, A. Y. S.; Pumera, M. Layered Metal Thiophosphite Materials: Magnetic, Electrochemical, and Electronic Properties. *ACS Appl. Mater. Interfaces* **2017**, *9*, 12563−12573.

(26) Gusmão, R.; Sofer, Z.; Pumera, M. Exfoliated Layered Manganese Trichalcogenide Phosphite (MnPX 3 , X = S, Se) as Electrocatalytic van der Waals Materials for Hydrogen Evolution. *Adv. Funct. Mater.* **2019**, *29*, 1805975.

(27) Gusmão, R.; Sofer, Z.; Sedmidubský, D.; Huber, Š.; Pumera, M. The Role of the Metal Element in Layered Metal Phosphorus Triselenides upon Their Electrochemical Sensing and Energy Applications. *ACS Catal.* **2017**, *7*, 8159−8170.

(28) Sanna, M.; Ng, S.; Pumera, M. Layered transition metal selenophosphites for visible light photoelectrochemical production of hydrogen. *Electrochem. Commun.* **2021**, *129*, 107077.

(29) Barua, M.; Ayyub, M. M.; Vishnoi, P.; Pramoda, K.; Rao, C. N. R. Photochemical HER activity of layered metal phospho-sulfides and -selenides. *J. Mater. Chem. A* **2019**, *7*, 22500−22506.

(30) Song, J. Sub-2 nm Thiophosphate Nanosheets with Heteroatom Doping for Enhanced Oxygen Electrocatalysis. *Adv. Funct. Mater.* **2021**, *31*, 2100618.

(31) Banks, C. E.; Davies, T. J.; Wildgoose, G. G.; Compton, R. G. Electrocatalysis at graphite and carbon nanotube modified electrodes: edge-plane sites and tube ends are the reactive sites. *Chem. Commun.* **2005**, 829−841.

(32) Wang, L.; Sofer, Z.; Pumera, M. Will Any Crap We Put into Graphene Increase Its Electrocatalytic Effect? *ACS Nano* **2020**, *14*, 21−25.

(33) Güell, A. G.; Cuharuc, A. S.; Kim, Y.-R.; Zhang, G.; Tan, S.; Ebejer, N.; Unwin, P. R. Redox-dependent spatially resolved electrochemistry at graphene and graphite step edges. *ACS Nano* **2015**, *9*, 3558−3571.

(34) Yuan, W.; Zhou, Y.; Li, Y.; Li, C.; Peng, H.; Zhang, J.; Liu, Z.; Dai, L.; Shi, G. The edge- and basal-plane-specific electrochemistry of a single-layer graphene sheet. *Sci. Rep.* **2013**, *3*, 2248.

(35) Bentley, C. L.; Kang, M.; Maddar, F. M.; Li, F.; Walker, M.; Zhang, J.; Unwin, P. R. Electrochemical maps and movies of the hydrogen evolution reaction on natural crystals of molybdenite (MoS2): basal vs. edge plane activity. *Chem. Sci.* **2017**, *8*, 6583−6593.

(36) Jaramillo, T. F.; Jørgensen, K. P.; Bonde, J.; Nielsen, J. H.; Horch, S.; Chorkendorff, I. Identification of Active Edge Sites for Electrochemical H 2 Evolution from MoS 2 Nanocatalysts. *Science* **2007**, *317*, 100−102.

(37) Takahashi, Y.; Kobayashi, Y.; Wang, Z.; Ito, Y.; Ota, M.; Ida, H.; Kumatani, A.; Miyazawa, K.; Fujita, T.; Shiku, H.; Korchev, Y. E.; Miyata, Y.; Fukuma, T.; Chen, M.; Matsue, T. High-Resolution Electrochemical Mapping of the Hydrogen Evolution Reaction on Transition-Metal Dichalcogenide Nanosheets. *Angew. Chem., Int. Ed.* **2020**, *59*, 3601−3608.

(38) Tan, S. M.; Ambrosi, A.; Sofer, Z.; Huber, Š.; Sedmidubský, D.; Pumera, M. Pristine Basal- and Edge-Plane-Oriented Molybdenite MoS2Exhibiting Highly Anisotropic Properties. *Chemistry* **2015**, *21*, 7170−7178.

(39) Tao, B.; Unwin, P. R.; Bentley, C. L. Nanoscale Variations in the Electrocatalytic Activity of Layered Transition-Metal Dichalcogenides. *J. Phys. Chem. C* **2020**, *124*, 789−798.

(40) Wert, S.; Iffelsberger, C.; Novčić, K. A.; Matysik, F.-M.; Pumera, M. Edges are more electroactive than basal planes in synthetic bulk crystals of TiS2 and TiSe2. *Appl. Mater. Today* **2022**, *26*, 101309.

(41) Sofer, Z.; Sedmidubský, D.; Huber, Š.; Luxa, J.; Bouša, D.; Boothroyd, C.; Pumera, M. Layered Black Phosphorus: Strongly Anisotropic Magnetic, Electronic, and Electron-Transfer Properties. *Angew. Chem., Int. Ed.* **2016**, *55*, 3382−3386.

(42) Marvan, P.; Huber, Š.; Luxa, J.; Mazánek, V.; Sedmidubský, D.; Sofer, Z.; Pumera, M. Edge vs. basal plane electrochemistry of layered pnictogens (As, Sb, Bi): Does edge always offer faster electron transfer? *Appl. Mater. Today* **2019**, *16*, 179−184.

(43) Djire, A.; Wang, X.; Xiao, C.; Nwamba, O. C.; Mirkin, M. V.; Neale, N. R. Basal Plane Hydrogen Evolution Activity from Mixed Metal Nitride MXenes Measured by Scanning Electrochemical Microscopy. *Adv. Funct. Mater.* **2020**, *30*, 2001136.

(44) Das, T.; Alam, K.; Chakraborty, S.; Sen, P. Probing active sites on MnPSe3 and FePSe3 tri-chalcogenides as a design strategy for better hydrogen evolution reaction catalysts. *Int. J. Hydrogen Energy* **2021**, *46*, 37928−37938.

(45) Bentley, C. L.; Edmondson, J.; Meloni, G. N.; Perry, D.; Shkirskiy, V.; Unwin, P. R. Nanoscale Electrochemical Mapping. *Anal. Chem.* **2019**, *91*, 84−108.

(46) https://www.2dsemiconductors.com/FePSe3/#description, accessed Aug 30, 2022.